



Durable Catalysts for Complete Methane Oxidation

Mortensen, Rasmus Lykke

Publication date:
2023

Document Version
Publisher's PDF, also known as Version of record

[Link back to DTU Orbit](#)

Citation (APA):
Mortensen, R. L. (2023). *Durable Catalysts for Complete Methane Oxidation*. Technical University of Denmark.

General rights

Copyright and moral rights for the publications made accessible in the public portal are retained by the authors and/or other copyright owners and it is a condition of accessing publications that users recognise and abide by the legal requirements associated with these rights.

- Users may download and print one copy of any publication from the public portal for the purpose of private study or research.
- You may not further distribute the material or use it for any profit-making activity or commercial gain
- You may freely distribute the URL identifying the publication in the public portal

If you believe that this document breaches copyright please contact us providing details, and we will remove access to the work immediately and investigate your claim.

Durable Catalysts for Complete Methane Oxidation

PhD dissertation by Rasmus Lykke Mortensen



DTU supervisors:
Assoc. Professor, Susanne Mossin
Senior Researcher, Jerrik Mielby

Umicore supervisors:
Dr. Kim Hougaard
Pedersen
Hendrik-David Noack

May 2023

Preface

This PhD project was carried out as a collaboration between Umicore Denmark ApS and the Department of Chemistry at the Technical University of Denmark as an Industrial PhD Program funded by Innovation Fund Denmark. The project was supervised by Dr. Kim Hougaard Pedersen from Umicore and by Associate Professor Susanne Mossin from DTU. The project lasted from April 2020 to May 2023 and included a 6-month stay at ITQ-UPV in Valencia, Spain in 2022. Being an Industrial PhD student, I have attempted to split my focus between scientific discoveries and industrial applications, and the thesis has been written to reflect this. The reader is encouraged to read Section 6 in its entirety, as the water deactivation project is by far the most interesting and innovative work of the PhD. Further, Section 6.8 contains an important discussion about realistic conditions for catalytic testing.

The publications produced during the project are included in the thesis, but the unpublished work of my PhD is also documented. Firstly, the design and construction of a catalytic test setup constituted a major part of the project, which is why it is given pages in the main thesis instead of just in an appendix. This choice is elaborated on further in Section 3. Secondly, the extensive effort to use rational catalyst design to synthesize a durable methane oxidation catalyst from palladium and metal oxides encapsulated in a hydrophobic zeolite. This project, which included two student projects, never lived up to its initial promise but the results are reported here to show the work. Results generated by students will be shown in either appendices or in the main report depending on how much additional analysis I can contribute. As methane oxidation is an active research area within our company, a series of oxidation catalysts were also evaluated on the catalytic test setup. This was done in parallel to the PhD project and the results are not included in the thesis.

Other than the three manuscripts (and a debate article in Danish tech/engineering outlet “Ingeniøren”) directly resulting from the PhD project, I participated in the publication of three other scientific articles during the period. These were, in part, the outcome of work I did during my masters program in collaboration with PhD students from Kegnæs Group at DTU Chemistry. The publications are not part of this PhD project, they are not affiliated with Umicore, and they are not funded by the Innovation Fund Denmark.

I would like to thank all my colleagues from DTU and Umicore who have supported me during the project. Especially Steen Riis Christensen and Ton Janssen for all their help and guidance in the world of chemical kinetics and for many fruitful discussions. I would like to thank fellow PhD students Mikkel Kock Larsen and Dimitra Iltsiou for good neighborliness in times of shared struggle and success. I’m happy to have been allowed in the Kegnæs Group labs throughout the project. The good people of the DTU Chemistry workshop assisted in countless practical matters regarding the test setup and Leif Bak of Ballerup Glas supplied invaluable high-quality quartz reactors, they all

have my profound gratitude. Avelino Corma and Manuel Moliner deserve warm thanks for letting me visit Valencia for a very inspiring 6 months and hosting me at ITQ. I would like to thank all my four supervisors for the things they have each contributed during the project. I have felt very well taken care of throughout the three years. Jerrik and Susanne, you were of invaluable help during our daily discussions about technical and scientific challenges. And finally, my family and my lovely soon-to-be wife Katrine. Without you and your support I would not have made it through.

Abstract

Replacing heavy fuel oil with liquefied natural gas in marine engines can potentially provide significant CO₂ savings due to the higher hydrogen to carbon ratio of natural gas. For many existing engines, the change can be done only minor modifications. One challenge remains to realize the potential green house gas savings: Methane slip. This longstanding issue with large engines revolves around the stability of the CH₄ molecule, resulting in significant amounts of unburned methane being emitted to the atmosphere. The high global warming potential (GWP) of methane means that the CO₂ savings are nullified by just a few percent of methane slip. To solve this challenge in the already highly optimized engines, a catalyst can be used to convert the last CH₄ to CO₂.

Methane oxidation catalysts have been in development for several decades and are essentially still faced with the same set of challenges as 40 years ago, namely three different types of deactivation. The first part of this dissertation aims to thoroughly present the progress in the field of methane oxidation and attempts to prevent catalyst deactivation. Arguably the most interesting leap forward has been the adoption of zeolite-supported catalysts which promises to solve both hydrothermal sintering and direct water-induced deactivation by offering nanoparticle encapsulation in a hydrophobic microporous structure. This topic is so novel and interesting that it was decided to cover it in a review article, presented here as Paper 1.

The first experimental project was an attempt to build on top of the promising work by others on zeolite-supported methane oxidation catalysts. A series of Pd/MO_x@S-1 catalysts (M = Ce, Ba) was synthesized and tested in a purpose-built catalytic test setup. None of the synthesized materials exhibited a catalytic performance or durability superior to the state-of-the-art Pd/Al₂O₃ catalyst and the work remains unpublished for that reason.

In the second project, the influence of the zeolite counter-ion on SO₂ tolerance was explored through a series of ion-exchanged materials. A Pd/H-CHA catalyst (CHA = zeolite with CHA framework) showed impressive stability when exposed to SO₂ for more than 200 hours. When the protons in the zeolite structure were exchanged to alkali metal ions, the catalyst quickly deactivated and irreversibly lost most of its methane oxidation activity. This result is remarkable since a lot of literature on water-induced deactivation points towards H-form zeolites being inferior to their alkali-exchanged counterparts due to the difference in hydrophobicity. This contradiction points out the importance of testing under realistic conditions when developing catalysts prone to multiple deactivation pathways. The results of the project were written into a manuscript, presented here as Paper 2.

The third and final experimental project describes our view on water-induced deactivation of palladium-based methane oxidation catalysts. The unique observation that deactivation requires methane to be converted at water-saturated sites opens up multiple new angles to improve the

understanding of the problem. The dependence of methane concentration, water concentration, temperature, and pressure was determined through a series of catalytic tests. Methane temperature programmed reduction (CH_4 -TPR) experiments were used to describe the deactivated PdO phase, showing that the deactivation is a bulk phenomenon. The reduction temperature of deactivated PdO increased steadily with deactivation time. Finally, a complete mechanism and model for water-induced deactivation is proposed based on the experimental data. The project is presented here as Paper 3, supplemented by some additional analysis and illustrations for the thesis.

Throughout the PhD project and this dissertation, realistic testing conditions is a recurring theme, as it should increasingly be viewed as a necessity for catalyst development. The challenges around designing a durable catalyst for complete methane oxidation are so numerous and interconnected that insisting on solving one isolated problem at a time will likely slow down progress significantly.

Resume

At erstatte traditionelt oliebaseret brændsel med flydende naturgas i skibsmotorer kan potentielt give markante CO₂-besparelser grundet det højere brint-til-kulstof forhold i naturgas. For mange eksisterende motorer kan ændringen af brændstof laves med kun få modifikationer. En udfordring står dog i vejen for at potentialet i drivhusgasbesparelser kan indfris: Metan slip. Dette velkendte problem ved store motorer skyldes den høje stabilitet af metanmolekylet og betyder at store mængder uforbrændt metan udledes til atmosfæren. Det store drivhusgaspotentiale (GWP) af metan betyder at CO₂ besparelserne ved at skifte til naturgas bliver udlignet ved nogle få procent metan slip. For at løse denne udfordring i de i forvejen højt optimerede motorer kan en katalysator bruges til at konvertere den sidste CH₄ til CO₂.

Katalysatorer til metanoxidation har været under udvikling i flere årtier og står essentielt stadig overfor den samme række af udfordringer som for 40 år siden, navnlig 3 forskellige slags deaktivering. Den første del af denne afhandling sigter efter at give en grundig gennemgang af de fremskridt der har været indenfor metanoxidation og forsøg på at forhindre katalysatordeaktivering. Det største fremskridt har muligvis været udviklingen af zeolit-baserede katalysatorer der tilstræber at løse både hydrotermisk sintring og direkte vand-induceret deaktivering ved at muliggøre indkapsling af nanopartiklerne i en hydrofob mikroporøs struktur. Dette emne er så nyt og interessant at det blev besluttet at dække det i et review, præsenteret her som Artikel 1.

Det første eksperimentelle projekt var et forsøg på at bygge ovenpå andres lovende arbejde med zeolit-baserede metanoxideringskatalysatorer. En serie af Pd/MOx@S-1 katalysatorer (M = Ce, Ba) blev syntetiseret og testet i en katalytisk testopstilling som blev bygget til formålet. Ingen af de syntetiserede materialer var mere katalytisk aktive eller stabile end den industrielle referencekatalysator Pd/Al₂O₃, og arbejdet blev af den grund ikke publiceret.

I det andet projekt blev betydningen af zeolit modionen for SO₂ tolerance udforsket gennem en serie af ionbyttede materialer. En Pd/H-CHA katalysator var stabil selv når den blev udsat for SO₂ i mere end 200 timer. Når protonerne i zeolitstrukturen blev byttet ud med alkalimetallioner deaktiverede katalysatoren hurtigt og mistede al sin katalytiske aktivitet. Dette resultat er bemærkelsesværdigt da en stor del af litteraturen om vand-induceret deaktivering påpeger at zeolitter i H-form er værre end zeolitter med alkalimetallioner på grund af forskellen i hydrofobicitet. Denne modsætning fremhæver vigtigheden af at teste under realistiske betingelser når man udvikler katalysatorer der er sårbare overfor mere end en form for deaktivering. Projektets resultater blev skrevet sammen til et manuskript præsenteret her som Artikel 2.

Det tredje og sidste eksperimentelle projekt sigtede efter at kortlægge de to typer vand-induceret deaktivering af palladiumbaserede metanoxideringskatalysatorer. Den unikke observation at deaktivering kræver at metan omsættes på vandmættede katalytiske sites åbner op for en bedre forståelse

af problemet. Afhængigheden af metankoncentration, vandkoncentration, temperatur og reaktortryk blev bestemt gennem en serie af katalytiske tests. CH_4 -TPR forsøg blev brugt til at beskrive den deaktiverede PdO-fase, hvilket viste at deaktivering er et bulk fænomen. Reduktionstemperaturen af deaktiveret PdO steg i takt med deaktiveringstiden. Til sidst bliver en komplet mekanisme og model for vand-induceret deaktivering foreslået baseret på de eksperimentelle data. Projektet er præsenteret her som Artikel 3 og suppleret med yderligere analyse og illustrationer til afhandlingen.

Igennem PhD projektet og denne afhandling er realistiske testbetingelser et gennemgående tema, da det i stigende grad bør anses som en nødvendighed for katalysatorudvikling. Udfordringerne i at designe en holdbar katalysator til komplet metanoxidation er så talrige og indbyrdes forbundne at et forsøg på at løse et enkelt isoleret problem af gangen sandsynligvis vil forsinke udviklingen markant.

List of publications

Publications authored by the PhD candidate as part of the PhD project:

Paper 1:

“Recent Advances in Complete Methane Oxidation using Zeolite-Supported Metal Nanoparticle Catalysts”

R. L. Mortensen, H. Noack, K. Pedersen, S. Mossin, & J. Mielby
ChemCatChem (2022), 14(16), e202101924

Paper 2:

“The Effect of Zeolite Counter-Ion on a Pd/H-CHA Methane Oxidation Catalyst with Remarkable Tolerance to SO₂”

R. L. Mortensen, H. Noack, K. Pedersen, S. Mossin, & J. Mielby

Submitted

Paper 3:

“Understanding Water-Induced Reversible Inhibition and Irreversible Deactivation of Methane Oxidation Catalysts”

R. L. Mortensen, H. Noack, K. Pedersen, J. Mielby, & S. Mossin

In progress

Debate article in Danish technology outlet Ingeniøren:

<https://ing.dk/artikel/fagligt-talt-naturgas-er-en-stoerre-klimasynder-end-foerst-antaget>

Other publications with contributions from the PhD candidate:

Paper 4:

“Heterogeneous Formic Acid Production by Hydrogenation of CO₂ Catalyzed by Ir-bpy Embedded in Polyphenylene Porous Organic Polymers” N. R. Bennedsen, D. B. Christensen, R. L. Mortensen, B. Wang, R. Wang, S. Kramer, & S. Kegnæs
ChemCatChem (2021), 13(7), 1781-1786

Paper 5:

“Study of CoCu Alloy Nanoparticles Supported on MOF-Derived Carbon for Hydrosilylation of Ketones”

D. B. Christensen, R. L. Mortensen, S. Kramer, & S. Kegnæs
Catalysis Letters (2020), 150(6), 1537–1545.

Paper 6:

“Palladium on carbon-catalyzed α -alkylation of ketones with alcohols as electrophiles: Scope and mechanism.”

N. R. Bennedsen, R. L. Mortensen, S. Kramer, & S. Kegnæs
Journal of Catalysis (2019), 371, 153–160

List of abbreviations

Abbreviation	Explanation
AR6	Sixth assessment report of the IPCC
a.u.	Arbitrary units
BET	Brunauer–Emmett–Teller theory for physisorption
BPR	Back-pressure regulator
BSc	Bachelor of Science
CDR	Carbon dioxide removal
CEM	Controlled evaporator mixer from Bronkhorst
CFCs	Chlorofluorocarbons
cpsi	Cells per square inch
CT	Carbon templating
DRIFTS	Diffuse reflectance infrared Fourier transform spectroscopy
DS	Desilication
EN	Ethylenediamine
EXAFS	Extended X-ray absorption fine structure
FID	Flame ionization detector
ft ³	Cubic feet
GC-MS	Gas chromatography-mass spectroscopy
GHG	Greenhouse gas
GWP	Global warming potential
HAADF-STEM	High-angle annular dark-field scanning transmission electron microscopy
HPDF	High-pressure dual-fuel
ICCT	International Council on Clean Transportation
ICP-OES	Inductively coupled plasma-optical emission spectroscopy
IPCC	Intergovernmental Panel on Climate Change
IUPAC	International Union of Pure and Applied Chemistry
LNG	Liquefied natural gas
LPDF	Low-pressure dual-fuel
MOC	Methane oxidation catalyst
MSc	Master of Science
NDIR	Non-dispersive infrared
NOAA	National Oceanic and Atmospheric Administration (US)
PDF	Pair distribution function
PID	Proportional–integral–derivative (control loop)
ppm	Parts per million
S-1	Silicalite-1
SCR	Selective catalytic reduction
SS-NMR	Solid state nuclear magnetic resonance
TC	Turbocharger
TEM	Transmission electron microscopy
TEOS	Tetraethyl orthosilicate
TGA	Thermogravimetric analysis
TPAOH	Tetrapropylammonium hydroxide
TPR	Temperature programmed reduction
WHSV	Weight hourly space velocity
XPS	X-ray photoelectron spectroscopy
XRF	X-ray fluorescence
XR(P)D	X-ray (powder) diffraction

Contents

Preface	i
Abstract	iii
Resume	v
List of publications	vii
List of abbreviations	viii
1 Introduction	1
1.1 Thesis scope	5
2 Background on complete methane oxidation	6
2.1 The state-of-the-art catalyst, Pd/Al ₂ O ₃	7
2.2 Palladium-based catalysts on alternative supports	10
2.3 Precious metal-free methane oxidation catalysts	10
2.4 Non-catalytic alternatives and exotic oxidants	12
2.5 Zeolite-based catalysts for complete methane oxidation (Paper 1)	13
3 Construction of catalytic test setup	30
3.1 Requirements	30
3.2 Equipment choices and automation software	32
4 Project 1: Rational design of a durable catalyst for methane oxidation using zeolite encapsulation	36
4.1 Material synthesis	37
4.1.1 Pd/MO _x @S-1	37
4.1.2 Pd@S-1 and PdPt@S-1	38
4.1.3 Others	38
4.2 Catalytic results	39
4.3 Characterization	43
4.4 Evaluation of Silicalite-1 encapsulation projects	50
5 Project 2: Influence of counter-ion on the sulfur tolerance of zeolite-supported methane oxidation catalysts	52
5.1 Initial screening of ion-exchanged zeolite-supported catalysts	52
5.2 Paper 2	54
6 Project 3: Uncovering the reason for water-induced deactivation of palladium-based methane oxidation catalysts	61
6.1 Description of the leading hypothesis for water-induced deactivation	61
6.2 Discovery of methane dependence	67
6.3 Methodology for water deactivation project	68
6.4 Paper 3	72
6.5 Further analysis of data from kinetic experiments	86
6.6 Attempts at elucidating the nature of deactivated PdO with spectroscopy	89
6.7 Hypothesis for water-induced deactivation	92

6.8	Discussion about the importance of realistic testing conditions	96
7	Conclusions	98
7.1	Industrial impact	99
7.2	Future perspectives	100
	References	101
	Appendices	117
	Appendix A - P&I diagram of test setup	117
	Appendix B - Construction drawing of test setup	118
	Appendix C - Example of poorly reproducible synthesis	119
	Appendix D - Characterization of PdPt@S-1 materials synthesized by BSc. students . . .	120
	Appendix E - Origin of discovery of methane dependence	122
	Appendix F - Calculations for accumulation plots (500 ppm CH ₄)	123
	Appendix G - Calculations for accumulation plots (5% H ₂ O)	124
	Appendix H - Supporting information for Paper 3	125
	Appendix I - Pictures of test setup	141
	Appendix J - TEM of Pd/CeO ₂ @S-1 without methane oxidation activity	146
	Appendix K - Solid-state ²⁹ Si NMR of fresh and deactivated Pd@S-1	147
	Appendix L - Virtual control panel for catalytic test setup	148
	Appendix M - N ₂ -physisorption isotherms	149
	Appendix N - XRD of fresh, deactivated, and regenerated catalyst for water deactivation project	150
	Appendix O - Co-author statements	151

1 Introduction

Mitigating climate change is no doubt a major challenge of the twenty-first century. In recent reports from the Intergovernmental Panel on Climate Change (IPCC),¹⁻³ emissions of methane are receiving increased attention due to its powerful effect as a greenhouse gas (GHG). This can be illustrated by comparing methane to carbon dioxide in terms of atmospheric concentration and greenhouse gas impact, so called radiative forcing, as shown in Figure 1. Despite making up less than 2 parts per million (ppm) of the atmosphere, and less than half a percent of the greenhouse gasses by volume, methane is currently responsible for at least one sixth of the total radiative forcing in the atmosphere.^{4,5}

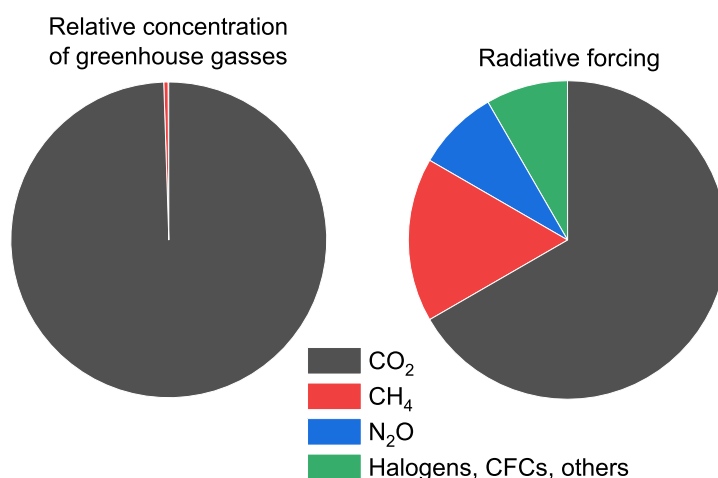


Figure 1 Difference between atmospheric concentration of various greenhouse gasses and their respective influences on radiative forcing. Greenhouse gasses make up 0.04% of the atmosphere, with CO₂ accounting for more than 99% of that. The main constituents of the atmosphere are nitrogen (78.08%), oxygen (20.95%), and argon (0.93%).⁶ RF data from National Oceanic and Atmospheric Administration (NOAA) of the United States of America.⁵

Methane has a global warming potential GWP₂₀ and GWP₁₀₀ of 81.2 and 27.9, respectively,² i.e. how much worse of a greenhouse gas than CO₂ it is on a mass basis over 20 and 100 years. The large difference in the GWP values comes from the fact that methane has a lifetime in the atmosphere of just 11.8 years, compared to the several centuries of carbon dioxide, meaning that most of its effect comes in the first decade after emission. This has caused lawmakers and scientists to focus on reducing methane emissions as an effective way of limiting global warming on the short term. As a result, even direct atmospheric methane removal is becoming an active research topic.⁷ As an example, the IPCC includes the following statements with the label "high confidence" in its recent synthesis report for the sixth assessment report (AR6):³

"The larger the overshoot, the more net negative CO₂ emissions would be needed to return to 1.5

°C by 2100. Transitioning towards net zero CO₂ emissions faster and reducing non-CO₂ emissions such as methane more rapidly would limit peak warming levels and reduce the requirement for net negative CO₂ emissions, thereby reducing feasibility and sustainability concerns, and social and environmental risks associated with CDR deployment at large scales.”

and:

”Strong, rapid and sustained reductions in methane emissions can limit near-term warming and improve air quality by reducing global surface ozone.”

Also, in its report on effective methods of climate change mitigation,¹ the IPCC writes:

”Global methane emissions from energy supply, primarily fugitive emissions from production and transport of fossil fuels, accounted for about 18% [13–23%] of global GHG emissions from energy supply, 32% [22–42%] of global CH₄ emissions, and 6% [4–8%] of global GHG emissions in 2019 (high confidence). About 50–80% of CH₄ emissions from these fossil fuels could be avoided with currently available technologies at less than USD50 tCO₂-eq⁻¹”

It can therefore be concluded that **lowering atmospheric methane concentrations by reducing methane emissions e.g. from industry is a highly effective and cost efficient method of mitigating climate change.**

An emission source with no widely adopted technical solution is unburned methane from large engines fueled with liquefied natural gas (LNG). These engines are either used on cargo/cruise ships for marine propulsion or stationed on land and used for electricity generation. The high stability of the methane molecule, which comes from the strong C-H bond (435 kJ/mol), makes it difficult to ignite if the local chamber temperature and mixing ratio is not ideal, which is often the case in crevasses and corners of the combustion chamber. This leads varying amounts of methane from the LNG fuel being emitted to the atmosphere unburned, so-called methane slip.^{8,9} The methane slip from a selection of engine types is shown in Table 1.

Table 1 Emission estimates from 2020 of large marine engines able to run fully or partially on liquefied natural gas. Adapted from Pavlenko et al.⁸ with methane slip in units of percentage instead of g/kWh using the following conversion: $\text{slip}(\%) = \frac{\text{slip}(\text{g/kWh})}{200 \text{ g CO}_2/\text{kWh}} \cdot \frac{M_{\text{CO}_2}}{M_{\text{CH}_4}} \cdot 100\%$

Engine type	Estimated number of vessels	Methane slip (%)
LPDF, medium-speed, four-stroke	At least 300	7.8
LPDF, slow-speed, two-stroke	At least 50	3.6
HPDF, slow-speed, two-stroke	At least 90	0.36

The environmental case for fueling large engines with LNG instead of diesel is the roughly 25% CO₂/kWh savings provided by the higher hydrogen to carbon ratio of natural gas.^{8,9} Figure 2 shows that these savings disappear when accounting for methane slip. Further, at high slippage

the greenhouse gas footprint of burning natural gas far exceeds that of the other hydrocarbons. At about 3% methane slip, the CO₂ savings from switching fuel from oil to gas are entirely negated, even when using the conservative GWP100.

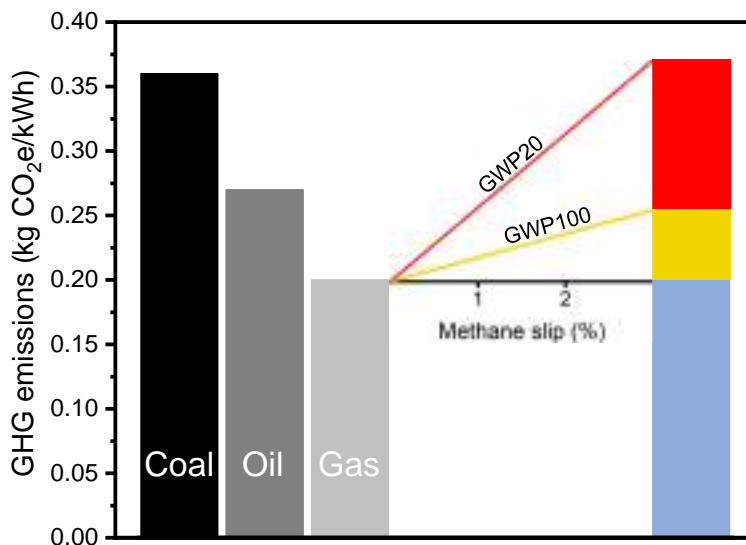


Figure 2 Comparison of the CO₂ equivalent greenhouse gas emissions of fossil energy sources when combusted for energy extraction. When taking methane slip into account, the emissions from natural gas increase significantly. Figure and analysis from Paper 1. Reprinted with permission from Mortensen et al.¹⁰ Copyright 2022 Wiley.

To realize the potential greenhouse gas savings of natural gas-fired engines, methane slip needs to be solved. A promising technology for emission control is catalytic complete methane oxidation. As with NO_x gasses emitted from high-temperature processes like combustion, methane can be removed from the exhaust through environmental catalysis, by converting the methane to carbon dioxide over a catalyst.¹¹ A catalyst is "a substance that increases the rate of a reaction without modifying the overall standard Gibbs energy change in the reaction", as defined by International Union of Pure and Applied Chemistry (IUPAC).¹² This means that a catalyst can enable chemical transformations that would otherwise be too slow or require too high temperatures for practical use. The reactants meet at the catalytic site, react, and leave the catalytic site as a newly formed product. Essential for the process is that the active site is returned to its original state in the end of the catalytic cycle, as illustrated in Figure 3.

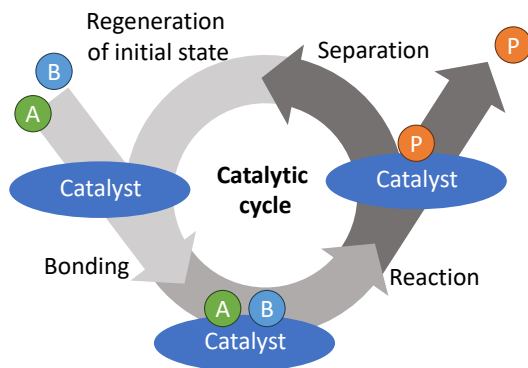


Figure 3 Illustration of a basic catalytic cycle. A catalyst is not consumed in the reaction, so it has to return to its initial state upon separation from the product. Inspired by similar figure from Chorkendorff and Niemantsverdriet.¹³

Environmental catalysts typically consist of catalytically active particles dispersed on a support material acting as a stabilizing carrier. The reactants and products are small-molecule gasses, meaning that the catalyst is heterogeneous from the perspective of the reactants. Homogeneous catalysts, e.g. dissolved molecules acting as catalysts for liquid-phase reactions, have limited relevance for emission control applications. Catalysts essentially allow for alternate reaction pathways with potentially lower energy barriers, measured as an activation energy. Since the rate constant k for a reaction depends on the size of the activation energy E_a , as described by the Arrhenius equation shown in Equation 1, catalysts can speed up reactions. R and T are the universal gas constant and temperature in Kelvin, respectively.

$$k = Ae^{\frac{-E_a}{RT}} \quad (1)$$

For a lot of applications however, the activity of the catalyst is not the primary concern. In many reaction environments, especially within environmental catalysis, the reactor conditions are very harsh. This can deactivate the catalyst, and since industrial catalysts often contain expensive precious metals, they need to maintain a certain lifetime to be profitable. A typical exhaust from an LNG-fueled large engine has a temperature of more than 400 °C, and contains 10% water and multiple pollutants which can render catalysts inactive in a short amount of time. Specifically, three distinct phenomena have stood in the way of the implementation of catalysts for complete oxidation of methane:

- The high temperature and water concentration of the exhaust drastically increases the mobility of surface species, causing sintering of active metal nanoparticles. The reduced surface area is directly proportional to the catalytic activity.
- Water in the exhaust interacts with the active sites which are initially saturated by hydroxyl

groups, lowering the activity. Over time, the activity decreases further for reasons that will be described in Section 6.

- Sulfur dioxide (SO_2), either from the natural gas or from combusted sulfur-containing lubricant oil, poisons the catalyst, causing deactivation as it accumulates over time.

1.1 Thesis scope

In this project, the aim is to develop durable catalysts for complete methane oxidation and to further the understanding of relevant deactivation phenomena. The aim of the thesis is to document and disseminate the project work.

Initially, the state-of-the-art will be presented with examples from scientific literature, and a short summary of how it has changed during five decades of catalytic methane oxidation. Alternative technologies will be explored, also those not relying on catalysis. Then, recent and promising developments within zeolite supported catalysts for complete methane oxidation will be covered.

The catalytic test setup built as part of the project will be described. It was designed and constructed taking into account both the shortcomings of catalytic experiments published in scientific literature and realistic conditions in the exhaust from an LNG-fueled large engine. The test setup was in many ways the foundation of the project and therefore required special attention to detail.

It will be attempted to synthesize durable catalysts for complete methane oxidation, able to withstand all three major deactivation phenomena at the same time, by employing a rational design approach based on previous achievements in scientific literature. The synthesized materials will be characterized by X-ray powder diffraction (XRD), transmission electron microscopy (TEM), N_2 -physisorption, hydrogen-temperature programmed reduction (H_2 -TPR), X-ray fluorescence (XRF), and inductively coupled plasma-optical emission spectroscopy (ICP-OES). Finally, the materials will be exposed to a series of catalytic tests to determine their potential for emission control.

Ion-exchange, i.e. replacing protons for alkali metal ions in zeolites, has been a go-to solution for increasing hydrophobicity and thereby water-tolerance of zeolite-supported methane oxidation catalysts (MOC). It will be shown that this approach can have a major drawback, which has so far not been addressed, namely that it significantly worsens the tolerance of the catalyst to SO_2 .

Finally, the least well understood deactivation pathway, direct water-induced deactivation, will be elucidated. Using low-cost but highly information-rich methods, it will be shown that deactivation by water is not purely a surface phenomenon, but involves the bulk palladium oxide as well. The dependence on relevant reaction parameters will be determined and a complete model for deactivation will be developed based on the measurements.

2 Background on complete methane oxidation

For a potentially explosive gas, methane is a surprisingly stable molecule with a C-H bond strength of 435 kJ/mol. This means that catalytic methane oxidation requires a highly efficient catalyst to operate at the temperatures in the exhaust from a natural gas-fired large engine, between 400 and 550 °C depending on engine load.¹⁴ For decades, realising a high activity at low temperature was the primary goal of methane oxidation catalyst development.^{15–17} A good example of a catalyst with exceptional methane oxidation activity under dry conditions is presented in the work by Cargnello et al. published in Science in 2012.¹⁸ The catalyst, which consisted of palladium encapsulated in cerium oxide anchored on an alumina support, managed to achieve a high conversion of methane at as little as 300 °C. About the same time, about 10 years ago, focus started shifting towards the deactivation observed in the catalysts when exposing them to more realistic conditions, i.e. including steam and SO₂ in the feed gas composition during catalytic testing. The deactivation of methane oxidation catalysts can be divided into three main topics:¹⁰

- Water-induced deactivation comes in two parts: Firstly, a quick and reversible interaction between gas-phase water and the active surface which causes a type of inhibition of the methane oxidation reaction, lowering the conversion rate while water is present in the feed gas. The degree of inhibition was shown by Keller et al. to depend on the water concentration.¹⁹ A key result from their publication is shown in Figure 4. Secondly, catalysts experience a type of time-dependent deactivation in the presence of water. The lost activity does not recover when water is no longer present, and if exposed for extended periods of time, the activity of the catalyst will go to zero. The two types of water-induced activity loss are the topic of Section 6 where they will be described further.
- SO₂ poisoning of methane oxidation catalysts has only received limited attention in literature compared to water-induced deactivation. Natural gas can be purified to contain essentially no sulfur-containing compounds, but combusted engine lubrication oils tend to produce small amounts SO₂ regardless, so some form of technical solution is necessary. SO₂ is a well-known poison for other emission control application, since many metals used for catalysis tend to form stable sulfates. The group of Mika Suvanto have done a significant amount of research into SO₂ deactivation of methane oxidation catalysts, on some specific topics which are highly relevant for the continued development. Most notably, they have shown how the PdSO₄ formed on the catalyst surface interacts with water,²⁰ and how an increased feed gas SO₂ concentration cannot be used for accelerated aging tests, as the stability of the formed sulfates depends on the SO₂ concentration.²¹
- Hydrothermal sintering describes the frequent observation that metal nanoparticles dispersed on a support surface have a tendency to agglomerate and grow when exposed to high temper-

atures, especially in the presence of steam.²² Since the exhaust from natural gas-fired engines contains very large amounts of steam, this is a highly relevant challenge for methane oxidation catalysts. However, as sintering is also an issue for other types of catalysts, a lot of research has been done on generalized means of prevention. In the context of this project, sintering was assessed to be the least critical mode of deactivation and was treated accordingly.

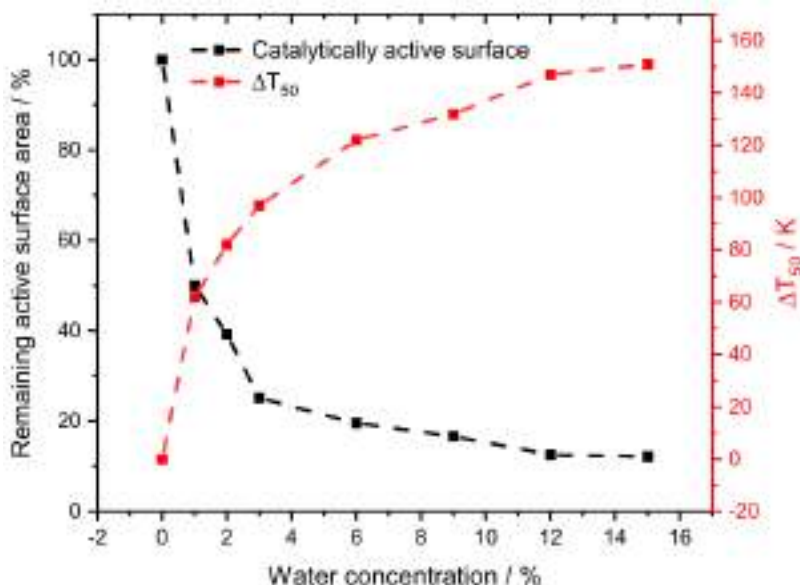


Figure 4 Relation between water concentration and extent of inhibition, compared with measurements of catalytically active surface area. The inhibition is defined as the difference between the T_{50} , the temperature at which conversion is exactly 50%, of light-off experiments with and without water. Reprinted with permission from Keller et al.¹⁹ Copyright 2020 MDPI.

Many types of catalysts have been developed for methane oxidation, but few seem to have made it to large scale tests in real exhausts, likely due to the deactivation challenges still persisting in laboratory experiments. The most notable catalyst is $\text{Pd}/\text{Al}_2\text{O}_3$, palladium oxide supported on aluminum oxide.^a Other promising catalysts have been developed, both with alternative active metals and with alternative support materials. The following sections will provide a brief overview of the various catalysts and present examples of competing emission control technologies not relying on catalysis to the same extent.

2.1 The state-of-the-art catalyst, $\text{Pd}/\text{Al}_2\text{O}_3$

In both materials oriented literature^{15,17,23–25} and reviews focusing more on processes and applications,^{16,26–30} palladium on aluminum oxide is and has always been the state-of-the-art catalyst for complete methane oxidation. The reason for this is the high activity of palladium and the ability of alumina to support and stabilize palladium nanoparticles. From a synthesis point of view,

^aThe convention is to write Pd instead of PdO when naming the catalyst, and to report the palladium content in terms of Pd wt% instead of PdO wt%, despite complete agreement about the active phase being the oxide.

Pd/Al₂O₃ is a relatively simple material, typically prepared by impregnation of an aqueous solution of pd precursor on high surface area γ -Al₂O₃.^{31–36} For this reason, it is also an attractive material in terms of large scale production compared catalysts produced with more advanced methods. Being the state-of-the-art catalyst, Pd/Al₂O₃ is frequently included in catalytic studies as a reference material.^{32,37–39} Indeed, in the water deactivation project in Section 6 of this thesis, a Pd/Al₂O₃ catalyst is also used as a representative methane oxidation catalyst.

Some support materials have a rather passive role in the catalytic action, but the alumina support of Pd/Al₂O₃ methane oxidation catalysts interacts with both water and sulfur dioxide present in the exhaust.^{40–45} In a very well-cited publication, Lampert et al.⁴⁶ show that the alumina support is able to scavenge SO₂ from the gas phase, forming aluminum sulfates and temporarily protecting the active palladium through a kind of sacrificial action. A key experiment from their article is shown in Figure 5. The shielding effect of sulfating supports is referenced frequently in methane oxidation literature, but it is arguable not very useful as the palladium will eventually be deactivated when the support is saturated. In the same manner, Huang et al. showed that the Al₂O₃ support can bind water and cause artificially high activities in catalytic testing.⁴⁵ In experiments both with H₂O and SO₂ adsorbing on alumina, they have been observed to spill over to the palladium oxide, further complicating practical use of the support to protect the active phase.^{21,46–48}

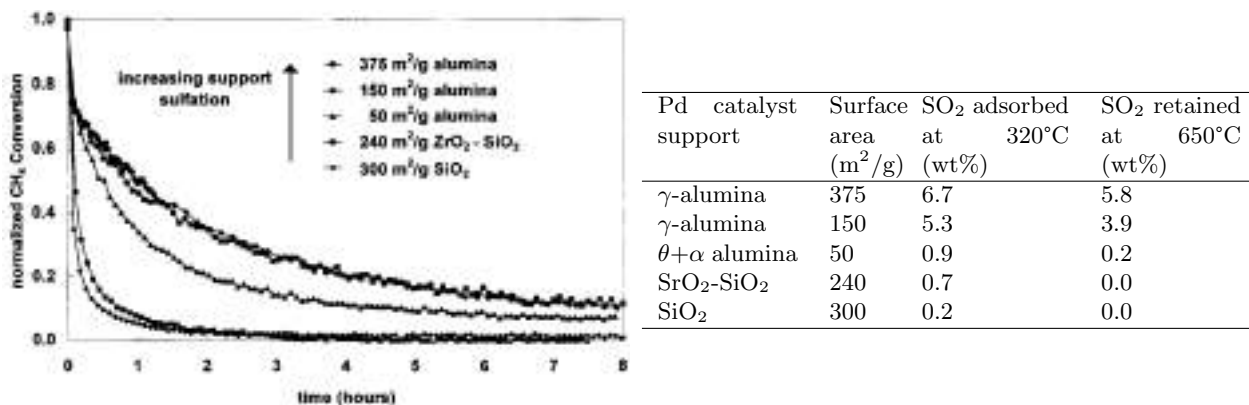


Figure 5 Left: Deactivation curves of monolithic catalysts (115 g/ft³ Pd, 400 cpsi) supported on different metal oxides, normalized to their respective initial activity. The catalysts supported on sulfating Al₂O₃ deactivate the slowest. Reaction conditions: 800 ppm CH₄, 8% O₂, 0.9 ppm SO₂, N₂ balance, 320 °C, 200 000 h⁻¹. Right: Adsorption of SO₂ at 320 °C and retained SO₂ at 650 °C. Both adsorption and desorption experiments were performed as a thermogravimetric analysis (TGA), in 2% SO₂ in air and pure air, respectively. Reprinted with permission from Lampert et al.⁴⁶ Copyright 1997 Elsevier.

Mobility of palladium species on the alumina surface is a topic which has attracted significant attention, primarily concerning the prevention of hydrothermal sintering.^{28,39,49–51} Recently however, Goodman et al.⁴⁹ showed that another type of deactivation, in which the palladium oxide is also redistributed, could be relevant for methane oxidation catalyst. At low metal loadings, in a mate-

rial synthesized via pre-forming of colloidal Pd nanoparticles distributed evenly on a γ -Al₂O₃, the authors show that the particles decompose to inactive single atoms at high temperature. Figure 6 shows the catalytic test of three samples with different metal loadings (particle densities) and an illustration of the hypothesized mechanism. The aging treatment entails 60 minutes at 775 °C in a dry gas consisting on 4% O₂ in Ar. The aging treatment is arguably not representative of realistic methane oxidation conditions, but the result is interesting and relevant none the less.

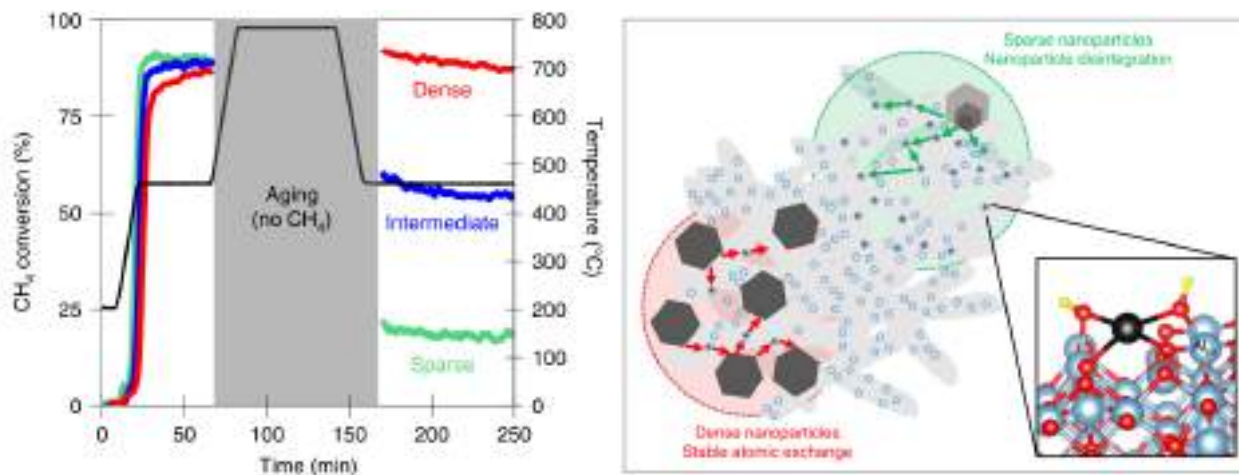


Figure 6 Left: Catalytic test of Pd/Al₂O₃ samples with different nanoparticle loadings. Reaction conditions: 0.5% CH₄, 4% O₂, Ar balance. Aging consisted of removing methane from the feed gas and heating to 775 °C for 1 hour. Right: Illustration describing the authors’ hypothesis for the observed deactivation. For both high and low particle loadings, the elevated temperature drastically increases the mobility of palladium. In the case of a densely populated surface, the palladium simply exchanges between the particles. On the sparsely populated surface, the particles disintegrate and the palladium forms single atom sites. The hypothesis is supported by a series of high-angle annular dark-field scanning transmission electron microscope (HAADF-STEM) images showing how the change of particle distribution depends on the initial particle loading. Reprinted with permission from Goodman et al.⁴⁹ Copyright 2019 Springer.

The activity loss caused by both water-induced deactivation and SO₂ poisoning can be regenerated by exposing the catalyst to a reducing atmosphere for a short amount of time, typically by shutting off oxygen at reaction temperatures in a so called rich pulse.^{40,42,52–54} This reduces palladium oxide to metallic palladium, removing sulfates and hydroxyl groups, and restoring the particles to their active state upon reintroduction of oxygen through reoxidation. SO₂ poisoning can also be regenerated thermally, by elevating the temperature above the decomposition temperature of the relevant metal sulfates.^{40,41,47} However, as simple as regeneration is in a laboratory setting with precise control over the feed gas composition, as difficult is it to realize in a real exhaust from a large natural gas-fueled engine. Shutting off oxygen or drastically elevating the exhaust temperature requires complex equipment and can have a wide range of consequences for engine control.^{29,55} Further, regeneration has been shown to speed up sintering, due to the increased mobility of metallic palladium.⁵⁶ It has been attempted to improve the tolerance towards both

water and sulfur dioxide of Pd/Al₂O₃ catalysts by introducing various promoters. As an example, catalysts with a small amount of platinum have been shown to deactivate less when exposed to both water^{43,44,47} and SO₂.^{41,46,47}

2.2 Palladium-based catalysts on alternative supports

Palladium being much superior to the alternatives can make optimization of the active metal nanoparticles a complex challenge. Possibly for that reason, a significant portion of catalyst research has revolved around the support material instead. Indeed, metal-support interactions are a very frequently discussed topic in methane oxidation literature.^{18,57–61} Palladium supported on various mixed metal oxides with either spinel or perovskite structure has received significant attention.^{62–76} The scope of the research seems to be centered around low temperature activity and not prevention of deactivation.

A support which seems to hold more potential for realizing a durable catalyst for complete methane oxidation is cerium oxide, the development of which has been covered in several dedicated reviews.^{77–79} Especially the combination of palladium and cerium oxide supported on alumina has resulted in promising performance,^{18,80–82} explained by the unique redox properties of cerium oxide providing increased oxygen exchange, indirectly participating in the methane oxidation reactions. The approach of using the support to tailor the catalytic properties of the active palladium nanoparticles was a key element of the material synthesis effort in the PhD project, which will be covered in Section 4. In the most recent decade, zeolites have attracted attention as support material for methane oxidation catalysts.^{10,83,84} This novel branch of methane oxidation catalysts was covered in Paper 1, shown in Section 2.5.

2.3 Precious metal-free methane oxidation catalysts

An radically different approach to methane oxidation for emission is catalysts where the active particles are made of base metals instead of palladium, most often cobalt or nickel. These metals, which in the periodic table are just above rhodium and palladium, respectively, share a lot of properties with their precious metal neighbors in terms of catalysis due to the similar electron structures. Their activity for complete oxidation of methane is significantly lower however, so the concept and business case relies on a few critical parameters:^{85–87}

- The availability of base metals is much higher than for precious metals, hence their names. Cobalt is almost 1000 times cheaper than palladium, meaning that the lower activity can to some extent be offset by simply adding more catalyst volume.
- The lower activity of the base metal catalysts can also be partially offset by a higher exhaust temperature. This can be achieved by positioning the catalyst upstream of the turbocharger

(TC), which would increase the temperature from about 450 °C to about 600 °C and the pressure from 1 to about 4 bar.^{14,55} A pre-TC position would likely prevent an increase in catalyst volume due to limited space however.

- Laboratory scale experiments have shown that some base-metal catalysts have good tolerance towards water and SO₂,^{88–91} the main obstacle for palladium-based catalysts. This defining feature needs more evidence however, as a lot of base metal catalysts suffer the same severe deactivation when exposed to e.g. water.^{92–94}

There is a significant overlap in literature between catalyst development for stationary emission control, emission control of heavy-duty LNG vehicles, and catalytic combustion.^{85–87,95–98} This is true for base metal catalysts especially, due to the higher operating temperatures in the other applications. The catalysts and conditions for the different applications are similar enough however that they can arguably be compared as equals. The promising work on water and SO₂ tolerant base metal catalysts can best be described as preliminary results, and it is rarely compared to a Pd/Al₂O₃ reference catalyst. In a recent study however, Caravaggio et al.⁹⁹ performed a well-thought-out experiment comparing a nickel-magnesium mixed oxide catalyst with a Pd/Al₂O₃ reference over multiple hours of methane oxidation in the presence of 10% water, shown in Figure 7.

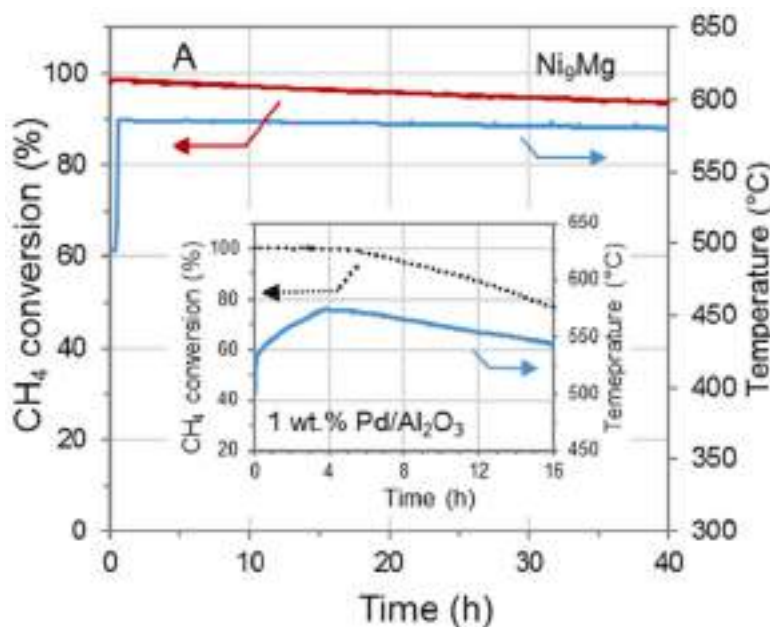


Figure 7 Catalytic test of mixed metal oxide catalyst in the presence of water, compared to Pd/Al₂O₃ reference catalyst. Reaction conditions: 1% CH₄, 10% O₂, 10% H₂O, 6% CO₂, N₂ balance, WHSV = 60 000 ml h⁻¹ g⁻¹. Reprinted with permission from Caravaggio et al.⁹⁹ Copyright 2021 Elsevier.

The tolerance towards water of the mixed metal oxide catalyst seemed good, but the temperature in the reference experiment was not stable and the conversion started at 100%, making it difficult

to conclude from. The concept of the experiment was exemplary though, and it is exactly that kind of thorough, long duration catalytic testing which should be used in the study of deactivation. This is further discussed in Section 6.8.

2.4 Non-catalytic alternatives and exotic oxidants

Returning to the origin of the methane slip challenge, marine engines have been optimized for efficiency over many generations. Higher efficiency often translates to smaller methane slip, as less wasted fuel means more delivered energy. However, engines which can run on LNG can still be optimized further in terms of lowering methane emissions.^{100,101} These modifications are especially relevant if they can be easily installed on existing engines, due to LNG mostly being viewed as a transitory fuel. The most widely used LNG-fueled engine for marine propulsion is a so-called low-pressure dual-fuel (LPDF) engine. More efficient, and expensive, alternatives exist however. The engine manufacturer MAN has developed a two-stroke high-pressure dual-fuel (HPDF) engine which is claimed to emit as little as 0.2–0.3 grams CH_4/kWh ,¹⁰² equivalent to an average of 20 grams $\text{CO}_2\text{e}/\text{kWh}$ using the 20-year global warming potential ($\text{GWP}_{20} = 81.2$) of methane. This corresponds to a methane slip of 0.35%, drastically lower than the almost 8% slip of the cheaper 4-stroke LPDF engines which currently dominate the market.¹⁰³ However, the roughly 175 ppm methane emitted by the new engines still increase the greenhouse gas emission of the engine by 10% compared to zero methane slip.¹⁰ This difference represents approximately one third of the CO_2 savings offered by changing from diesel oil to LNG, not accounting for the significant losses associated with transport and storage of natural gas.¹⁰⁴ A catalyst would therefore likely still be necessary in case strict methane regulation is put in place. The new engines also face a challenge concerning user adoption, as LNG is predominantly viewed as a transitory fuel to be replaced by E-fuels as soon as they are ready. Indeed, according to The International Council on Clean Transportation (ICCT), the market share of the efficient HPDF engines will shrink towards 2030 while the market share for the less efficient LPDF engines will grow.¹⁰³ Large investments in efficient LNG engines are therefore not a given, but that discussion is outside the scope of this thesis.

Alternative emission control technologies, that do not rely on catalysts, are also being developed. An example of this is the plasma reduction system developed by Daphne Technology under the product name SlipPure.¹⁰⁵ Using about 4% of the total engine output as electricity, a non-thermal electron plasma is generated which interacts with the exhaust, forming hydroxyl radicals which oxidize the methane to carbon monoxide and water.¹⁰⁶ The ability to remove methane emissions from the exhaust have been demonstrated on laboratory scale, and scale-up efforts are supposedly underway. The technology is not as temperature reliant as catalytic methane oxidation, which requires a high exhaust temperature to function, but the envisioned emission control system is both complex and reduces the efficiency of the engine,¹⁰⁶ minimizing the advantage of switching from

diesel to LNG.

Finally, a niche branch of catalyst development revolves around the use of more reactive oxidizers, in many cases ozone.^{107–111} The concept works by using an electric ozone generator to add an amount of ozone to the hot exhaust upstream of the methane oxidation catalyst layer. The reaction with ozone has a lower activation energy than the traditional reaction between methane and molecular oxygen.¹⁰⁸ This hypothetically lowers the demands on the catalyst in terms of activity, but very little research has been done on how this approach influences catalyst deactivation, so it is questionable if the technology can be fully developed before LNG is replaced by E-fuels.

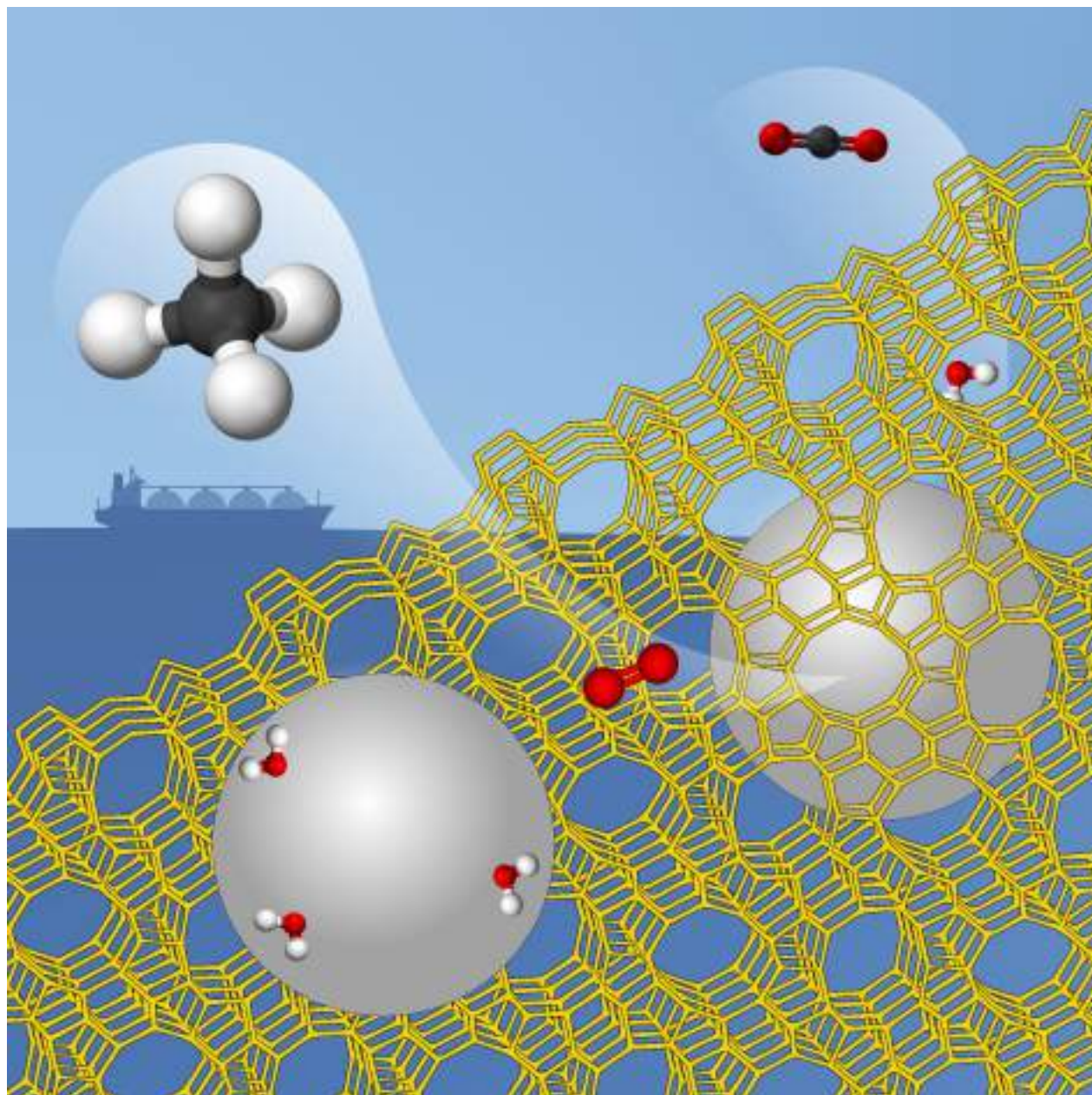
2.5 Zeolite-based catalysts for complete methane oxidation (Paper 1)

Despite the exotic alternatives, a durable catalyst based on palladium is likely the most feasible way of dealing with methane slip due to its innate advantage of being retrofittable in the exhaust of existing engines. After decades of research on the state-of-the-art Pd/Al₂O₃ catalyst, a new class of catalysts emerged around 2015 and quickly attracted attention from both industry and academia. In the following years, many interesting findings concerning zeolite-based methane oxidation catalysts were published in scientific literature, which has been covered in Paper 1, presented on the following pages.



Recent Advances in Complete Methane Oxidation using Zeolite-Supported Metal Nanoparticle Catalysts

Rasmus Lykke Mortensen,^[a, b] Hendrik-David Noack,^[b] Kim Pedersen,^[b] Susanne Mossin,^[a] and Jerrik Mielby^{*[a]}



The high fuel efficiency of natural gas makes it an attractive alternative to coal and oil during the transition towards renewable energy resources. Natural gas engines are needed to ensure a stable power grid that can accommodate fluctuations in renewable energy production. Unfortunately, these engines emit as much as 3–4% of the methane (CH_4) in the natural gas under lean-burn conditions. This methane slip has a high environmental cost since CH_4 is a potent greenhouse gas. Complete catalytic oxidation of CH_4 can potentially control the emission. Unfortunately, the best performing $\text{Pd}/\text{Al}_2\text{O}_3$ catalysts suffer from severe deactivation under operating conditions.

After decades of little progress, zeolite-supported catalysts have recently attracted increased attention. Here, we review the current status, challenges, and prospects for controlling methane emissions from large engines using zeolite-based catalysts. The determining factors for catalytic activity and stability are the zeolite topology, alumina content, counter-ion, and active metal nanoparticles incorporation. In addition, we highlight the importance of testing under realistic operation conditions. Thus, the review provides a framework for developing a catalyst technology critically needed to fulfill the Paris Climate Agreement.

Introduction

Despite making up less than 2 ppm of the atmosphere, methane is responsible for at least one-sixth of the total radiative forcing,^[1,2] a measure of the greenhouse gas (GHG) effect causing global warming. Therefore, the United Nations Environment Programme director recently stated that “Cutting methane emissions is the best way to slow down climate changes over the next 25 years.”^[3] A significant source of anthropogenic methane originates from large stationary natural gas engines used for power production and maritime applications. This methane slip occurs when a part of the natural gas hides in small so-called dead volumes of the engine and leaves the combustion chamber unburned.^[4] Unfortunately, the methane slip is currently emitted into the atmosphere because there are no regulations on methane emissions and no practical solutions to remove it from the highly diluted exhaust gas.^[5,6]

The most promising technology to control methane emissions is to pass the exhaust gas over a catalyst and convert the remaining CH_4 into CO_2 by complete oxidation. Although CO_2 is another well-known greenhouse gas, it is far less potent than methane. For comparison, methane’s 100 year global warming potential is around 28 times higher than CO_2 ($\text{GWP}_{100} = 27.9$), and on a 20 year term, its GWP is even higher ($\text{GWP}_{20} = 81.2$).^[1,7] These values are discussed in the most recent report from the Intergovernmental Panel on Climate Change (IPCC), which also emphasized the alarming consequences of the accelerating methane emissions.^[8] Table S1 in the

supporting information summarises methane’s relative environmental impact.

Figure 1 shows how the high energy-to-carbon ratio of natural gas results in lower CO_2 equivalent emissions than coal and oil. Unfortunately, the figure also shows how an untreated methane slip significantly increases the relative environmental impact. Considering the high energy demand and the projected increase in natural gas production, this underlines the critical need for an effective technology to control methane emissions.

Although methane has a high standard enthalpy of combustion ($\Delta H_c = -891 \text{ kJ/mol}$), the high C–H bond energy (435 kJ/mol) in the stable CH_4 molecule kinetically hinders the reaction. Therefore, complete methane oxidation requires an efficient catalyst that can lower the activation energy and allow the reaction to occur at reasonable temperatures, typically below $< 500 \text{ }^\circ\text{C}$. Unfortunately, the catalyst still has to operate under demanding conditions in the presence of both sulfur-containing compounds from the fuel and large amounts of steam from the combustion process. These conditions cause fast and severe deactivation, which prevents commercial applications.

After decades of little progress in complete methane oxidation, new advances in the use of zeolite-encapsulated metal nanoparticles have recently attracted increasing atten-

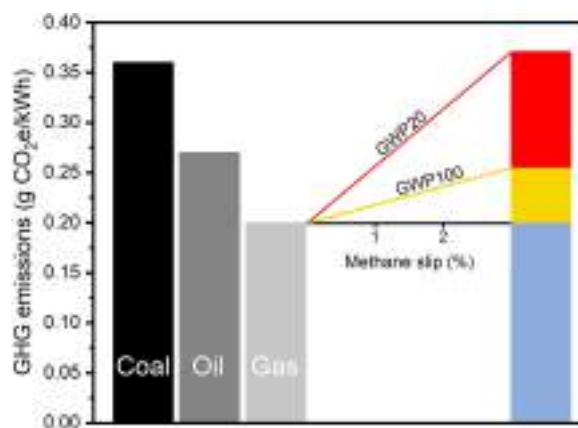


Figure 1. Impact of 0–3% methane slip on the total GHG emissions (in CO_2 equivalents) of large natural gas-fired engines compared to coal and oil on a 20 and 100 year perspective, respectively.

[a] R. L. Mortensen, Prof. S. Mossin, Dr. J. Mielby
DTU Chemistry
Technical University of Denmark
Kemitorvet 207
DK-2800 Kgs. Lyngby (Denmark)
E-mail: jjmie@kemi.dtu.dk

[b] R. L. Mortensen, H.-D. Noack, Dr. K. Pedersen
Umicore Denmark Aps
Kogle Allé 1
DK-2970 Hørsholm (Denmark)

Supporting information for this article is available on the WWW under <https://doi.org/10.1002/cctc.202101924>

This publication is part of the Catalysis Talents Special Collection. Please check the ChemCatChem homepage for more articles in the collection.

© 2022 The Authors. ChemCatChem published by Wiley-VCH GmbH. This is an open access article under the terms of the Creative Commons Attribution License, which permits use, distribution and reproduction in any medium, provided the original work is properly cited.

tion. These advances are not only relevant for the specific application of stationary methane emission control but also for a range of related applications, including 1) compressed natural gas-fueled lean-burn vehicles such as cars, busses, and trucks, which belong to the area of automotive catalysis but deal with many of the same challenges as stationary engines,^[9,10] 2) catalytic combustion as a low-temperature method for extracting energy from natural gas without producing NO_x,^[11–13] 3) oxidation of ventilation air methane (VAM) for cleaning the emissions from coal mines,^[14–16] and 4) flue gas oxygen removal as a means of CO₂ purification.^[17] Despite some differences in feed gas compositions, these applications have many similarities, aiming to mitigate emissions or recover energy. In this review, we have therefore treated these applications together. Table 1 shows the typical differences in the realistic feed gas compositions of the different applications.

Palladium-based catalysts are by far the most investigated catalysts for complete methane oxidation. The palladium is sometimes mixed with platinum and typically dispersed on various high-surface-area metal oxide supports. Specifically, Pd/Al₂O₃ has attracted much attention over the years.^[11,12,20–22] Figure 2 illustrates a typical Mars-van Krevelen mechanism on Pd/Al₂O₃ accompanied by the three most common types of deactivation.^[23–25] Although several excellent reviews have covered most of the recent literature on methane oxidation,^[20,22] the recent advances in zeolite-based systems have not been covered as extensively. P. Gélin and M. Primet thoroughly

reviewed the work done with zeolites for complete methane oxidation until 2002. Still, they mainly focused on the light-off temperatures like most other work on metal oxide-based methane oxidation catalysts (MOCs).^[11]

Several prominent researchers have pointed out the lack of real progress in the field,^[26,27] and it is clear that methane oxidation catalysts still suffer from the same challenges with deactivation as 30 years ago.^[22] Zeolites offer several significant advantages over alumina for methane oxidation to prevent hydrothermal deactivation,^[28,29] and Jackson et al.^[11] even suggested that zeolite-based methane oxidation catalysts may even find applications as a means of atmospheric restoration.

Recently, another possibly game-changing development has occurred. Several researchers have suggested moving the catalyst upstream and installing it before the turbocharger.^[30,31] This increases the reactor temperature by roughly 150 °C and the pressure by 2–3 bar. The higher temperature not only reduces the need for low-temperature activity but may also reduce the chemical deactivation caused by water, which is particularly severe below 450 °C. This transition could favor zeolite-based technologies because of their unique ability to encapsulate metal nanoparticles as a means to prevent thermal-induced sintering.^[32–34]

With the increasing attention from industry,^[35] and regulators,^[5] and the development to focus more on the stability than the light-off temperatures, the recent advances in complete methane oxidation indicate that a breakthrough in



Rasmus Mortensen obtained his Master's degree in Applied Chemistry from the Technical University of Denmark in 2019. He then joined Umicore Denmark ApS to pursue an Industrial PhD in Chemistry in collaboration with the Technical University of Denmark. He is engaged in the development of durable catalysts for complete methane oxidation. His research focuses on elucidating and preventing deactivation under realistic testing conditions.



Hendrik-David Noack is holding a Diploma in Mechanical Engineering from the Berlin School of Economics and Law (2003) and a Master of Engineering degree in Automotive Technology from the Ostfalia University of Applied Sciences (2015). He has worked for Umicore since 2003 focusing on exhaust after-treatment systems for diesel passenger cars. Lately he joined the R&D team of Umicore's Stationary Emission Control Catalysis division developing catalysts for methane oxidation, large diesel engines and alternative fuels in the marine industry.



Kim Hougaard Pedersen received his PhD in Chemical Engineering from the Technical University of Denmark in 2008. His career has since then focused on emission control from industry sources including marine and in 2017 he joined Umicore as head of global R&D for stationary emission control. Here he works with developing and industrializing catalytic technologies that can be part of the solution toward more sustainable shipping and energy generation.



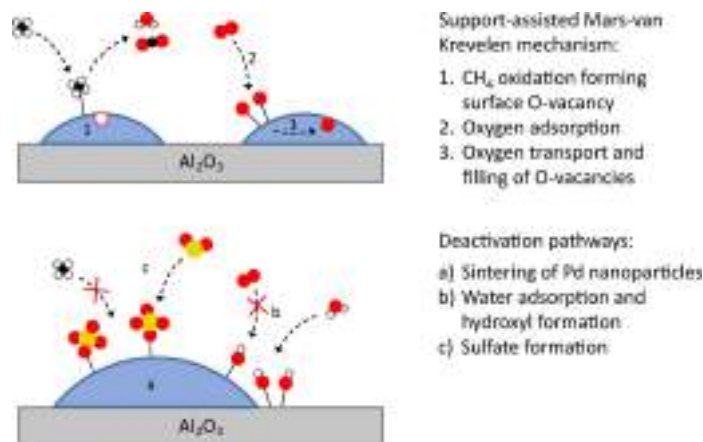
Susanne Mossin received her PhD from University of Copenhagen in 2006. After a post-doc at Friedrich-Alexander University of Erlangen-Nuremberg she started her independent research at the Technical University of Denmark in 2009. She is working with in-situ and operando spectroscopy of heterogeneous catalysts for emission control and spectroscopic, electronic and magnetic properties of inorganic materials including metal containing zeolites.



Jerrik Mielby received his PhD from the Technical University of Denmark in 2014 and is currently a Senior Researcher at DTU Chemistry. His research focuses on the design of advanced nanostructured catalysts for C1-chemistry and he has published several papers and patents on the synthesis and application of zeolite-encapsulated metal nanoparticles.

Table 1. Typical feed gas compositions for various applications that involve complete methane oxidation.

Application	CH ₄ [%]	O ₂ [%]	H ₂ O [%]	CO ₂ [%]	Other pollutants	Heat source
Lean-burn emission control ^[18,19]	0.1	10	10	5	1–10 ppm SO ₂	Exhaust
Catalytic combustion ^[11–13,20]	3	20	None	None	H ₂ S	Self-heated
VAM oxidation ^[14–16]	1	20	2	None	H ₂ S	Self-heated
CO ₂ purification ^[17]	1.5	3	None	85.5	H ₂ S	Exhaust

**Figure 2.** Working principle and deactivation of a typical Pd/Al₂O₃ catalyst for complete methane oxidation.

the field is not only imminent, it is happening right now. This review focuses on zeolite-based catalysts for complete methane oxidation in stationary emission control and summarizes the most significant results published since 2015. We explain why zeolites are promising support materials and look ahead to determine where further improvements are still required. Finally, we suggest a guideline for future research that highlights the importance of testing under realistic operation conditions.

Deactivation of Methane Oxidation Catalysts

The main challenge that prevents the practical implementation of methane oxidation catalysts in large natural gas-fired engines is the catalytic deactivation caused by the demanding reaction conditions and the exhaust gas composition. Although the exact pathways and mechanisms of deactivation are still not fully understood, three main challenges contribute to the problem. These challenges are illustrated in Figure 2 and described in further detail below.

Deactivation by Water

In general, there are two types of direct steam-induced deactivation: 1) A fast and reversible deactivation by molecular adsorption causing site blocking and 2) a slower formation of more stable hydroxyl groups on the catalyst surface.^[18,36,37] The hydroxyl groups can form on both the active metal and on the

surface of the support material, in the latter case preventing oxygen uptake and hindering efficient methane oxidation by the Mars-van Krevelen mechanism.^[24,28,38] Li et al.^[10] recently published a comprehensive study of the hydroxyl formation phenomenon in which they used ambient pressure X-ray photoelectron spectroscopy (APXPS). These studies showed how water causes two simultaneous effects on the palladium surface: 1) The formation of palladium hydroxyls block the coordinatively unsaturated sites for methane adsorption and adjacent oxidic sites for methane activation, and 2) the hydroxyls prevent oxygen vacancies being filled by bulk migration. The fast type of steam-induced deactivation is a simple adsorption phenomenon in the vicinity of active sites that reversibly raises the T₅₀ by around 40–150 °C depending on the water concentration.^[27,39,40] More than two decades ago, van Giezen et al. studied the kinetics of water inhibition on alumina-supported Pd catalysts.^[41] The authors determined the reaction order of water to be negative, with a value of around –0.8 over the relevant temperature range. Methane was found to have a reaction order of 0.9–1, and oxygen was found to have a reaction order close to zero. More recent studies using zeolite supports reported similar values.^[27,42,43] The kinetics of complete methane oxidation has received much attention in the literature^[11,24,44–46] but is outside the scope of this review and will not be discussed in further details here.

In 2017, Sadokhina et al.^[36] described a complete water deactivation model by coupling adsorption with hydroxyl formation. Generally, the two types of direct water deactivation are more problematic below 450 °C. Hydrothermal sintering becomes a severe threat to catalyst stability at higher

temperatures.^[28,47] Huang et al.^[48] highlighted the consequences of not accounting for transient water effects in light-off experiments. Essentially, the authors showed that running some types of catalytic experiments without the addition of water will result in artificially high activity since the reactor diluent may adsorb the water produced by the reaction. For a short duration, the diluent will therefore maintain an almost water-free environment around the active sites. Later, the same authors expanded on this work by suggesting the addition of more diluent to maintain highly active and water-free active states for a longer time.^[49] The authors also noted that such an approach would rely heavily on regeneration cycles to remove adsorbed water from the diluent. In a lean-burn natural gas-fired engine, about 10–12% of the exhaust gas is water vapor from the combustion of methane. However, it is not uncommon to see work published where less than 5% of the feed stream is water,^[27] probably due to instrumental limitations. Importantly, Zhang et al.^[39] investigated the effect of water concentrations between 0 and 15% and showed that water deactivation still intensifies beyond 5% water in the feed. Recently, Wang et al.^[50] showed the significant difference in catalyst deactivation caused by 4.5% and 10% water. Considering the possible effect of steam on zeolites, Hosseiniamoli et al.^[14] pointed out that water can damage acidic zeolites through dealumination at high temperatures.^[51–54] Most recent work with zeolites for methane oxidation applies either very high Si/Al values or ion-exchange of protons with Na⁺, where dealumination is less prone to occur. The detailed scientific literature on this steam-assisted dealumination seems to lack, and more thorough studies on the structural integrity of zeolite supports during long-term operation under realistic operation conditions would therefore be highly relevant for the field of complete methane oxidation.

Deactivation by Sintering

Like other metal catalysts, supported palladium are also prone to sintering, a thermal deactivation caused by irreversible Ostwald ripening or particle migration.^[55] In general, it is sometimes possible to improve the thermal stability by tuning the catalyst composition and metal-support interaction or supporting the active nanoparticles in ordered mesoporous or core-shell materials. A more recent strategy is to encapsulate the active metal nanoparticles inside the framework of a microporous zeolite.^[56] As previously mentioned, hydrothermal sintering becomes relevant at the temperature where the typical issues with hydroxyl formation decrease.^[47] However, it may be difficult to distinguish the effects of the two types of deactivation at intermediate temperatures from activity measurements alone. In this case, transmission electron microscopy (TEM) may be used to resolve the cause of deactivation.^[15,18] The presence of steam increases the mobility of PdO, which significantly accelerates the sintering of Pd-containing particles.^[14,27,28] Concerning the Si/Al of the zeolite, there are some discrepancies in the literature. Some researchers suggest that the acidic sites related to Al in the zeolite accelerate

sintering,^[27,29,37] whereas others suggest they prevent sintering.^[13,14,57–59] The arguments for accelerated sintering generally refer to the increased mobility of palladium oxide on zeolites with a low Si/Al value (i.e. a zeolite with a high Al content), while the arguments for increased stability refer to stronger metal-support interactions. We will discuss this topic in more detail later in the review.

Deactivation by SO₂ Poisoning

Natural gas contains a small amount of sulfur-containing compounds, such as H₂S. During combustion, the sulfur compounds oxidize to SO₂, a well-known poison to many noble metal catalysts. In general, natural gas contains significantly less sulfur than e.g. fuel oil.^[5] However, the lubricants used for large engines also contain sulfur, which eventually ends up as SO₂ in the exhaust. Realistic values for SO₂ concentrations are on the order of 1 ppm. Alternatively, it is possible to decrease this value by installing various sorbent materials in a guard bed before the MOC reactor. While such efforts may significantly reduce the SO₂ concentration, they cannot remove all contaminants.

The deactivation of methane oxidation catalysts by SO₂ is still not fully understood, but recently several authors have started to address this issue in more detail. Essentially, the active metal oxidizes SO₂ to SO₃, which quickly forms sulfates on the surface of the catalysts. The formation of sulfates may block the active site but also have consequences related to the support material. On sulfate-forming materials, such as Al₂O₃, the formation of aluminum sulfates may delay the deactivation of the active metal. Unfortunately, these sulfates may spill over from the support and slow down regeneration efforts.^[60] For comparison, non-sulfate forming supports, such as SiO₂, typically deactivate faster but regenerate more efficiently.

To achieve the lowest possible light-off temperature, many research groups have tested their catalysts under dry and SO₂-free conditions. Realistically, however, deactivation by SO₂ remains one of the most significant challenges preventing the practical implementation of MOC systems. Several studies have tested the catalytic activity at relatively high SO₂ concentrations to shorten experiments. For investigation of deactivation, however, Auvinen et al.^[19] argued that this may not be a representative approach since sulfates formed at higher SO₂ concentrations are less stable than those formed at low concentrations. Furthermore, Zhang et al.^[33] showed that high concentrations of SO₂ do not necessarily result in faster or more severe deactivation.

The thermal stability of the relevant sulfates plays an essential role, and as with water deactivation, SO₂ poisoning is strongly temperature-dependent.^[33] Zhang et al. recently described the deactivation as a fully reversible surface coverage phenomenon where, as soon as the coverage equilibrium has settled, the activity stabilizes at a lower level.^[32] For palladium-based catalysts, this level of stabilization happens at such a low activity that it essentially means complete deactivation. Zhang et al.^[32] investigated a rhodium-based catalyst with a notable

tolerance for SO_2 and some remaining activity upon stabilization. The authors argued that the degree of deactivation at equilibrium coverage likely depends on the decomposition temperature of the specific sulfates involved. RhSO_4 decomposes at a lower temperature than PdSO_4 and therefore remains active in a broader operation range with SO_2 present.^[32,61]

Suvanto et al.^[62] recently showed that the deactivation caused by SO_2 poisoning and water are interconnected, emphasizing the importance of having both species present during catalytic testing. The authors used density-functional theory (DFT) calculations to show that the $\text{PdSO}_4(111)$ surface strongly adsorbs water. Since this surface contains the unsaturated and catalytically active Pd sites, this water causes blocking and deactivation. The calculated energy barrier for methane oxidation on the sulfated surface was comparable to the clean Pd surface with no water present. With water present, however, the calculated energy barrier increased dramatically.

Zhang et al. draw the same conclusions from experiments with a set of Pd and Rh-based catalysts.^[33] Figure 3 shows the results of a light-off experiment in which a Rh/ZSM-5 catalyst achieves a conversion of 50 % at a temperature that is 50 °C less than Pd/ZSM-5 when both water and SO_2 is present, which may be explained by the lower decomposition temperature of RhSO_4 compared to PdSO_4 . Figure 4 shows the DFT model of water adsorbed on the unsaturated Pd atom of a clean PdSO_4 surface proposed by Suvanto et al.^[62]

Based on these results, it appears that the design of catalysts that form unstable sulfates or have hydrophobic environments that keep excess water from the active sites may be a reasonable strategy to achieve a high catalytic activity and stability.

Other Types of MOC Deactivation

In addition to the three main deactivation modes, Hosseini-moli et al.^[14] investigated spent catalysts by energy-dispersive X-ray spectroscopy (TEM-EDS) analysis and reported that some methane oxidation catalysts could suffer from the deposition of carbonaceous species. Although the combustion reaction occurs under strongly oxidizing conditions, the authors observed the presence of carbonaceous species on both Pd/ZSM-5 ($\text{Si}/\text{Al} = 140$)^[14] and Pd/silicalite-1 (no Al).^[15] To the best of our knowledge, these are the only reports on this phenomenon, although several groups have studied similar Pd/ZSM-5^[9,13,63] and Pd/silicalite-1 catalysts.^[39,50,64,65]

Friberg et al.^[18] investigated the resilience of zeolite-based catalysts towards NO and showed a small advantage compared to alumina supports. Very recently, Suvanto et al.^[66] also investigated the interaction between SO_2 and NOx ($x = 1$ or 2). Although a detailed discussion of the effect of NOx on methane oxidation catalysts is outside the scope of this review, we note that the feed composition of exhaust gas is complex and that many of the components have interconnected effects on the activity and stability of the catalyst. These effects emphasize the importance of testing under as realistic conditions as possible.

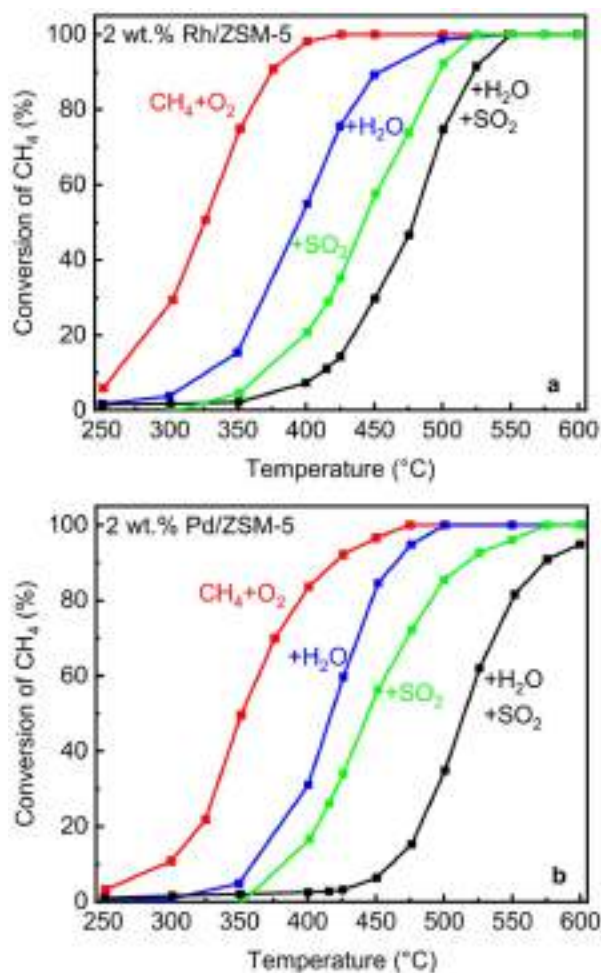


Figure 3. Top and bottom: Light-off experiments that show the effect of water and SO_2 on the catalytic activity of Pd and Rh supported on ZSM-5. Conditions: 2500 ppm CH_4 , 10 % O_2 , 5 % H_2O (if present), 20 ppm SO_2 (if present), balanced with N_2 . GHSV = 150,000 $\text{ml/g}_{\text{cat}} \text{h}^{-1}$. Reprinted with permission from Zhang et al.^[32] Copyright 2020, American Chemical Society.

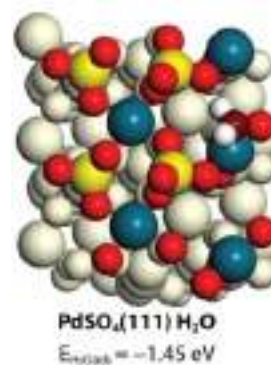


Figure 4. DFT model of a sulfated Pd surface with adsorbed water. The oxygens in H_2O and hydroxyl groups are dark red, while lattice oxygens are bright red. Palladium atoms are blue, and sulfur atoms are yellow. Reprinted with permission from Auvinen et al.^[62] Copyright 2019, American Chemical Society.

Methane Oxidation with Zeolite Supported Catalysts

The choice of support material is important for methane oxidation catalysts. Compared to conventional high-surface-area metal oxides, such as Al_2O_3 , microporous zeolites offer several advantages, including simple loading through ion-exchange,^[27] hydrophobic properties,^[18,39,50] encapsulation of the active nanoparticles,^[27,39,50,65,67,68] and high control of the structure and composition. For instance, Petrov et al. recently showed that complete removal of the acidic sites by post-exchange with Na^+ and confinement of the Pd nanoparticles within the zeolite resulted in a highly active and stable catalyst that resisted steam-induced sintering and zeolite degradation. Furthermore, the authors used operando X-ray absorption spectroscopy to investigate the catalyst's beneficial redox properties, characterized by a rapid Pd reduction and slow reoxidation. However, the non-reducible nature of zeolites may also entail some limitations. Pd is typically reduced more easily on zeolites than on Al_2O_3 ^[27,69] but has a lower initial activity under both dry and wet conditions.^[18,28] Despite some challenges with steaming and dealumination, recent work indicates that zeolite-based catalysts can also handle more water than $\text{Pd}/\text{Al}_2\text{O}_3$.^[58]

Zeolite encapsulated metal nanoparticles have recently attracted increasing attention for several processes, ranging from environmental remediation to renewable energy and biomass conversion.^[56,70,71] For many of the same reasons, zeolite encapsulated nanoparticles also hold great promise for complete methane oxidation.^[28] For instance, encapsulation typically results in a high dispersion of small and uniform metal nanoparticles. The inherent microporous framework allows the reacting gasses to diffuse to and from the active sites while keeping the encapsulated nanoparticles from sintering. Therefore, zeolite encapsulated nanoparticles are often stable at high temperatures.

Material Synthesis

The successful synthesis of zeolite encapsulated metal nanoparticles requires an efficient encapsulation strategy. Conventional preparation procedures, such as impregnation followed by calcination, typically cause the nanoparticles to end up on the external surface.^[14,32,57,72,73] For example, Fan et al.^[57] produced a Pd/ZSM-5 catalyst with active nanoparticles dispersed on the external zeolite by adding H-ZSM-5 ($\text{Si}/\text{Al} = 36$) into a solution of polyvinyl alcohol, H_2PdCl_4 , and NaBH_4 . After washing, drying, and calcination, the final material experienced significant sintering even under dry reaction conditions. Friberg et al.^[18,47] investigated the effect of Si/Al and prepared a series of catalysts by impregnation and calcination in air. Then, the authors used a degreening and pre-treatment procedure involving reduction under H_2 , high-temperature steaming, and reoxidation in air to redisperse the Pd. Although some particles appeared to enter the micropores, a significant amount of the metal, especially the large particles, remained on the external surface. Ryou et al.^[74–76]

used a similar hydrothermal treatment to disperse Pd nanoparticles in zeolite-based passive NO_x absorbers (PNAs).^[74–76] These methods exploit the high mobility of PdO on acidic zeolites under hydrothermal conditions. As previously mentioned, however, the same mobility may also cause steam-induced sintering during the reaction.

Ion-exchange is another method to prepare zeolite-supported methane oxidation catalysts.^[9,27,29,32,33,58] Typically, the zeolites are ion-exchanged with Pd^{2+} , dried, and then calcined at high temperatures to form well-dispersed nanoparticles of PdO. Although ion-exchanged Pd sites possess some activity, several studies showed that nanoparticles are more active for complete methane oxidation.^[18,37,73] As long as the solvated metal precursor is small enough to enter the microporous framework, ion-exchange is a simple and effective method to achieve well-dispersed inside the zeolite. After calcination, the metal nanoparticles are typically a little larger than the micropores. This size difference indicates that the zeolite has to form local defects to accommodate the metal nanoparticles.^[50,77–79] Lim et al.^[58] performed a thorough study of the effect of different framework types, Si/Al , and Pd loadings. Based on these studies, the authors suggested that the ion-exchange may reduce the total pore volume by partially blocking the micropores. Furthermore, their TEM analysis showed that the ion-exchange did not result in a complete encapsulation since Pd nanoparticles appeared both within and on the external surface of the zeolite supports. Consequently, the catalysts also suffered from deactivation by sintering. Recently, Petrov et al.^[29] ion-exchanged a mesoporous zeolite prepared by a mild desilication procedure. After calcination, the authors closed the mesopores in an additional crystallization step. This synthesis resulted in complete encapsulation that effectively prevented steam-induced sintering. To distinguish between supported and encapsulated metal nanoparticles, we will use the standard notation M/support if the metal is dispersed on the external surface and M@support if the metal is confined inside the support.

In 2016, Wang et al.^[80] reported another simple and effective method to encapsulate Pd metal nanoparticles inside an MFI zeolite. In this method, ethylenediamine is used as a ligand to form a stable Pd complex that prevents the metal from premature precipitation in the alkaline zeolite gel. Furthermore, the ethylenediamine complex interacts with the negatively charged silica species that traps the metal precursor during hydrothermal crystallization. Upon calcination, the complex decomposes to form highly dispersed metal oxide clusters inside the zeolite. Several research groups have adopted this synthesis procedure and showed that the encapsulated Pd nanoparticles are highly active for the complete oxidation of methane.^[16,39,50,65] Figure 5 shows a schematic illustration of the so-called *in situ* synthesis using ethylenediamine. The figure also shows how Wang et al. reduced their catalyst under H_2 in their original work. We note that this step may be skipped since PdO is the active phase for methane oxidation.

Interestingly, this Pd@zeolite catalyst has good stability against steam and high temperatures.^[39,50] Furthermore, Zhang

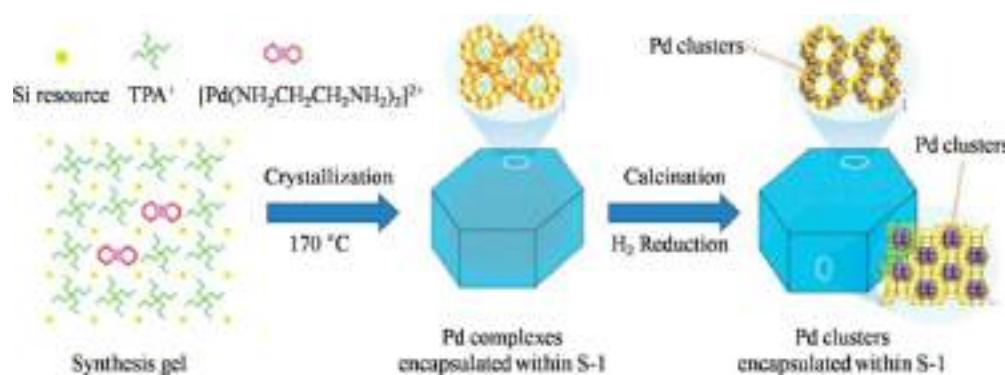


Figure 5. Schematic illustration of the synthesis of Pd@S-1 using ethylenediamine. Reprinted with permission from Wang et al.^[80] Copyright 2016, American Chemical Society.

et al. suggested that the tight confinement also improves the stability towards SO_2 .^[39] Niu et al.^[16] showed that the ethylenediamine synthesis resulted in significantly higher activity and stability than the corresponding catalysts prepared by impregnation under dry and sulfur-free conditions. Since this work dealt with the oxidation of 1% ventilation air methane, the author did not investigate the effect of adding more water to the feed.

Losch et al. dispersed preformed colloidal Pd nanoparticles on various mesoporous zeolites prepared by selective desilication.^[28,81,82] In this way, the authors achieved a high control over the particle size, which made their catalysts directly comparable and allowed them to investigate the catalytic effects of Si/Al and the hydrophobic properties.

Zeolite Type

So far, the zeolite topology does not seem to play the most important role in determining the catalytic activity of zeolite-based methane oxidation catalysts. Instead, other properties such as the Si/Al ratio, the nanoparticle distribution, the choice of counter-ions, and promoters are more critical. Although researchers have supported Pd nanoparticles on many different zeolite topologies, the most common ones are MOR, MFI (ZSM-5), FAU, BEA, and CHA (SSZ-13), respectively.

For example, Lim et al.^[58] tested four Pd-exchanged small-pore zeolites and compared their catalytic activity to Pd/ZSM-5 and Pd- Al_2O_3 . Despite some differences in the Si/Al ratios, Pd loadings, and particle size distributions, the study showed that the Pd-SSZ-13 catalyst resulted in the highest activity and stability under wet conditions (10% water). To explain these results, the authors suggested that the higher acidity of SSZ-13 compared to the other zeolites caused a stronger interaction with PdO, which suppressed both sintering and dealumination during the reaction.

Recently, Zhang et al.^[33,37] impregnated Rh on different ZSM-5 zeolites (Si/Al = 15–140) and compared their catalytic activity to Rh/SSZ-13 (Si/Al = 12), Rh/ SiO_2 , and Rh/ Al_2O_3 in the

presence and absence of 5% water and 20 ppm SO_2 . The results showed that that Rh supported on Si-rich zeolites showed good stability during long-term experiments. However, since the study focused on the catalytic effects of the Si/Al ratio, the authors did not further investigate the differences between the SSZ-13 and ZSM-5.

Petrov et al.^[29] studied the effects of various acid and base treatments on MFI, MOR, and BEA before introducing Pd by ion-exchange. The authors were able to modify the catalytic properties of the materials by removing extra-framework aluminum, changing the pore structure, and stabilizing the palladium nanoparticles to prevent hydrothermal sintering. In general, they concluded that it was possible to change the properties of the different zeolites by the same structural manipulations. However, as expected, some pre-treatments required specific adjustments since each zeolite exhibits different susceptibility to acid and base treatments. The optimal modification of both ZSM-5, MOR, and BEA samples with Si/Al ratios around 10–15 consisted of 1) a mild desilication in $\text{NaOH} + \text{TPABr}$, 2) a selective dealumination in $\text{HNO}_3/\text{oxalic acid}$, 3) Pd loading by ion-exchange and calcination, and 4) a final titration of residual acid sites with sodium bicarbonate to obtain a fully Na-exchanged material. We will later discuss this particular choice of counter-ion in more detail.

High-silica zeolites with the MFI framework have recently received much attention,^[15,16,39,50,65,80] which may be explained by the issues with water and increasing interest in hydrophobic properties.^[18,27–29] For example, silicalite-1 (S-1) is an MFI zeolite that contains no Al and, therefore, has no acidic sites but high hydrophobicity and hydrothermal stability. Several studies have shown that Pd@S-1 is significantly more active than Pd/ SiO_2 .^[28,37] Hosseini et al.^[15] also investigated titanium silicalite-1 (TS-1) as catalyst support but added Pd by incipient wetness impregnation with Pd^{2+} in an aqueous solution. Although S-1 and TS-1 have similar hydrophobic properties, the authors showed that Pd/TS-1 showed less sintering after a 100 h tests with 3–4% water.

In their recent studies of the importance of hydrophobic properties, Losch et al.^[28] studied the effect of the zeolite

topology. By supporting preformed colloidal Pd particles on mesoporous zeolites with identical Si/Al ratios, they compared MOR, ZSM-5, beta, and FAU type zeolites to the typical alumina-based catalysts that serve as a benchmark in many studies. In general, the results showed that the catalysts made from large-pore zeolites (BEA and FAU with pores of 0.7–0.8 and 0.8–1.2 nm, respectively) typically performed better than those made from medium-pore zeolites (MFI and MOR with pores of <0.6 and 0.5–0.7 nm, respectively). Therefore, the authors proposed that the medium-pore zeolite retains the produced water more strongly through increased polar interaction and dispersion forces. Friberg et al.^[83] and Cui et al.^[73] also investigated the difference in activity between medium- and large-pore zeolites for methane oxidation. Interestingly, both groups concluded that small pore zeolites were preferable. However, it is important to mention that these studies focused on hydrothermal sintering, while the previous research focused on the direct deactivation by water adsorption. In general, all three groups seem to agree that Si/Al of the zeolite is more important than the zeolite type.

Si/Al Ratio

In the literature, the effect of the amount of aluminum on the catalytic activity have recently attracted much interest. The value is either given as Si/Al (silicon to aluminum ratio) or SiO₂/Al₂O₃ (silica to alumina ratio).^[18] In zeolites, substituting the tetravalent silicon with trivalent aluminum results in a negative charge compensated by a cation or a proton, which gives the zeolite acidic and hydrophilic properties. These properties significantly impact the catalyst's activity for methane oxidation because of the high amounts of water present in the exhaust from large natural gas engines.

Several studies have shown that hydrophobic zeolites with high Si/Al suffer less from deactivation by water.^[18,27,28,84] Additionally, the high Si/Al zeolites typically undergo the fast and reversible kind of water deactivation that results from molecular adsorption instead of forming more stable hydroxyl groups.^[18,37] Although several groups have focused on highly silicious zeolites with Si/Al > 300, recent results suggest that the optimal Si/Al value is, perhaps surprisingly, around 40.^[18,28,37] To explain the need for some acidity, Osman et al.^[85] proposed that a small number of protons could assist Pd reoxidation, which is essential to sustain a high catalytic activity. Losch et al.^[28] used *operando* diffuse reflectance infrared Fourier transform spectroscopy (DRIFTS) to study their catalyst's activation energies as a function of the zeolite's hydrophilicity. Based on these studies, the authors proposed an alternative explanation, where the acidic sites are needed to remove the water produced by the methane oxidation reaction. Figure 6 and Figure 7 show how the rapid adsorption/desorption process in the acidic micropores may assist the removal of water from the active PdO sites.

As highlighted in the previous sections, zeolites may prevent some challenges with water-induced deactivation and nanoparticle sintering. However, concerning the issues with

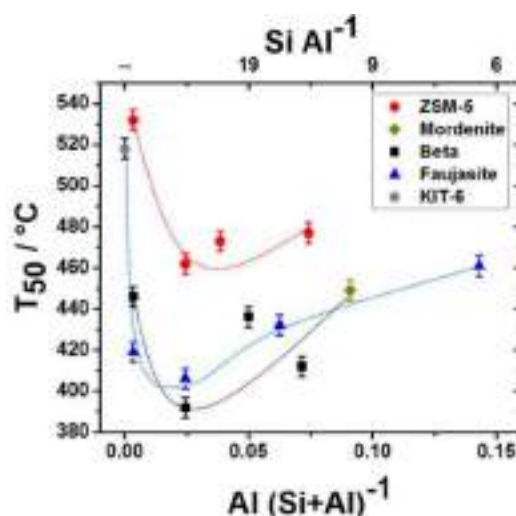


Figure 6. Results from light-off experiments showing the T_{50} as function of the aluminium content using a range of different Pd/zeolite catalysts. Conditions: 0.5% CH₄, 4% O₂, and 4.2% H₂O, balanced with Ar, and GHSV = 69,000 mL/(g_{cat}h). Reprinted with permission from Losch et al.^[28] Copyright 2019, American Chemical Society.

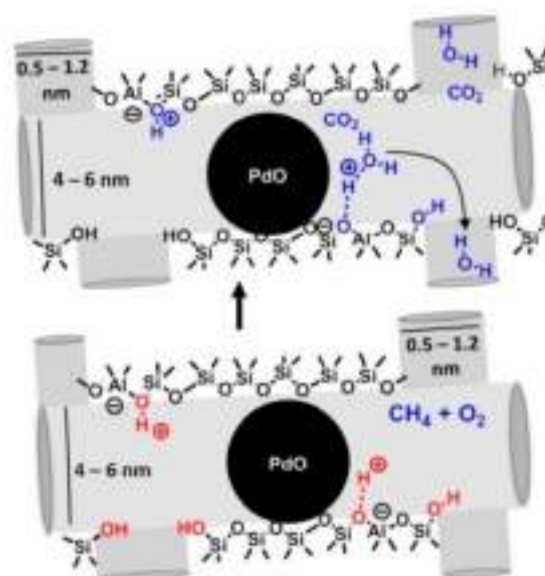


Figure 7. Illustration of the molecular transport of water via adsorption/desorption processes on the internal surface of an acidic mesoporous zeolite. Reprinted with permission from Losch et al.^[28] Copyright 2019, American Chemical Society.

SO₂ poisoning, it may be more important to optimize the composition of the active metal nanoparticles than the zeolite support. In some cases, such as Al₂O₃-based catalysts, the support can act as a sulfur sink that temporarily protects the active sites. However, for commercial applications that favor continuous operation without periodic regenerations, it may be needed to lower the decomposition temperature of the

sulfates. Unfortunately, this point has received relatively little attention in recent studies.

Zhang et al.^[37] investigated the influence of the support and rhodium speciation on total methane oxidation in the presence of water and SO₂. Water significantly inhibited all catalysts, particularly those supported on amorphous SiO₂ and Al-rich zeolites. Furthermore, the authors related a high Si/Al ratio with good sulfur tolerance, indicating that the sulfur primarily binds to the Al sites.

As previously mentioned, steaming is a widespread method to disperse metal nanoparticles on zeolite-supported catalysts.^[18,47,63,74–76,86] Interestingly, this method exploits the same steam-induced mobility of PdO species that causes sintering under reaction conditions. The method is generally more effective for low Si/Al zeolites.^[18] However, the high acidity of these materials also results in increased sintering since the mobility of PdO is higher on hydrophilic surfaces.^[27] This contradiction results in a challenging balancing act between nanoparticle dispersion and long-term stability.

Multiple authors have discussed how Si/Al determines both the ion-exchange capacity of the zeolite and its tendency to form metal nanoparticles.^[18,37] Petrov et al.^[27] showed that the Si/Al can determine the particle size distribution because the acidity controls the PdO mobility and dispersion. The authors also point out that a low Si/Al value results in a high metal dispersion (high ion-exchange capacity and high PdO mobility). In contrast, a high Si/Al value typically results in high stability (high hydrophobicity and low PdO mobility). In general, a high Si/Al appears to reduce sintering and water deactivation. However, it also requires more complex synthesis procedures to disperse the active metal, including various pre- and post-treatments.

Counter Ions and Role of Acidic Sites

Petrov et al.^[27,29] ion-exchanged Pd into commercial dealuminated MOR and then calcined the material at 500 °C. After the calcination, the authors then ion-exchanged the protons with sodium ions to remove all remaining acidity. Compared to other methods, this approach is relatively simple and well-suited for large-scale production. The Na-exchanged sites improved the stability of the support and effectively prevented steam-induced sintering by confining the Pd nanoparticles within the zeolite.^[27,37] Furthermore, they pointed out that reducing zeolite acidity by ion-exchange over e.g. dealumination, may prevent the formation of unwanted extra-framework aluminum.

Several studies have shown that it is challenging to achieve a high dispersion of Pd within high silica zeolites due to their high hydrophobicity and small ion-exchange capacity. Recently, Lei et al.^[72] highlighted the advantage of having some acidity present when loading Pd. The authors impregnated an aqueous palladium solution onto Na-form ZSM-5 followed by drying and calcination. TEM analysis showed that the Pd ended up on the external surface of the Na-ZSM-5 as rather large particles. The particle size distributions of the

three Na-form samples with Si/Al = 20, 40, 80 did not follow a clear trend. Repeating the syntheses with H-ZSM-5 confirmed that low Si/Al ratios resulted in higher dispersions. The authors tested the activity over 50 hours and showed that the catalysts achieved up to 90 % conversion at 450 °C of 1 % methane in air (neither water nor SO₂ was present in the tested feed).

In general, the literature describes some significant discrepancies regarding the stabilizing effects of the Si/Al value. Over the last decade, a series of publications^[13,14,57–59] have suggested that the presence of acidic sites might prevent sintering by anchoring the PdO particles. We note that these suggestions all have references to the same three publications.^[42,87,88] Several of these publications also hypothesized that the acid sites could assist in cleaving the first and most difficult C–H bond in methane, initiating the reaction through protolysis.^[13,57,59] Later, some of the authors seemed to have abandoned this hypothesis. For example, Wang et al. suggested an anchoring and activating effect in 2016,^[13] but already in 2018,^[63] the same authors showed that the Si/Al value had a significant impact on the metal dispersion, but only a negligible effect on methane activation. Similarly, Stockenhuber et al. suggested an anchoring effect in 2018.^[14] In 2020, the same authors related high catalytic stability to low acidity. Therefore, the most recent results support the commonly accepted hypothesis that a high acidity is increasing the mobility of PdO, as presented in this review.^[15]

In 2017, van Bokhoven and co-workers showed why the acidity of the zeolite is a critical parameter for methane oxidation.^[9] The authors loaded palladium by ion-exchange on H-ZSM-5 but did not exchange the remaining protons with sodium. Therefore, they obtained a material that contained small and well-dispersed nanoparticles inside the zeolite framework but with significant Brønsted acidity. The nanoparticles sintered from around 1–2 nm to 5–10 nm under so-called dry conditions with 1 % CH₄ in the feed. However, under wet conditions with 5 % added H₂O, the sintering accelerated significantly, resulting in up to 100 nm nanoparticles. Figure 8 shows one of van Bokhovens experiments that demonstrate how the deactivation occurs at different timescales. The red ellipse shows the fast deactivation caused by water inhibition, and the green ellipse shows the slow deactivation caused by a combination of nanoparticle sintering and hydroxyl formation. Although the XRD patterns of the fresh and spent catalysts looked identical, changes in the solid-state ²⁷Al-NMR and physisorption analysis did indicate some gradual degradation of the zeolite framework.

In general, zeolite acidity may help disperse the active metal during synthesis but also enhance hydrothermal sintering under realistic operating conditions. On the one hand, high dispersions are critical for achieving low-temperature activity and reducing costs. On the other hand, it may be worthwhile to value stability over low-temperature activity, especially if the final catalyst is installed before the turbo-charger where the reaction temperature is relatively high.

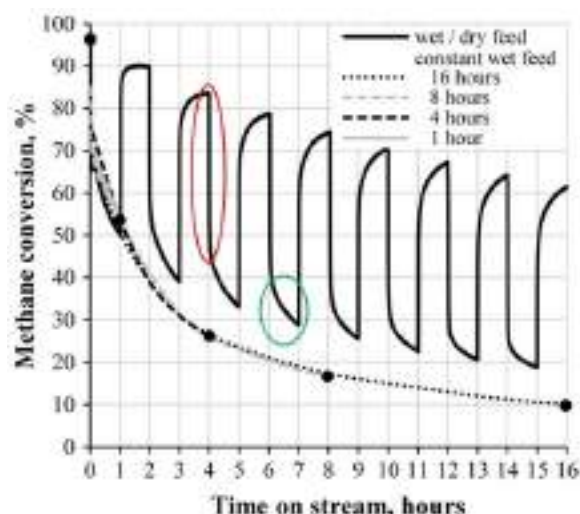


Figure 8. A deactivation experiment where water is periodically added to the feed gas. Colored markings are added to the original figure. Red: Fast deactivation by water adsorption. Green: Slow deactivation by a combination of hydroxyl build-up and hydrothermal sintering. Conditions: 450 °C, 1 % CH₄, 4 % O₂, 0 or 5 % H₂O, balanced with N₂. Adapted with permission from Petrov et al.^[9] Copyright 2016, Springer Nature.

Additives

It is well-known that additives and promoters significantly affect the catalytic activity of Pd/Al₂O₃ catalysts in complete methane oxidation.^[11,22] Therefore, several researchers have also investigated different additives and promoters in Pd-based zeolite systems.

Xie et al.^[89] exchanged the protons with other counter-ions than Na, but these modifications did not have much effect. However, a mixture of La and Na resulted in higher catalytic activity than pure Na-exchanged Pd/ZSM-5. To explain these results, the authors suggested that La had a size-reducing effect on the Pd nanoparticles.

Zhang et al.^[39] used the in-situ ethylenediamine approach to synthesize a series of Pd-Ni@ZSM-5 materials with varying ratios between the two metals. The authors found that the addition of Ni improved the activity and stability but accelerated the deactivation caused by water and SO₂.

Most additives for methane oxidation catalysts facilitate the reoxidation of the catalyst to provide lattice O²⁻, which is the active species in a Mars-van Krevelen mechanism. For this reason, redox-active metal oxides such as CeO₂ and ZrO₂ have found extensive use to partially or fully substitute conventional support materials such as SiO₂ or Al₂O₃. Furthermore, redox-active metal oxides result in strong metal-support interactions with PdO, increasing thermal stability.^[16,90,91] With few exceptions, investigating such composite metal oxide-zeolite composites is still a relatively new field in the area of complete methane oxidation. Niu et al.^[16] recently synthesized Pd@S-1 and then covered the exterior surface of the zeolite with 13 wt% ceria through wet impregnation and calcination.

The material exhibited slightly lower initial activity but improved stability under dry conditions. The authors related the increased stability to the strong metal support interactions between Pd and CeO₂. However, based on the expected separation between the Pd nanoparticles encapsulated inside the zeolite and the CeO₂ supported outside the zeolite, the degree of direct contact is still unclear.

Osman et al.^[85] reported another example of zeolite-based catalysts modified by metal oxides. In this work, the authors synthesized a series of Pt-Pd/TiO₂/ZSM-5 catalysts by a sonication-assisted impregnation adding the dissolved Pt- and Pd-precursors into a slurry of anatase and ZSM-5. The Pt and Pd loadings were 2 and 5 wt%, respectively, and the TiO₂ content was 17–25 wt%. The addition of TiO₂ had a remarkable effect on the low-temperature activity under dry conditions. The authors attributed this to the oxygen storage and transport abilities of TiO₂ and its interaction with the precious metals. The authors did not discuss the specific role of the zeolite in further detail.

Several studies have investigated the effects of combining Pd and Pt in Al₂O₃-supported methane oxidation catalysts.^[11,21,61,92–95] In general, the introduction of Pt decreases the catalytic activity by stabilizing Pd⁰,^[96] but increases the stability towards SO₂. Osman et al.^[85] and Nguyen et al.^[97] also investigated some bimetallic zeolite-based PdPt catalysts but did not investigate their stability in the presence of SO₂.

Influence of Active Metal Loading and Particle Size

For zeolite-supported methane oxidation catalysts, metal nanoparticles are significantly more active than single-metal sites.^[18,37,73,84,98] Friberg et al. explained this by the more facile reduction and reoxidation of metallic nanoparticles over ion-exchanged single metal sites.^[18] For methane oxidation, Pd-based catalysts follow a Mars-van Krevelen mechanism, in which the active phase is PdO.^[24,28,99] Therefore, Goodman et al.^[100] also confirmed that oxidative pretreatments are better than reductive for methane oxidation catalysts. Although the pretreatment of methane oxidation catalyst continues to attract much attention,^[57] this topic, which mainly deals with the Pd/PdO distribution, is outside the scope of this review. The interested reader is referred to the recent review by Ciuparu et al.^[101]

The metal loading varies greatly for zeolite-supported Pd-based methane oxidation catalysts. Niu et al.^[16] synthesized a Pd@S-1 material with only 0.123 wt% palladium, while Doyle et al.^[102] synthesized a Pd/Na-FAU with 6.21 wt% palladium. Losch et al.^[28] noted that loadings between 0.1 and 4 wt% were commonly used in literature and performed a thorough study of the effect of the Pd loading. Figure 9 shows T₅₀ as function of the metal loading (0.05, 0.1, 0.25, 0.5, 1, and 2 wt %) for six mesoporous zeolite catalysts supporting 3.2 nm Pd nanoparticles. The authors found that 0.5 wt% Pd was optimal and explained how higher loadings might cause pore blocking and mass transfer limitations. Wang et al.^[50] studied the metal loading of Pd nanoparticles encapsulated in silicalite-1 (MFI),

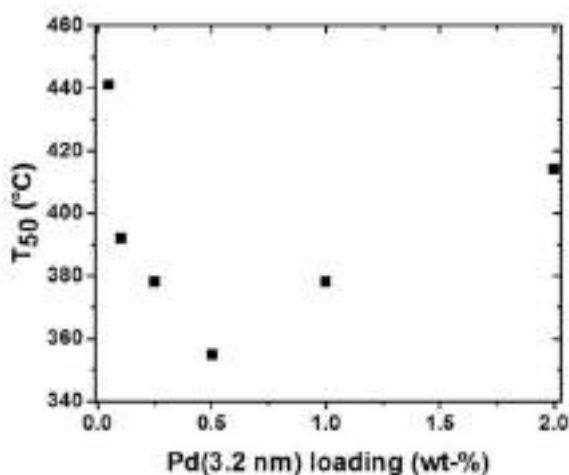


Figure 9. Results from light-off experiments showing the T_{50} as function of the metal loading for six mesoporous zeolite catalysts supporting 3.2 nm Pd nanoparticles. Conditions: 0.5 % CH_4 , 4 % O_2 , and 4.2 % H_2O , balanced with Ar, and GHSV = 69,000 $\text{ml}/(\text{g}_{\text{cat}} \cdot \text{h})$. Bed was diluted with alumina (20 mg/180 mg) and heating rate was 10 $^\circ\text{C}/\text{min}$. Reprinted with permission from Losch et al.^[28] Copyright 2019, American Chemical Society.

and observed a volcano-shaped relation with an optimum activity at 0.6 wt%, in good agreement with the previous study. In general, a high metal loading results in larger nanoparticles, although the synthesis method is the most decisive factor. Typically, ion-exchange followed by calcination yields nanoparticles with a size of 1–1.5 nm,^[9,27] in-situ encapsulation using ethylenediamine^[80] gives nanoparticles with a size of 1–3 nm,^[16,39,50,80] and impregnation results in relatively large nanoparticles with a size range of 3–40 nm.^[14,16,17] Hydrothermal treatments are sometimes used to reduce the particle size after synthesis by impregnation.^[18] In general, the two first methods result in small and stable nanoparticles situated inside the micropores of the zeolite. In contrast, simple impregnation typically results in larger nanoparticles supported outside the micropores of the zeolite.

Although small nanoparticles expose a higher fraction of unsaturated metal active sites, there are cases where larger particles are preferred. Several researchers have determined that Pd nanoparticles within a specific size range have optimal activity for complete methane oxidation.^[50,57,92,103,104] Although this size range varies greatly, there seems to be some agreement that the optimum size is around 3–7 nm concerning both activity and stability. The exact reasons for these effects depend on the support material and the metal-support interactions but are still not fully understood. Murata et al.^[104] showed how the turn-over frequency (TOF) of a series of α - Al_2O_3 and θ - Al_2O_3 supported Pd catalysts had a volcano-shaped dependence on the Pd particle size that achieved the highest activity at around 7 nm. The authors related this behavior with the fraction of step-sites combined with an effect of different metal-support interactions. The particle size can also influence the deactivation of SO_2 . For example, Wilburn et al.^[92] found that larger Pd nanoparticles supported

on Al_2O_3 mainly adsorbed molecular SO_2 that easily desorbed at intermediate temperatures. In contrast, smaller particles formed more stable sulfate species that needed higher temperatures to decompose. The work on Pd particle sizes for zeolites-based methane oxidation catalysts is more limited. Wang et al.^[50] synthesized Pd@silicalite-1 with different metal loadings and described how the particle size increased at higher loadings. The most active catalyst contained 0.6 % Pd nanoparticles with a size of 2.3 nm. Fan et al.^[57] produced a series of Pd/H-ZSM-5 catalysts and exposed them to different calcination, reduction, and oxidation treatments to change the particle size. The authors described how the methane oxidation TOF had a volcano-shaped dependency on the Pd particle size that achieved the highest activity at around 5 nm.

Among others, Friberg et al.^[18] showed that some degree of ion-exchange may occur during the reaction. The authors explained that this phenomenon is less pronounced at high Pd loadings. Furthermore, the ion-exchange is less significant in Na-form zeolites compared to H-form.^[105] Therefore, it also seems likely that zeolite-based catalysts with a low ion-exchange capacity (high Si/Al) will form fewer of these less active metal-exchanged sites. The Si/Al can also influence the active metal nanoparticles in other ways. For example, Nguyen et al.^[97] reported a Pd/Pt catalyst where the fraction of a bimetallic phase increased with decreasing acidity (increasing Si/Al). The authors showed that the bimetallic phase possessed a surprisingly high metallic character and that its fraction correlated linearly with the activity.

Catalytic Performance of Zeolite-based Materials under Realistic Testing Conditions

In principle, Pd-based catalysts have had sufficient low-temperature activity to convert methane in the exhaust from large lean-burn natural gas-fueled engines for more than ten years.^[91] However, the issues with fast and severe deactivation continue to prevent practical applications, which drive the research and development to focus more on increasing the stability under realistic operation conditions. To this end, zeolites may help prevent some of the most significant issues with hydroxyl formation and water deactivation.^[27–29,82] Still, most catalysts lose some activity when exposed to high amounts of steam, which increases the T_{50} by 40–150 $^\circ\text{C}$.^[27,39,40] Even under so-called “dry” test conditions, methane oxidation still produces water that affects the catalytic activity.^[48] These effects are more pronounced in studies using high methane concentrations. For example, the oxidation of 1–2 % methane results in 2–4 % steam at full conversion.

It is also important to remember that methane oxidation is a highly exothermic reaction and that oxidation of 1 % methane-in-air heat the gas by > 300 $^\circ\text{C}$, its so-called adiabatic heating. Therefore, too high methane concentrations often cause significant heat transfer problems. The problems may result in hot spots and too high conversions if the catalysts bed is undiluted or the generated heat is not effectively removed.^[97]

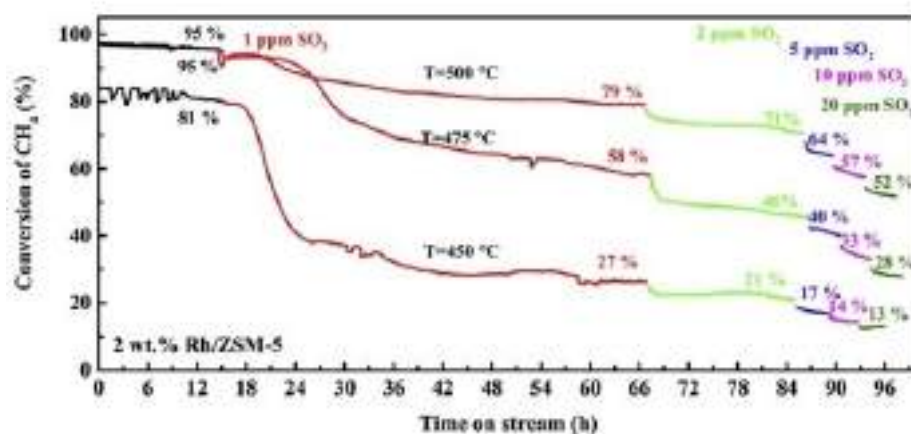


Figure 10. Catalytic activity of 2 wt.% Rh/ZSM-5 under 2500 ppm CH₄, 10% O₂, 5% H₂O and 0–20 ppm SO₂ balanced with N₂. GHSV = 150,000 ml/(g_{cat}h). Reprinted with permission from Zhang et al.^[33] Copyright 2020, Elsevier.

Zeolites may also help prevent sintering since they can hold the encapsulated nanoparticles in a firm grip inside the microporous framework.^[27–29,82] This leaves the challenge of chemical deactivation by SO₂. Zhang et al.^[39] suggested that encapsulation might reduce SO₂ poisoning if the confinement inside the zeolite was tight enough to limit the space for PdSO₄ formation. Furthermore, the authors suggested that the small size of such sulfate nanoparticles decreases their decomposition temperature, effectively reducing the deactivation.

In four recent publications,^[32,33,37,106] Zhang et al. published their work on Rh-based zeolite catalysts for methane oxidation. These exhibited a remarkable tolerance towards SO₂ poisoning, maintaining significant activity after exposure to close-to-realistic conditions. Unfortunately, the synthesis of the catalysts relied on impregnation, which was insufficient to get the Rh inside the zeolite micropores. Consequently, the catalysts also suffered due to some sintering. Although these results show that Rh is an interesting alternative to Pd, the high cost of Rh may limit practical applications. Figure 10 shows the catalytic activity of Rh/ZSM-5 in the presence of both water and SO₂.

Only a few studies have supported the zeolite catalyst on actual monoliths. For example, Xiao et al.^[64] synthesized silicalite-1 on the surface of a cordierite monolith via steam-assisted crystallization. The monolith was then calcined and dip-coated in an aqueous solution of Pd(NH₃)₂Cl₂. Although the Pd distribution and the zeolite's actual effect remain unclear, the prepared catalyst was active for more than 70 h at 450 °C (tested under dry model conditions and at 100% conversion).

Conclusions and Future Outlook

In summary, zeolites offer an exciting alternative to conventional metal oxides for supporting metal nanoparticles for complete methane oxidation. The ideal zeolite is relatively hydrophobic and has low acidity, either from a high Si/Al ratio or the exchange of remaining H⁺ with alkali metal counterions such as Na⁺. The micropores can have small 8-membered rings (e.g. CHA), medium 10-membered rings (e.g. MFI) or large 12-membered rings (BEA, FAU, MOR), but the zeolite has to be stable under relatively demanding reaction conditions, at high temperatures, and in the presence of steam. In addition, the active metal should be well-dispersed and preferably encapsulated inside the zeolite to prevent sintering by particle migration. For Pd, the ideal particle size is around 3–7 nm.

Some researchers argue that the field of methane oxidation has focused too much on achieving the lowest possible light-off temperature under ideal conditions.^[27] With the recent developments in complete methane oxidation, now might be the right time to direct more attention towards improving the catalytic stability under realistic operation conditions. While zeolites hold great promise to limit sintering and water-induced deactivation, their potential for preventing SO₂ poisoning is still unclear. Based on the experience with Al₂O₃-supported catalysts, it may be possible to improve the SO₂ tolerance by introducing dopants, alloys, or redox-active metal oxides such as CeO₂. Although zeolites attract increasing interest, it is important to underline that Al₂O₃-supported catalysts still receive much attention.^[60,107–111] Regardless of the support material, however, it is paramount that the testing conditions become more realistic for two reasons:

- 1) Long-term stability is more important than low-temperature activity for controlling the methane emissions from large lean-burn natural gas-fired engines. Existing catalysts already have sufficient low-temperature activity but still suffer

from deactivation by sintering, water, and SO_2 . While promising results show how it is possible to address these issues individually, studies investigating the interconnected and enhanced deactivation when both SO_2 and H_2O are present are critically needed. Preferably, these studies should also account for the increased pressure before the turbocharger (typically up to 5 bar).

- 2) The direct comparison of results from different research groups, companies, and end-users is challenging when the testing conditions vary too much. While it might be possible to account for differences in e.g. space velocity or oxygen concentration, it is almost impossible to compare results obtained under wet and dry conditions with or without SO_2 . Therefore, a set of standard reaction conditions (see Table 1) would accelerate the development of new and more durable catalysts, critically needed for controlling methane emissions.

Several studies have used testing conditions that differ significantly from actual applications. For example, many researchers use a feed gas composition of 1% CH_4 , 4% O_2 , 95% Ar, or 1% CH_4 in air.^[9,102,107,112] More and more studies investigate the effect of water, but often 5% or less. Real exhaust from natural gas engines usually contains up to 10% water. Few studies examine the impact of both H_2O and SO_2 , and even fewer consider the effect of pressure. Testing on real engine exhaust and laboratory test benches both have their advantages. Still, we argue that the field of methane oxidation will benefit from testing under a set of standard conditions with more realistic gas compositions.

Although the recent developments in complete methane oxidation demonstrate that zeolite-supported metal nanoparticle catalysts hold great promise, there are still significant challenges to overcome. For example, high-silica zeolites have high hydrothermal stability, but their ability to withstand 3 bar of 10% steam at 500 °C for thousands of hours is still unknown. In addition, Pd nanoparticles suffer from significant deactivation by SO_2 . While regeneration may be an option, such operations complicate the reactor design, especially if the catalyst sits before the turbocharger. Therefore, modifying the Pd nanoparticles to give less stable sulfate species seems like one promising strategy.

The recent advances in complete methane oxidation show that zeolite-supported metal nanoparticle catalysts hold great promise for future emission control systems. However, there is still room for improvement concerning their long-term stability. Therefore, it is crucial to understand the complex causes of deactivation and start testing under more realistic operation conditions.

Acknowledgements

This work is funded by Umicore Denmark and Innovation Fund Denmark (IFD) under File No. 0153-00064. R.L.M., H.-D.N., and K.H.P. are employed at Umicore Denmark and have commercial interests in developing new emission control technologies.

Conflict of Interest

The authors declare no conflict of interest.

Keywords: Catalysis · Emission control · Methane oxidation · Palladium nanoparticles · Zeolites

- [1] R. B. Jackson, E. I. Solomon, J. G. Canadell, M. Cargnello, C. B. Field, *Nat. Sustain.* **2019**, 2, 436–438.
- [2] M. Etminan, G. Myhre, E. J. Highwood, K. P. Shine, *Geophys. Res. Lett.* **2016**, 43, 12,614–12,623.
- [3] M. Caltagirone, T. Chung, “New global methane pledge aims to tackle climate change,” can be found under <https://www.unep.org/news-and-stories/story/new-global-methane-pledge-aims-tackle-climate-change>, **2021**.
- [4] Y. Wang, P. Hu, J. Yang, Y.-A. Zhu, D. Chen, *Chem. Soc. Rev.* **2021**, 50, 4299–4358.
- [5] N. Pavlenko, B. Comer, Y. Zhou, N. Clark, D. Rutherford, *ICCT Work. Pap.* **2020–02 2020**.
- [6] D. Stenersen, O. Thonstad, *GHG and NOx Emissions from Gas Fuelled Engines*, **2017**.
- [7] G. Weisser, D. Schneider, I. Nylund, in *CIMAC Congr. 2019*, Vancouver, **2019**.
- [8] V. Masson-Delmotte, P. Zhai, A. Pirani, S. L. Connors, C. Péan, S. Berger, N. Caud, Y. Chen, L. Goldfarb, M. I. Gomis, M. Huang, K. Leitzell, E. Lonnoy, J. B. R. Matthews, T. K. Maycock, T. Waterfield, O. Yelekçi, R. Yu, B. Zhou, *IPCC: Climate Change 2021: The Physical Science Basis. Contribution of Working Group I to the Sixth Assessment Report of the Intergovernmental Panel on Climate Change*, Cambridge University Press, **2021**.
- [9] A. W. Petrov, D. Ferri, M. Tarik, O. Kröcher, J. A. van Bokhoven, *Top. Catal.* **2017**, 60, 123–130.
- [10] X. Li, X. Wang, K. Roy, J. A. van Bokhoven, L. Artiglia, *ACS Catal.* **2020**, 10, 5783–5792.
- [11] P. Gélin, M. Primet, *Appl. Catal. B* **2002**, 39, 1–37.
- [12] T. V. Choudhary, S. Banerjee, V. R. Choudhary, *Appl. Catal. A* **2002**, 234, 1–23.
- [13] Y. Lou, J. Ma, W. Hu, Q. Dai, L. Wang, W. Zhan, Y. Guo, X. M. Cao, Y. Guo, P. Hu, G. Lu, *ACS Catal.* **2016**, 6, 8127–8139.
- [14] H. Hosseiniamolli, G. Bryant, E. M. Kennedy, K. Mathisen, D. Nicholson, G. Sankar, A. Setiawan, M. Stockenhuber, *ACS Catal.* **2018**, 8, 5852–5863.
- [15] H. Hosseiniamolli, A. Setiawan, A. A. Adesina, E. M. Kennedy, M. Stockenhuber, *Catal. Sci. Technol.* **2020**, 10, 1193–1204.
- [16] R. Niu, P. Liu, W. Li, S. Wang, J. Li, *Microporous Mesoporous Mater.* **2019**, 284, 235–240.
- [17] Q. Zheng, S. Zhou, M. Lail, K. Amato, *Ind. Eng. Chem. Res.* **2018**, 57, 1954–1960.
- [18] I. Friberg, N. Sadokhina, L. Olsson, *Appl. Catal. B* **2019**, 250, 117–131.
- [19] P. Auvinen, N. M. Kinnunen, J. T. Hirvi, T. Maunula, K. Kallinen, M. Keenan, R. Baert, E. van den Tillaart, M. Suvanto, *Appl. Catal. B* **2019**, 258, 117976.
- [20] L. He, Y. Fan, J. Bellettre, J. Yue, L. Luo, *Renewable Sustainable Energy Rev.* **2020**, 119, 109589.
- [21] J. Matthey, A. Raj, *Johnson Matthey Technol. Rev.* **2016**, 60, 228–235.
- [22] M. Monai, T. Montini, R. J. Gorte, P. Fornasiero, *Eur. J. Inorg. Chem.* **2018**, 2884–2893.
- [23] P. Lott, P. Dolcet, M. Casapu, J. D. Grunwaldt, O. Deutschmann, *Ind. Eng. Chem. Res.* **2019**, 58, 12561–12570.
- [24] H. Stotz, L. Maier, A. Boubnov, A. T. Gremminger, J. D. Grunwaldt, O. Deutschmann, *J. Catal.* **2019**, 370, 152–175.
- [25] M. Schaube, R. Merkle, J. Maier, *J. Phys. Chem. C* **2020**, 124, 18544–18556.
- [26] R. J. Farrauto, *Science* **2012**, 337, 659–660.
- [27] A. W. Petrov, D. Ferri, F. Krumeich, M. Nachtegaal, J. A. Van Bokhoven, O. Kröcher, *Nat. Commun.* **2018**, 9.
- [28] P. Losch, W. Huang, O. Vozniuk, E. D. Goodman, W. Schmidt, M. Cargnello, *ACS Catal.* **2019**, 9, 4742–4753.
- [29] A. W. Petrov, D. Ferri, O. Kröcher, J. A. Van Bokhoven, *ACS Catal.* **2019**, 9, 2303–2312.
- [30] R. Bank, U. Etzien, B. Buchholz, H. Harndorf, *MTZ Ind.* **2015**, 5, 14–21.

- [31] B. Torkashvand, A. Gremminger, S. Valchera, M. Casapu, J. D. Grunwaldt, O. Deutschmann, *SAE [Tech. Pap.]* **2017**, 2017-01-10, DOI 10.4271/2017-01-1019.
- [32] Y. Zhang, P. Glarborg, K. Johansen, M. P. Andersson, T. K. Torp, A. D. Jensen, J. M. Christensen, *ACS Catal.* **2020**, *10*, 1821–1827.
- [33] Y. Zhang, P. Glarborg, M. P. Andersson, K. Johansen, T. K. Torp, A. D. Jensen, J. M. Christensen, *Appl. Catal. B* **2020**, *277*, 119176.
- [34] A. Gremminger, P. Lott, M. Merts, M. Casapu, J.-D. Grunwaldt, O. Deutschmann, *Appl. Catal. B* **2017**, *218*, 833–843.
- [35] A. Guliaeff, K. Wanning, F. Klose, G. Maletz, A. Tissler, *SAE Technical Paper* **2013**, DOI 10.4271/2013-01-0531.
- [36] N. Sadokhina, F. Ghasempour, X. Auvray, G. Smedler, U. Nylén, M. Olofsson, L. Olsson, *Catal. Lett.* **2017**, *147*, 2360–2371.
- [37] Y. Zhang, P. Glarborg, M. P. Andersson, K. Johansen, T. K. Torp, A. D. Jensen, J. M. Christensen, *Catal. Sci. Technol.* **2020**, *10*, 6035–6044.
- [38] P. Velin, F. Hemmingsson, A. Schaefer, M. Skoglundh, K. A. Lomachenko, A. Raj, D. Thompson, G. Smedler, P. Carlsson, *ChemCatChem* **2021**, *13*, 3765–37711–8.
- [39] Z. Zhang, L. Sun, X. Hu, Y. Zhang, H. Tian, X. Yang, *Appl. Surf. Sci.* **2019**, *494*, 1044–1054.
- [40] K. Keller, P. Lott, H. Stotz, L. Maier, O. Deutschmann, *Catalysts* **2020**, *10*, 1–21.
- [41] J. C. Van Giezen, F. R. Van Den Berg, J. L. Kleinen, A. J. Van Dillen, J. W. Geus, *Catal. Today* **1999**, *47*, 287–293.
- [42] K. Okumura, S. Matsumoto, N. Nishiaki, M. Niwa, *Appl. Catal. B* **2003**, *40*, 151–159.
- [43] C. R. Florén, C. Demirci, P. A. Carlsson, D. Creaser, M. Skoglundh, *Catal. Sci. Technol.* **2020**, *10*, 5480–5486.
- [44] P. Velin, M. Ek, M. Skoglundh, A. Schaefer, A. Raj, D. Thompson, G. Smedler, P. A. Carlsson, *J. Phys. Chem. C* **2019**, *123*, 25724–25737.
- [45] C. R. Florén, M. Van Den Bossche, D. Creaser, H. Grönbeck, P. A. Carlsson, H. Korpi, M. Skoglundh, *Catal. Sci. Technol.* **2018**, *8*, 508–520.
- [46] T. Guo, J. Du, J. Wu, S. Wang, J. Li, *Chem. Eng. J.* **2016**, *306*, 745–753.
- [47] I. Friberg, A. Wang, L. Olsson, *Catalysts* **2020**, *10*, 517.
- [48] W. Huang, E. D. Goodman, P. Losch, M. Cargnello, *Ind. Eng. Chem. Res.* **2018**, *57*, 10261–10268.
- [49] W. Huang, X. Zhang, A. C. Yang, E. D. Goodman, K. C. Kao, M. Cargnello, *ACS Catal.* **2020**, *10*, 8157–8167.
- [50] W. Wang, W. Zhou, W. Li, X. Xiong, Y. Y. Wang, K. Cheng, J. Kang, Q. Zhang, Y. Y. Wang, *Appl. Catal. B* **2020**, *276*, 119142.
- [51] S. M. Campbell, D. M. Bibby, J. M. Coddington, R. F. Howe, *J. Catal.* **1996**, *161*, 350–358.
- [52] L. H. Ong, M. Dömök, R. Olindo, A. C. Van Veen, J. A. Lercher, *Microporous Mesoporous Mater.* **2012**, *164*, 9–20.
- [53] H. K. Beyer, *Dealumination Techniques for Zeolites. Post-Synthesis Modification I. Molecular Sieves (Science and Technology)*, Springer, Berlin, Heidelberg, **2002**.
- [54] W. Zhang, X. Han, X. Liu, H. Lei, X. Liu, X. Bao, *Microporous Mesoporous Mater.* **2002**, *53*, 145–152.
- [55] T. W. Hansen, A. T. Delariva, S. R. Challa, A. K. Datye, *Acc. Chem. Res.* **2013**, *46*, 1720–1730.
- [56] D. Farrusseng, A. Tuel, *New J. Chem.* **2016**, *40*, 3933–3949.
- [57] C. Fan, L. Yang, L. Luo, Z. Wu, Z. Qin, H. Zhu, W. Fan, J. Wang, *New J. Chem.* **2020**, *44*, 3940–3949.
- [58] J. Bin Lim, D. Jo, S. B. Hong, *Appl. Catal. B* **2017**, *219*, 155–162.
- [59] O. M'Ramadj, D. Li, X. Wang, B. Zhang, G. Lu, *Catal. Commun.* **2007**, *8*, 880–884.
- [60] P. Lott, M. Eck, D. E. Doronkin, A. Zimina, S. Tischer, R. Popescu, S. Belin, V. Briois, M. Casapu, J.-D. Grunwaldt, O. Deutschmann, *Appl. Catal. B* **2020**, *278*, 119244.
- [61] M. S. Wilburn, W. S. Epling, *ACS Catal.* **2019**, *9*, 640–648.
- [62] P. Auvinen, J. T. Hirvi, N. M. Kinnunen, M. Suvanto, *ACS Catal.* **2020**, *10*, 12943–12953.
- [63] Q. Dai, Q. Zhu, Y. Lou, X. Wang, *J. Catal.* **2018**, *357*, 29–40.
- [64] C. Xiao, Y. Yang, D. Meng, L. Dong, L. Luo, Z. Tan, *Appl. Catal. A* **2017**, *531*, 197–202.
- [65] T. Li, A. Beck, F. Krumeich, L. Artiglia, M. K. Ghosal, M. Roger, D. Ferri, O. Kröcher, V. Sushkevich, O. V. Safonova, J. A. van Bokhoven, *ACS Catal.* **2021**, *11*, 7371–7382.
- [66] P. Auvinen, N. M. Kinnunen, J. T. Hirvi, T. Maunula, K. Kallinen, M. Keenan, M. Suvanto, *Chem. Eng. J.* **2020**, *417*, 128050.
- [67] H. Rasmussen, F. Goodarzi, D. B. Christensen, J. Mielby, *ACS Appl. Nano Mater.* **2019**, *2*, 8083–8091.
- [68] Y. Wang, C. Wang, L. Wang, L. Wang, F.-S. Xiao, *Acc. Chem. Res.* **2021**, *54*, 2579–2590.
- [69] Y. Li, J. N. Armor, *Appl. Catal. B, Environ.* **1994**, *3*, 275–282.
- [70] F. Goodarzi, L. Kang, F. R. Wang, F. Joensen, S. Kegnaes, J. Mielby, *ChemCatChem* **2018**, *10*, 1566–1570.
- [71] H. J. Cho, D. Kim, B. Xu, *ACS Catal.* **2020**, *10*, 4770–4779.
- [72] J. Lei, R. Niu, S. Wang, J. Li, *Solid State Sci.* **2020**, *101*, 106097.
- [73] Y. Cui, B. Peng, L. Kovarik, J. Zheng, J. Szanyi, Y. Wang, F. Gao, in *Small Pore Zeolite Supported Pd as Highly Active and Stable Low-Temperature Methane Combustion Catalysts*, North American Catalysis Society Meeting, NAM, **2019**.
- [74] Y. S. Ryou, J. Lee, H. Lee, C. H. Kim, D. H. Kim, *Catal. Today* **2019**, *320*, 175–180.
- [75] J. Lee, Y. Ryou, S. Hwang, Y. Kim, S. J. Cho, H. Lee, C. H. Kim, D. H. Kim, *Catal. Sci. Technol.* **2019**, *9*, 163–173.
- [76] Y. S. Ryou, J. Lee, S. J. Cho, H. Lee, C. H. Kim, D. H. Kim, *Appl. Catal. B* **2017**, *212*, 140–149.
- [77] J. Zečević, A. M. J. Van Der Eerden, H. Friedrich, P. E. De Jongh, K. P. De Jong, *ACS Nano* **2013**, *7*, 3698–3705.
- [78] Y. Chai, S. Liu, Z. J. Zhao, J. Gong, W. Dai, G. Wu, N. Guan, L. Li, *ACS Catal.* **2018**, *8*, 8578–8589.
- [79] J. Tang, P. Liu, X. Liu, L. Chen, H. Wen, Y. Zhou, J. Wang, *ACS Appl. Mater. Interfaces* **2020**, *12*, 11522–11532.
- [80] N. Wang, Q. Sun, R. Bai, X. Li, G. Guo, J. Yu, *J. Am. Chem. Soc.* **2016**, *138*, 7484–7487.
- [81] J. J. Willis, E. D. Goodman, L. Wu, A. R. Riscoe, P. Martins, C. J. Tassone, M. Cargnello, *J. Am. Chem. Soc.* **2017**, *139*, 11989–11997.
- [82] J. J. Willis, A. Gallo, D. Sokaras, H. Aljama, S. H. Nowak, E. D. Goodman, L. Wu, C. J. Tassone, T. F. Jaramillo, F. Abild-Pedersen, M. Cargnello, *ACS Catal.* **2017**, *7*, 7810–7821.
- [83] I. Friberg, A. H. Clark, P. H. Ho, N. Sadokhina, G. J. Smales, J. Woo, X. Auvray, D. Ferri, M. Nachtegaal, O. Kröcher, L. Olsson, *Catal. Today* **2020**, *382*, 3–12.
- [84] Y. Cui, J. Zhu Chen, B. Peng, L. Kovarik, A. Devaraj, Z. Li, T. Ma, Y. Wang, J. Szanyi, J. T. Miller, Y. Wang, F. Gao, *J. Am. Chem. Soc.* **2021**, *1*, 396–408.
- [85] A. I. Osman, J. K. Abu-Dahrieh, F. Laffir, T. Curtin, J. M. Thompson, D. W. Rooney, *Appl. Catal. B* **2016**, *187*, 408–418.
- [86] K. Khivantsev, N. R. Jaegers, L. Kovarik, M. Wang, J. Z. Hu, Y. Wang, M. A. Derewinski, J. Szanyi, *Appl. Catal. B* **2021**, *280*, 119449.
- [87] J. Sommer, R. Jost, M. Hachoumy, *Catal. Today* **1997**, *38*, 309–319.
- [88] M. J. Truitt, S. S. Toporek, R. Rovira-Hernandez, K. Hatcher, J. L. White, *J. Am. Chem. Soc.* **2004**, *126*, 11144–11145.
- [89] Y. Xie, L. Zhang, Y. Jiang, S. Han, L. Wang, X. Meng, F.-S. Xiao, *Catal. Today* **2021**, *364*, 16–20.
- [90] K. Persson, A. Ersson, S. Colussi, A. Trovarelli, S. G. Järås, *Appl. Catal. B* **2006**, *66*, 175–185.
- [91] M. Cargnello, J. J. D. Jaen, J. C. H. Garrido, K. Bakhmutsky, T. Montini, J. J. C. Gamez, R. J. Gorte, P. Fornasiero, *Science* **2012**, *337*, 713–717.
- [92] M. S. Wilburn, W. S. Epling, *Appl. Catal. A* **2017**, *534*, 85–93.
- [93] M. S. Wilburn, W. S. Epling, *Emiss. Control Sci. Technol.* **2018**, *4*, 78–89.
- [94] M. S. Wilburn, W. S. Epling, *Appl. Catal. B* **2017**, *206*, 589–598.
- [95] M. S. Wilburn, W. S. Epling, *Catal. Today* **2019**, *320*, 11–19.
- [96] H. Nassiri, K.-E. Lee, Y. Hu, R. E. Hayes, R. W. J. Scott, N. Semagina, *ChemPhysChem* **2017**, *18*, 238–244.
- [97] T. S. Nguyen, P. McKeever, M. Arredondo-Arechavala, Y. C. Wang, T. J. A. Slater, S. J. Haigh, A. M. Beale, J. M. Thompson, *Catal. Sci. Technol.* **2020**, *10*, 1408–1421.
- [98] K. Giewont, E. A. Kyriakidou, E. A. Walker, *J. Phys. Chem. C* **2021**, *125*, 15262–15274.
- [99] P. Mars, D. W. Van Krevelen, *Chem. Eng. Sci.* **1954**, *3*, 41–59.
- [100] E. D. Goodman, A. A. Ye, A. Aitbekova, O. Mueller, A. R. Riscoe, N. Taylor, A. S. Hoffman, A. Boubnov, K. C. Bustillo, M. Nachtegaal, S. R. Bare, M. Cargnello, *J. Chem. Phys.* **2019**, *151*, 154703.
- [101] D. Ciuparu, M. R. Lyubovskiy, E. Altman, L. D. Pfefferle, A. Datye, *Catal. Rev.* **2002**, *44*, 593–649.
- [102] A. M. Doyle, R. Postolache, D. Shaw, R. Rother, L. Tosheva, *Microporous Mesoporous Mater.* **2019**, *285*, 56–60.
- [103] K. Murata, J. Ohyama, Y. Yamamoto, S. Arai, A. Satsuma, *ACS Catal.* **2020**, *10*, 8149–8156.
- [104] K. Murata, Y. Mahara, J. Ohyama, Y. Yamamoto, H. Arai, A. Satsuma, *Angew. Chem. Int. Ed.* **2017**, *56*, 15993–15997; *Angew. Chem.* **2017**, *129*, 16209–16213.
- [105] B. J. Adelman, W. M. H. Sachtler, *Appl. Catal. B* **1997**, *14*, 1–11.
- [106] Y. Zhang, Catalytic Oxidation of Methane, Technical University of Denmark, **2019**.

- [107] K. Murata, T. Shiotani, J. Ohyama, R. Wakabayashi, H. Maruoka, T. Kimura, A. Satsuma, *Catal. Sci. Technol.* **2021**, *11*, 2374–2378.
- [108] C. Cui, Y. Zhang, W. Shan, Y. Yu, H. He, *J. Environ. Sci.* **2022**, *112*, 38–47.
- [109] Y. Xu, X. Chen, Z. Wang, S. Fan, W. Zhang, H. Liu, Y. Zheng, *Int. J. Hydrogen Energy* **2021**, *46*, 15526–15538.
- [110] B. Cen, W. Wang, P. Zhao, C. Liu, J. Chen, J. Lu, M. Luo, *Catal. Lett.* **2021**, *152*, 863–871.
- [111] K. Murata, D. Kosuge, J. Ohyama, Y. Mahara, Y. Yamamoto, S. Arai, A. Satsuma, *ACS Catal.* **2020**, *10*, 1381–1387.
- [112] J. Xiong, J. Yang, X. Chi, K. Wu, L. Song, T. Li, Y. Zhao, H. Huang, P. Chen, J. Wu, L. Chen, M. Fu, D. Ye, *Appl. Catal. B* **2021**, *292*, 120201.

Manuscript received: December 17, 2021
Revised manuscript received: March 4, 2022
Accepted manuscript online: April 1, 2022
Version of record online: April 21, 2022

3 Construction of catalytic test setup

This section details a critical part of the PhD project. Not only did the design and construction of the test setup represent a significant fraction of the three years of the PhD, it also constituted a small research project in itself. The motivation for including this section in the main thesis instead of as an appendix is multifaceted:

- The test setup and its features are essentially the core of the PhD project, and the success of the catalytic experiments performed is a direct consequence of the design effort.
- The design considerations for the test setup show that awareness of realistic testing conditions were indeed something that pervaded the whole project from start to finish.
- One purpose of this thesis is to document the research contribution of the PhD project. Considering the impact of studies that will be performed on the test setup in the future, it is possibly the single biggest contribution to research of the entire PhD project.
- The constructed test setup is possibly the most advanced of its kind for complete methane oxidation, involving far more features and reaction specific control parameters than its international counterparts that are often built more flexibly towards multiple reactions and purposes.

3.1 Requirements

Complete methane oxidation is a simple, yet extremely condition dependent reaction. It is very sensitive to a myriad of parameters and catalysts will undergo multiple interconnected deactivation phenomena. The approach in most literature is to isolate the various challenges and attempt to solve them one at a time; a completely reasonable approach given that the complexity of the system would otherwise complicate rational catalyst design. However, what seems to happen in many cases is that overly simplistic experiments are performed, so much so that potential positive results can be difficult to reproduce under more realistic conditions. The first part of the design process therefore consisted of going through recent literature to collect a list of pitfalls to avoid. This list is shown in Table 2.

Table 2 Features seemingly lacking in catalytic test setups used for complete methane oxidation in literature. Specific references are intentionally not included, but the occurrence rate of the listed items in methane oxidation literature is high.

Challenge	Explanation
Low measurement frequency	Many use a GC-MS for quantification which has the major advantage of being able to measure most outlet gas species. However, the time between injections is typically between 5 and 15 minutes, resulting in a very low data density.
Low measurement accuracy	The signal-to-noise ratio of some published work is likely insufficient to see certain sensitive phenomena and to perform in-depth analysis of the data. This is likely caused by a combination of poor gas flow control and unstable quantification methods.
Too high methane concentration	A methane slip of 0.36-7.8% results in an exhaust containing 180-3900 ppm CH ₄ . In a lot of literature however, 10 000 ppm (1%) methane is used, significantly higher than what can be considered realistic. The adiabatic temperature rise for complete methane oxidation is 306 °C for each percent of methane converted. This will inevitably heat up the catalyst bed and skew results.
Insufficient water dosing	The exhaust of a natural gas-fired engine contains about 10% water. In a lot of literature about wet methane oxidation however, only 2-4% water is added, likely due to instrumental limitations.
No SO ₂ or CO ₂ dosing	The exhaust from a natural gas-fired engine is complex and contains many pollutants. Seeing as the primary challenges to overcome in the development of durable methane oxidation catalysts is tolerance to various poisons, it seems highly relevant to include known poisons and major exhaust components.
Simple experiments	Light-off experiments dominate the field of methane oxidation. To advance from these simplistic experiments, that offer limited knowledge gain, a programmable test setup is required.
No pressure elevation	Being able to test catalysts at elevated pressure is increasingly relevant, but requires specialized equipment and precautions. Few seem to have prioritized to include this option in their test setup.

Based on the observations in literature, knowledge the of real-world application, and on the overall goals for the PhD project, a list of requirements for the test setup was formulated:

- Online quantification
 - High accuracy measurements
 - Possibility to accurately add between 1 and 20% water
 - Possibility to add ppm levels of SO₂ and 5% CO₂
 - Automation and programmability for extended experiments
 - Possibility to elevate reactor pressure
 - Possibility to swap or add new pollutant gasses, like CO, NO_x, etc.
-

3.2 Equipment choices and automation software

The basic layout for the test setup consisted of three parts. A segment for mixing of feed gas, a segment containing the heated reactor, and a segment for outlet quantification. A complete piping and instrumentation diagram can be seen in Appendix A. For planning the actual construction, a more dimension-realistic construction drawing was prepared, shown in Appendix B. A handful of photos showing segments of the test setup are presented in Appendix I. The various components will be described in the following section.

Tubing, gas line features, and mass flow controllers

For practical reasons, and to protect the sensitive flow meters, the gas lines were designed with filters and needle valves before the mass flow controllers and check valves after. The tubing itself was 1/8" stainless steel from Swagelok with a wall thickness of 0.028". A flow of 420 ml/min would correspond to a linear flow velocity of 2.9 m/s, enough to ensure a quick response time when changing between gas compositions. The mass flow controllers used were of the model EL-FLOW Select from Bronkhorst.

Gasses

By consulting emission data from engine manufacturers and scientific literature, a methane oxidation model gas was composed to represent the emission gas from natural gas-fired engines. With a very wide range for methane slippage, as shown in Table 1, 1000 ppm was selected as a representative value. The range of the specific mass flow controller enabled concentrations from 100 to 2500 ppm. The model gas composition is shown in Table 3. Using diluted gases was necessary for realizing the low model gas concentrations of e.g. SO₂. This had the added benefit of avoiding explosive or overly toxic gasses to be stored in shared labs, at the cost of increased gas consumption and more frequent bottle replacement.

Table 3 Model gas composition used in the design of the catalytic test setup, and the type of gas bottles delivering the various components. The exact gas composition for a catalytic test varies from experiment to experiment, but this composition is considered "realistic" in the context of the PhD project.

Gas	Concentration	Source
CH ₄	1000 ppm	2% in N ₂
O ₂	10%	21% in N ₂
H ₂ O	10%	Deionized water
CO ₂	5%	Pure CO ₂
SO ₂	2 ppm	100 ppm in N ₂
N ₂	Balance	Pure N ₂

Water addition to feed gas

As water-induced deactivation is one of the major challenges to be overcome in methane oxidation catalyst development, the ability to add an accurate, stable, and sufficient amount of steam to

the feed gas is critical. For this purpose, a controlled evaporator-mixer (CEM) from Bronkhorst was used. It was fed from a custom-built water container pressurized with nitrogen. To avoid condensation of water in the gas line, it was heat traced from the outlet of the CEM to the inlet of the last detector. Additionally, the heat tracing was set to a temperature high enough to avoid condensation of sulfuric acid. With a catalyst likely able to oxidize SO_2 to SO_3 , and a pressurized gas containing high amounts of steam, formation of sulfuric acid via the reaction between SO_3 and H_2O could not be ruled out. Calculations of the dew point of sulfuric acid were performed according to the work of Verhoff and Banchero.¹¹²

Reactor and furnace

Catalysts for complete methane oxidation require high temperatures to operate. For catalytic testing on milligram scale, a quartz reactor placed inside a tube furnace is a common choice. Despite its fragility, quartz was preferred over a stainless steel reactor, both for practical reasons and because it is a more inert material. 400 mm quartz reactors with an inner diameter of 10 mm were acquired from Ballerup Glas. Positioning the reactor and furnace in a vertical orientation meant that convection would create an airflow upwards in the furnace channel around the reactor. For this and other reasons, the temperature across the length of the reactor would not be constant. As the catalytic bed itself had a non-zero length, the temperature gradient across it needed to be minimized. For this, a temperature profile of the reactor was measured at three different furnace temperatures while flowing nitrogen gas through the reactor to simulate the cooling effect of the feed gas. Based on these, a 50 mm isothermal zone was determined, centered around the point of highest temperature. The bed, at an estimated average length of 18 mm, was to be positioned in the end of the isothermal zone, to allow for optimal preheating of the reaction gas. The quartz filter of the reactor was then positioned 12 mm from the catalyst bed to allow for the placement of a quartz wool plug and quartz sand to get a leveled and flat base for the bed. Figure 8 shows the temperature profiles of the reactor during stable furnace temperature, $T = 300, 400, 500\text{ }^\circ\text{C}$, along with lines indicating the position of the furnace openings, the isothermal zone, the approximate bed position, and the quartz filter.

To accurately monitor the reactor temperature in the bed and not just the furnace temperature, a thermocouple was installed, just touching the bottom of the quartz filter, after the catalyst bed. Opting for controlling the temperature inside the reactor directly instead of the furnace temperature introduced a significant delay, as heat had to transfer to the air in the furnace, then to the walls of the reactor, and then to the gas in the reactor. This delay significantly complicated temperature control, so a PID control loop was introduced. After a series of failed manual attempts, controller tuning was performed using the Ziegler–Nichols method, resulting in PID terms of $P = 0.5$, $I = 8$, $D = 10$, which were then fed into the control software.

Pressure regulation in the reactor

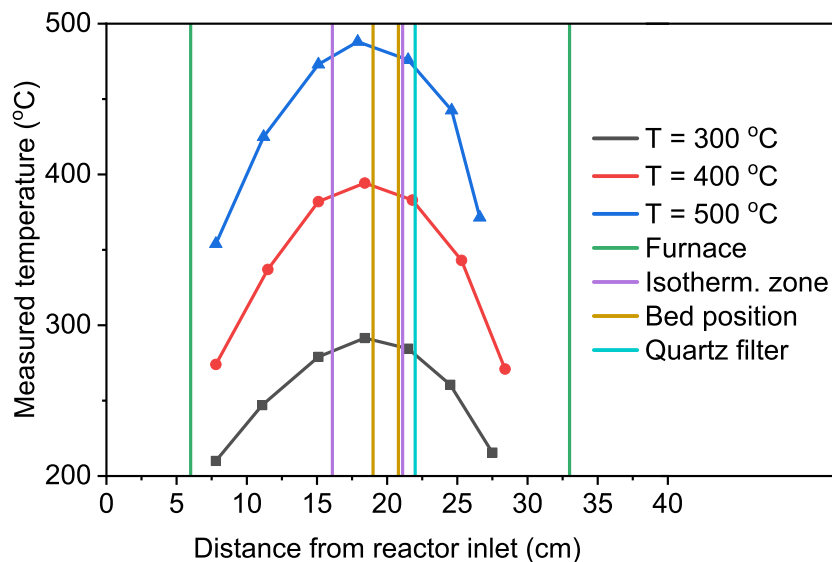


Figure 8 Temperature measurements of the reactor during simulated catalytic testing at three different temperatures. The goal was to determine an isothermal zone of the furnace-reactor system, for correctly positioning the catalytic bed.

Due to the option of a catalyst placement upstream of the turbo-charger, as described in Section 2.3, being able to increase the reactor pressure in the test setup was assessed to be relevant. For this purpose, a LF Series Precision Back Pressure Regulator was acquired from Equilibar. A back pressure regulator (BPR) is essentially a valve maintaining a defined pressure upstream of its own inlet by restricting flow until the pressure setpoint is reached. This requires gasses to, at all times, be fed to the mass flow controllers at a pressure higher than the highest possible process pressure.

Detectors for outlet gas quantification

Complete methane oxidation is a simple reaction in which tracking just one species, methane, is sufficient as long as side reactions are not occurring. For continuous measurements of just methane, a standalone flame ionization detector (FID) is an excellent option due to its accuracy and low maintenance requirements. The main drawback of an FID is the narrow scope of analytes, essentially just hydrocarbons, but for that it is great. An FID converts hydrocarbons to CO_2 in the measuring process, so naturally it has to be last in the detector train. In this project, a Thermo-FID ES from SK Elektronik was used. To be able to close the atom balance, and verify that methane was being oxidized all the way to carbon dioxide, and not just e.g. carbon monoxide, a secondary detector was necessary. A BINOS-100 from Rosemount Analytical was used for quantifying CO and CO_2 in the outlet gas. This non-dispersive infrared (NDIR) detector had some amount of cross sensitivity between H_2O and CO_2 , so water had to be condensed in a cold trap just before the detector inlet. The BINOS was only used occasionally to verify the absence of side reactions. The detectors were calibrated before every experiment with a common calibration gas consisting of 500 ppm CH_4 , 2.5% CO_2 , and 100 ppm CO in N_2 using pure N_2 as zero-gas.

Safety measures

Safety was, for obvious reasons, a critical design parameter for the test setup. Firstly, the furnace was fitted with both hardware and software to prevent overheating in case of a partial power outage or system failure. The SO₂ gas line was connected to a secondary N₂ line and a ventilation line, to allow for flushing in case it had to be taken apart and whenever the gas bottle was swapped out. Industrial-grade pressure relief valves from Leser were positioned along the gas line in positions with a hypothetical risk of rapid over pressure in case of the following sequence of events: Heat tracing failure → water condensation → heat tracing reestablished → condensate evaporation and rapid expansion. Further, the setup was placed inside a ventilated polycarbonate cupboard to mitigate the risk of leaks and to prevent quartz shards from flying around in case of a reactor failure.

Software and automation

For controlling the test setup and collecting data from the various instruments and sensors, a virtual control panel was put together in LabView. The front end of the control panel can be seen in Appendix L. Step-wise experiments were programmed in a spreadsheet where each step contained a setpoint temperature, ramp speed, hold time, total flow, total pressure, and concentration of the various gasses. The control software would then convert the file to timestamped setpoints for the various instruments, run the loaded experiment, and generate a log file with second-by-second setpoints and process value readings from thermocouples, gas detectors, mass flow controllers, back-pressure regulator, differential pressure gauge, CEM temperature, and furnace output. It cannot be counted how many times the exhaustive log file enabled fast troubleshooting and how much having it available directly contributed to research findings. Having an automated and programmable setup enabled an estimated up-time of 75% over 1.5 years of intensive testing, resulting in roughly 10 000 hours of testing data, about 2000 of which made it into the thesis or the manuscripts in some form.

4 Project 1: Rational design of a durable catalyst for methane oxidation using zeolite encapsulation

Catalysts for complete methane oxidation have historically suffered from three different modes of deactivation; water-induced deactivation, SO_2 poisoning, and hydrothermal sintering, each described in Section 2. Researchers have employed a wide range of catalyst designs in their attempt to prevent deactivation, typically by isolating the three modes and working on them individually. In recent literature, significant progress has been reported for all three deactivation types. However, a durable catalyst for complete methane oxidation needs to prevent all three modes of deactivation at the same time. Hypothetically, by utilizing the progress reported in literature and combining the catalyst designs shown to prevent the individual deactivation types, a durable catalyst could possibly be developed.

The original key idea for the PhD project was to design a hierarchical catalyst comprised of multiple components. Each component would assist in solving one or more of the challenges concerning catalyst deactivation. The approach was heavily inspired by recent literature on both general heterogeneous catalysis and methane oxidation. In 2016, Wang et al.¹¹³ published a clever synthesis of palladium nanoparticles fully encapsulated in the all silica zeolite Silicalite-1 (S-1). Encapsulation of active metal nanoparticles in the porous network of a zeolite have been shown to prevent sintering.^{28,37,50} As described in Section 2.5, zeolites can be very hydrophobic which has been used for improving the water-tolerance in methane oxidation catalysts.^{32,37,38} The promising potential of hydrophobic zeolites as support material for methane oxidation catalysts was covered in Paper 1. An alternative to the procedure developed by Wang et al. for encapsulating metal nanoparticles inside Silicalite-1 was recently developed by Rasmussen et al.¹¹⁴ It involves significantly more steps, as the metal nanoparticles are not formed in-situ during zeolite crystallization, but allows for more flexibility and a wider selection of active metals. This procedure was assessed to be ideal for the envisioned hierarchical catalyst design where complete control over the synthesis was, to begin with, valued over efficiency. For preventing the final mode of deactivation, SO_2 poisoning, we looked to the many studies which have found that supporting palladium on redox-active metal oxides can improve catalytic properties, and in many cases SO_2 tolerance.^{115–119} The novel material conceptualized for this project essentially combines zeolite encapsulation with a metal oxide support to protect the palladium oxide nanoparticles from both sintering, water deactivation, and SO_2 poisoning while keeping low temperature activity reasonably high. This concept is illustrated in Figure 9 where a rough synthesis pathway is also presented.

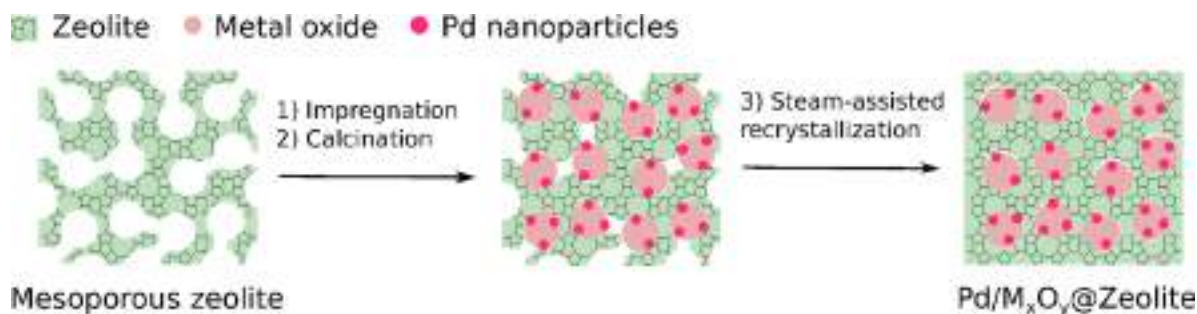


Figure 9 Catalyst design concept and synthesis outline for the zeolite encapsulation project. First, a mesoporous starting material is prepared by growing Silicalite-1 around a carbon template. The active components are then added through impregnation and nanoparticles are formed during calcination. The open mesoporous network is closed by a recrystallization step, encapsulating both the palladium and the metal oxide. The figure was prepared by co-supervisor Jerrik Mielby.

4.1 Material synthesis

All chemicals used for material synthesis were reagent grade, purchased from Merck/Sigma Aldrich, and used without further purification.

4.1.1 Pd/MO_x@S-1

5 grams of mesoporous Silicalite-1 were synthesized by impregnating 8 grams of spherical carbon particles (20-40 nm) with 29.06 grams of 20% (1M in H₂O) tetrapropylammonium hydroxide (TPAOH). After overnight drying, the powder was impregnated with 16.66 grams of tetraethyl orthosilicate (TEOS) after which it was dried overnight again. The powder was then transferred to a small polytetrafluoroethylene (PTFE) beaker and placed inside a PTFE-lined 500 ml stainless steel autoclave with 60 ml H₂O in the bottom of the autoclave liner. The autoclave was sealed and heated to 180 °C for 72 hours. After the autoclave had cooled down, the zeolite-covered carbon powder was collected and washed until neutral pH. It was then dried and calcined for 20 hours at 550 °C.

For synthesizing approximately 1.3 grams of catalyst, to 1 gram of mesoporous S-1 was added dropwise a solution of the relevant metal nitrate dissolved in 0.2 ml H₂O. For producing a material with 1 wt% Pd and 10 wt% CeO₂, 37.3 mg Pd(NO₃)₂·2H₂O and 391.6 mg Ce(NO₃)₃·6H₂O were required. The impregnated powder was stirred for 30 minutes and dried overnight. It was calcined for 2 hours at 250 °C to decompose the nitrates. The calcination temperature was kept relatively low to avoid unnecessary nanoparticle sintering. For growing a recrystallized shell around the zeolite particles, closing the mesopores, 1.2 grams of 40% (2M in H₂) TPAOH were impregnated onto the calcined powder. A more concentrated TPAOH solution had to be used as to not wet the powder excessively. After overnight drying, 1.43 grams of TEOS were impregnated onto the powder, and it was dried again. The powder was then transferred to a small PTFE beaker and placed inside a

PTFE-lined 200 ml stainless steel autoclave with 15 ml H₂O in the bottom of the autoclave liner. The autoclave was sealed and heated to 180 °C for 72 hours. After the autoclave had cooled down, the recrystallized material was collected and washed until neutral pH. It was then dried and calcined for 20 hours at 550 °C.

4.1.2 Pd@S-1 and PdPt@S-1

For producing 2 grams of zeolite catalyst, 16.17 grams of 20% (1M) TPAOH were diluted with 22.05 grams of H₂O and stirred for 10 minutes. 8.32 grams of TEOS were added, and the mixture was stirred for 6 hours. This hydrolysed the Si-O bonds in the TEOS and resulted in a clear gel. For synthesizing a material with 1 wt% Pd, 0.048 grams of Pd(NO₃)₂·2H₂O were dissolved in 3 ml H₂O. To this, 0.3 ml ethylenediamine (EN) were added to form a solution of Pd(EN)₂ complexes. The Pd solution was added dropwise to the silica gel and the mixture was stirred for another 30 minutes before it was transferred to a PTFE-lined 200 ml stainless steel autoclave. The autoclave was sealed and heated to 180 °C for 24 hours. After the autoclave had cooled down, the zeolite powder was collected by filtration and washed three times in water and three times in ethanol. It was then dried overnight and calcined for five hours at 550 °C. For producing catalysts with both Pd and Pt, a mixed precursor liquid of both metal complexes was used. Metal-free S-1 was synthesized using the same procedure where the metal complexes were omitted.

4.1.3 Others

Chen et al.¹²⁰ recently published an alternative, and potentially fast, method for synthesizing mesoporous Silicalite-1. The method involves a recrystallization step to close the mesopores around the added metal nanoparticles. The method is termed “filtrate recrystallization” in this thesis and is summarized in the following. Instead of synthesizing mesoporous S-1 through carbon templating, mesoporosity is introduced to conventional S-1 by a treatment with TPAOH. The base selectively dissolves part of the zeolite, creating cavities in its surface. The solid is collected and the filtrate, containing both TPAOH structure directing agent and Si building blocks, is saved for later. After washing, drying, and calcining the solid, a solution of metal precursors is added and it is calcined again to decompose the metal complexes. The solid is then impregnated with the filtrate from the TPAOH treatment and the mixture is recrystallized, closing the mesopores with a new layer of S-1.

In an effort to make more hydrophobic Pd@S-1, it was attempted to reduce the number of silanol defects through a treatment with hydrofluoric acid.^{121–124} The procedure was inspired by Bregante et al.¹²¹ and is summarized here. The synthesis was identical to that of conventional Pd@S-1 with the following exceptions:

- Between TEOS addition and Pd(EN)₂ addition, 636 µl 50% HF was added during vigorous stirring.

- After $\text{Pd}(\text{EN})_2$ addition, 120 mg S-1 powder was added as seed crystals and stirred with the gel for 10 minutes.
- The zeolite was allowed to precipitate from the gel for 48 hours instead of 24.
- After collecting the zeolite powder by filtration, the filtrate was neutralized with excess CaCO_3 .

For most of the project, a 2.4 wt% $\text{Pd}/\text{Al}_2\text{O}_3$ oxidation catalyst from Umicore was used as reference during catalytic testing. For the early parts of the project however, a simple 1 wt% $\text{Pd}/\text{Al}_2\text{O}_3$ was synthesized by impregnating a concentrated palladium nitrate solution onto crushed high surface area γ -alumina pellets. 27.4 mg $\text{Pd}(\text{NO}_3)_2 \cdot 2\text{H}_2\text{O}$ was dissolved in 0.2 ml H_2O and added to 1 gram alumina powder crushed to $<500\mu\text{m}$. It was then dried overnight and calcined for 1 hour at 250°C and for 6 hours at 600°C .

4.2 Catalytic results

The steam-assisted recrystallization synthesis of $\text{Pd}/\text{MO}_x@\text{S-1}$ was not very reproducible in terms of catalytic activity. About half the batches would barely have any activity at all. The batches which had activity were however very similar and the catalytic results shown in this section are from a successful synthesis of $\text{Pd}/\text{CeO}_2@\text{S-1}$. Under dry and SO_2 -free conditions, it was comparable to a $\text{Pd}@\text{S-1}$ material with similar Pd loading. However, compared to catalysts supported on alumina, the activity was low, as can be seen in Figure 10.

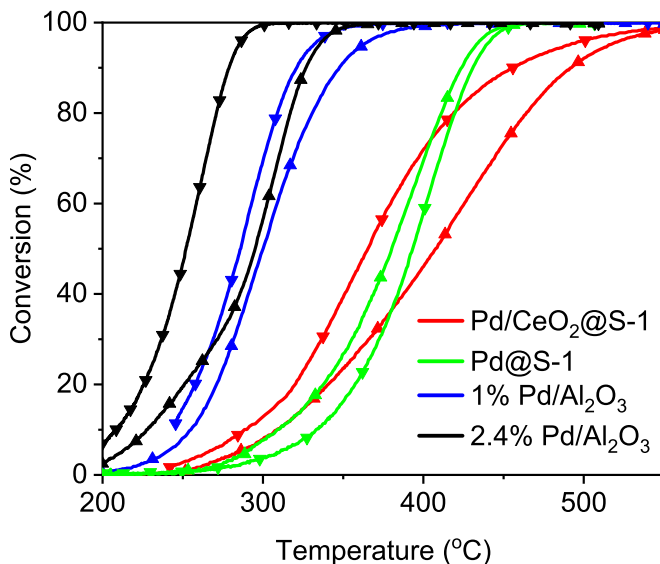


Figure 10 Light-off curves of encapsulated palladium catalysts and alumina-supported catalysts. Reaction conditions: 1000 ppm CH_4 , 10% O_2 , 5% CO_2 , N_2 balance, $\text{WHSV} = 126\,000\text{ ml h}^{-1}\text{ g}^{-1}$.

The stability under dry and SO_2 -free conditions of the $\text{Pd}/\text{CeO}_2@\text{S-1}$ catalyst was good, as shown in Figure 11.

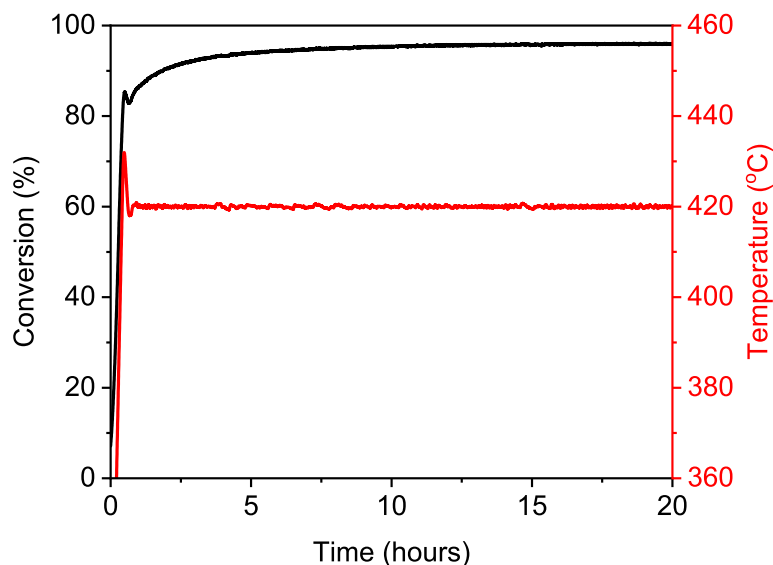


Figure 11 20-hour catalytic test of Pd/CeO₂@S-1 material. Reaction conditions: 1000 ppm CH₄, 10% O₂, 5% CO₂, N₂ balance, WHSV = 126 000 ml h⁻¹ g⁻¹.

The exhaust from a natural gas-fueled large engine is neither dry nor SO₂-free however. Figure 12 shows a series of light-off experiments where the activity of the catalyst is measured in the presence of water and SO₂ and compared to the activity of a Pd/Al₂O₃ reference catalyst.

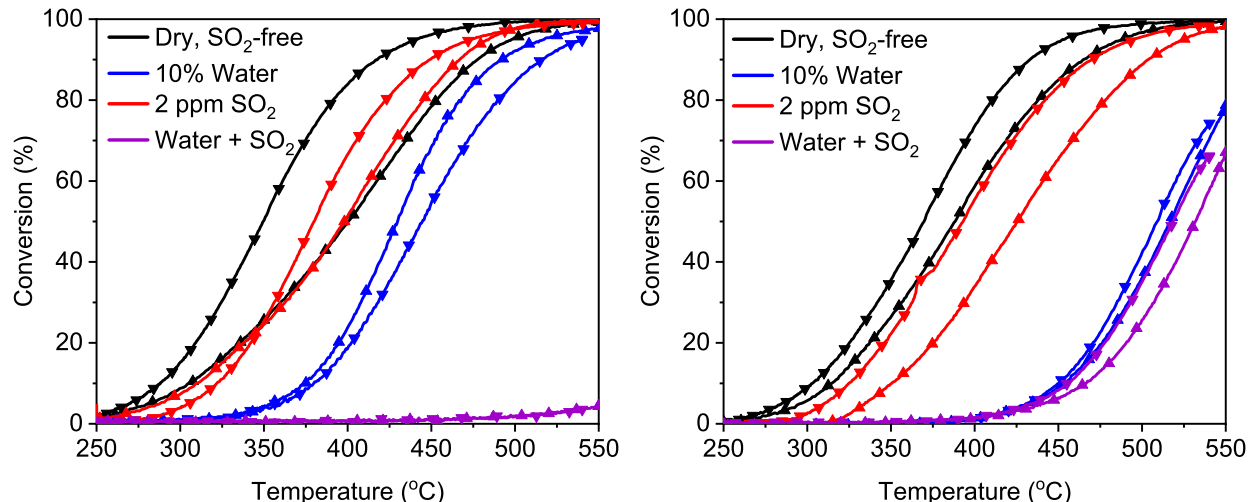


Figure 12 Light-off experiments with Pd/CeO₂@S-1 catalyst (left) and 1 wt% Pd/Al₂O₃ reference (right). Reaction conditions: 1000 ppm CH₄, 10% O₂, 5% CO₂, 10% H₂O (when present), 2 ppm SO₂ (when present), N₂ balance, WHSV = 126 000 ml h⁻¹ g⁻¹.

In the light-off tests, the Pd/CeO₂@S-1 catalyst has a higher immediate activity than the reference in the presence of water and SO₂ individually. When exposed to a feed gas containing both water and SO₂ however, it has barely any activity at all. Light-off tests are not the best method of assessing catalyst stability or tolerance to pollutants, although they are frequently used for that

purpose in methane oxidation literature. When testing the catalyst with either water or SO₂ in the feed gas for extended periods of time, it deactivates severely, as can be seen in Figure 13.

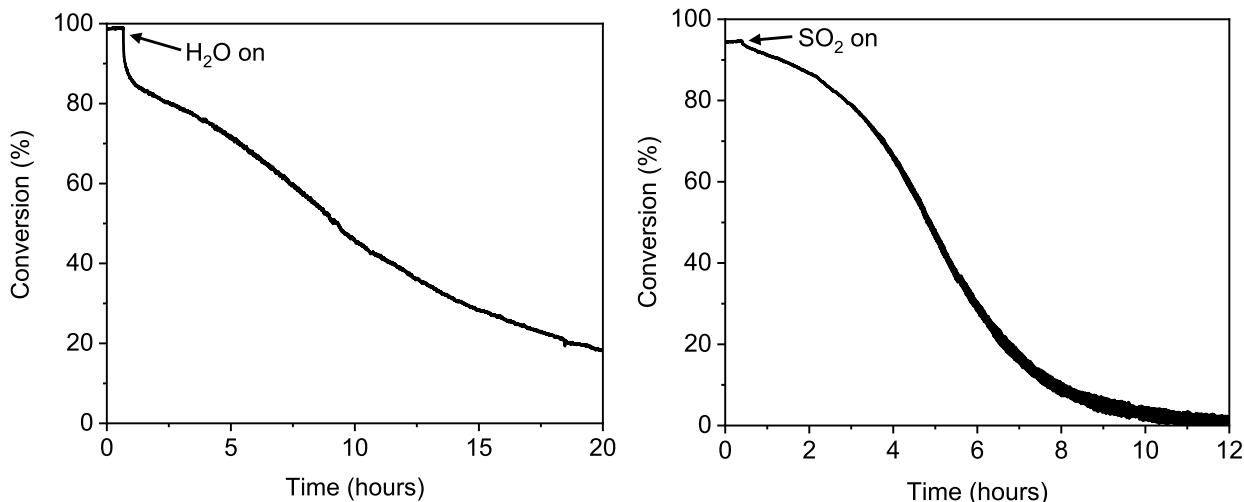


Figure 13 Left: Deactivation by water at 500 °C. Right: Deactivation by SO₂ at 420 °C. Reaction conditions: 1000 ppm CH₄, 10% O₂, 5% CO₂, 10% H₂O (when present), 2 ppm SO₂ (when present), N₂ balance, WHSV = 126 000 ml h⁻¹ g⁻¹.

Although the deactivation from water and SO₂ is extensive, it could arguably be a lot worse, and maintaining significant conversion after 20 hours of methane oxidation in the presence of 10% water is not bad. The effects of, and reasons for, water-induced deactivation will be discussed further described in Section 6. At the time of performing these experiments, the result seemed mediocre at best compared to the catalytic performance reported in literature, much of which employed similarly synthesized S-1 catalysts.^{37–39,125–129} As explained previously, one premise of the catalyst concept was the ability of the hydrophobic Silicalite-1 support to shield the active palladium nanoparticles against water-induced deactivation. As detailed in Paper 1, this feature had received significant support in literature. Taking a step back, it was natural to replicate the synthesis of those who had accomplished near-complete water tolerance with a Pd@S-1 catalyst. This well-defined task was formulated as a Master’s Thesis Project and a student was brought on to assist in the investigation, Panagiotis Dimitriou 2021.¹³⁰ A Pd@S-1 material was successfully synthesized using the in-situ encapsulation procedure originally published by Wang et al.¹¹³ which later inspired a significant amount of work on methane oxidation catalysts. In the masters project, many batches of the same material were synthesized and activity tested. As with the steam-assisted recrystallization synthesis of Pd/CeO₂@S-1, about half of the attempts did not produce an acceptable material. In some cases the powder was grainy or contained significant amounts of discolored particles, in others the activity was almost non-existent. When the synthesis was successful, a homogeneous-looking fine powder was produced with reproducible activity across the different batches. These were then mixed and the combined sample assumed to represent a successful synthesis of Pd@S-1. Figure 14 shows a

catalytic test of the material in the presence of SO₂ and water.

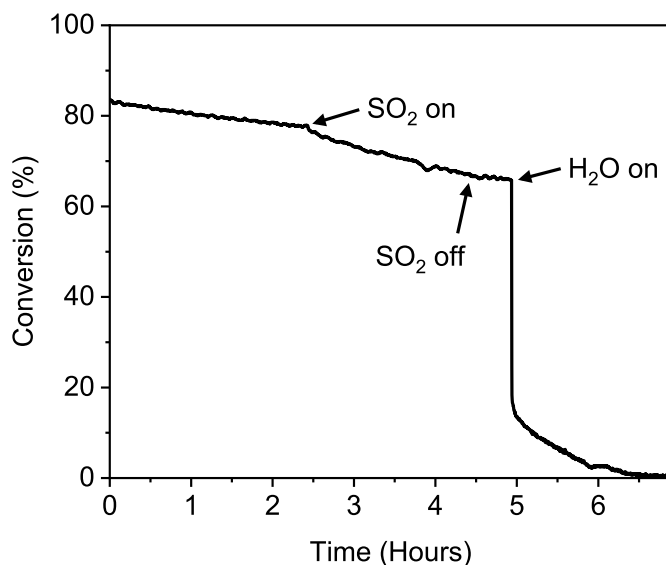


Figure 14 Catalytic test of Pd@S-1 material synthesized in MSc project. Reaction conditions: 1000 ppm CH₄, 10% O₂, 5% CO₂, 10% H₂O (when present), 2 ppm SO₂ (when present), N₂ balance, WHSV = 126 000 ml h⁻¹ g⁻¹, T = 430 °C. Adapted from MSc. project by Panagiotis Dimitriou.¹³⁰

The catalyst deactivated slightly even under dry and SO₂ free conditions. Curiously, upon exposure to SO₂, the deactivation only accelerated slightly. When exposed to water however, the catalyst quickly lost all activity. The water tolerance was far from what had been published in literature of materials synthesized using an identical procedure. This discrepancy will be discussed further in Section 4.4.

Before abandoning the zeolite encapsulation project, a last concept needed to be evaluated. Palladium is recognized as the most active metal for methane oxidation, but alloying it with platinum can improve the water-tolerance.^{44,47,131,132} The ethylenediamine synthesis was originally designed for a Pd-based hydrogen evolution catalyst,¹¹³ but could potentially be applied to synthesize mixed palladium-platinum particles encapsulated in S-1. This was successfully done in another student project, where a series of PdPt@S-1 catalysts were produced, Frederik Feddersen and Signe Tronsen 2021.¹³³ As can be seen from Figure 15, a catalyst with both metals is more stable than its pure palladium counterpart, and deactivates less rapidly when exposed to a wet feed gas.

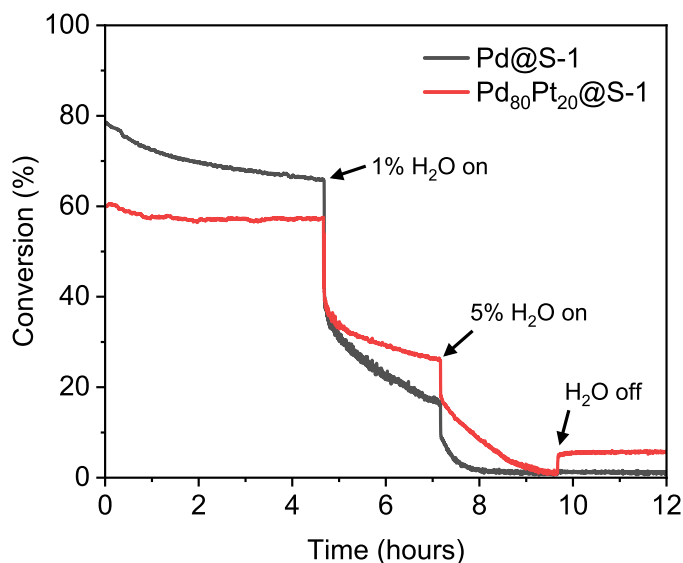


Figure 15 Catalytic test of a catalyst with both palladium and platinum compared to a pure palladium catalyst. The addition of platinum makes the catalyst deactivate more slowly when exposed to different concentrations of water. Reaction conditions: 1000 ppm CH₄, 10% O₂, 0-5% H₂O, 5% CO₂, N₂ balance, WHSV = 126 000 ml h⁻¹ g⁻¹, T = 500 °C. Adapted from BSc. project by Frederik Feddersen and Signe Tronsen.¹³³

Although the catalytic results from the student projects were not significantly more promising than those from the Pd/CeO₂@S-1 project, they provided important understanding of Silicalite-1 catalysts. A synthesis from literature was carefully replicated, over many attempts by four individuals, and the resulting material was confirmed to be of the intended structure by a series of characterization techniques, presented in the next section. The fact that the catalytic performance, especially the water-tolerance, was so far from what had been published in literature somewhat explained why the Pd/MO_x@S-1 materials had not been more successful. For this reason, a selection of the materials characterization done in collaboration with the students has been included in the next section where it was meaningful. Materials produced with the HF modification, filtrate recrystallization, and BaO as metal oxide all had little to no activity for methane oxidation and were therefore not tested further. For an example of what the catalytic performance looks like for a failed synthesis, see Appendix C.

4.3 Characterization

Although the catalytic performance was sometimes lacking, the synthesis of Silicalite-1 derived materials was almost always successful from a materials characterization perspective. The zeolitic support consisted of a single phase of MFI-structured Silicalite-1, as can be seen from the X-ray diffractogram in Figure 16. Also, broad peaks from both CeO₂ and PdO can be seen, indicating a relatively small particle size, as per the Scherrer equation.¹³⁴

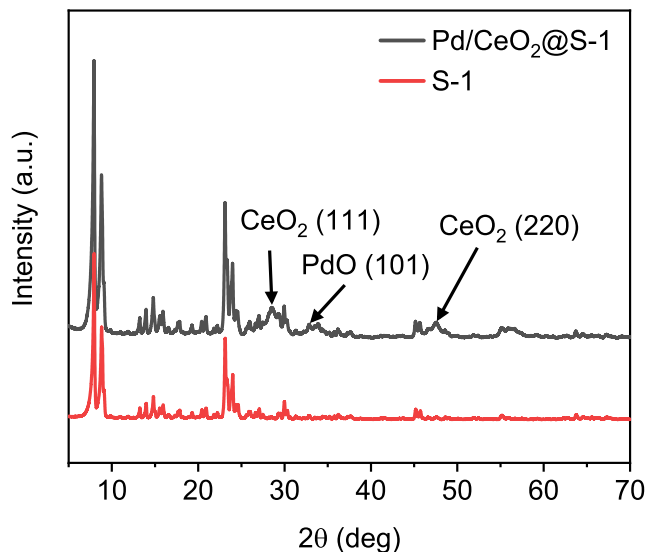


Figure 16 X-ray powder diffraction of Pd/CeO₂@S-1 and the metal-free support. The characteristic sets of double peaks from the MFI structure are clearly visible around $2\theta = 8^\circ$, 24° , and 46° .

It was often difficult to tell successful and failed synthesis attempts from each other based solely on characterization. An example of this is shown in Appendix C where XRPD's of two samples with drastically different methane oxidation activity are compared.

The synthesis method was also relatively successful in terms of incorporating the correct amount of metal oxide and precious metal. The Pd/CeO₂@S-1 material was synthesized to contain 1 wt% PdO and 10 wt% CeO₂. From the ICP-data in Table 4 it can be seen that both metal contents were about 20% below the target for the specific sample. Part of discrepancy comes from the fact that the recrystallization step involves growing new zeolite around the existing crystals from new TEOS, the zeolite precursor. When determining the amounts needed for the synthesis, it was assumed, based on previous results by others, that the growth of new zeolite would be around 10%, but in reality it was closer to 20%, lowering the relative concentrations of the active metals. The thickness of the encapsulating layer could potentially be reduced by tuning the recrystallization conditions in the autoclave to grow just enough new zeolite. The Pd@S-1 sample synthesized in a single step via the ethylenediamine in-situ route was closer to the 1% target. Both samples contained significant amounts of potassium, possibly from impurities of the precursors or deionized water used in the syntheses.

Table 4 Inductively coupled plasma - optical emission spectrometry (ICP-OES) data for zeolite-supported catalysts. Samples were prepared for injection by acid digestion. Measurements were performed by Umicore technicians in Analytical Competence Center Hanau, Germany.

Sample	PdO content (wt%)	CeO ₂ content (wt%)	K content (wt%)
Pd@S-1	0.88	n/a	0.54
Pd/CeO ₂ @S-1	0.82	8.05	0.53

Verifying that the palladium and cerium oxide had been incorporated into the material was followed up by electron microscopy to determine whether it was placed inside or on the external surface of the zeolite particles. The benefits of encapsulation concerning sintering prevention are only relevant if the active metal is dispersed in the cavities inside the zeolite and not on the external surface. A selection of transmission electron microscopy (TEM) images of a Pd/CeO₂@S-1 sample are shown in Figure 17.

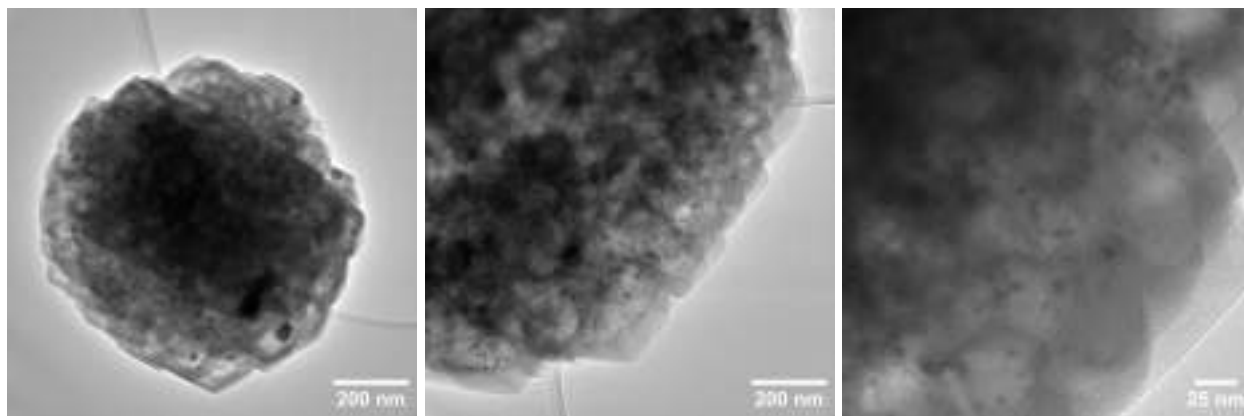


Figure 17 Bright-field TEM images of Pd/CeO₂@S-1. Images of a similarly synthesized material without catalytic activity can be seen in Appendix J.

The TEM micrographs reveal a lot of information about the sample:

- The roughly spherical Silicalite-1 crystals are of a size between 600 and 1000 nanometers.
- Inside the crystals are still mesopores originating from the carbon template, seen as lightly colored channels in the otherwise dark center of the particles.
- Dispersed homogeneously throughout the zeolite crystals, but not on the surface, are nanoparticles of heavier elements. They are between 5 and 15 nanometers in size.

It is a challenge that palladium and cerium are so close in atomic weight, since it makes it difficult to assess which of them are present in the nanoparticles visible in the TEM. On one hand, it would be reasonable to assume that PdO and CeO₂ are co-located as the impregnation liquid contained precursors for both. On the other hand, given the size and number of the visible particles, it is questionable if they can make up 9% of the sample mass, as per the ICP determination, even when they are much heavier than silicon. To accurately determine the distribution of palladium and cerium, a type of elemental mapping technique is required. Despite the novelty of the material and the interesting hierarchical concept, elemental mapping was not pursued due to the lacking catalytic performance and the reproducibility challenges. Materials combining precious metal nanoparticles, a metal oxide, and a zeolite support have been presented in literature,^{135–138} but never with our stepwise and highly controlled synthesis and never with this exact combination of components. If

an application can be found for the Pd/CeO₂@S-1 material, that would certainly be publishable.

Further attempts to synthesize Pd/MO_x@S-1 catalysts were not promising due to lacking catalytic performance. Figure 18 shows TEM images of a Pd/BaO@S-1 material which was synthesized. Several features stand out, especially the large and heavy objects around the particle surface. Generally the sample seemed less homogeneous and it was difficult to spot any nanoparticles, even from images of higher resolution than those shown here.

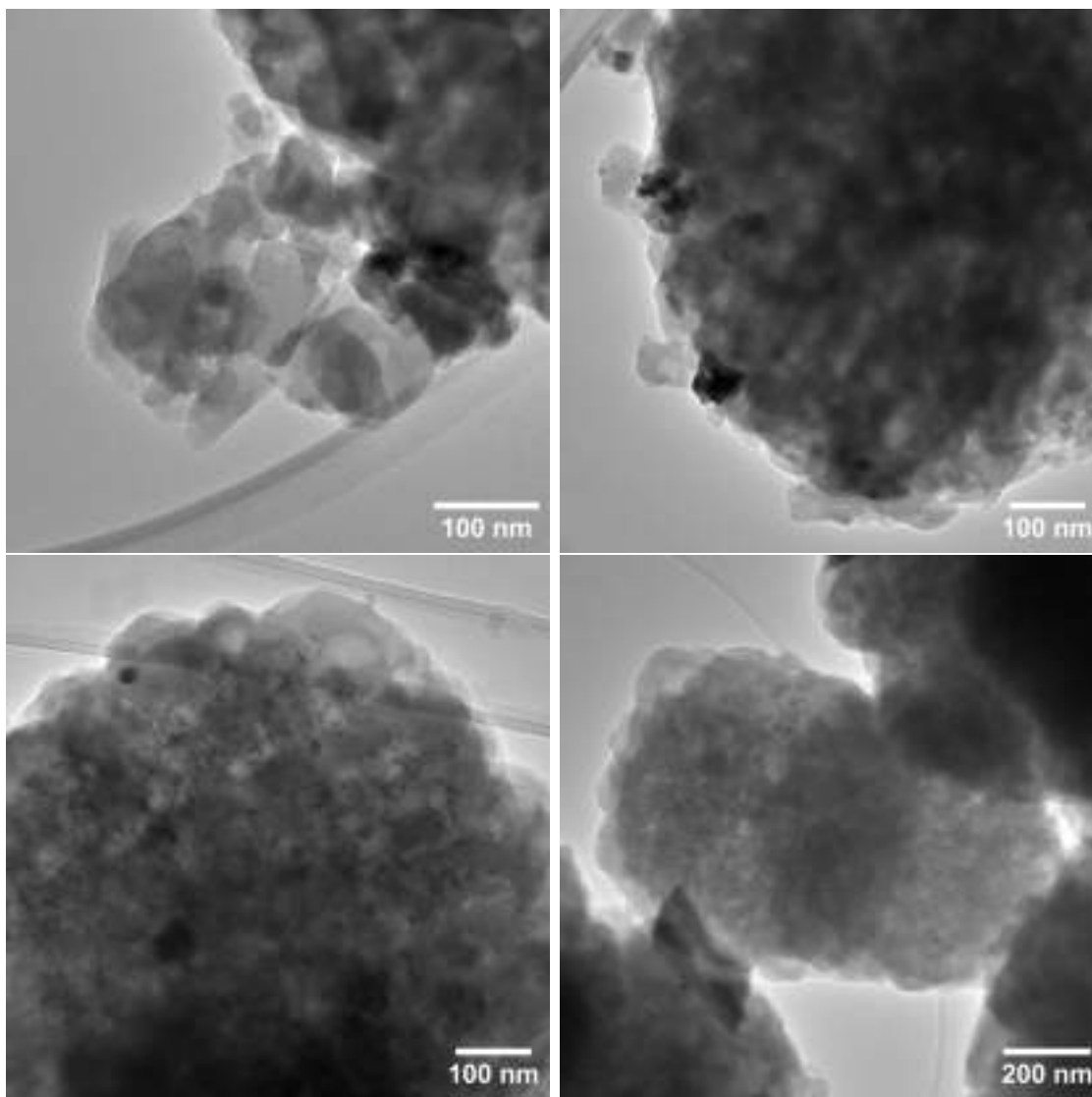


Figure 18 Bright-field TEM images of Pd/BaO@S-1.

In an attempt to speed up the synthesis of the Pd/MO_x@S-1 catalysts to improve iteration time, a faster method for making the mesoporous S-1 starting material was conceptualized. Selective desilication with the alkaline structure directing agent TPAOH of conventional S-1 can yield a material with a range of pore sizes.^{120,139} Additionally, the desilication liquid collected during the

filtration of the treated material can be used for the recrystallization step as it contains enough silica precursor species and structure directing agent to complete the encapsulation. From an industrial perspective this is highly attractive as it would improve the synthesis efficiency drastically from both a green chemistry¹⁴⁰ and cost perspective. The first attempt at replicating the procedure from Chen et al.¹³⁹ resulted in complete dissolution of the parent zeolite. After shortening the treatment and adjusting the conditions, a highly porous material was collected, but at a yield of 28%. Using N₂-physisorption and Brunauer–Emmett–Teller theory (BET), the porosity and surface area was investigated, shown in Entry 6 of Table 5. For comparison, the table also shows the porosity data for the conventional S-1 and mesoporous S-1 synthesized via the week-long carbon templating (CT) route, as well as that of a Pd/CeO₂@S-1 catalyst after steam-assisted recrystallization. The TPAOH treatment was likely still too harsh but no further attempts were made to optimize it.

Table 5 N₂-physisorption data from select zeolite encapsulation materials. Adapted from MSc. project by Panagiotis Dimitriou¹³⁰ and supplemented with additional data from Pd/MO_x@S-1 project. Isotherms are shown in Appendix M.

Entry	Sample	BET surface area (m ² /g)	Total pore volume (cm ³ /g)	Micropore volume (cm ³ /g)
1	S-1 ^a	344	0.202	0.135
2	Pd@S-1 (fresh) ^a	328	0.184	0.106
3	Pd@S-1 (deactivated) ^a	324	0.197	0.104
4	S-1 (meso, CT)	395	0.242	0.102
5	Pd/CeO ₂ @S-1	361	0.214	0.068
6	S-1 (meso, DS)	499	0.903 ^b	0.112

^a Data from MSc project¹³⁰

^b The desilication process resulted in a sample mass loss of 72%

In order to better understand the impact of the desilication treatment, an XRD was recorded of the mesoporous S-1. This is shown in Figure 19 along with an XRD of the parent S-1 and a mesoporous S-1 synthesized via carbon templating. The diffractograms are similar in the sense that they all have the MFI structure, but the peaks for the desilicated sample seems to have broader peaks. This could possibly be explained by the severe loss of mass (72%), since a solid which has been hollowed out to the point where it mostly consists of void space and a "skeleton" holding it together would likely have fewer consecutive crystallographic layers for diffraction, resulting in peak broadening as per the Scherrer equation.¹³⁴ This would be consistent with the general appearance of the powder, as it had become even lighter and more fluffy than the non-mesoporous S-1.

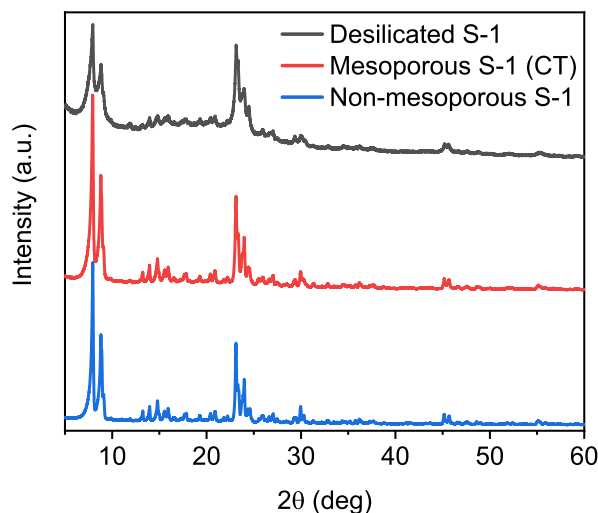


Figure 19 Powder XRD of mesoporous S-1 samples produced via different routes compared to conventional S-1.

In some studies of deactivation in methane oxidation catalysts, the focus is on the support instead of the active palladium nanoparticles. For zeolites, dealumination of the framework is a concern in some cases.^{141,142} In order to investigate if the structural integrity of the zeolite support was being compromised during deactivation, a Pd@S-1 sample was exposed to wet methane oxidation conditions for two hours. In Table 5 the deactivated sample is compared to a fresh in terms of porosity, and it can be seen that the total pore volume increases by 7% while the micropore volume, which makes up more than half of the total volume, remains relatively constant. The change in non-micropore volume is 19%, which is rather surprising. The deactivated sample has maintained its MFI structure, as seen in the powder XRD in Figure 20.

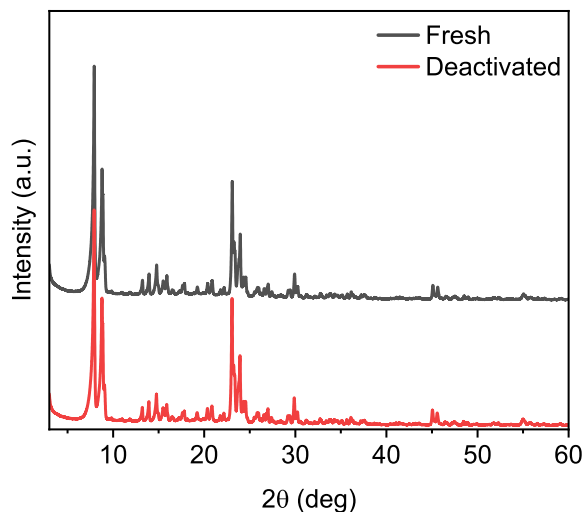


Figure 20 Powder XRD of fresh and deactivated Pd@S-1. Reaction conditions for 2-hour deactivation treatment: 1000 ppm CH₄, 10% O₂, 5% CO₂, 10% H₂O, N₂ balance, WHSV = 126 000 ml h⁻¹ g⁻¹, T = 430 °C, p = 3 bar. Adapted from MSc. project by Panagiotis Dimitriou.¹³⁰

TEM images were recorded of the fresh and deactivated Pd@S-1 samples, shown in Figures 21 and 22. The zeolite crystals appear very uniformly shaped and have a size between 400 and 600 nanometers, a bit smaller than those synthesized via the recrystallization pathway. More interesting however are the bright areas in the zeolite crystals of the deactivated sample which were not present in the images of the fresh sample. These look a lot like internal mesopores, which would fit well with the 19% increased non-micropore volume. It is surprising if additional pores have formed from the deactivation treatment, although the high temperature, high steam concentration, and elevated pressure are similar to the conditions during zeolite synthesis. The Pd nanoparticles are difficult to spot in the fresh sample, likely due to their small size. The ethylenediamine in-situ synthesis is known to produce Pd particles between 1 and 3 nanometers.^{39, 113, 127, 129, 143, 144}

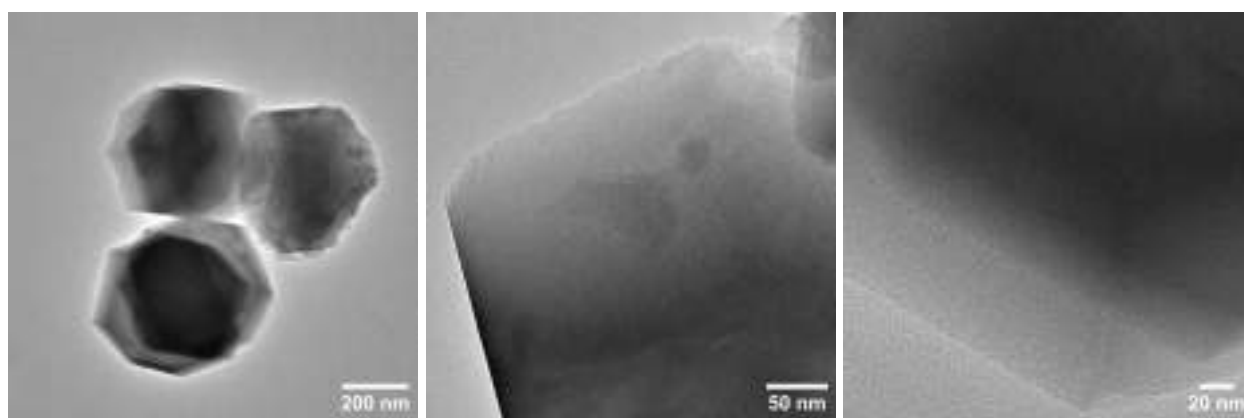


Figure 21 Bright-field TEM images of fresh Pd@S-1. Adapted from MSc. project by Panagiotis Dimitriou.¹³⁰

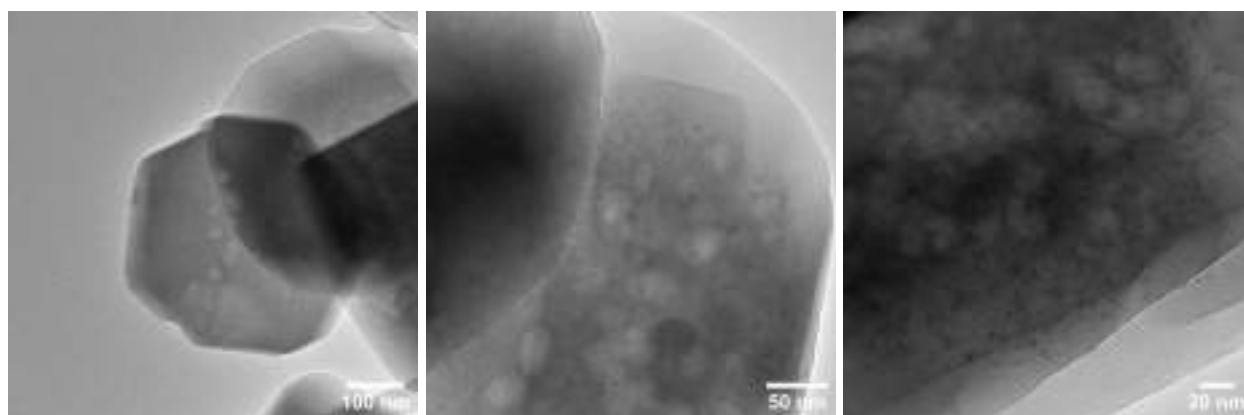


Figure 22 Bright-field TEM images of deactivated Pd@S-1. Adapted from MSc. project by Panagiotis Dimitriou.¹³⁰

In the TEM images of the deactivated sample it is much easier to spot the palladium nanoparticles. The reason for this is unknown but it can not be ruled out that it is because they have agglomerated during the deactivation. Regardless of the extent of these physical changes, they are unlikely to be

behind all of the deactivation experienced by the catalyst. As will be explained and explored in Section 6, deactivation by water is primarily due to chemical interactions with the active palladium nanoparticles.

A ^{29}Si solid state nuclear magnetic resonance (SS-NMR) was performed to investigate if the chemical environment around the silicon atoms in the S-1 structure had changed. Spectra for a fresh and a deactivated sample are shown in Appendix K, but were inconclusive. Lastly, a series of TEM images were recorded of the Pd@S-1 material synthesized in the presence of hydrofluoric acid, one of which is shown in Figure 23. The material appears more opaque in the TEM, which is surprising as it should have the same elemental composition and structure, except for fewer hydroxyl defects. Further, the materials seems less homogeneous than the conventional Pd@S-1 in Figure 21, containing large dark areas, i.e. higher concentration of heavier elements.

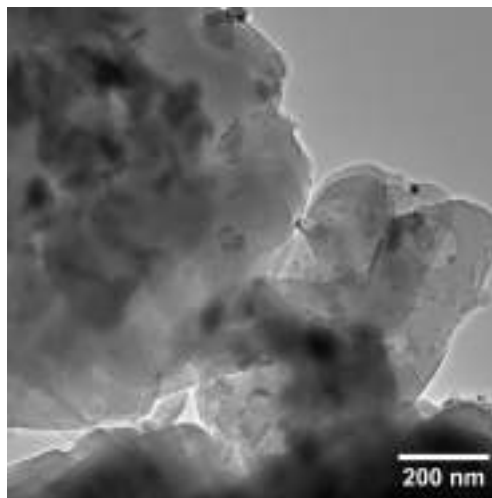


Figure 23 Bright-field TEM image of HF-modified Pd@S-1

A range of characterization techniques were performed of the PdPt@S-1 materials as part of the second student project. Appendix D shows a powder XRD of the samples, as well as an attempt to confirm the Pd/Pt ratios with X-ray fluorescence using the samples themselves as a kind of internal standard. Finally, Appendix D also includes a series of H_2 -temperature programmed reduction (H_2 -TPR) experiments where the reduction peak of the mixed metal nanoparticles encapsulated in S-1 moves to higher temperatures as the Pd/Pt ratio increases.

4.4 Evaluation of Silicalite-1 encapsulation projects

The interesting catalyst concept developed here might not have had its potential fully explored due to time limitations. Although certain results were promising, the synthesis had issues with reproducibility. It was attempted to synthesize a Pd/BaO@S-1 material twice, but neither had much activity for methane oxidation. Initially, it was planned to also synthesize variations with oxides of

Sn, Ti, Mn, Zr, Co, Ni inspired by interesting results from literature.^{52, 61, 77, 145–153} CeO₂ and BaO were the first metal oxides attempted due to overwhelming number of publications using these as supports or promoters.^{31, 52, 58, 77, 148, 152, 154–160} Eventually it was determined that the other ongoing projects had better prospects of scientific and industrial impact, and time had to be prioritized accordingly.

As described in Paper 1, when reading literature on catalytic methane oxidation, water-induced deactivation appears to have been solved by hydrophobic zeolite supports. At least many researchers seem to have developed catalysts which do not deactivate when exposed to model conditions for wet methane oxidation. In this project it was not possible to reproduce the results of a promising class of materials, the Silicalite-1 encapsulated palladium oxide nanoparticles. Judging from the characterization performed (XRD, TEM, N₂-physisorption) it seems plausible that the synthesis was successful in terms of zeolite structure and nanoparticle size, but the catalytic performance was not as those published in literature. A reason for this is possibly the way methane oxidation catalysts are often tested, with 10 times too high methane concentration, lower than realistic water concentration, overly simplistic experiments, testing at 100% conversion, etc. Since the methane oxidation reaction is so sensitive, testing under unrealistic conditions might invalidate the results, or at least make comparison very difficult. Also, if the deactivation problems had actually been solved, there would be an enormous market for that catalyst technology and there would likely be many patents showing up. To the best of my knowledge, that is not the case. A more lengthy discussion about the importance of realistic testing conditions can be found in Section 6.8.

5 Project 2: Influence of counter-ion on the sulfur tolerance of zeolite-supported methane oxidation catalysts

This project investigates the role of the counter-ion in zeolite-supported methane oxidation catalysts in terms of resistance to SO₂ poisoning. The project is relevant as the main result points in the opposite direction of recent studies on water-induced deactivation. The section includes a short description of the initial experiments leading up to those included in Paper 2 and of course the manuscript itself as submitted to the journal.

5.1 Initial screening of ion-exchanged zeolite-supported catalysts

As part of the validation of the catalytic test setup, and to have to zeolite-supported reference catalysts, a series of Pd/zeolite materials with different framework topologies and Si/Al ratios were acquired from Umicore. The synthesis of the materials is described in Paper 2, and their characteristics are shown in Table 6.

Table 6 Pd/zeolite samples from Umicore used for ion-exchange experiments.

Sample name	Framework	SiO ₂ /Al ₂ O ₃ ratio
Pd/H-CHA30	CHA	30
Pd/H-CHA25	CHA	25
Pd/H-CHA13	CHA	13
Pd/H-MFI29	MFI	29
Pd/H-MOR19	MOR	19
Pd/H-AEI22	AEI	22

The samples were all exposed to the same experiment consisting of segments with different deactivation conditions, shown in Figure 24. Four of the samples, those supported on zeolites with either CHA or AEI framework, exhibited a surprising behavior when exposed to a feed gas containing 2 ppm SO₂. The catalysts would quickly lose a significant portion of their activity, but regain most of it over the following hours. Neither of the catalysts had any tolerance towards water, and in a feed gas containing both water and SO₂ all catalysts immediately dropped to less than 5% conversion.

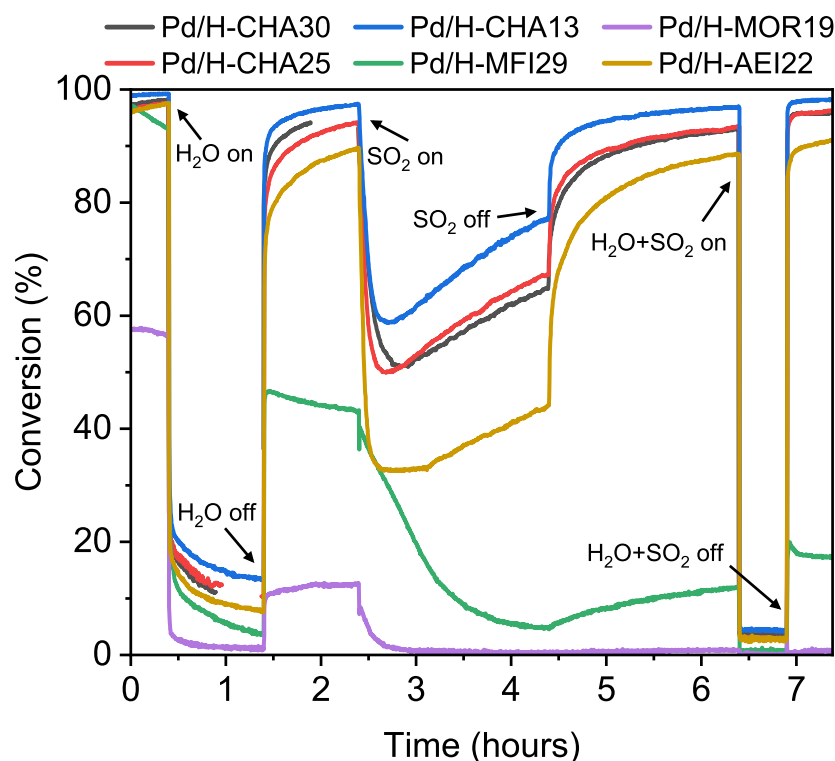


Figure 24 Screening experiment designed to test the catalysts under a series of different reaction conditions. The catalytic behavior was as expected except for the curious behavior of 4 of the catalysts when exposed to SO_2 where they initially drop in conversion but then recover. Reaction conditions: 1000 ppm CH_4 , 10% O_2 , 5% CO_2 , 10% H_2O (when present), 2 ppm SO_2 (when present), N_2 balance, $\text{WHSV} = 126\,000 \text{ ml h}^{-1} \text{ g}^{-1}$, $T = 420^\circ\text{C}$.

The interesting interaction with SO_2 exhibited by several of the sample was difficult to explain. To gain a better understanding, it was decided to modify the samples and observe how the interaction changed. The most straightforward modification was to exchange the protons in the H-form zeolites with an alkali metal ion. Using the procedure explained in Paper 2, all six samples were ion-exchanged to Na-form. The catalytic screening experiment was repeated with the Na-exchanged samples, shown in Figure 25. The recovery of the CHA and AEI catalysts did not persist in their Na-form, meaning that protons in the zeolite structure likely played a part in the SO_2 tolerance of the original catalysts. Importantly, this result stood in contrast to those of Petrov et al.¹²⁶ which showed that exchanging protons for sodium ions can improve the water tolerance of similar methane oxidation catalysts.

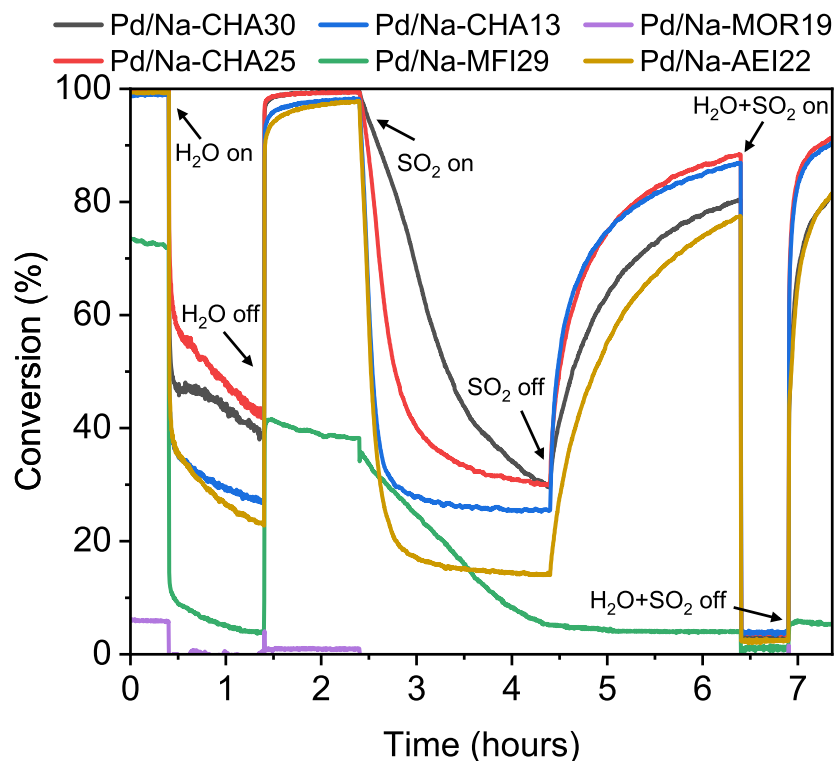


Figure 25 Same screening experiment as Figure 24, but with Na-exchanged catalysts. Now the drop-and-recover behavior of the four catalysts are gone. The activity in absence of water and SO_2 has increased though. Reaction conditions: 1000 ppm CH_4 , 10% O_2 , 5% CO_2 , 10% H_2O (when present), 2 ppm SO_2 (when present), N_2 balance, $\text{WHSV} = 126\,000 \text{ ml h}^{-1} \text{ g}^{-1}$, $T = 420^\circ\text{C}$.

For Paper 2, only the Pd/H-CHA13 material was used. It contained the most aluminum and therefore had the highest theoretical capacity for ion exchange, depending of course on the unknown amount of extra-framework aluminum.

5.2 Paper 2

On the following pages, the manuscript for Paper 2 is presented as it was submitted for peer review.

The Effect of Zeolite Counter-Ion on a Pd/H-CHA Methane Oxidation Catalyst with Remarkable Tolerance to SO₂

Received 00th January 20xx,
Accepted 00th January 20xx

DOI: 10.1039/x0xx00000x

Rasmus Lykke Mortensen,^{a,b} Hendrik-David Noack^b, Kim Pedersen^b, Susanne Mossin^{*a} and Jerrik Mielby^{*a}

Zeolites find increasing use as support material for catalysts used in complete methane oxidation to reduce sintering and water-induced deactivation of the active PdO nanoparticles. Especially zeolites in Na-form have been investigated towards water-tolerance. This paper presents a Pd/H-CHA catalyst with good low-temperature activity and remarkable tolerance to SO₂, a well-known catalytic poison. The catalyst withstands more than 200 hours on stream with a realistic methane concentration of 1000 ppm in the presence of 2 ppm SO₂ without losing any activity and maintains a stable conversion of 94% at 400 °C and 126.000 ml h⁻¹ g⁻¹. The counter-ions play a key role in the SO₂ tolerance of the Pd/CHA material and it is expected from the literature that ion-exchange with sodium and other alkali metals provide better water-tolerance. Here we show, however, that they possess inferior sulfur resistance compared to the parent Pd/H-CHA. Deactivation, especially by the combined effect of SO₂ and water remains an unsolved challenge for complete methane oxidation catalysts.

Introduction

Using natural gas as a replacement for fuel oil during the transition to a fully sustainable energy society is not simple. Unburned methane emitted into the atmosphere limits the potential savings in greenhouse gases from the marine and energy production sectors. Catalytic methane oxidation is the most promising way of realizing the potential of existing natural gas engines by converting the unburned methane to CO₂, which has a much lower global warming potential.¹ A catalyst with excellent stability is required due to the harsh exhaust conditions present in relevant applications, the high cost of raw materials, and the difficulties associated with regeneration technologies. Specifically, the high exhaust temperatures can cause active metal particle sintering, and both water and SO₂ contribute to deactivation.² Palladium oxide nanoparticles are considered to be the most active for complete methane oxidation, and the current state-of-the-art is to have them supported on high surface area alumina.³ Recently, zeolites have attracted attention as an alternative support for the active PdO nanoparticles. The zeolites can protect the PdO in two main ways: 1) Hydrophobic zeolites, typically with high Si/Al ratios, are hypothesized to keep water away from the active sites, limiting the deactivation caused by water.^{4–6} 2) The zeolite can prevent sintering by confining the particles inside the microporous framework, which keep them separated at high

temperatures.^{7,8} Another significant deactivation phenomenon for palladium-based methane oxidation catalysts is poisoning by SO₂, which originates from small amounts of sulfur-containing molecules in natural gas and engine lubricants. SO₂ deactivation has been explored extensively for Pd/Al₂O₃,^{9–14} but has only received limited attention for zeolite-based methane oxidation catalysts.^{2,3} The few available publications point towards SO₂ deactivation being even faster for zeolite-based catalysts since the support does not bind to sulfate, unlike for alumina-based catalysts where the support can, to some extent, temporarily shield the palladium oxide particles.^{6,15}

Friberg et al.⁶ showed that a series of zeolite-based catalysts with different zeotypes and Si/Al ratios suffer a quick and complete deactivation upon exposure to 10 ppm SO₂ at 450 °C, as opposed to a state-of-the-art Pd/Al₂O₃ sample which deactivated much more slowly. All the zeolite samples were in the H-form, as is often the case, as this has been shown to aid palladium dispersion during nano particle synthesis.^{4,16} On the other hand, H-form zeolites are hypothesized to be less favorable during operation in the presence of water as they are less hydrophobic.^{17,18}

Z. Zhang et al.⁸ have suggested using nanoparticle encapsulation to increase SO₂ tolerance. By confining the active palladium oxide inside the microporous network of the pure silica zeolite S-1, they show that a palladium catalyst can maintain activity in a feed gas with SO₂. The authors use SO₂-TPD results to hypothesize that the increased SO₂ tolerance is caused by restricting the size of formed PdSO₄ particles. Researchers have also reported promising results using other active metals than palladium. For example, Y. Zhang et al.^{19,20} showed that rhodium has better SO₂ tolerance than palladium

^a DTU Chemistry, Technical University of Denmark, Kemitorvet 207, DK-2800 Kgs. Lyngby, Denmark.

^b Umicore Denmark Aps, Kogle Allé 1, DK-2970 Hørsholm, Denmark.

due to the formation of less stable sulfates. For industrial applications however, a catalyst with rhodium as the only active ingredient could be difficult to realize since the price is close to an order of magnitude higher than that of palladium, while its activity is similar.

In a recent publication, Wu et al.²¹ highlighted the shortcomings of current palladium-based methane oxidation catalysts in terms of H₂O and SO₂ tolerance and showed how nickel oxide nanoparticles have significant methane oxidation activity in the presence of SO₂. There are many examples of transition metal catalysts with slow or non-existing SO₂ poisoning, although rarely supported on zeolites.^{21–28} All these have significantly lower activity than palladium-based catalysts and therefore require very high exhaust temperatures. In addition, several of these catalysts rely on chromium, which gives concerns regarding safety and toxicity.

Petrov et al. have shown that exchanging protons for e.g. sodium makes zeolite-supported methane oxidation catalysts more water tolerant.^{4,18} The authors argue that this approach is a viable alternative to using a high Si/Al ratio for hydrophobicity, while still being able to produce a material with highly dispersed nanoparticles. However, they do not evaluate the effect of the ion-exchange on other deactivation mechanisms relevant for methane oxidation. Herein, we present a highly active Pd/zeolite methane oxidation catalyst with unprecedented tolerance to SO₂ and explore the influence of the zeolite counter-ions by exchanging protons for a series of alkali metal ions. This highlights the important role of the counter-ion as not just a synthesis tool to aid palladium dispersion, but as a critical parameter for catalyst performance and stability.

Results and discussion

SO₂ tolerance

The exhaust of a lean-burn natural gas-fired large engine contains a few ppm of SO₂ and about 10% water. Although very different in concentration, both molecules dramatically affect palladium-based methane oxidation catalysts. These two challenges are typically addressed separately: catalytic tests are often performed in the presence of only one pollutant, despite recent evidence that the deactivation is enhanced when both water and SO₂ are present simultaneously.²⁹ Here, we focus on the deactivation caused by SO₂ in a dry feed gas, see Figure 1.

After obtaining a stable high conversion of 1000 ppm methane at 420 °C, 2 ppm SO₂ is added to the feed gas. The methane conversion decreases instantly, but then recovers almost fully over the following 10 hours. The catalyst is stable with a high conversion at a relatively low temperature for more than 200 hours.

Figure 1 shows a shortened SO₂ exposure experiment with different SO₂ concentrations and at a lower temperature. The initial drop depends directly on the SO₂ concentration. At 0.2 ppm the drop is smaller and at 10 ppm it is significantly larger than in the original experiment with 2 ppm SO₂. The same recovery effect was seen and the conversion continued to climb after 4 hours to levels seemingly determined by the SO₂ concentration. The decreased temperature did not significantly

change the behavior of the catalyst or the size of the drop in terms of rate loss compared to initial activity, other than the expected lower initial conversion. Work is ongoing to understand the drop-and-recovery behavior.

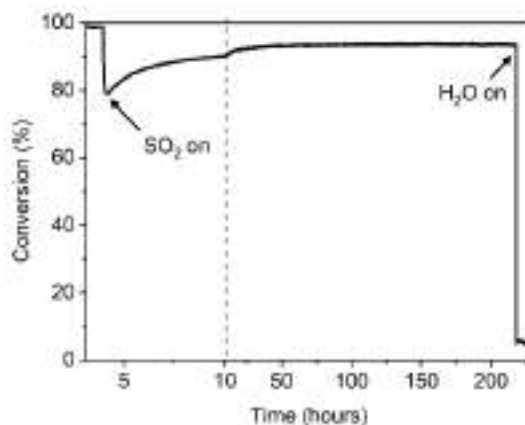


Figure 1. Catalytic test of Pd/H-CHA in the presence of SO₂. The catalyst was degreened at 500 °C for 1 hour before the temperature was lowered to 420 °C. Without SO₂ the conversion was 98%, just after SO₂ addition it was 79%, and after prolonged exposure it was stable at 94%. The timescale changes at the dashed line. Reaction conditions: 1000 ppm CH₄, 10% O₂, 5% CO₂, 2 ppm SO₂ (when present), N₂ balance, GHSV = 126.000 ml h⁻¹ g⁻¹.

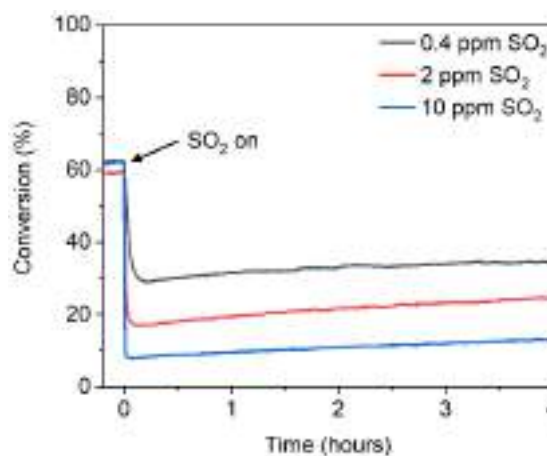


Figure 2. SO₂ exposure experiment at lower temperature, with three different concentrations of SO₂. Reaction conditions: 1000 ppm CH₄, 10% O₂, 5% CO₂, N₂ balance, 360 °C, GHSV = 126.000 ml h⁻¹ g⁻¹.

SO₂ tolerance: Dependence on the counter-ion

Often, the effect of the counter-ion is not attributed much attention when it comes to the performance of methane oxidation catalysts. Here, we show that exchanging the protons in the Pd/H-CHA material, results in a significant decrease in SO₂ tolerance. Using the procedure described below, we exchanged the protons in Pd/H-CHA with various alkali metals and tested their catalytic activity. We also exchanged the Na-ions with NH₄⁺ and calcined again to bring the zeolite back on H-form to confirm that the effect was caused by the counter-ion and not the ion-exchange procedure.

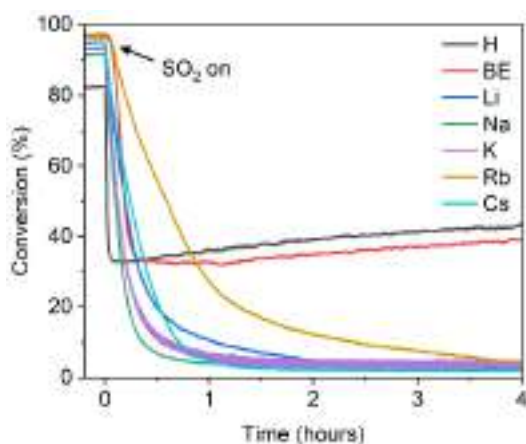


Figure 3. Catalytic test of Pd/M-CHA (M=H, Li, Na, K, Rb, Cs) in the presence of SO_2 . BE = back-exchanged to H-form. The catalyst was degreased at 500 °C for 1 hour prior to the experiment. Reaction conditions: 1000 ppm CH_4 , 10% O_2 , 5% CO_2 , 2 ppm SO_2 , N_2 balance, $T = 380^\circ\text{C}$, GHSV = 126.000 $\text{ml h}^{-1} \text{g}^{-1}$.

Figure 3 shows a prolonged SO_2 exposure experiment at 380 °C for all seven samples. When the acidic protons are exchanged by alkali metal ions, the SO_2 tolerance and the recovery phenomenon disappear completely.

To quantify the effect of the ion-exchange procedure and better see the difference between the alkali metal samples, we performed a series of light-off experiments, see Figure 4a and b. More specifically, we used the ramp-down temperature at 50% conversion, T_{50} , as a measure for catalytic activity. The T_{50} values are presented as column bars in Figure 4c both with and without SO_2 . All the ion-exchanged samples, even the one back-exchanged to H-form, show a moderately higher activity under dry and SO_2 -free conditions (T_{50} is on average 30 °C lower). The increased activity of alkali-exchanged catalysts is in good agreement with the results of Petrov et. al.⁴ Interestingly, the activity in the presence of SO_2 was drastically lowered for all samples with alkali metals as counter-ion. The T_{50} increase ranged from 41 to 87 °C compared to the original H-form catalyst.

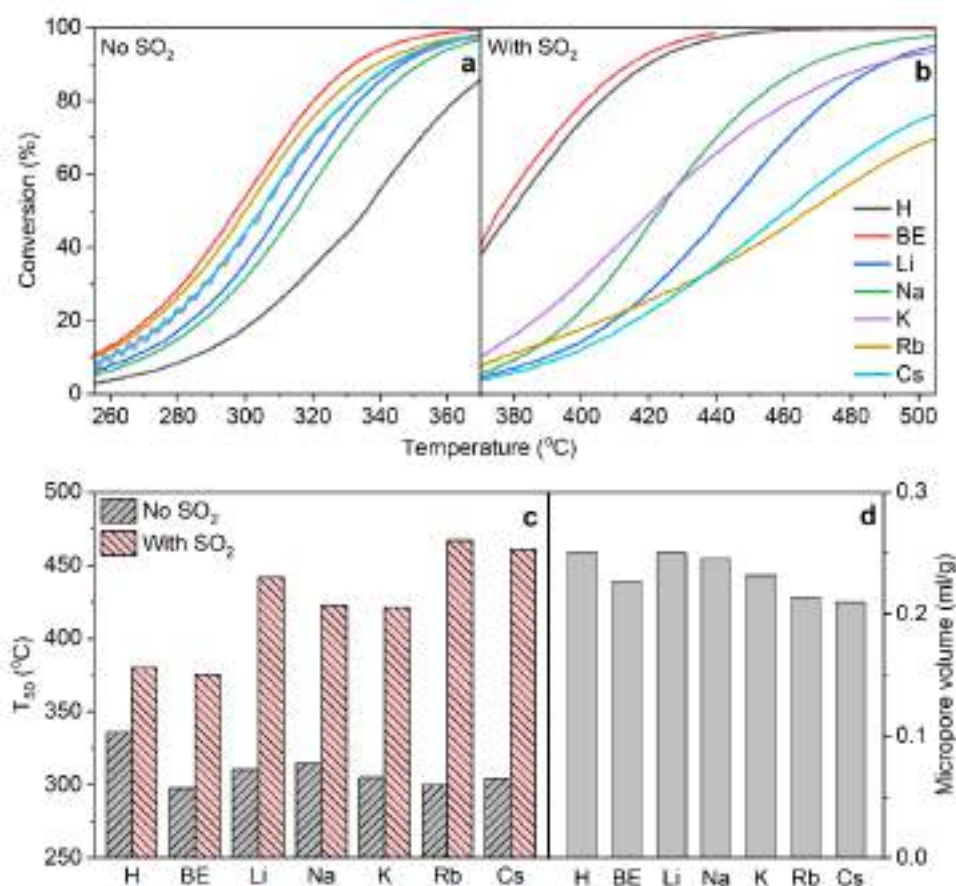


Figure 4. Experimental data for Pd/CHA materials with different counter-ions. Conditions during catalytic tests: 1000 ppm CH_4 , 10% O_2 , 5% CO_2 , 2 ppm SO_2 (when present), N_2 balance, GHSV = 126.000 $\text{ml h}^{-1} \text{g}^{-1}$. Light-down catalytic test: a) without SO_2 , b) with SO_2 , c) T_{50} values. d) Micropore volumes determined by N_2 -physorption.

The back-exchanged catalyst had the same activity as the original H-form catalyst in presence of SO₂. To investigate the structural effects of incorporation of counter-ions of very different sizes, we analyzed all samples by N₂ physisorption, see Figure 4d. In general, the micropore volume of the samples were not significantly affected by the ion-exchange procedure. When the zeolite was ion-exchanged by larger, more heavy alkali metal ions, a slight decrease in micropore volume was detected. Since we prepared the catalysts by incipient wetness impregnation, the PdO nanoparticles were mainly on the external surface of the zeolite. Consequently, we did not observe any direct relation between the micropore volume and the catalytic performance.

We hypothesize that the accessible protons in the H-form zeolite may lower the stability of palladium sulfate in the catalyst. This hypothesis is supported by several literature works.^{30,31} The investigated materials are almost identical with the exception of the counter ions, but nevertheless show drastically different catalytic behavior. Since the degradation of sulfate (SO₄²⁻) to gas phase SO₂ and H₂O will require available protons, H⁺, the limited availability of protons in the alkali metal exchanged materials will hinder the degradation at low temperature. Presently, this hypothesis has not been supported by spectroscopic data, but work is ongoing to investigate the relation between sulfate stability, surface acidity, and catalytic performance.

Perspectives on deactivation by simultaneous water and SO₂

In the literature presenting hydrophobic zeolites as a means of solving water-induced deactivation, the problem of SO₂ is rarely addressed. As we show here, sodium and other alkali metal ions significantly enhance the vulnerability towards SO₂ deactivation. We emphasize the importance of testing under realistic conditions with a gas mixture that accurately represents the exhaust of a lean-burn natural gas engine, including both water and SO₂.² Auvinen et al. recently showed that the deactivation caused by water and SO₂ reinforce each other.²⁹ Indeed, the best catalyst in this work deactivated rapidly in a feed with both water and SO₂ present, as shown to the very right of Figure 1. The challenge of a sufficiently durable methane oxidation catalyst is still not overcome, and more work is required both in understanding the complex interplay between the several deactivation phenomena and the various features of the catalyst.

Conclusions

A Pd/H-CHA methane oxidation catalyst was presented and tested for dry methane oxidation (1000 ppm CH₄, 420 °C GHSV

126.000 ml h⁻¹ g⁻¹, 2 ppm SO₂) for more than 200 hours with minimal activity loss due to the SO₂ in the feed. The protons of the zeolite support were necessary for the SO₂ tolerance since Pd/M-CHA ion-exchanged with alkali metal ions (M=Li, Na, K, Rb, Cs) had a significantly lowered tolerance towards SO₂. The SO₂-tolerance can be reintroduced by selectively removing Na⁺ from Pd/Na-CHA by back-exchange to produce a Pd/H-CHA catalyst. The significant deactivation observed when water and SO₂ are present together underlines the importance of testing under realistic conditions in the development of more durable methane oxidation catalysts for emission control.

Experimental

Materials

Commercially available H-form Chabazite zeolite (SSZ-13) with Si/Al = 6.5 was used as starting material. Palladium loading was performed by incipient wetness impregnation, using an aqueous solution of PdNO₃ with a concentration that would yield a material with 3 wt% Pd in the final material upon the addition of 80% of the total pore volume. Following impregnation, the samples were dried for 10 hours at 60 °C and calcined for 16 hours in air with 10 vol% water at 750 °C.

Ion-exchange was performed using a procedure inspired by the work of Petrov et al.⁴ 2 g Pd/H-CHA was added to a round-bottomed flask and dispersed in 20 ml demineralized water. While stirring, a 0.01 M solution of M₂CO₃ (M=Li, Na, K, Rb, Cs) was added dropwise until the slurry reached pH 7. It was then stirred for another 30 minutes, and the solids were collected by centrifugation. The samples were dried overnight at 80 °C and calcined for 2 hours at 500 °C. The samples were denoted Pd/M-CHA (M=Li, Na, K, Rb, Cs).

A back-exchanged material was prepared by dispersing 2 g Pd/Na-CHA in 50 ml 1 M NH₄NO₃ and stirring it for 24 hours at 80 °C. The solid was collected by centrifugation, and the ammonium exchange was repeated 2 more times, after which the solid was dried overnight at 80 °C and calcined for 2 hours at 500 °C. This sample was denoted Pd/BE-CHA, with BE instead of H, to distinguish it from the original H-form zeolite material.

Characterization

The micropore volume of the samples was measured with N₂ physisorption using a Micrometrics 3Flex system at 77 K. All samples were degassed for 24 hours in a Micrometrics VacPrep 061 Sample Degas System at 400 °C.

Catalytic tests

All catalytic testing was performed at ambient pressure in a continuous flow quartz reactor with an inner diameter of 10 mm. The reactor was fitted with an internal thermocouple and

placed inside a programmable furnace. Mass flow controllers fed five gasses: Air, N₂, CO₂, 1% CH₄ in N₂, 100 ppm SO₂ in N₂ using a total feed gas flow rate of 420 ml/min. The bed consisted of 200 mg catalyst diluted with 2 g quartz sand, resting on a quartz wool plug leveled flat by 500 mg quartz sand, and topped by another quartz wool plug. The catalyst sample and quartz sand were both fractionated to 150–300 µm. The methane concentration in the outlet gas was analyzed with a Thermo-FID ES from SK Elektronik and conversion calculated as:

$$\text{Conversion} = (C_{\text{in}} - C_{\text{out}})/C_{\text{in}} \times 100\%$$

Where C_{in} and C_{out} are the methane concentrations in the inlet and outlet gas, respectively. Light-off tests were performed with a ramp of ±5 °C/min. Data displayed from these tests are from the cooling segment of the experiment, i.e. a light-down instead of a light-off. We have found this to be a more accurate and reproducible approach. An example of a complete standard experiment is shown in Figure 5.

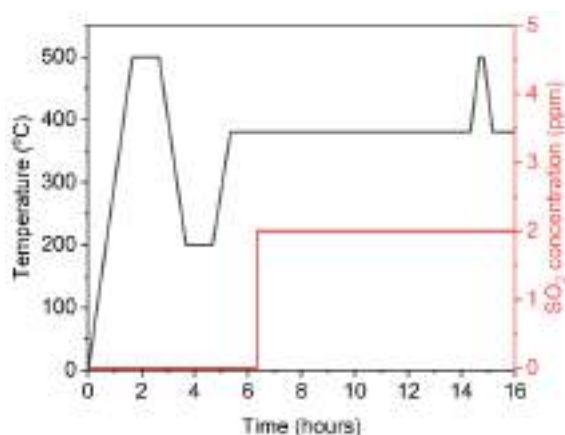


Figure 5. Standard experimental protocol for all samples. Reaction conditions: 1000 ppm CH₄, 10% O₂, 5% CO₂, 2 ppm SO₂ (when present), N₂ balance, GHSV = 126,000 ml h⁻¹ g⁻¹.

Author Contributions

RLM performed all the experimental work, developed the methodology and wrote the first draft. KP and HDN provided resources, funding and methodology and revised and edited the paper, SM and JM conceptualized the work, secured funding, supervised the project and revised and performed final editing of the paper.

Conflicts of interest

There are no conflicts to declare.

Acknowledgements

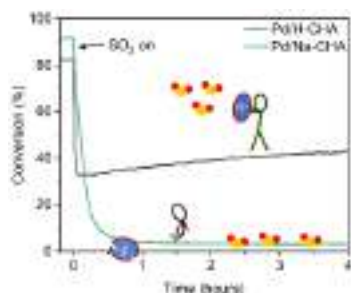
This work is funded by Umicore Denmark and Innovation Fund Denmark (IFD) under File No. 0153-00064. R.L.M., H.N., and K.H.P. are employed at Umicore Denmark and have commercial interests in developing new emission control technologies.

References

- 1 C. Smith, Z. R. J. Nicholls, K. Armour, W. Collins, P. Forster, M. Meinshausen, M. D. Palmer and M. Watanabe, The Earth's Energy Budget, Climate Feedbacks, and Climate Sensitivity Supplementary Material. In: Climate Change 2021: The Physical Science Basis. Contribution of Working Group I to the Sixth Assessment Report of the IPCC., Cambridge University Press, Cambridge, United Kingdom and New York, NY, USA, 2021.
- 2 R. L. Mortensen, H. Noack, K. Pedersen, S. Mossin and J. Mielby, *ChemCatChem*, 2022, **14**, e20210192.
- 3 H.-Y. Chen, J. Lu, J. M. Fedeyko and A. Raj, *Appl. Catal. A Gen.*, 2022, **633**, 118534.
- 4 A. W. Petrov, D. Ferri, F. Krumeich, M. Nachtegaal, J. A. van Bokhoven and O. Kröcher, *Nat. Commun.*, 2018, **9**, 2545.
- 5 P. Losch, W. Huang, O. Vozniuk, E. D. Goodman, W. Schmidt and M. Cargnello, *ACS Catal.*, 2019, **9**, 4742–4753.
- 6 I. Friberg, N. Sadokhina and L. Olsson, *Appl. Catal. B Environ.*, 2019, **250**, 117–131.
- 7 T. Li, A. Beck, F. Krumeich, L. Artiglia, M. K. Ghosalya, M. Roger, D. Ferri, O. Kröcher, V. Sushkevich, O. V. Safonova and J. A. van Bokhoven, *ACS Catal.*, 2021, **11**, 7371–7382.
- 8 Z. Zhang, L. Sun, X. Hu, Y. Zhang, H. Tian and X. Yang, *Appl. Surf. Sci.*, 2019, **494**, 1044–1054.
- 9 R. Burch, D. J. Crittle, B. W. L. Southward and J. A. Sullivan, *Catal. Letters*, 2001, **72**, 153–155.
- 10 D. L. Mowery, M. S. Graboski, T. R. Ohno and R. L. McCormick, *Appl. Catal. B Environ.*, 1999, **21**, 157–169.
- 11 P. Gélin, L. Urfels, M. Primet and E. Tena, *Catal. Today*, 2003, **83**, 45–57.
- 12 N. M. Kinnunen, V. H. Nissinen, J. T. Hirvi, K. Kallinen, T. Maunula, M. Keenan and M. Suvanto, *Catalysts*, 2019, **9**, 427.
- 13 F. Arosio, S. Colussi, A. Trovarelli and G. Groppi, *Appl. Catal. B Environ.*, 2008, **80**, 335–342.
- 14 P. Auvinen, N. M. Kinnunen, J. T. Hirvi, T. Maunula, K. Kallinen, M. Keenan, R. Baert, E. van den Tillaart and M. Suvanto, *Appl. Catal. B Environ.*, 2019, **258**, 117976.
- 15 J. Lampert, M. Kazi and R. Farrauto, *Appl. Catal. B Environ.*, 1997, **14**, 211–223.
- 16 J. Lei, R. Niu, S. Wang and J. Li, *Solid State Sci.*, 2020, **101**, 106097.
- 17 Y. Zhang, P. Glarborg, M. P. Andersson, K. Johansen, T. K. Torp, A. D. Jensen and J. M. Christensen, *Catal. Sci. Technol.*, 2020, **10**, 6035–6044.
- 18 A. W. Petrov, D. Ferri, O. Kröcher and J. A. van Bokhoven, *ACS Catal.*, 2019, **9**, 2303–2312.
- 19 Y. Zhang, P. Glarborg, M. P. Andersson, K. Johansen, T. K. Torp, A. D. Jensen and J. M. Christensen, *Appl. Catal. B Environ.*, 2020, **277**, 119176.
- 20 Y. Zhang, P. Glarborg, K. Johansen, M. P. Andersson, T. K. Torp, A. D. Jensen and J. M. Christensen, *ACS Catal.*, 2020, **10**, 1821–1827.
- 21 J. Wu, K. Du, J. Che, S. Zou, L. Xiao, H. Kobayashi and J. Fan, *J. Phys. Chem. C*, 2021, **125**, 2485–2491.
- 22 S. Ordóñez, J. R. Paredes and F. V. Díez, *Appl. Catal. A Gen.*, 2008, **341**, 174–180.
- 23 M. García-Vázquez, K. Wang, J. M. González-Carballo, D. Brown, P. Landon, R. Tooze and F. R. García-García, *Appl. Catal. B Environ.*, 2020, **277**, 119139.
- 24 S. A. Singh, G. Madras and I. Sreedhar, *Top. Catal.*, 2021, **64**, 243–255.
- 25 I. Rossetti, O. Buchneva, C. Biffi and R. Rizza, *Appl. Catal. B Environ.*, 2009, **89**, 383–390.
- 26 D. Trong On, S. V. Nguyen and S. Kaliaguine, *Phys. Chem. Chem. Phys.*, 2003, **5**, 2724–2729.
- 27 Y. Dai, H. Wang, S. Liu, K. J. Smith, M. O. Wolf and M. J. MacLachlan, *CrystEngComm*, 2020, **22**, 4404–4415.

- 28 S. N. Hernández Guiance, I. D. Coria, I. M. Irurzun and E. E. Mola, *Chem. Phys. Lett.*, 2016, **660**, 123–126.
- 29 P. Auvinen, J. T. Hirvi, N. M. Kinnunen and M. Suvanto, *ACS Catal.*, 2020, 10, 12943–12953.
- 30 A. M. Venezia, G. Di Carlo, L. F. Liotta, G. Pantaleo and M. Kantcheva, *Appl. Catal. B Environ.*, 2011, 106, 529–539.
- 31 Y. Ding, S. Wang, L. Zhang, L. Lv, D. Xu, W. Liu and S. Wang, *Chem. Eng. J.*, 2020, 382, 122969.

TOC entry:



A Pd/CHA catalyst for methane oxidation is shown to have remarkable resistance towards SO₂ in the feed gas and to lose it all again upon ion exchange with alkali metal ions.

6 Project 3: Uncovering the reason for water-induced deactivation of palladium-based methane oxidation catalysts

This project revolves around the important discovery, that water-induced deactivation has two components, taking place at different time scales. They have been termed fast reversible inhibition and slow irreversible deactivation. Contrary to the currently leading hypothesis, we found that the slow irreversible deactivation requires methane to be converted on the catalyst. The section will provide a background on the leading hypothesis revolving around the formation of hydroxyl groups. The context for our findings will be given, and key parts of the methodology used for the project will be discussed. Then follows the manuscript for Paper 3, which is undergoing final preparations for submission. After that, additional analysis of the deactivation data is provided along with attempts at gaining a deeper understanding of deactivated palladium oxide via spectroscopy. Finally, the section will end on a discussion about the importance of realistic testing conditions and useful deactivation experiments.

6.1 Description of the leading hypothesis for water-induced deactivation

Paper 1 provides a thorough explanation for the, in literature, most prominent hypothesis for water-induced deactivation. By backtracking through the citations on the topic, this section will provide a deeper analysis of the experimental evidence behind the hypothesis and justify how it could potentially be the result of a misinterpretation of the original experimental findings.

From the beginning, research in the field of complete methane oxidation consisted, as it does today, of a mixture between the two applications catalytic combustion and emission control. Catalytic combustion is an alternative to thermal combustion for extracting energy from fuel, where the fuel is converted over a catalyst instead of being burned. The point is to keep the combustion temperatures low enough that formation of thermal NO_x is completely avoided. In catalytic combustion there is no water in the feed gas, but the interaction with water has been researched extensively, as the methane oxidation reaction itself produces two water molecules for each converted methane molecule. Around the year 2000, a handful of research groups, primarily in the United States, were in particular contributing to the work on the interaction of the catalyst with water in the gas stream.^{16,47,161–168} Already in 1972 however, Cullis et al.¹⁶⁹ observed deactivation of a palladium-based methane oxidation catalyst in the presence of added water vapor over a 25 minutes long experiment. The authors hypothesized that the formation of inactive $\text{Pd}(\text{OH})_2$ was the reason for deactivation. In 1983, Card et al.¹⁷⁰ contributed to dismantling that hypothesis by showing that $\text{Pd}(\text{OH})_2$ decomposes to palladium oxide at 250 °C. The work by Cullis, Card, and their co-workers was cited in the work published during the late 1990s.

In 1995, Burch et al.¹⁶¹ investigated the effect of carbon dioxide and water on the activity of

palladium-based methane combustion catalysts, by adding and removing the pollutants to the feed gas, much in the same way as the experiments shown in Paper 3. A key experiment performed by the authors is shown in Figure 26. Here, it can be seen that the short-term interaction with water is both fast and fully reversible. A small irreversible deactivation can be seen, as the catalyst end up with a slightly lower conversion upon removal of water from the feed gas across most temperatures. This is most noticeable at 325 and 350 °C (triangle and star symbols respectively).

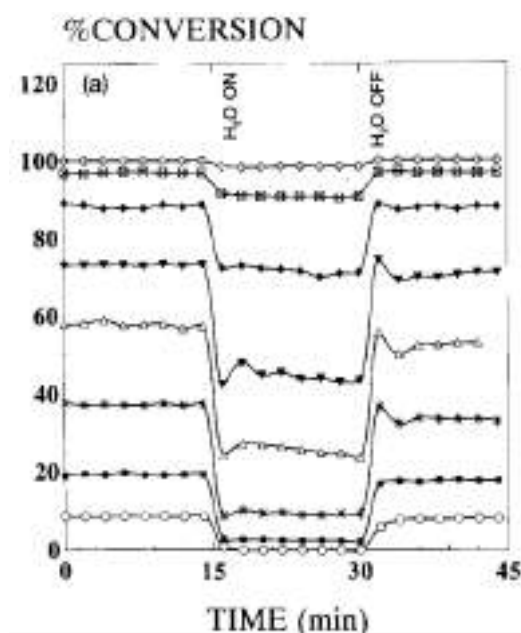


Figure 26 Experiment showing the inhibition by water at different temperatures. The lowest conversion experiment (circle) takes place at 275 °C. The experiment with the highest conversion (plus) takes place at 450 °C. The remaining experiments are distributed with 25 °C intervals. Reprinted with permission from Burch et al.¹⁶¹ Copyright 1995 Elsevier.

As with $\text{Pd}(\text{OH})_2$, surface hydroxyl groups were mentioned frequently in literature in the 1990s. However, they started attracting much more attention after the publication of an in-situ DRIFTS study by Ciuparu et al.¹⁶⁸ in which it was shown that hydroxyl groups are present on the surface of palladium oxide during methane oxidation with added water. Further, the authors show that more hydroxyl groups are formed on a sample which has oxidized methane in the presence of water for 10 minutes at 350 °C than one exposed to wet air for the same amount of time, the results of which are presented to the left in Figure 27. They describe that the hydroxyl groups are the reason for inhibition and do not perform any long-duration studies. In 2007, Persson et al.¹⁷¹ followed up with another DRIFTS study on hydroxyl groups. The study confirmed many of the findings from three years earlier by Ciuparu et al., but included an interesting hydroxyl adsorption/desorption experiment in the absence of water at 200 °C, i.e. in a gas stream of methane and air, shown to the right in Figure 27. After 30 minutes, the hydroxyl coverage has almost stabilized, and upon removal of methane from the feed gas, hydroxyl groups start desorbing. Performing the experiment at 200

°C means that the stability of surface hydroxyls is drastically increased and desorption is slowed down, compared to what would be the case at a more realistic temperature, which is acknowledged by the authors.

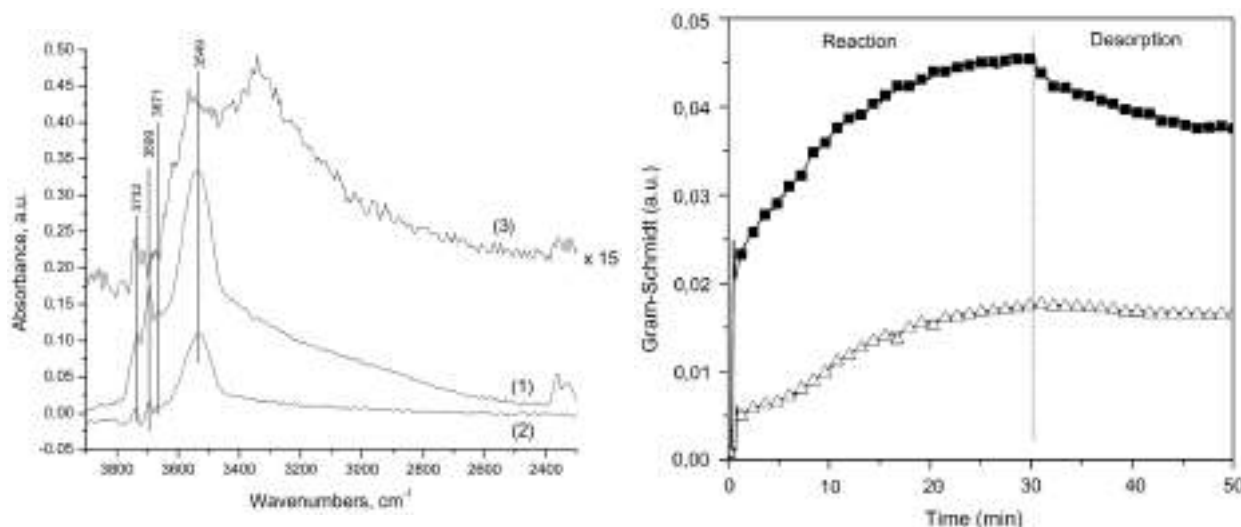


Figure 27 Left: DRIFTS spectra recorded at 350 °C of (1) Pd/Al₂O₃ exposed to wet methane conditions for 10 minutes, (2) Pd/Al₂O₃ exposed to moist air pulses, and (3) the Pd-free alumina support exposed to moist air. Spectrum 3 has been multiplied by 15. Reprinted with permission from Ciuparu et al.¹⁶⁸ Copyright 2004 Elsevier. Right: Hydroxyl adsorption and desorption at 200 °C on the surface of Pd/Al₂O₃ (black squares) and 2:1PdPt/Al₂O₃ (white triangles). Reprinted with permission from Persson et al.¹⁷¹ Copyright 2007 Elsevier.

The study by Persson et al.¹⁷¹ also included many interesting catalytic experiments. In one of these, a Pd/Al₂O₃ catalyst is deactivated for 12 hours under the following dry reaction conditions: 1.5% CH₄ in air, gas hourly space velocity = 250 000 h⁻¹, T = 500 °C. Long deactivation experiments with methane oxidation catalysts were rare at the time, as literature had been focused on inhibition. To describe the severe deactivation over time, the authors hypothesized that “the gradually decreasing activity may be due to the slow formation of surface hydroxyls and consequent buildup.” This is, to the best of my knowledge, the first time hydroxyl formation was used to explain irreversible deactivation over time, and not just inhibition. This hypothesis has later been propagated by others,^{28,31,32,52,125,159,172–177} including in our own review on zeolite-based methane oxidation catalysts.¹⁰ However, no evidence has been provided of a slow build-up of hydroxyl groups leading to deactivation over time.

Today, the fact that deactivation takes place on two different timescales is well-established. Petrov et al.⁵⁰ performed an insightful experiment on a Pd/H-ZSM-5 catalyst by alternating a wet and dry feed and comparing it to experiments with constant water feed, shown in Figure 28. The fast interaction occurs instantaneously upon water addition, and is fittingly termed reversible inhibition in other works.^{19,48,178–180} The slow and irreversible deactivation in the experiment with alternating water addition follows the experiments with constant water concentration, i.e. connecting the bottoms of the valleys.

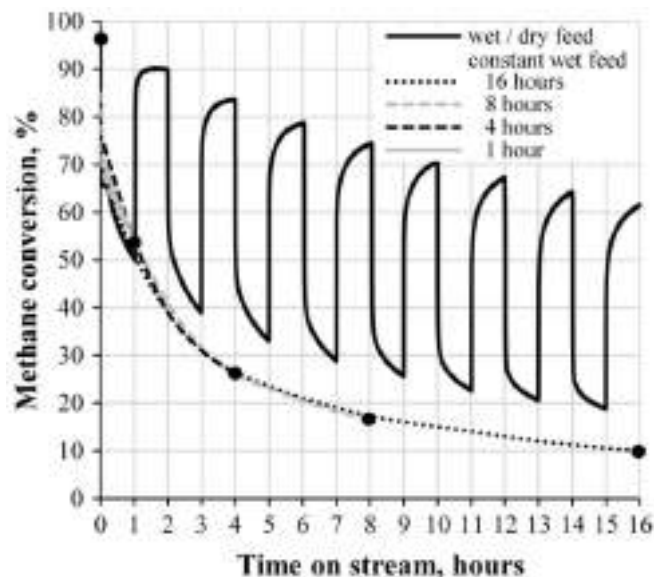


Figure 28 Catalytic test of Pd/H-ZSM-5 with constant and periodic addition of water. Reaction conditions: 1% CH₄, 4% O₂, 5% H₂O (when present), N₂ balance, GHSV = 80 000 h⁻¹, T = 450 °C. Reprinted with permission from Petrov et al.⁵⁰ Copyright 2017 Springer.

More evidence for hydroxyl groups being the cause of inhibition was presented recently by Li et al.¹⁸¹ In their publication, the authors used ambient pressure X-ray photoelectron spectroscopy (XPS) to show that hydroxyl groups are present on a palladium foil under both wet and dry methane oxidation conditions. As can be seen from Figure 29, the concentration of hydroxyl groups under wet conditions was several times higher though. It is not clearly stated in the article for how long time the samples were exposed to reaction conditions before the measurements were performed, but it appears to be a few minutes. Although the existence of hydroxyl groups had already been showed by IR studies, it was valuable to have it confirmed by a different method.

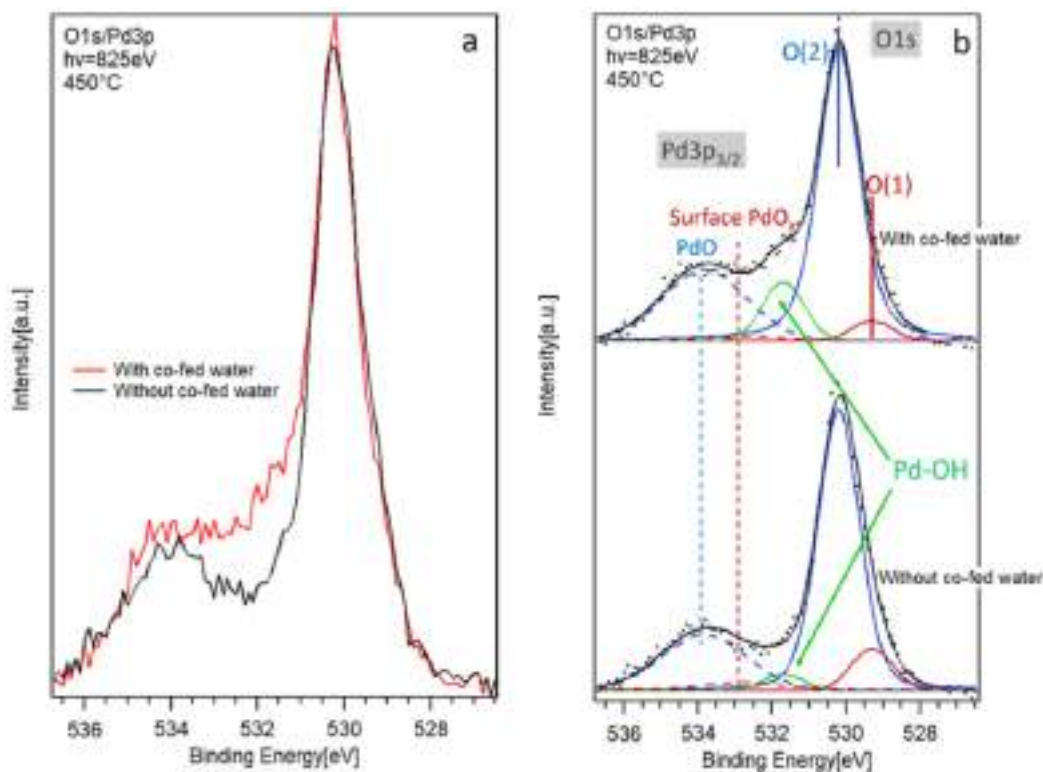


Figure 29 a) Ambient pressure X-ray photoelectron spectroscopy of O 1s and Pd 3p_{3/2} in a dry and wet methane oxidation gas mixture over a palladium foil at 450 °C. b) deconvolution of the spectra. Reprinted with permission from Li et al.¹⁸¹ Copyright 2020 American Chemical Society.

Even more recently, Velin et al.¹⁸⁰ followed up the DRIFTS studies by Ciuparu and Persson with an in-situ inhibition experiment showing hydroxyls on the catalyst surface during operation. The authors exposed a Pd/Al₂O₃ catalyst to methane oxidation conditions for 20 minutes and detected a small signal in the hydroxyl region around 3500 cm⁻¹. Water was then added to the feed gas and a strong absorbance signal appeared. The signal grew to full strength almost immediately, but seemed to stabilize after 10 minutes. After 20 minutes, water was removed from the feed gas, and, importantly, the signal quickly faded to the initial levels during dry methane oxidation before water addition. Although the original work does not discuss irreversible deactivation, the observation holds remarkable implications within the context of irreversible water-induced deactivation. This finding suggests that hydroxyl groups are exclusively associated with fast reversible inhibition. Notably, when water is removed from the feed gas, the additional hydroxyl groups visibly depart from the surface, dynamically adjusting the equilibrium to accommodate the new conditions.

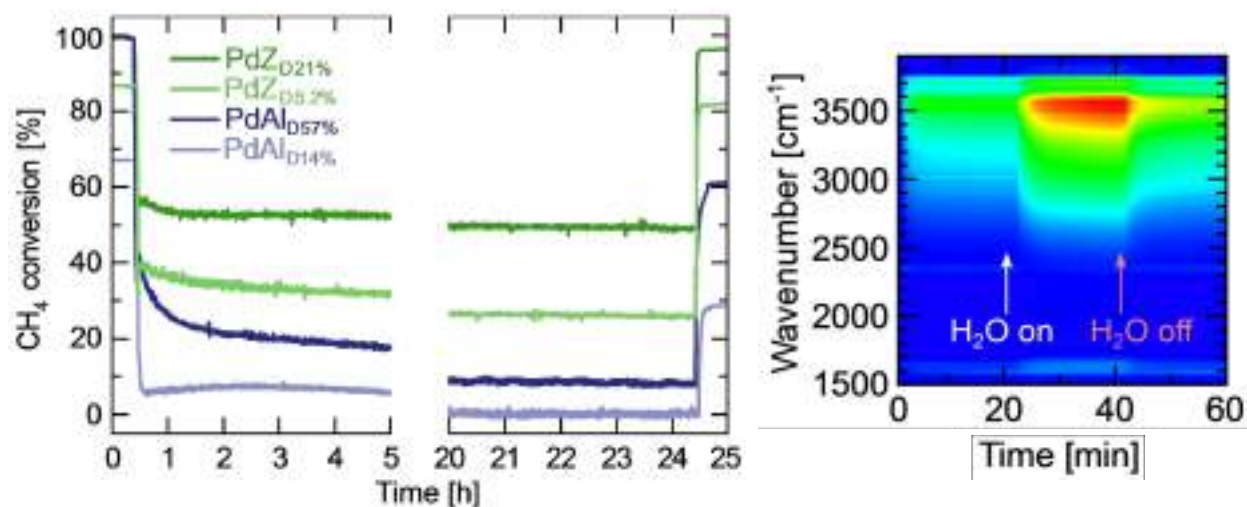


Figure 30 Left: Catalytic tests of palladium supported on alumina (PdAl) and ZSM-5 (PdZ) with palladium dispersion as percentage written as part of the sample names. All catalysts are inhibited by water, and slowly deactivate further over 24 hours. Reaction conditions: 1000 ppm CH₄, 2% O₂, 10% H₂O (when present), Ar balance, gas hourly space velocity = 32 000 h⁻¹, T = 400 °C. Right: DRIFTS measurements of hydroxyl groups on the surface of Pd/Al₂O₃ catalyst. Experimental conditions: 1000 ppm CH₄, 2% O₂, 2% H₂O (when present), Ar balance, T = 300 °C. Reprinted with permission from Velin et al.¹⁸⁰ Copyright 2021 Wiley.

To summarize, in a time of simple and short catalytic experiments, a hypothesis for water-induced inhibition was formulated: *When exposed to steam, and in particular when oxidizing methane in the presence of water, palladium-based catalysts will rapidly form an amount of hydroxyl groups on the palladium oxide surface. The amount of formed hydroxyls will quickly stabilize at an equilibrium level determined by the water concentration and the temperature.* When longer and more advanced deactivation experiments became available, a second type of activity loss was observed, which was not reversible upon removal of water from the gas feed. In the absence of a better explanation, the hypothesis for water-induced inhibition and the evidence behind it was extrapolated so that hydroxyl formation could explain both fast reversible inhibition and slow irreversible deactivation. That sums up the analysis of the evidence for the hydroxyl hypothesis for water-induced deactivation of methane oxidation catalysts.

A really interesting finding in the original water inhibition literature, which has not received much attention, is the leading hypothesis on why surface hydroxyls temporarily suppress methane oxidation. A slow-down of methane activation on the blocked sites has been given as the explanation for the lowered activity,^{181–183} but others point towards a delayed surface reoxidation as the reason.^{82, 167, 173, 177} An example of the latter is the work by Ciuparu et al.¹⁶⁷ in which the authors write: "surface hydroxyls resulting from methane oxidation impede surface reoxidation, leading to a certain degree of catalyst deprivation of oxygen and formation of bulk oxygen vacancies". That observation helped inspire our hypothesis for water-induced deactivation, described in Section 6.7.

6.2 Discovery of methane dependence

After building the catalytic test setup in the first year of the PhD project, hundreds of validation tests were performed to confirm that the equipment was working as intended. One of these, which also served to confirm the reaction order of methane determined by others,^{38,181,184} is shown in Figure 31. The experiment consisted of determining the conversion of methane oxidation at different methane concentrations. Assuming a first order reaction, a reaction rate could be calculated for the different concentrations as:

$$r = -\frac{F \cdot [\text{CH}_4]}{m_{\text{cat}}} \cdot \ln(1 - X) \quad (2)$$

Where r is the first order reaction rate, F is the total molar flow, $[\text{CH}_4]$ is the methane concentration, X is the fractional conversion and m_{cat} is the catalyst mass. If the assumption of a first order reaction is correct, the rate will be a linear function of methane concentration. Indeed, judging from the slight curvature of the rate versus methane concentration plot, the order of methane in complete oxidation is just below 1.

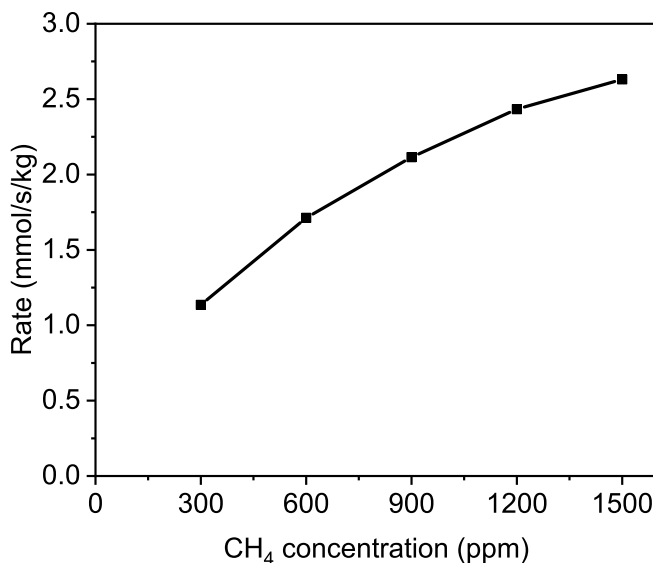


Figure 31 Figure showing methane oxidation rate of Pd/Al₂O₃ catalyst versus methane concentrations, assuming a reaction order of 1. The lines do not represent measurements, they are simply a guide for the eye. As the line is not linear, but bends slightly, the order in methane is slightly below 1. This fits well with results in literature.^{38,181,184} Reaction conditions: 300-1500 ppm CH₄, 10% O₂, N₂ balance, WHSV = 126 000 ml h⁻¹ g⁻¹, T = 300 °C.

Next, it was attempted to determine the order of methane in the presence of water. The experiment, shown in Appendix E, involved testing the conversion at different concentrations of methane again, but with water in the feed gas. Due to deactivation hindering measurements at a steady state, this was rather challenging. The conversion changed with the methane concentration as in the

experiment without water, implying a reaction order smaller than 1. More interesting however, was that the slope of the deactivation curve would also change with the methane concentration. This was very surprising, as it did not fit with the hydroxyl coverage hypothesis. The observation was repeated in a separate experiment to confirm the phenomenon, also shown in Appendix E. To observe the effect over a longer time-span, the experiment shown in Figure 32 was performed. A fundamental question emerged: Why is water-induced deactivation depending so heavily on methane concentration?

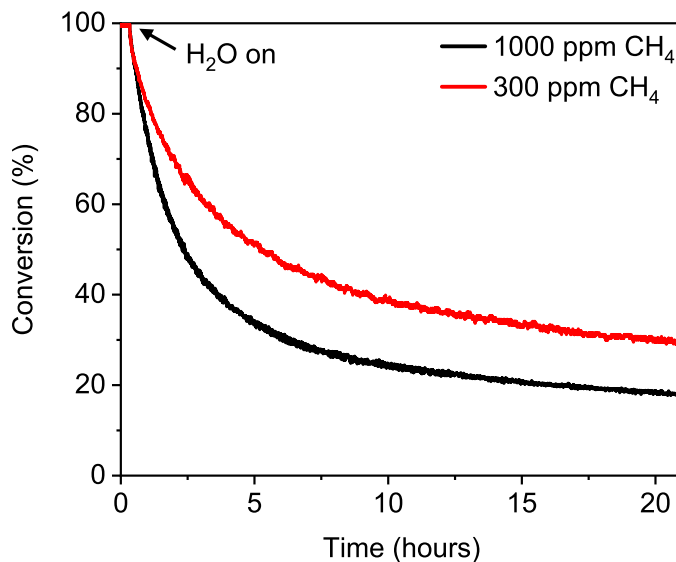


Figure 32 Extended experiment with Pd/Al₂O₃ catalyst showing that the rate of water-induced deactivation depends on methane concentration. Reaction conditions: 300 or 1000 ppm CH₄, 10% O₂, 10% H₂O, N₂ balance, WHSV = 126 000 ml h⁻¹ g⁻¹, T = 400 °C.

6.3 Methodology for water deactivation project

This section is located here for chronological reasons, but to understand its context, reading Paper 3 in advance is highly recommended. The goal of the project was to investigate both reversible inhibition and the slower, methane-dependent irreversible deactivation over time, shown in Figure 33.

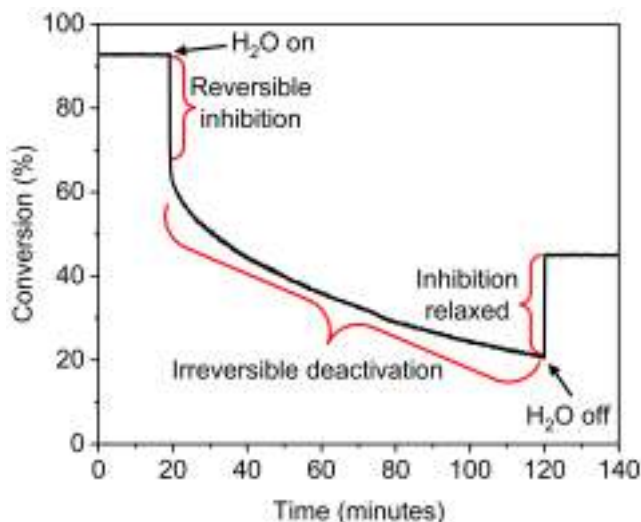


Figure 33 Experiment showing the two types of water-induced activity loss: Inhibition and time-dependent deactivation. When water is removed from the feed gas, the inhibition reverses, but the irreversible deactivation remains. Reaction conditions: 500 ppm CH₄, 10% O₂, 5% CO₂, 10% H₂O (when present), N₂ balance, WHSV = 1 260 000 ml h⁻¹ g⁻¹, T = 440 °C. Reprinted from Paper 3.

For the inhibition, calculating the height of the instantaneous activity drop upon water addition would provide a basis of comparison. Similarly, for characterising the deactivation curves during exposure to water, a measure for deactivation rate was needed. One approach was to imagine deactivation as a batch reaction converting activity, assign it an order in e.g. conversion (X), and then fit the experiments with traditional kinetics. Initially at $t = 0$, the “concentration” of fractional conversion would be $0 < X_0 < 1$, and when fully deactivated at some time t , $X = 0$. Depending on the assumed order in conversion, the rate law and the derived deactivation constant would take the form shown in Table 7.

Table 7 Integrated rate laws and methods for finding the rate constants under the various reaction orders. The concentration $[A]$ has been replaced by the fractional conversion X to reflect the fact that k_D is a deactivation rate constant.¹⁸⁵

Reaction order	Integrated rate law	Deactivation constant
0 th	$X = X_0 - k_D \cdot t$	-slope of X vs. time
1 st	$X = X_0 \cdot e^{-k_D \cdot t}$	-slope of $\ln(X)$ vs. time
2 nd	$\frac{1}{X} = \frac{1}{X_0} + k_D \cdot t$	slope of $1/X$ vs. time

As the deactivation curves clearly have curvature, zeroth order seemed implausible. Initially, a first order approach was decided upon as it seemed the simplest and least presumptive. This had to be adjusted however, when experiments with high concentrations of methane and water, i.e. with very fast deactivation, were performed. The difference between first and second order fits of experiments with moderate and rapid deactivation is shown in Figure 34. Under most circumstances, i.e. most concentrations of water and methane, the first order fit is able to capture the shape of the

deactivation curve. At high concentrations of water and methane however, only the second order fit can capture the high curvature of the experimental data. For this reason, the kinetic analysis in Paper 3 was performed assuming second order deactivation.

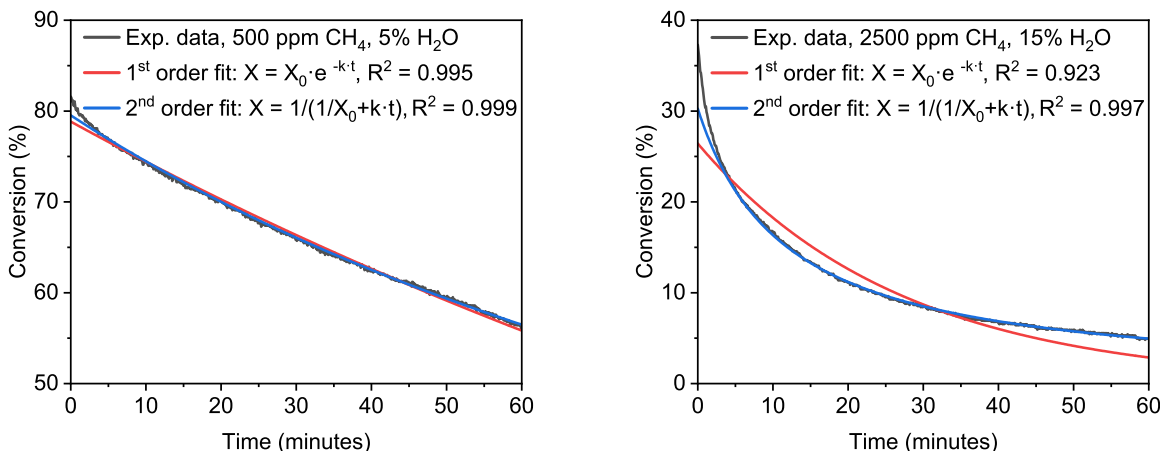


Figure 34 Kinetic experiments with moderate (left) and rapid (right) deactivation. When deactivation is very fast, only the second order fit can accurately represent the experimental data, whereas both fits are roughly equal at moderate and slow rates of deactivation. Reaction conditions: 500 or 2500 ppm CH₄, 10% O₂, 5 or 15% H₂O, 5% CO₂, N₂ balance, WHSV = 1 260 000 ml h⁻¹ g⁻¹, T = 440 °C.

In Figure 34 there is a curious detail which stands out around $t=0$. In every single experiment with water, the deactivation seemed to be particularly fast during the first 1-2 minutes after water was introduced to the feed gas. Indeed, the second order fit is has exactly no error with respect to the experimental data from $t=5$ to $t=60$, but a very significant error during the first few minutes. Our 2-part hypothesis for water-induced deactivation consisted of time-independent (fast) inhibition and time-dependent (slow) irreversible deactivation. After much contemplation, the discrepancy during the first minutes after water addition was assessed to actually be caused by inhibition. Water is obviously present in great excess, but as the reaction between gas-phase water and the catalyst forming hydroxyl groups near-instantaneously approaches equilibrium, adsorption sites become sparse. This likely slows down the process dramatically, to the point of it being measurable on the time scale of the deactivation experiments. The inhibition effect is so pronounced and depends so strongly on water that even minor discrepancies are clearly visible in well-resolved catalytic experiments.

For Paper 3, 36 experiments with different methane and water concentrations were planned out and performed. Due to the wildly different levels of inhibition caused by a very wide range of water concentrations, it was challenging to select a common temperature for the experiments where all measurements would fall within a reasonable conversion range. Eventually, it was decided to measure inhibition at 380 °C and deactivation at 440 °C, and then determine the influence of temperature on the two phenomena. From the kinetic experiments, 36 values for the second order

deactivation coefficient k_D were calculated. In an attempt to find a correlation between reaction conditions and catalytic deactivation, k_D was plotted against the feed gas concentrations of water and methane, as shown in Figure 35. The most simple description, and the one best fitting with the hydroxyl coverage hypothesis, would be that deactivation follows water concentration. As shown in Figure 35A, this is however a poor predictor for k_D , and the same is true for just methane, as shown in Figure 35B. The ratio between water and methane seemed like an important metric, considering the argument that they are competing for the same adsorption sites. Surprisingly, the correlation of k_D with the water-to-methane ratio was very poor. Instead, fitting k_D to the product of the concentrations, as shown in Figure 35D, decisively demonstrated that the deactivation rate depends on both water and methane concentration.

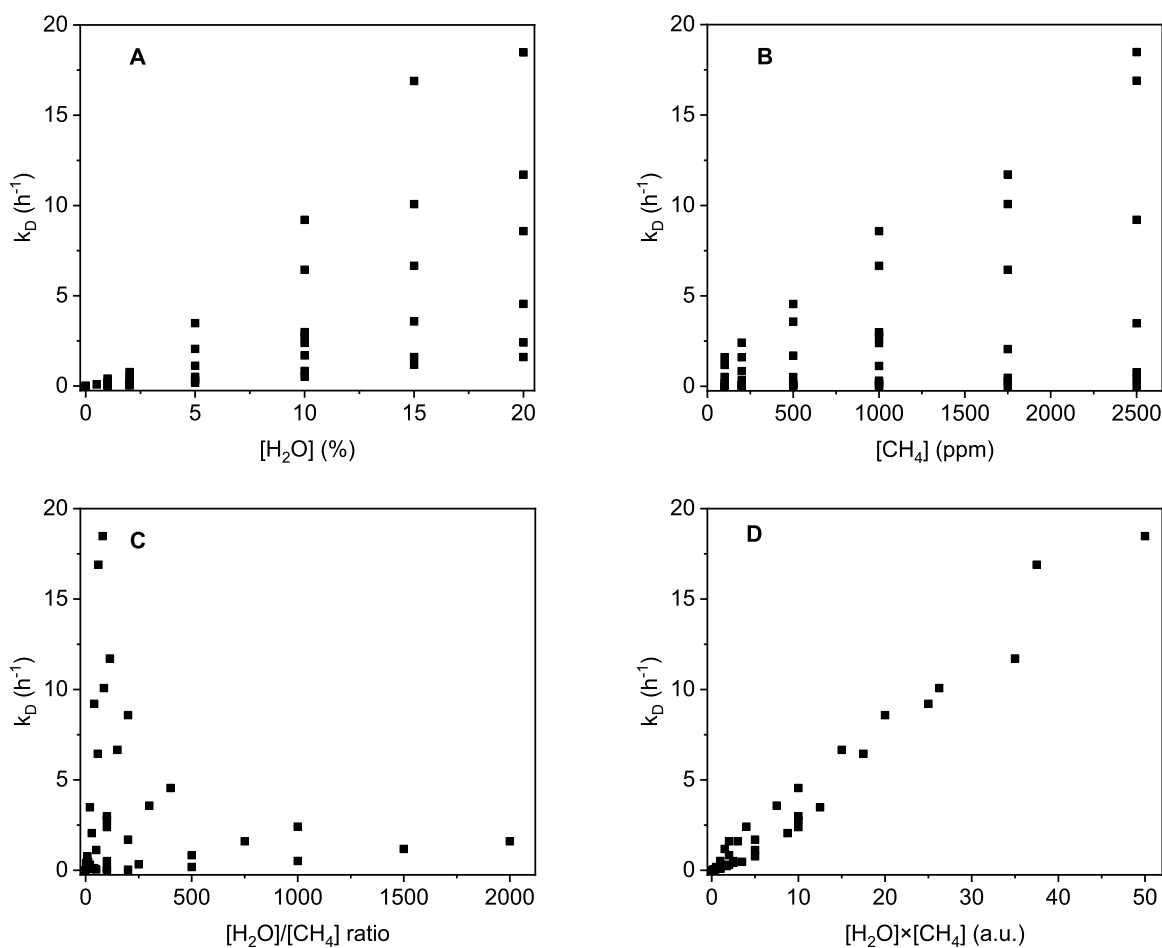


Figure 35 Second order deactivation coefficients from kinetic experiments plotted against combinations of water and methane concentration.

A key experiment of Paper 3 is the CH_4 -temperature programmed reduction (TPR) of a $\text{Pd}/\text{Al}_2\text{O}_3$ catalyst deactivated to different extents. TPR experiments on methane oxidation catalysts have been performed before,^{31,155,174} but to our knowledge never on thoroughly deactivated samples. The method was extremely powerful for the project as it provided a lot of valuable, easy-to-interpret

information, while being able to run on the catalytic test setup, which is relatively simple equipment compared to e.g. a synchrotron facility, which is often needed for alternative methods. The first iteration of the experiment is shown in Figure 36 along with the final version prepared for Paper 3. Even from the crude first attempt it was clear that the palladium oxide phase had changed during deactivation.

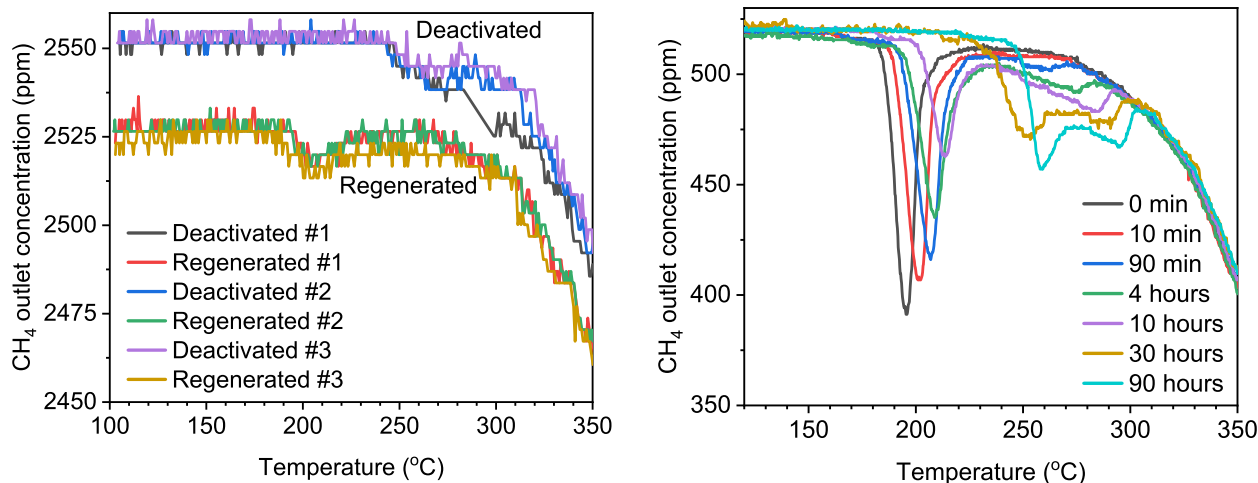


Figure 36 Left: First attempt at CH₄-TPR of deactivated and regenerated Pd/Al₂O₃ with repetitions to evaluate reproducibility. The experiments were performed in the chronological order of the figure legend. The measurements for the regenerated catalyst have been offset by -25 ppm. The sample was deactivated for 4 hours under the following conditions: 2500 ppm CH₄, 10% O₂, 10% H₂O, N₂ balance, flow = 420 ml/min, T = 450 °C. The sample was regenerated according to the procedure described in Paper 3. Right: CH₄-TPR experiment from Paper 3.

The several orders of magnitude improvement in quality going from Figure 36 left to right is a result of the following optimizations, instated after multiple iterations:

- Sample amount increased from 20 to 200 mg
- Sample dilution omitted to shorten the bed and consequently reduce the temperature difference across it in the thermal gradient of the furnace
- Temperature ramp reduced from 5 to 2.5 °C/min
- Methane concentration reduced from 2500 to 500 ppm
- Gas flow reduced by 11%
- FID detector re-calibrated to the specific measurement range

6.4 Paper 3

On the following pages, the manuscript for Paper 3 is presented in the form it had upon thesis submission. The supporting information for the manuscript can be seen in Appendix H.

Understanding Water-Induced Reversible Inhibition and Irreversible Deactivation of Methane Oxidation Catalysts

Rasmus Lykke Mortensen,^[a,b] Hendrik-David Noack^[b], Kim Pedersen,^[b] Susanne Mossin,^[a] and Jerrik Mielby*^[a]

[a] R. L. Mortensen, Prof. S. Mossin, and Dr. J. Mielby
DTU Chemistry
Technical University of Denmark
Kemitorvet 207, DK-2800 Kgs. Lyngby, Denmark
E-mail: slmo@kemi.dtu.dk

[b] H.-D. Noack, Dr. K. Pedersen
Umicore Denmark Aps
Kogle Allé 1, DK-2970 Hørsholm, Denmark

Abstract

Catalysts for complete methane oxidation suffer from water-induced deactivation due to the high concentrations of steam in the exhaust from natural gas-fired large engines. Here, we show simple catalytic experiments that convincingly disprove the commonly accepted explanation for water-induced deactivation. Instead, we present evidence for an alternative deactivation pathway, consisting of two separate deactivation phenomena, one of them requiring methane molecules to be converted at water-saturated sites, irreversibly changing active palladium oxide to inactive palladium oxide. The two types of palladium oxide are distinguished between and characterized by a series of novel temperature programmed reduction experiments where the relation between structural change and loss of activity can be accurately monitored. The dependence of both deactivation speed and inhibition depth on H₂O concentration, CH₄ concentration, temperature, and pressure is quantified in a series of kinetic experiments. Finally, we propose a simple model of three chemical equations which together describe deactivation during wet methane oxidation.

Introduction

Emission control of methane slip is required to realize the potential greenhouse gas savings of LNG as a maritime fuel. Environmental catalysts for complete oxidation of methane suffer from a series of deactivation phenomena which have hindered the development of a functioning exhaust treatment technology for decades. Direct water-induced deactivation is the least well understood deactivation pathway, the others being hydrothermal sintering and SO₂ poisoning. Despite recent advancements revolving around hydrophobic catalyst supports,^{1–5} it is still the main obstacle to be overcome, largely due to its illusive nature. The prevailing hypothesis revolves around hydroxyl groups forming on the active surface.^{3,6–12} Ciuparu et al. used in-situ diffuse reflectance-Fourier transform infrared (DR-FTIR) spectroscopy to show that hydroxyl groups form over time on a Pd/Al₂O₃ catalyst exposed to wet methane oxidation conditions, and that more hydroxyl groups form than when the material is exposed to just wet air.¹² A more recent example is the work by Li et al. who use ambient pressure X-ray photoelectron spectroscopy (XPS) to show the existence of a PdOH phase on the surface of a palladium foil during wet methane oxidation.⁶ The evidence for the hydroxyl formation hypothesis has two weaknesses: 1) The spectroscopic data is always collected with high concentrations of steam in the gas phase. This will inevitably result in a lot of signal from water adsorbed or bonded to every surface in the sample and not necessarily just from active sites deactivated by hydroxyl groups. 2) The “deactivated” samples that are spectroscopically investigated are exposed to wet methane oxidation conditions for a very short time, often minutes. For a methane oxidation catalyst to be considered deactivated, it should have lost a significant amount of activity, preferably measured under stable and dry conditions before and after the deactivation

sequence respectively. The hydroxyl groups should then be detected spectroscopically without steam in the gas phase. Post-catalysis characterization after long time-on-stream experiments have previously been focused on hydrothermal sintering.

Several research groups have discovered that repeated short reducing pulses effectively negate the irreversible loss of activity resulting from the catalyst's interaction with water over time.^{13–16} A reducing pulse, which in practice consist of shutting off oxygen for a few seconds, rapidly reduces the PdO nanoparticles to metallic palladium, whereafter they are re-oxidized to a regenerated state. In their work on regeneration through reducing pulses, Franken et al.¹⁴ provide an alternative explanation for what happens on a structural level with the catalyst in time-on-stream experiments in the presence of water. Essentially, the hypothesis revolves around the finding that surface sites offering methane oxidation activity are generally less crystalline, in the sense that they contain some amount of defects, oxygen vacancies or crystallographic strain. Another description is that the active palladium oxide is coordinatively unsaturated.¹⁷ The loss of activity comes from healing of defects or relief of strain, which causes crystallization and densification, resulting in a surface with fewer active sites. This new perspective inspired our work in which we further justify that water adsorption/hydroxyl formation is likely not the sole reason for irreversible activity loss in methane oxidation catalysts. Instead, it is merely a component of the real mechanism behind, which involves a bulk change to the palladium oxide itself.

Results

Two Distinct Types of Water-Induced Activity Loss

To investigate the mechanism of water-induced deactivation, a catalyst with significant water-tolerance is required, preferably one representing the state-of-the-art. An off-the-shelf hydrocarbon oxidation catalyst from Umicore was used, consisting mainly of palladium on alumina. This catalyst has a high initial activity for both dry and wet methane oxidation and water-induced activity losses can be regenerated by a reducing pulse (Supplementary Fig. 1). Light-off experiments are a common catalytic test, but these are typically not of high value on their own when addressing permanent losses of activity, due to the temporal element of most deactivation phenomena.¹⁸ Instead, more information can be gained by leaving a catalyst under conditions where it deactivates, and then analyzing the resulting deactivation curve. This is typically done for methane oxidation by running the same time-on-stream experiment with and without water. From these, it can easily be concluded that water plays a critical role in the deactivation of methane oxidation catalysts. Furthermore, when adding water periodically as done by Petrov et al.¹⁹ it becomes clear that some of the activity loss experienced by the catalyst is reversible. The reversible part is reasonably well understood and is often described as a form of inhibition. The irreversible and slowly progressing part of the activity loss is termed deactivation and is less well understood. An experiment presenting both phenomena is shown in Figure 1.

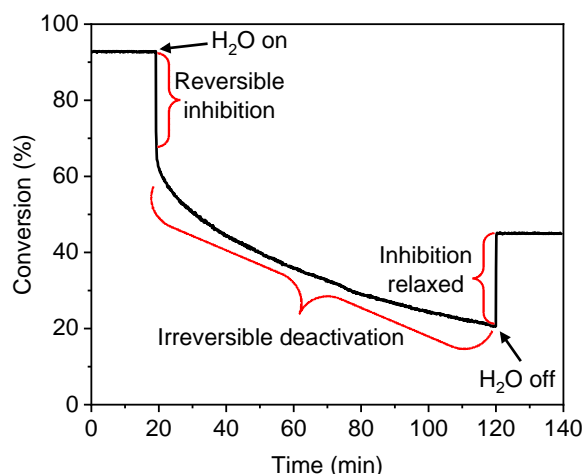


Figure 1 | Experiment illustrating the two types of activity loss investigated in this paper. One is quick and reversible, the other is slower and irreversible, respectively termed inhibition and deactivation. Upon addition of water, the rate almost instantaneously drops by 61% but recovers the same exact fraction when water is removed from the feed gas. Reaction conditions: 500 ppm CH₄, 10% O₂, 10% H₂O (when present), N₂ balance, T = 440 °C, WHSV = 1.260.000 ml h⁻¹ g⁻¹.

Changing the water concentration mid-experiment clearly shows that, although water is always present in orders of magnitude higher concentrations than methane, the exact amount of water determines the deactivation rate (Supplementary Fig. 2). In a similar manner, we ran an unorthodox deactivation experiment where methane was left out, except for five minutes every four hours to get an activity reading for following the deactivation. This experiment is shown in Figure 2 together with a reference experiment with constant methane feed.

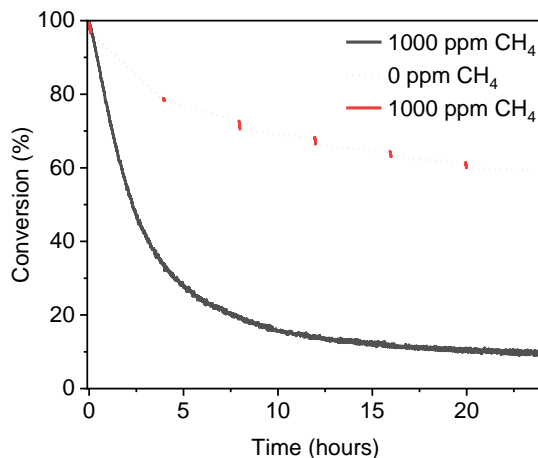


Figure 2 | Deactivation experiment with and without methane. Experiments were run in sequence and preempted by a reducing pulse regenerating the catalyst bed. Reaction conditions: 1000 ppm CH₄ (when present), 10% O₂, 10% H₂O, N₂ balance, T = 380 °C, WHSV = 126.000 ml h⁻¹ g⁻¹.

The catalyst in the methane-free experiment deactivates rapidly whenever methane is present, but otherwise seems to be relatively stable. The currently accepted hypothesis for water-induced deactivation consisting of water adsorption and hydroxyl build-up is independent of methane and would predict the same degree of deactivation in the two experiments. Instead, this experiment points towards methane playing a role in the irreversible loss of activity experienced by palladium-based methane oxidation catalysts.

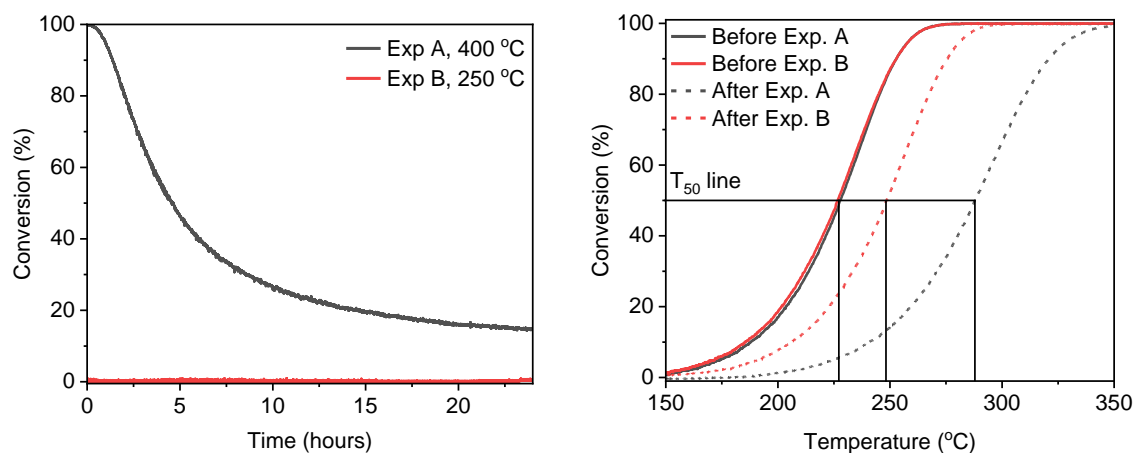


Figure 3 | Deactivation experiment with and without methane conversion. Left: Time-on-stream experiment in the presence of water performed at two different temperatures. Right: Light-down curves before and after ToS experiments. Before the ToS experiments, the starting point is the same for A and B (T_{50} of 228 °C and 227 °C respectively). After the ToS experiment, the T_{50} values are 288 °C and 248 °C for A and B respectively. Reaction conditions during deactivation segments: 1000 ppm CH_4 , 10% O_2 , 10% H_2O , N_2 balance, $\text{WHSV} = 126.000 \text{ ml h}^{-1} \text{ g}^{-1}$. Reaction conditions for light-down tests: 1000 ppm CH_4 , 10% O_2 , N_2 balance, ramp = 5 °C/min, $\text{WHSV} = 126.000 \text{ ml h}^{-1} \text{ g}^{-1}$.

There are two possibilities. Either, 1) the presence of methane is involved in deactivation, or 2) the conversion of available methane is involved in deactivation. To distinguish between these two cases, we designed an experiment where methane would be present, but the temperature would be low enough to avoid significant oxidation activity. This experiment is shown in Figure 3, along with a reference experiment at 400 °C and light-down curves before and after each run. From the light-down curves it can be concluded that the sample at 400 °C deactivated the most. This is counter intuitive according to the water adsorption/hydroxyl formation hypothesis which predicts more water adsorption and more strongly bound hydroxyl groups for the experiment at lower temperature. At 250 °C the conversion is negligible in the presence of water, and the catalyst deactivates much slower than at 400 °C. This indicates that the methane oxidation reaction itself is part of whatever is causing an irreversible loss of activity. The difference in T_{50} before/after deactivation for the two experiments is 60 °C and 21 °C, meaning that the effect is quite substantial. In the experiment at 250 °C, between 1 and 4 ppm of methane is being converted throughout the experiment which explains the observed non-zero deactivation.

Having established that irreversible activity loss requires methane conversion, it is clear that deactivation and inhibition cannot be caused by the same chemical phenomenon, i.e. hydroxyl build-up quickly at first and slower over time. We will distinguish between the two by calling irreversible activity loss deactivation, and the reversible activity loss inhibition. Although the catalyst can be regenerated, the term irreversible refers to the fact that simply removing water from the gas feed does not bring back activity. When measuring steep deactivation curves like those shown here, catalytic tests are performed across a wide conversion range. We have attempted to stay within reasonable limits to avoid approaching a diffusion limited regime.

Dependency of deactivation and inhibition on water and methane concentration

After having established that not just water, but also methane, are reactants in the chemical reaction causing irreversible loss of activity in methane oxidation catalysts, the exact dependency should be determined. This was done by running 36 kinetic experiments with different concentrations of methane and water, shown in Table 1.

Table 1 | Six concentrations of water and six concentrations of methane giving 36 individual kinetic experiments.

Concentrations of methane (ppm)	100, 200, 500, 1000, 1750, 2500
Concentrations of water (vol%)	0, 1, 2, 5, 10, 15

In the 36 kinetic experiments, a short segment was included to measure the depth of the drop of conversion caused by reversible inhibition (Supplementary Fig. 4). The depth of the inhibition drop was measured as a percentual decrease in first order methane conversion rate, calculated as:

$$\Delta r = \frac{r_1 - r_2}{r_1} \cdot 100\%$$

Where r_1 and r_2 are the first order methane conversion rates for the top and the bottom of the inhibition drop respectively, calculated as:

$$r = \frac{F \cdot [\text{CH}_4]}{m_{\text{cat}}} \cdot \ln(1 - X)$$

Where F is the total molar flow, $[\text{CH}_4]$ is the concentration of methane in the feed gas, m_{cat} is the catalyst mass and X is the fractional conversion. As a first approximation, the deactivation curve was fitted to a second order expression (Supplementary Fig. 4) to obtain a rate constant for the irreversible loss of activity over time:

$$\frac{1}{X} = \frac{1}{X_0} + k_D \cdot t$$

Where X is the fractional conversion at time t , X_0 the initial conversion (just after introduction of water to the gas feed), t is the time in hours, and k_D the deactivation rate constant with the unit h^{-1} . Raw data from the 36 kinetic experiments can be found under supplementary information on the journal website.

The values for Δr and k_D were extracted and plotted as functions of methane and water concentration, shown in the top of Figure 4. Other than some minor irregularities at very low methane concentrations, Δr can be seen to depend exclusively on water concentration and not methane concentration. On the contrary, k_D depends on both water and methane concentration. In experiments with no water, the deactivation rate constant k_D has the value 0. Upon introduction of water however, k_D grows rapidly. The dependencies presented in both contour plots appear smooth and continuous (except for the difference between 0 and 1% water), indicating good reproducibility. To further verify the methodology, the experiment with 10% water and 1000 ppm CH_4 was repeated twice. The standard deviation for Δr was less than 1% of the average value while it was 9% for k_D . Below the contour plots, the same data is shown in two dimensional plots as functions of the concentration of water and methane. Inhibition depends linearly on the water concentration to the power of 0.25 and the deactivation rate depends linearly on the product $[\text{CH}_4]^{0.85}[\text{H}_2\text{O}]^{1.15}$. The exponents 0.25, 0.85, and 1.15 can be interpreted as scaling factors of the various components' influence on inhibition and deactivation and will be discussed further in a later section.

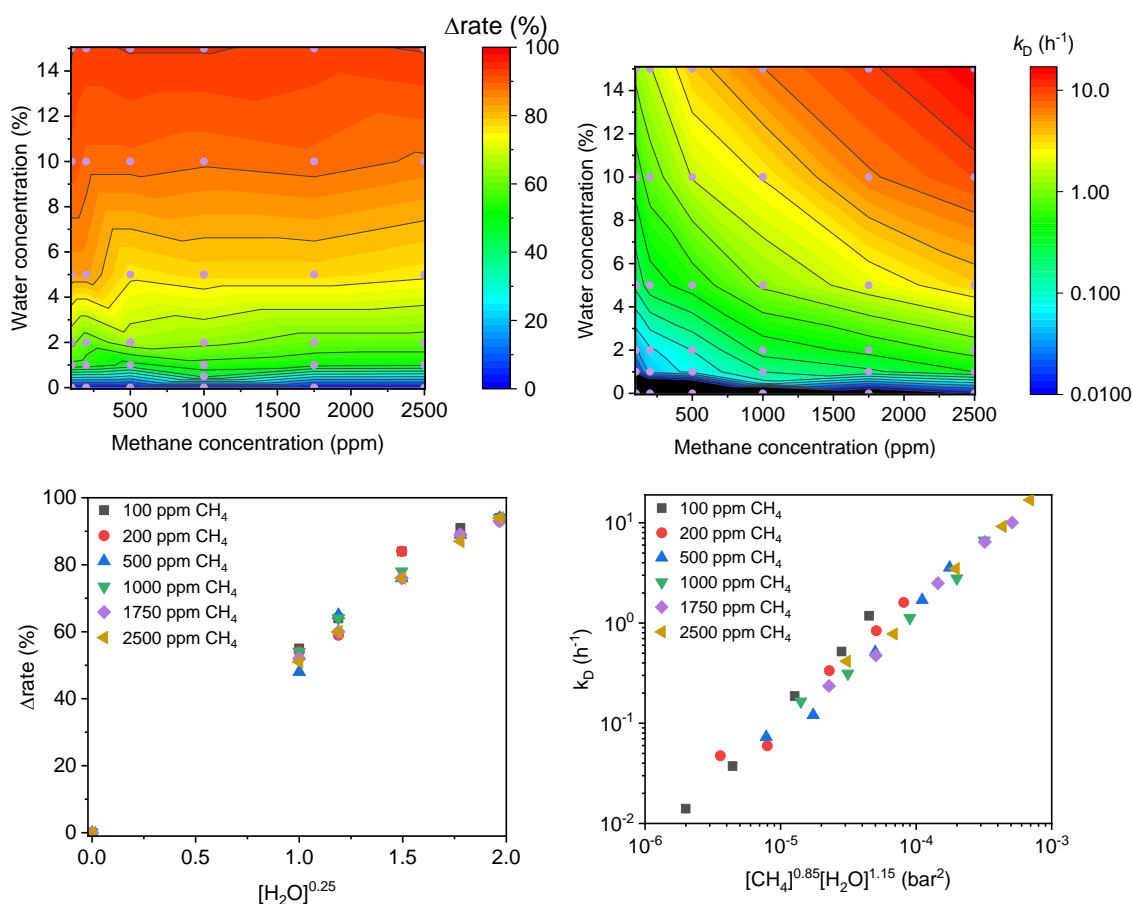


Figure 4 | Determination of dependence on water and methane concentration. Top left: Contour plot describing how much the methane oxidation rate is decreased upon water addition as a function of methane and water concentration. Top right: Contour plot describing how deactivation rate depends on water and methane concentration. Bottom left: Inhibition data as function of water concentration to the power of 0.25. Bottom right: Deactivation rate constants plotted against a product of CH_4 and H_2O partial pressures where the total order is 2, corresponding to the assumed total order of the deactivation rate.

The reversible inhibition depends on water concentration in a manner which agrees with the findings of Keller et al.²⁰ In their work, the inhibition is measured as the difference in T_{50} (the temperature at which conversion is 50%) between two light-off experiments, one dry and one in the presence of water. For better comparison, the inhibition data was plotted against the water concentration to the power of 1 (Supplementary Fig. 5). In the work by Keller et al. it is concluded that inhibition increases the most at low concentrations of water. From Figure 4, it is clearly visible that both inhibition and deactivation continue to increase drastically beyond 5% water. This common feature is important, as it ties them closer together, in that they both continue to worsen almost limitlessly as more water is added.^{21,22} The dependency of inhibition and deactivation on temperature and pressure was found using the same methodology as in the above. Above 500 °C deactivation starts to be less pronounced, and at 575 °C it is only taking place to a very small degree (Supplementary Fig. 6). These temperatures correspond well with previous observations of irreversible deactivation where hydroxyl formation was thought to be the culprit.^{5,7} Elevated pressure greatly accelerates water induced deactivation, as k_D steadily increases between 1 and 4 bar (Supplementary Fig. 7). Reversible inhibition by water is also strongly temperature dependent, worsening gradually as the temperature is lowered (Supplementary Fig. 8). Finally, elevated pressure also deepens inhibition (Supplementary Fig. 9). The fact that irreversible deactivation and reversible

inhibition shares the same dependencies on water concentration, temperature, and pressure suggests that they are both a function of water/hydroxyl surface coverage, as illustrated in Table 2. This is likely why most literature points towards essentially the same explanation for inhibition and deactivation.

Table 2 | Diagram describing the relation between extent of catalytic phenomena and changes in reaction conditions.
Arrow up symbolizes an effect that worsens when the specific parameter is increased.

	T	p	[H ₂ O]
Reversible inhibition	↓	↑	↑
Irreversible deactivation	↓	↑	↑
H ₂ O surface coverage	↓	↑	↑

What separates active PdO from Inactive PdO?

Considering that the activity of methane oxidation catalysts is closely linked to the reducibility of PdO, it seems natural to investigate how deactivation influences reducibility. For this, we have performed a series of temperature programmed reduction experiments, shown in Figure 5. The freshly regenerated sample has a regularly shaped and relatively narrow reduction peak at 195 °C. When exposed to conditions for complete methane oxidation in the presence of water, the reduction peak gradually shrinks and moves to higher temperatures. The shift to higher reduction temperatures for deactivated catalysts makes sense given that PdO reduction is part of the Mars-van Krevelen (MvK) mechanism and a slow-down of oxidation state changes will reduce activity.

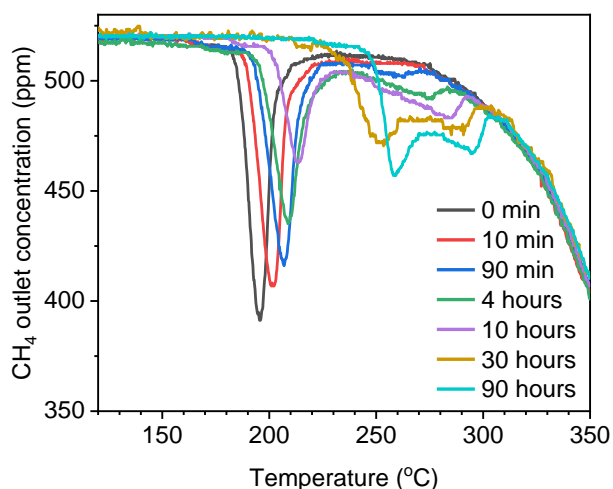


Figure 5 | CH₄-TPR experiment with samples deactivated to different extents. As the catalyst is deactivated more, the palladium oxide nanoparticles become significantly more difficult to reduce. Samples deactivated for 2 and 30 minutes were also recorded but they were almost on top of 0 and 10 minutes respectively. To make a less cluttered figure they were left out. Between each run the bed was regenerated and a CH₄-TPR experiment performed to verify that all deactivation experiments had the same starting point (Supplementary Fig. 10). The background reaction taking place from 280 °C is assumed to be decomposition of methane to carbon and hydrogen taking place on the surface of metallic palladium particles. Conditions during CH₄-TPR: 500 ppm CH₄ in N₂, 2.5°C/min, GHSV = 111.000 ml h⁻¹ g⁻¹. Conditions during deactivation: 1000 ppm CH₄, 10% O₂, 5% H₂O, N₂ balance, 420°C, GHSV = 126.000 ml h⁻¹ g⁻¹.

In parallel with the shrinkage and displacement of the main reduction peak caused by extended deactivation, a pair of reduction peaks grow out at higher reduction temperatures. After 30 hours, the main peak has almost completely disappeared, being replaced by two broader peaks at 260 and 290 °C with comparable combined area. The total peak area is relatively constant throughout the series (Supplementary Fig. 11) and the average area of the CH₄-TPR signal corresponds to reduction of 100% of the amount of palladium oxide present in the sample, as determined by inductively

coupled plasma optical emission spectrometry (ICP-OES, Supplementary Table. 1). Activity loss and changes to PdO reducibility happen in parallel and in the exact same fashion. They happen quickly to begin with and gradually slow down, but never fully stop taking place. It seems straight-forward that the two are connected. Looking at the TPR peaks, the deactivation seems to be a bulk phenomenon, as the whole PdO particle is clearly being restructured. That water-induced irreversible deactivation should not just be a surface phenomenon is perhaps surprising but considering that the MvK mechanism relies on bulk oxygen transport it seems plausible that a lowered reducibility of the bulk phase could lead to deactivation beyond that caused by surface changes.

Instead of deactivating the catalyst for different amounts of time to manipulate the deactivation temperature of PdO, running two-hour deactivation cycles in the presence of different water concentrations will similarly result in different PdO reduction temperatures (Supplementary Fig. 12). The changing identity of palladium oxide is currently being investigated, especially what structural difference is behind the significant increase in reduction temperature exhibited by the deactivated catalyst, including various X-ray and spectroscopy techniques.

Characterization of the reversible inhibition phenomenon

As shown, the irreversible loss of activity over time can be linked to changes in the reducibility of the active palladium oxide nanoparticles. Using a novel type of TPR experiment, the reversible inhibition caused by water can also be explored. Boucly *et al.*¹⁷ recently used ambient pressure X-ray photoelectron spectroscopy (XPS), in the presence and absence of water, to show that water on the nanoparticle surface changes reducibility of PdO. In the same fashion, we ran a series of CH₄-TPR experiments on the same freshly regenerated sample, with different concentrations of water vapor in the reducing gas. These are shown in Figure 6 along with a summary of the catalytic inhibition data.

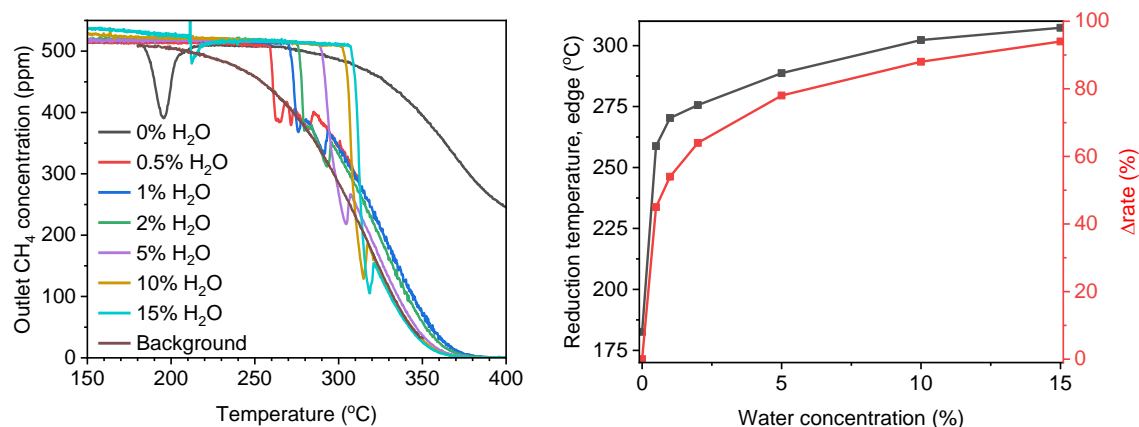


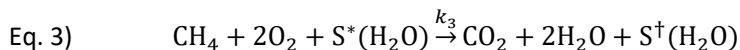
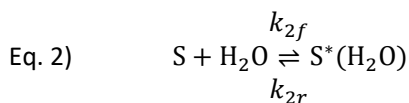
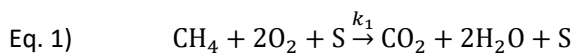
Figure 6 | CH₄-TPR in the presence of water. Left: CH₄-TPR experiment with identical regenerated samples but with different concentrations of water. For recording the background reaction in the presence of water, a pre-reduced sample was cooled down at 2.5°C/min in a gas flow consisting of 500 ppm CH₄ and 5% H₂O in N₂. Conditions during CH₄-TPR: 500 ppm CH₄ in N₂, 2.5°C/min, GHSV = 111.000 ml h⁻¹ g⁻¹, water concentration: see figure legend. Right: Reduction peak temperatures from wet TPR experiment plotted with catalytic inhibition data from kinetic experiments (see Figure 4), as

Having water present during the TPR experiment enabled a new type of background reaction, steam reforming. As with the background reaction in the dry experiment, it only started to occur after the sample had been reduced, indicating that it is catalyzed by metallic Pd and not palladium oxide. This made many of the reduction peaks difficult to interpret. Instead, the edge formed by the sequential rapid reduction and initialization of water-gas shift reaction was used for the wet TPR experiments. Comparing the reduction temperatures of the catalyst exposed to different water concentrations

with the effect of water on immediate catalytic activity, shown to the right in Figure 6, a reasonable hypothesis for the inhibition phenomenon can be formulated: Water is adsorbing to the surface to an extent determined by an equilibrium at relevant conditions, making it inaccessible to methane and therefore more difficult to reduce. The less reducible palladium oxide has lower activity for methane oxidation, as PdO reduction is central in the Mars van Krevelen mechanism. The fact that both irreversible deactivation and reversible inhibition can be linked to their respective effects on methane oxidation activity with relatively simple TPR experiments open new possibilities to understand catalytic behavior.

A combined kinetic model for inhibition and deactivation

To summarize, our results show that the activity loss of PdO during methane oxidation in the presence of water is caused by a fast and reversible inhibition and a slow and irreversible deactivation. The inhibition is an equilibrium phenomenon that scales indefinitely with the concentration of water present. On the other hand, the slow deactivation is irreversible at oxidizing conditions and depend on methane being converted. To explain these key observations, we propose the following three equations:



Equation 1 is the reaction of CH₄ with O₂ to give CO₂ and H₂O. The reaction occurs on a surface-active site S that is unchanged by the reaction. Equation 2 is the reaction of water with the surface-active site S to give an inhibited site S*(H₂O) corresponding to an adsorbed water molecule, a hydroxyl-group or similar on the site. This site has limited activity for methane oxidation compared to S. Equation 3 is conversion of methane on the inhibited site, which results in complete deactivation and loss of the surface active site.

Since S*(H₂O) immediately reacts to changes in the water concentration, we expect that the rate constants for water adsorption k_{2f} and desorption k_{2r} are high. Although methane oxidation forms water, the catalyst does not deactivate under dry methane oxidation conditions where there is no additional water in the feed. Therefore, we also expect that k_1 is significantly higher than k_3 . If the dry methane oxidation reaction was kept under 350°C, a mild deactivation caused by the reaction with product water was observed (Supplementary Fig. 13). This indicates that also the formed water is absorbed on the catalyst's surface at low temperatures.¹²

On the basis of Equations 1-3, we developed a simple quasi-empirical model to test our understanding of the deactivation mechanism. Equation 4 shows a typical Langmuir-Hinshelwood expression that assumes a first order reaction in methane and zero order reaction in CO₂ and H₂O concentration.

$$\text{Eq. 4)} \quad r_{\text{CH}_4} = K_1 \cdot [\text{CH}_4] \cdot \theta_s$$

Here, K_1 is the rate constant, $[\text{CH}_4]$ is the methane concentration, and θ_s is the fraction of remaining surface-active sites. The rate constant K_1 is given by the following Arrhenius equation:

$$\text{Eq. 5)} \quad K_1 = A \cdot e^{\frac{-E_a}{R \cdot T}}$$

where A is the preexponential factor, and E_a is the apparent activation energy as determined from catalytic experiments (Supplementary Fig. 14). Furthermore, we expressed the total deactivation as a fast (time-independent) and a slow (time-dependent) decrease in the fraction of surface-active sites, corresponding to reversible inhibition and irreversible deactivation, respectively, in the following equation:

$$\text{Eq. 6)} \quad \theta_S = \frac{1}{1 + K_2 \cdot [\text{H}_2\text{O}]^{0.25} + K_3 \cdot [\text{H}_2\text{O}]^{1.15} [\text{CH}_4]^{0.85} \cdot t}$$

The powers of methane and water concentrations in Eq. 6 were obtained as the values where the results of all 36 experiments performed collapsed to the best single line as evaluated by least squares fitting, as shown in Figure 4.

Using the method of lines, we then modelled the plug flow reactor by a set of ordinary differential equations and fitted the proposed rate expression to our data sets of conversion versus time. More specifically, we divided the reactor volume into 20 sections and fitted K_2 and K_3 using the least squares method. Figure 7 shows how the resulting model compares to our experimental data with 1000 ppm methane and 1 %, 5 %, and 10 % water, respectively. As a first approximation, the model results in an excellent fit that will give a good basis for more advanced modelling. The conversion vs time data from our kinetic study is available for download on the journal website.

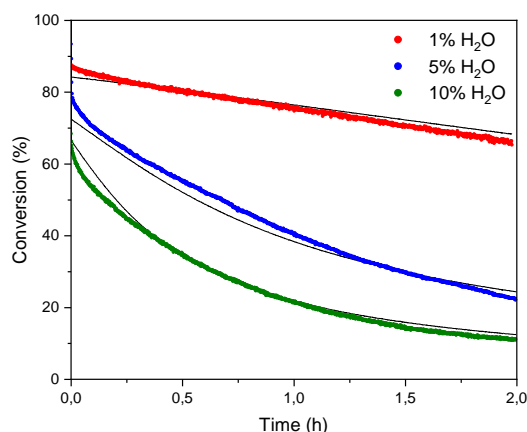


Figure 7 | Comparison of the predictions of the kinetic model (solid lines, calculated at $K_2 = 122$ and $K_3 = 384$) with the experimental results at 1000 ppm CH₄ and 3 different concentrations of water.

In conclusion, this study showed how a Pd/Al₂O₃ catalysts deactivated during methane oxidation under realistic operation conditions. The total deactivation was a combination of a fast, reversible blocking of the active sites (inhibition) and a slow, irreversible loss of the surface active sites (deactivation). Both phenomena significantly increased the reduction temperature of PdO as probed by CH₄-TPR, and the observed shift of reduction temperature was an excellent descriptor for the degree of deactivation. Furthermore, the increase in reduction temperature of all PdO present indicated that the deactivation was not a surface phenomenon on PdO nanoparticles, but was better described as a complete restructuring of the active PdO phase that is initiated by a methane oxidation event on a PdO site with adsorbed hydroxyl groups. The deactivation was quite slow during wet methane oxidation, but could always be reversed quickly and reproducibly through a reductive treatment. Based on a comprehensive kinetic study, we proposed three reaction equations and a simple quasi-empirical kinetic model that captured the key trends in catalytic activity.

The restructured surface phase is only subtly different from the original PdO phase. Powder X-ray diffraction of fresh, deactivated, and regenerated catalyst gave exactly the same diffractogram. No

additional phases compared to the support material were found. Further spectroscopic investigations are in progress to identify the origin of the observed difference in methane oxidation activity.

Methods

Catalytic testing

Complete methane oxidation reactions were carried out using a fixed-bed reactor with an inner diameter of 10 mm. The reactor was positioned in a temperature-controlled furnace and fitted with thermocouple inside the reactor just after the bed. The catalyst (Pd/Al₂O₃ oxidation catalyst from Umicore Denmark ApS) was ground, pressed, and crushed into particles ranging from 150 to 300 µm. The bed was diluted with 2 g SiO₂ sand (150-300 µm) for experiments with 200 mg catalyst, and with 1 g for experiments with 20 and 5 mg catalyst to avoid excessive local heating. The bed was positioned on a quartz wool plug and 500 mg quartz sand to get a level base. Four gasses were fed by independent mass flow controllers from Bronkhorst: Air, N₂, CO₂, and 2% CH₄ in N₂ with a total flow rate of 420 ml/min. Steam was added to the gas stream by a Controlled Evaporator-Mixer (CEM, Bronkhorst), which was fed by a stainless steel water container pressurized by N₂. The reactor was pressurized by an Equilibar LF Series Precision Back Pressure Regulator. Feed and outlet methane concentration was measured using a Thermo-FID ES from SK Elektronik and conversion calculated as:

$$\text{Conversion} = (C_{\text{in}} - C_{\text{out}})/C_{\text{in}} \times 100\%$$

Where C_{in} and C_{out} are the methane concentrations in the inlet and outlet gas respectively. Light-off tests were performed at a ramp of ± 5 °C/min. Data displayed from these tests are from the cooling segment of the experiment, i.e. a light-down instead of a light-off. We have found this to be a more accurate and reproducible approach. Catalyst regeneration consisting of reduction and reoxidation was carried out in the same catalytic setup. It was performed by exposing the reactor bed to 1000 ppm CH₄ in N₂ in a total gas flow of 380 ml/min for 5 minutes followed by 10 minutes at standard methane oxidation conditions (1000 ppm CH₄, 10% O₂ in N₂). Prior to kinetic experiments, using fresh catalyst beds every time, the catalyst was degreed for 1 hour at 500 °C in the same standard gas mixture.

Using the right equipment and conditions, light-off experiments can be a helpful and reliable way of determining the deactivation state of a catalyst. In our work, we often took advantage of the fact that water-deactivated methane oxidation catalysts can be regenerated by a short reducing pulse.^{14-16,23} This allowed us to always have the same starting point for deactivation experiments. The activity of the regenerated catalyst is slightly higher than that of the fresh (Supplementary Fig. 1). This is also observed in the work by others, in which the regenerated catalyst is described to be in a temporary "highly active state".^{14,15} In our case however, the activity gained from regeneration was not short-lived (Supplementary Fig. 3).

CH₄-TPR

Methane temperature programmed reduction (CH₄-TPR) experiments were conveniently performed in the same reactor setup as the catalytic testing. The sample was placed on a plug of quartz wool leveled off by 500 mg SiO₂ sand. Since the TPR experiment essentially regenerated the catalyst, multiple deactivation experiments could be performed on the same bed. After a deactivation segment, the sample was dried for 1 hour at 420 °C and cooled down, both in a flow of dry N₂, in preparation for TPR. Numerous measures were taken to achieve high-quality TPR data, some notable examples being:

- Signal-to-noise from FID detector was maximized by running at a lowered methane concentration (500 ppm).
- Peak sharpness was improved by ramping at 2.5 °C/min instead of the typical 5 °C/min.
- Catalyst samples were undiluted to ensure a short bed and thereby minimal thermal variation across the length of the bed.

ICP

The palladium content of the Pd/Al₂O₃ catalyst was determined with inductively coupled plasma optical emission spectrometry (ICP-OES) on a Varian Agilent 725-ES spectrometer. The sample was prepared for injection by acid digestion.

References

1. Losch, P. *et al.* Modular Pd/Zelite Composites Demonstrating the Key Role of Support Hydrophobic/Hydrophilic Character in Methane Catalytic Combustion. *ACS Catal.* **9**, 4742–4753 (2019).
2. Petrov, A. W., Ferri, D., Kröcher, O. & van Bokhoven, J. A. Design of Stable Palladium-Based Zeolite Catalysts for Complete Methane Oxidation by Postsynthesis Zeolite Modification. *ACS Catal.* **9**, 2303–2312 (2019).
3. Friberg, I., Sadokhina, N. & Olsson, L. The effect of Si/Al ratio of zeolite supported Pd for complete CH₄ oxidation in the presence of water vapor and SO₂. *Appl. Catal. B Environ.* **250**, 117–131 (2019).
4. Hosseiniamoli, H., Setiawan, A., Adesina, A. A., Kennedy, E. M. & Stockenhuber, M. The stability of Pd/TS-1 and Pd/silicalite-1 for catalytic oxidation of methane – understanding the role of titanium. *Catal. Sci. Technol.* **10**, 1193–1204 (2020).
5. Mortensen, R. L., Noack, H., Pedersen, K., Mossin, S. & Mielby, J. Recent Advances in Complete Methane Oxidation using Zeolite-Supported Metal Nanoparticle Catalysts. *ChemCatChem* **14**, (2022).
6. Li, X., Wang, X., Roy, K., van Bokhoven, J. A. & Artiglia, L. Role of Water on the Structure of Palladium for Complete Oxidation of Methane. *ACS Catal.* **10**, 5783–5792 (2020).
7. Sadokhina, N. *et al.* An Experimental and Kinetic Modelling Study for Methane Oxidation over Pd-based Catalyst: Inhibition by Water. *Catal. Letters* **147**, 2360–2371 (2017).
8. Zhang, Y. *et al.* Influence of the support on rhodium speciation and catalytic activity of rhodium-based catalysts for total oxidation of methane. *Catal. Sci. Technol.* **10**, 6035–6044 (2020).
9. Velin, P. *et al.* Hampered PdO Redox Dynamics by Water Suppresses Lean Methane Oxidation over Realistic Palladium Catalysts. *ChemCatChem* **13**, 3765–3771 (2021).
10. Murata, K., Ohyama, J., Yamamoto, Y., Arai, S. & Satsuma, A. Methane Combustion over Pd/Al₂O₃ Catalysts in the Presence of Water: Effects of Pd Particle Size and Alumina Crystalline Phase. *ACS Catal.* **10**, 8149–8156 (2020).
11. Gholami, R., Alyani, M. & Smith, K. Deactivation of Pd Catalysts by Water during Low Temperature Methane Oxidation Relevant to Natural Gas Vehicle Converters. *Catalysts* **5**, 561–594 (2015).
12. Ciuparu, D., Perkins, E. & Pfefferle, L. In situ DR-FTIR investigation of surface hydroxyls on γ-Al₂O₃ supported PdO catalysts during methane combustion. *Appl. Catal. A Gen.* **263**, 145–153

(2004).

13. Roger, M., Kröcher, O. & Ferri, D. Assessing the effect of O₂ dithering on CH₄ oxidation on Pd/Al₂O₃. *Chem. Eng. J.* **451**, 138865 (2022).
14. Franken, T. *et al.* Effect of Short Reducing Pulses on the Dynamic Structure, Activity, and Stability of Pd/Al₂O₃ for Wet Lean Methane Oxidation. *ACS Catal.* **11**, 4870–4879 (2021).
15. Petrov, A. W. *et al.* Stable complete methane oxidation over palladium based zeolite catalysts. *Nat. Commun.* **9**, 2545 (2018).
16. AROSIO, F., COLUSSI, S., TROVARELLI, A. & GROPPi, G. Effect of alternate CH₄-reducing/lean combustion treatments on the reactivity of fresh and S-poisoned Pd/CeO₂/Al₂O₃ catalysts. *Appl. Catal. B Environ.* **80**, 335–342 (2008).
17. Boucly, A. *et al.* Water inhibition and role of palladium adatoms on Pd/Al₂O₃ catalysts during methane oxidation. *Appl. Surf. Sci.* **606**, 154927 (2022).
18. Huang, W., Goodman, E. D., Losch, P. & Cargnello, M. Deconvoluting Transient Water Effects on the Activity of Pd Methane Combustion Catalysts. *Ind. Eng. Chem. Res.* **57**, 10261–10268 (2018).
19. Petrov, A. W., Ferri, D., Tarik, M., Kröcher, O. & van Bokhoven, J. A. Deactivation Aspects of Methane Oxidation Catalysts Based on Palladium and ZSM-5. *Top. Catal.* **60**, 123–130 (2017).
20. Keller, K., Lott, P., Stotz, H., Maier, L. & Deutschmann, O. Microkinetic Modeling of the Oxidation of Methane Over PdO Catalysts—Towards a Better Understanding of the Water Inhibition Effect. *Catalysts* **10**, 922 (2020).
21. Zhang, Z. *et al.* Anti-sintering Pd@silicalite-1 for methane combustion: Effects of the moisture and SO₂. *Appl. Surf. Sci.* **494**, 1044–1054 (2019).
22. Wang, W. *et al.* In-situ confinement of ultrasmall palladium nanoparticles in silicalite-1 for methane combustion with excellent activity and hydrothermal stability. *Appl. Catal. B Environ.* **276**, 119142 (2020).
23. Nilsson, J. *et al.* Methane oxidation over Pd/Al₂O₃ under rich/lean cycling followed by operando XAFS and modulation excitation spectroscopy. *J. Catal.* **356**, 237–245 (2017).

6.5 Further analysis of data from kinetic experiments

In the process of trying to understand the results from the water deactivation project, it was suggested to plot deactivation as a function of something else than time: 1) as a function of accumulated methane conversion throughout the experiment and 2) as a function of the accumulated amount of water added to the reactor through the feed gas. These variables were extracted from the 36 kinetic experiments performed in Paper 3, as demonstrated in Figure 37 for the experiment performed with 500 ppm CH₄ and 5% H₂O. The remaining figures with extracted variables used for this analysis are shown in Appendices F and G. The **conversion** data is taken from the two-hour segment of the kinetic experiments used for estimating the dependence of the deactivation rate coefficient on CH₄ and H₂O concentration. **Rate loss** is used as measure of “the degree of deactivation” and is calculated as the relative difference between the first order methane oxidation rates at $t = 0$ and t , in percent. The rate loss variable serves two purposes: 1) Assuming methane turnovers are part of the deactivation mechanism, using the rate instead of conversion normalises the experiments in terms of methane concentration. 2) Using a loss-compared-to-initial-value metric normalizes the experiments in terms of the deactivation curves not having the same starting point, i.e. initial conversion. **Methane converted** is essentially the area under the conversion curve, collected by stepwise integration. **Water accumulated** is a function of the feed water concentration and time. Water obviously doesn’t accumulate in the catalyst bed, but an accumulated amount of water has passed through the bed at any given time since the start of the experiment.

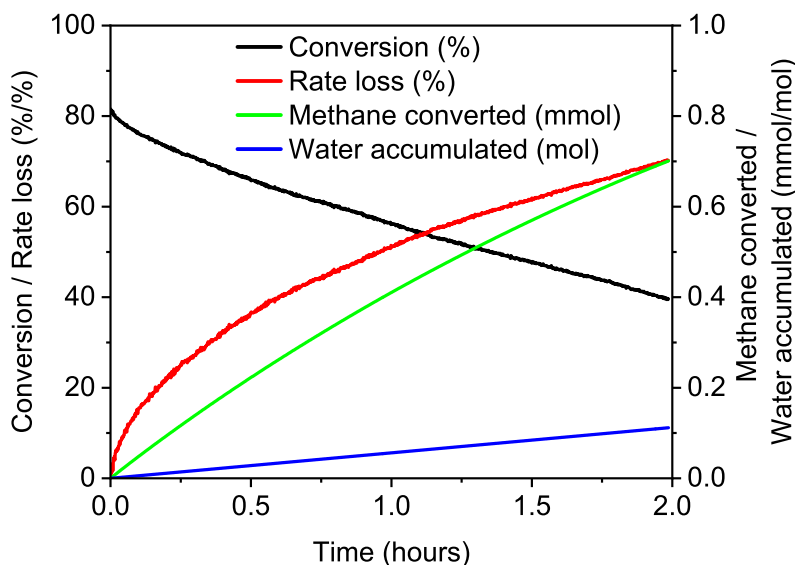


Figure 37 Example of data extraction used for accumulation plot analysis. Conversion and rate loss on left axis both have percentage as unit. On the right axis, methane converted has the unit mmol while water accumulated has the unit mol. Reaction conditions: 500 ppm CH₄, 10% O₂, 5% H₂O, 5% CO₂, N₂ balance, flow = 420 ml/min, WHSV = 1 260 000 ml h⁻¹ g⁻¹, T = 440 °C.

As described in Paper 3, the rate of deactivation, when water is added to the feed gas of methane

oxidation catalysts, depends on the methane concentration. Six experiments with 5% H₂O and different methane concentrations are shown to the left in Figure 38, and they all follow unique deactivation curves when conversion is plotted against time. However, when the same experiments are plotted as rate loss against accumulated methane conversion, as is done to the right in Figure 38, a new pattern emerges. Now it is clearly seen that the six experiments follow roughly identical deactivation curves, only at different velocities determined by the methane concentration.

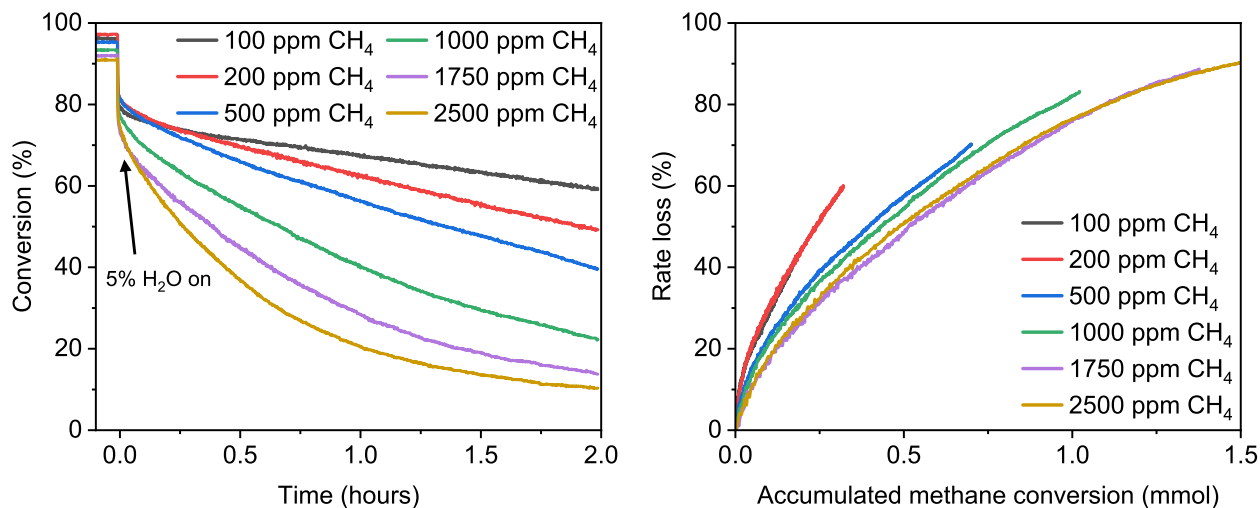


Figure 38 Left: Deactivation experiments with Pd/Al₂O₃ reference catalyst. Right: Same six experiments but plotted as rate loss versus accumulated methane conversion. Reaction conditions: 100-2500 ppm CH₄, 10% O₂, 5% CO₂, 5% H₂O, N₂ balance, WHSV = 1 260 000 ml h⁻¹ g⁻¹, T = 440 °C.

Similarly, a plot of experiments with the same methane concentration, but different water concentrations can be constructed, shown to the left in Figure 39. In Paper 3, it is demonstrated that the second order deactivation coefficient k_D has a linear relationship with the product $[\text{CH}_4]^{0.85} \cdot [\text{H}_2\text{O}]^{1.15}$. Multiplying the data in the accumulation plot by the water concentration in each of the experiments to the power of 1.15 makes all the deactivation curves follow identical paths. This is shown in the right side of Figure 39.

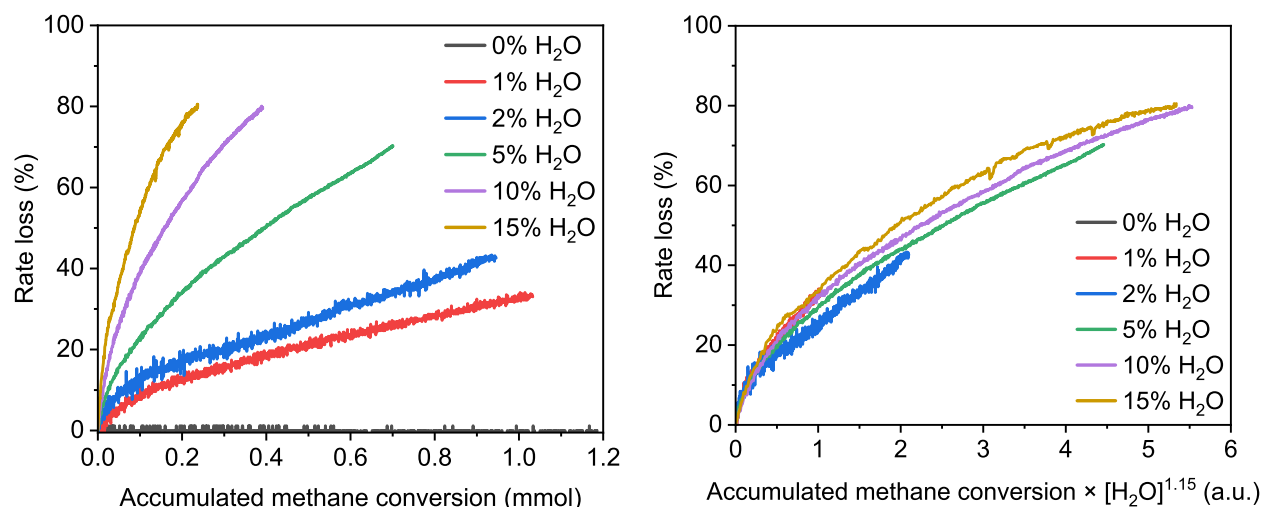


Figure 39 Left: Deactivation experiments with Pd/Al₂O₃ reference catalyst plotted as rate loss versus accumulated methane conversion. Right: Same figure, but with a modified x-axis. Reaction conditions: 500 ppm CH₄, 10% O₂, 0-15% H₂O, 5% CO₂, N₂ balance, WHSV = 1 260 000 ml h⁻¹ g⁻¹, T = 440 °C.

The exact meaning of the exponent, and its value 1.15, is difficult to evaluate. It is clearly a factor which describes the influence of the water concentration, but it is unclear how to chemically interpret that. However, the fact that a number exists which cause the deactivation curves to align is very interesting in itself.

The goal of this analysis was to use the kinetic data to illustrate the hypothesis raised in Paper 3 about the mechanism for water-induced deactivation. This approach had the advantage of not requiring the assumption of a deactivation rate order for the extraction of rate constants. Although the analysis did not add new information in itself, the two accumulation plots to the right in Figures 38 and 39 are nice visual assets to help communicate the central message:

During methane oxidation in the presence of water, every methane turnover has the potential to deactivate a site, and the probability of that occurring is determined by the water concentration

Figure 38 explains the first part of the message by showing that experiments with different methane concentrations produces deactivation of equal rate when scaled to the methane converted in the individual experiments. The last part of the message is explained by Figure 39 which shows that experiments with different water concentrations produces identical deactivation per methane turnover when scaled to the concentration of water in the individual experiments. This analysis contributed greatly to the understanding required for proposing a new hypothesis for water-induced inhibition and deactivation, presented in Section 6.7.

6.6 Attempts at elucidating the nature of deactivated PdO with spectroscopy

After making the CH₄-TPR observations, shown in Paper 3, of active and inactive PdO having a radically different bulk reduction temperature, it was natural to investigate the structure of deactivated palladium oxide on the Pd/Al₂O₃ catalyst. For this purpose, a series of materials were prepared for experiments:

- The palladium-free support was acquired.
- A deactivated sample was prepared by placing 400 mg undiluted Pd/Al₂O₃ in a reactor and treating it for 60 hours under the following reaction conditions: 1000 ppm CH₄, 10% O₂, 5% CO₂, 10% H₂O, N₂ balance, flow = 420 ml/min, T = 450 °C. After the deactivation sequence, the sample was dried and cooled under nitrogen flow in the reactor.
- A regenerated sample was prepared by placing 400 mg undiluted Pd/Al₂O₃ in a reactor and heating it to 400 °C under nitrogen flow. It was then exposed to dry methane oxidation conditions for one hour, after which oxygen was cut off, creating a reducing atmosphere in the reactor. After two minutes, oxygen was reintroduced to re-oxidize the sample. Lastly, it was dried and cooled under nitrogen flow in the reactor.

Others have speculated that water-induced deactivation might be accompanied by structural changes in the form of crystallographic strain, defects, vacancies, or surface roughness,^{38,54,186,187} largely based on the agreement in literature about the connection between the presence of these features and methane oxidation activity. Using X-ray diffraction to detect differences in the PdO crystal structure was hindered by the crystalline support, since the sample only contained 2.4 wt% palladium. The signal from the support was dominating the diffractogram, see Appendix N. Raman spectroscopy was attempted, as changes to the lattice distances would likely also be visible from this technique. Palladium oxide is Raman active and has a clear and well-defined peak around 640 cm⁻¹.¹⁸⁸ Figure 40 shows Raman spectra for the deactivated and regenerated samples along with a PdO reference made from calcined palladium on carbon. Both catalyst spectra have had the spectrum for the support material subtracted, as the alumina and promoters also gave a spectrum. The hope was to see a clear shift of the peak position between the two samples, or possibly a change to the peak shape, but the signal-to-noise was insufficient for that kind of analysis despite many attempts to improve it.

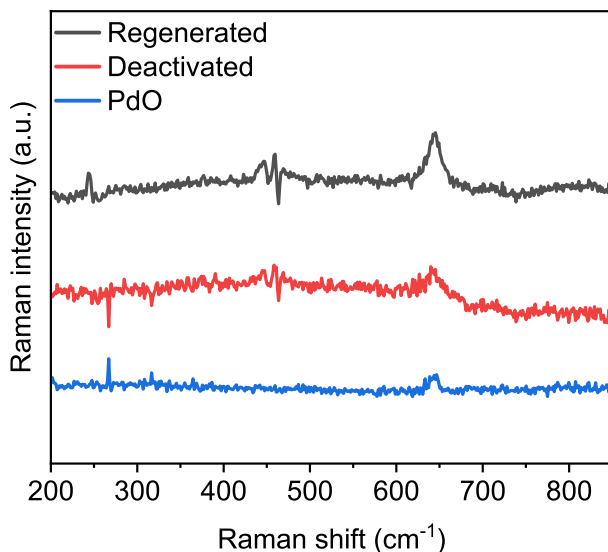


Figure 40 Raman spectra of deactivated and regenerated Pd/Al₂O₃ and of a pure PdO reference.

Considering the drastic decrease in CH₄-TPR reducibility and catalytic activity experienced by the deactivated catalyst, a probe-molecule approach seemed promising. The hypothesis was that an active and a deactivated catalyst would interact differently with a probe molecule like carbon monoxide, CO. A diffuse reflectance infrared Fourier transform spectroscopy (DRIFTS) cell was loaded with a dry sample, and the following sequence was performed at room temperature:

1. The chamber was flushed with N₂ (150 ml/min) for 10 minutes and a background spectrum was collected.
2. For 10 minutes, 1% CO in air was dosed to the chamber at 150 ml/min, collecting a spectrum every 90 seconds.
3. For 30 minutes, the chamber was flushed with N₂, collecting a spectrum every 90 seconds.

An example of the spectra collected during a sequence with a fresh sample is shown in Figure 41. Starting out, there is no absorbance in the region. Upon CO addition, the IR spectrum of gas-phase CO appears.¹⁸⁹ By the end of CO dosing, a broad peak has emerged around 2100 cm⁻¹, corresponding to CO bound to palladium.¹⁹⁰ After removing gas-phase CO by N₂ flushing, only the Pd-CO signal remains, but after extended flushing, it disappears.

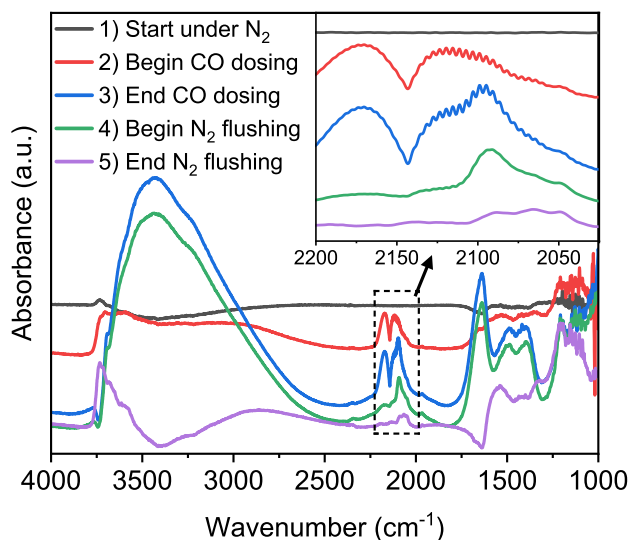


Figure 41 Carbon monoxide adsorption experiment with a fresh Pd/Al₂O₃ catalyst using DRIFTS. The five spectra represents the different segments of the experiment before, during, and after CO is adsorbed on the palladium oxide surface. Spectrum number 4, in green, shows the pure but weak signal from CO bound to palladium, right as gas phase CO has been flushed out of the DRIFTS cell. Insert: Zoom of the carbon monoxide region of the same spectra.

The spectrum collected right after CO gas has been flushed from the DRIFTS cell shows that the fresh sample has some ability to bind to carbon monoxide at room temperature. Figure 42 shows the corresponding spectra for a deactivated and a regenerated catalyst, as well as that for the Pd-free support. Also, it shows a second run with the fresh catalyst where the cell was re-loaded, indicating excellent reproducibility of the method. From the spectra, it can be seen that the regenerated catalyst forms a broad peak similar to that of the fresh catalyst, while the Pd-free support does not bind to CO. The deactivated catalyst forms a weak signal, but it is differently shaped and shifted slightly down in energy. Interestingly, the signal for the deactivated catalyst resembles that of the thoroughly flushed fresh catalyst shown in purple in Figure 41. It therefore seems like there are multiple Pd-CO interactions, one exclusive to the active catalyst and one shared by all Pd-containing samples.

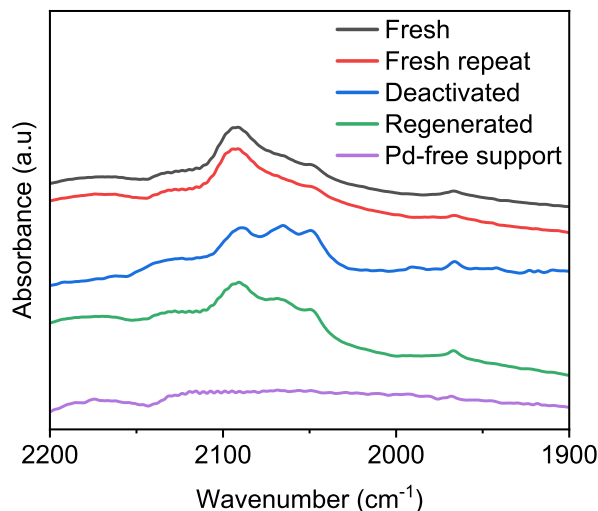
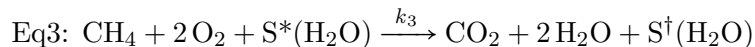
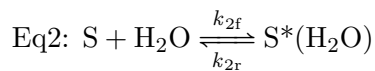
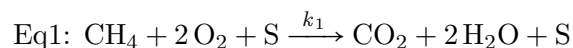


Figure 42 Carbon monoxide adsorption experiment with a fresh, deactivated, and regenerated Pd/Al₂O₃ catalyst. The spectra are recorded just after gas phase CO has been flushed from the DRIFTS cell, showing only the carbon monoxide region. No CO was adsorbed on the Pd-free support.

As exciting as it is to show a difference in active and deactivated PdO, the result was difficult to interpret. The CH₄-TPR experiments indicated that deactivation is a bulk phenomenon, and as a surface method, CO adsorption gives another type of information. Regrettably, conventional TEM imaging was not an option as the Pd/Al₂O₃ catalyst contained high amounts of a relatively heavy promoter, making it difficult to track the location of palladium nanoparticles without some form of elemental mapping. Unfortunately there was not enough time to employ more advanced characterization methods, but both extended X-ray absorption fine structure (EXAFS), XRD with pair distribution function (PDF) analysis,^{191,192} and XPS were considered.

6.7 Hypothesis for water-induced deactivation

In Paper 3, chemical equations describing water-induced inhibition and deactivation are proposed:



Despite their novelty and usefulness for kinetic modelling, the equations fail to address one critical question: What is the nature of S[†]? In the hydroxyl accumulation hypothesis described in Section 6.1, S[†] would be the same as S*, a surface covered in hydroxyl groups. The CH₄-TPR experiments in Paper 3 point towards a bulk phenomenon however, as the entire palladium mass is changing in reduction temperature and not just the particle surface. When analyzing the deacti-

vation experiments at first glance, the fast and reversible interaction with water has to be ascribed to inhibition, but the slow irreversible deactivation could seemingly be explained by hydrothermal sintering. There are two major reasons why this cannot be the case however:

1. The rate constant for the slow irreversible deactivation depends inversely on temperature, as shown in Paper 3, meaning deactivation is faster at lower temperatures. As sintering accelerates at elevated temperatures, due to the increased mobility of surface species, it is unlikely the reason for slow irreversible water-induced deactivation.
2. The deactivation can be regenerated by reducing and reoxidizing the nanoparticles. This procedure is unlikely to reverse the effects of sintering.

Instead, we propose nanoparticle dispersion as the reason for deactivation. It has been observed that under similar conditions, supported precious metal nanoparticles will tend to decompose and disperse, eventually to single atoms if the total metal loading is low enough.^{49,162,193} The dispersion is enabled by a mobile quasi-metallic state, formed by oxygen depletion of the palladium oxide when the surface is covered in hydroxyl groups during methane oxidation in the presence of water.^{82,167,173,177} During dry methane oxidation, there is a tolerable amount of hydroxyl groups on the surface,¹⁷¹ and a steady state of oxygen can reoxidize the palladium oxide and stabilize the particle. When steaming the catalyst, the palladium oxide surface is covered by hydroxyl groups,¹⁶⁸ but the palladium oxide does not become oxygen deficient as there is no methane present. However, when oxidizing methane in the presence of water, on a surface covered in hydroxyl groups, the particle will gain mobility and slightly smear out over the support surface. Due to methane oxidation being an very structure sensitive reaction,^{10,183,194–196} i.e. activity highly dependent on nanoparticle shape and size, the catalytic activity will be reduced. As have been shown in DRIFTS studies,^{168,171,180} there are plenty of hydroxyl groups on the catalyst surface during dry methane oxidation. The hydroxyl groups are free to combine and desorb however, as there is no gas phase water to “push against”. This means that the lifetime of surface hydroxyls is low under dry conditions. When water is added to the feed gas, hydroxyl combination is slow, and the lifetime is extended far enough to allow deactivation to take place. In this way, inhibition becomes a prerequisite for deactivation, as only a surface sufficiently covered in hydroxyl groups will experience enough oxygen deficiency to become unstable and mobile. This explains why inhibition and deactivation have very similar dependencies on temperature, pressure, and water concentration, as shown in Paper 3. Further, as the rate of deactivation will be directly related to the degree of inhibition, any feature which prevents inhibition will also prevent deactivation. In this context, past attempts at minimizing inhibition by supporting palladium nanoparticles on a more redox-active metal oxide like ceria appear very interesting.^{167,168} The proposed hypothesis for water-induced inhibition and deactivation is illustrated in Figure 43. To further substantiate the hypothesis, more experimental evidence is required, in particular about the nature of deactivated palladium oxide.

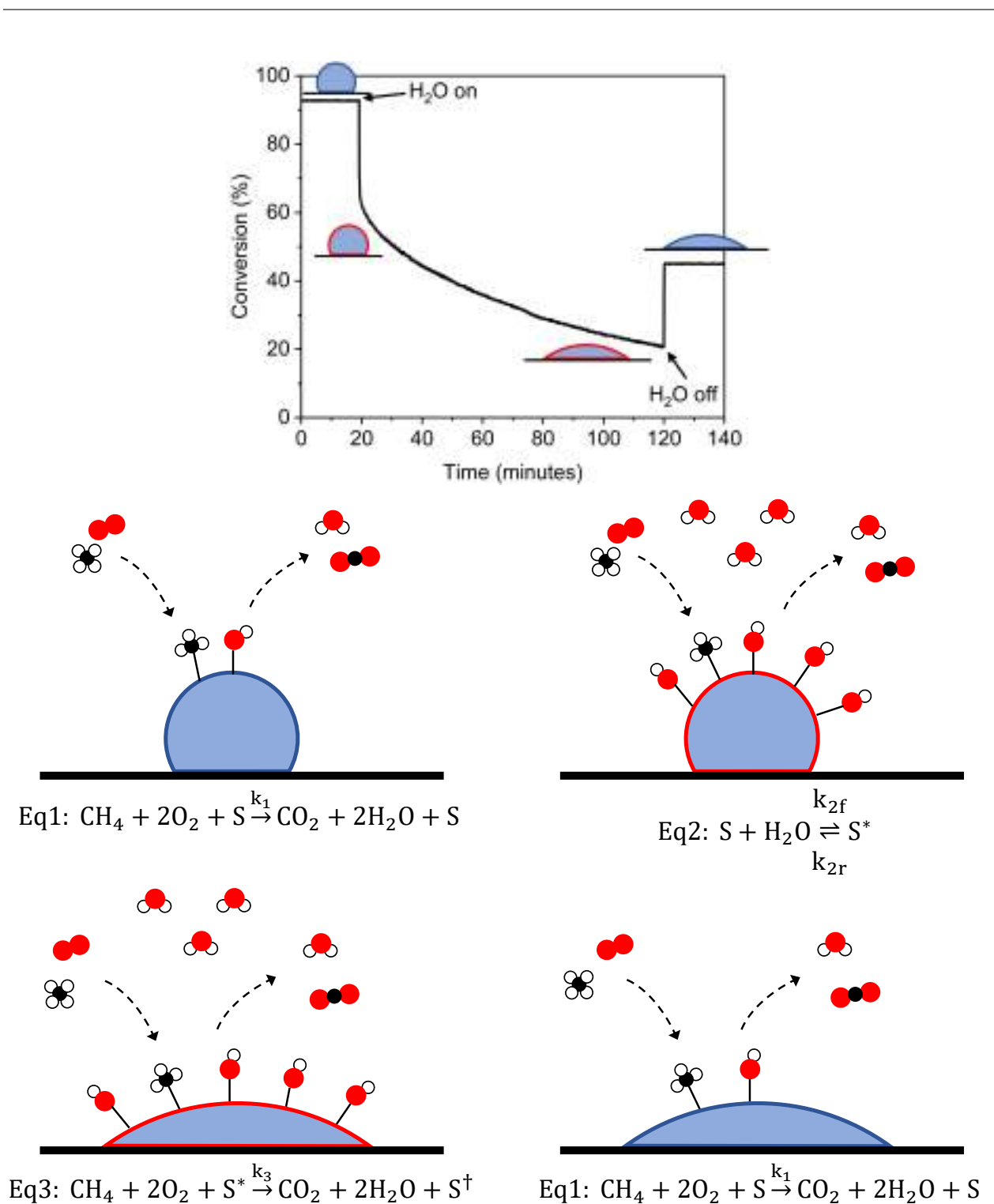


Figure 43 Hypothesis for water-induced inhibition and deactivation. Under dry conditions (middle-left), methane oxidation takes place on nanoparticles with low hydroxyl coverage. Upon introduction of water (middle-right), hydroxyl combination and water desorption is slowed down, delaying surface reoxidation. The local oxygen depletion creates a mobile quasi-metallic state, which begins to spread out on the support surface. After extended exposure (bottom-left), the nanoparticles are smeared out. The highly structure sensitive methane oxidation reaction is slowed down, i.e. the catalyst has been deactivated. Upon removal of water from the feed gas (bottom-right), the hydroxyl coverage decreases, but the nanoparticles remain in the deactivated state, although the inhibition reverses, as demonstrated in the catalytic experiment (top).

Sadokhina et al.¹⁷⁵ developed a kinetic model in 2017 for water-induced inhibition and deactivation, based on the hypothesis that hydroxyl groups are the reason for both phenomena. The work was inspired by modelling work by Groppi et al.^{197,198} and also included interactions between the catalyst and NO gas. Although it is rather unclear how the authors introduced time-dependence into their expression, the concept of developing a combined model for inhibition and deactivation was great. Based on the kinetic data and the chemical equations proposed for deactivation, a kinetic model was developed in Paper 3. Our model is rather similar to that of Sadokhina et al. with the exception that we introduce a term for the methane and time dependence of the irreversible deactivation. The exponents to the concentrations of water and methane originate from the 36 kinetic experiments and are derived in Paper 3. Both models are shown in Figure 44. In our model, the rate constant parameters K_1 , K_2 , and K_3 are capitalized to distinguish them from the rate constants k_1 , k_2 , and k_3 in the three chemical equations. Figure 45 shows a comparison of the model prediction with experimental results across different water concentrations.

$$r = \frac{k_1 \cdot y_{CH_4} \cdot \theta_{S^*}}{1 + k_{H_2O}^{inhib} \cdot y_{H_2O} + k_{NO}^{inhib} \cdot y_{NO}} \quad \theta_S = \frac{1}{1 + K_2 \cdot [H_2O]^{0.25} + K_3 \cdot [H_2O]^{1.15} \cdot [CH_4]^{0.85} \cdot t}$$

$$r = K_1 \cdot [CH_4] \cdot \theta_S$$

Figure 44 Left: Kinetic model for inhibition and deactivation, including the inhibition by NO, proposed by Sadokhina et al.¹⁷⁵ Right: Our kinetic model for water-induced inhibition and deactivation developed in Paper 3. The model includes the specific dependencies on methane and water concentration as the power of the various components. The rate constant for methane oxidation, K_1 , was found via an Arrhenius plot, having a value comparable to those found in literature. Values for the model parameters K_2 (inhibition) and K_3 (deactivation) were determined by fitting the model to a test sample of the kinetic data.

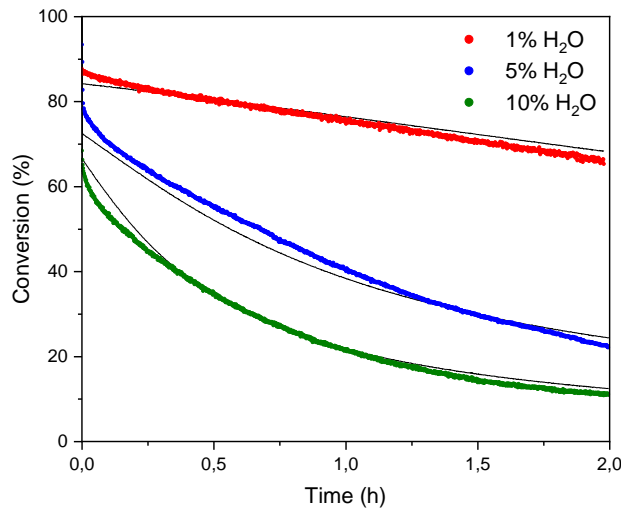


Figure 45 Model prediction of the deactivation in three experiments with 1000 ppm CH_4 and 1, 5, and 10% H_2O , compared to experimental data. The model parameters K_2 and K_3 had the values 122 and 384 respectively. From Paper 3.

6.8 Discussion about the importance of realistic testing conditions

In catalyst development, catalytic tests traditionally take place on different scales: Lab scale where milligrams of catalyst powder are placed in a narrow tubular reactor, pilot scale where hundreds of grams of catalyst on a monolithic substrate are tested in a larger facility, and full scale tests of catalytic elements in the exhaust from power plants or ships. Performing tests at small scale has the advantage of flexibility, allowing for quick turn-around and rapid iterations in catalyst design. Based on real-world expectations, a set of model conditions are selected to represent the exhaust to be treated in the eventual emission control application. As outlined in Section 3.1 a reasonable model gas composition for complete methane oxidation could be: 1000 ppm CH₄, 10% O₂, 5% CO₂, 10% H₂O, 2 ppm SO₂, balanced in N₂. Studies have also been performed with NO in the feed gas,^{199,200} but NO_x gasses are typically omitted, possibly due to an assumption that a selective catalytic reduction (SCR) catalyst is located upstream of the MOC. In a large number of published articles, a similar model gas composition is used. In many cases however, there are significant deviations. As an example, a methane concentration of 1%, corresponding to 10 000 ppm, is very commonly used. The exothermic reaction in this case produces an adiabatic temperature rise of 306 °C at full conversion. If not dealt with, the increase in gas temperature will heat up the catalyst, artificially raising the activity. This challenge can be alleviated by mixing the catalyst with an inert diluent like quartz sand, since the increased bed surface area will lead to an increased heat loss, but the common mixing ratios of 1:1 and 1:3 are likely not sufficient. In this project, catalysts were diluted between 10 and 50 times for this reason. As shown earlier in this section, at 1000 ppm CH₄, just 2% water causes significant deactivation. At 1% CH₄, the oxidation reaction itself produces 2% water at full conversion, but curiously this does not cause deactivation. Methane concentrations as high as 6.7% have been used in emission control-oriented literature,²⁰¹ resulting in a theoretical adiabatic temperature rise of more than 2000 °C. It is also not uncommon to see oxygen concentrations lower than 10%, in fact 1% CH₄ and 4% O₂ is a common combination. Although it is still over-stoichiometric, the 1:4 CH₄/O₂ ratio is far from the more realistic 1:100 ratio, which is a more oxidizing environment. Using an unrealistic model gas composition does not necessarily invalidate the obtained results, it just makes them difficult to benchmark against. For this reason, agreeing on a common set of model conditions for a given application would likely be greatly beneficial for the catalyst community.

Methane oxidation catalysts suffer from multiple deactivation phenomena. It is common practise to isolate the problems and attempt to solve one at a time. This is a both clever and efficient approach, but it should be balanced against the drawback of losing sight of potential negative synergy effects. As Auvinen et al.²⁰ showed, deactivation by water and SO₂ intensify each other. Attempting to solve one challenge while disregarding the other therefore might be counterproductive. An example of this is Paper 2 where it is concluded that prevention of SO₂ poisoning favors H-form zeolites,

while modifications to obtain Na-form zeolites favors prevention of water-induced deactivation in the work of others on similar materials. Isolation of problems in a structured effort to prevent deactivation therefore needs to be balanced against adhering to realistic testing conditions as much as possible.

When discussing realistic model gas compositions and testing conditions, a short remark on deactivation procedures is warranted. Catalytic tests examining deactivation are frequent, and before/after microscopy imaging are often used to determine if a material is sintering at the reaction conditions. Spectroscopic investigations of long term deactivation are very rare however. Interestingly, the common claim, described in Section 6.1, that hydroxyl coverage accelerates beyond the first few minutes is not supported by experimental evidence. The term “hydroxyl build-up”, arguably indicating a time-dependent process, is used frequently in methane oxidation literature when citing the work of others, but in the cited publication the sample is rarely exposed to wet methane oxidation conditions for more than 10 minutes. This is also reported in our own Paper 1, as the hydroxyl coverage hypothesis seemed plausible at the time. In hindsight, it was an unsupported extrapolation of evidence for inhibition to build an explanation for slow irreversible deactivation. The lack of scientific evidence in literature describing water-induced deactivation makes the results in Paper 3 stand out, as they are undeniably measurements of actual deactivation caused by the presence of water over long periods of time. Likewise, the kinetic model and the hypothesis for water-induced deactivation presented in Section 6.7 might need more evidence to be fully substantiated, but are a completely new take on a phenomenon which has been evading researchers for decades.

7 Conclusions

In this work, the field of complete methane oxidation was advanced on several fronts. The most recent major advance in the field, the introduction of zeolite-supported catalysts, was covered in a review article. The many promises of zeolite-derived catalysts were discussed and evaluated, in an effort to provide an overview which could serve as foundation for continued development. For the thesis to provide a complete picture, the review was supplemented by a section summarizing the remaining field, including state-of-the-art, base-metal catalysts, alternative oxidants, as well as non-catalytic alternatives.

A catalytic test setup was built to, as accurately as possible on lab-scale, simulate realistic testing conditions. Methane oxidation is a sensitive reaction and the testing equipment was designed to support thorough investigations of the various relevant deactivation phenomena. The design and construction were documented in the thesis to showcase what is required to build equipment for catalyst development where most aspects can be accounted for at the same time. The setup functioned as intended throughout the project and was a determining factor in the various discoveries made.

Based on the assumption that zeolite supports could alleviate the challenges with water-induced deactivation and metal nanoparticle sintering, the last major deactivation phenomenon, SO_2 poisoning, was the attempted to tackle first. A series of materials were successfully synthesized, consisting of palladium encapsulated in the pure silicon zeolite Silicalite-1. Additional materials were synthesized with platinum and various base-metal oxides as promoters. Most synthesized materials were active for catalytic methane oxidation, but all suffered severely from water-induced deactivation, despite a small improvement from the introduction of platinum. A Pd@S-1 catalyst deactivated in wet methane oxidation had its non-micropore volume increased by 19% and seemed to develop mesopores from the deactivation treatment. Despite the promise of the Silicalite-1-supported catalysts in literature, they were found to not prevent water-induced deactivation under realistic testing conditions.

It was shown that the counter ion in a series of zeolite-supported catalysts with Al/Si ratios ranging from 6.5 to 15 had strong influence on the SO_2 tolerance of the materials. A Pd/H-CHA catalyst was able to maintain high conversion for more than 200 hours in the presence of 2 ppm SO_2 . When exchanging the protons in the zeolite with sodium ions, the catalyst had a higher initial activity but quickly deactivated from SO_2 poisoning. This result is particularly interesting as others have shown that exchanging protons for sodium ions in similar catalysts is beneficial in terms of preventing water-induced deactivation, a contradiction which could complicate development of a zeolite-based methane oxidation catalyst.

Water-induced deactivation is arguably the least well-understood deactivation mechanism for methane

oxidation catalysts. Very little evidence exists in literature to explain the fundamental deactivation mechanism. Mostly by luck, it was discovered that water-induced deactivation requires methane to be converted on the catalyst. Through a carefully designed series of kinetic experiments, the dependencies on methane concentration, water concentration, temperature, and pressure were determined, both of reversible inhibition and irreversible deactivation. Using CH₄-TPR experiments it was shown that water-induced deactivation leads to structural changes in the bulk palladium oxide, and not just the surface region. The methane consumption calculated from the reduction peaks corresponded to reduction of exactly 100% of the PdO content of the samples, as determined by ICP-OES. Extended deactivation of a Pd/Al₂O₃ catalyst increased the reduction temperature of the palladium oxide by as much as 100 °C. A completely novel type of wet CH₄-TPR experiment was designed in which different amounts of water were present in repeated measurements of identical samples. The influence of water concentration on reduction temperature was shown to be closely correlated with the influence of water concentration on reversible inhibition. A set of chemical equations describing the deactivation mechanism was proposed, differing radically from past attempts in literature of describing the phenomenon. From these and the kinetic data, a new hypothesis for water-induced deactivation was proposed, and a kinetic model was developed, able to accurately simulate deactivation experiments. Other than the implications for catalytic methane oxidation, the results likely have relevance to the broader field of emission control catalysis, as various types of deactivation to a large extent dictate catalyst development.

7.1 Industrial impact

The thesis provides an overview of technologies for complete methane oxidation by describing the state-of-the-art catalyst, catalytic alternatives, and radically different technologies not based on catalysis. This overview might be valuable when assessing the technological readiness of solutions for methane slip emission control.

The three experimental projects revolve around catalyst deactivation, means of prevention, and the interplay between catalyst composition and the harsh environment in the hot exhaust from a large natural gas-fueled engine. Neither project were successful in developing a durable catalyst for complete methane oxidation, but several trends and correlations relating to deactivation were discovered. Decades of development have resulted in only a few steps forward, best exemplified with the fact that palladium supported on alumina is still the state-of-the-art and still suffers severe deactivation. Elucidating the possible mechanism for water-induced deactivation will hopefully bring the industry one step closer to a durable catalyst for complete methane oxidation.

The important finding that water-induced deactivation depends on methane conversion opens up for the possibility to effectively use it in combination with another methane slip reduction technology, like the high-pressure two-stroke engines described in Section 2.4. Low-emission engines still suffer

from methane slip, although it is significantly lower than that of the most common engines. Due to the methane dependence of deactivation, a conventional Pd/Al₂O₃ catalyst would likely survive for longer in an exhaust with less methane. The climate impact of such a combined solution would be small and the equipment would be rather complex, but if strict methane regulation is introduced it might be necessary and the only functioning solution.

As explained in Section 2.3, placing the catalyst element upstream of the turbocharger has been proposed as a method of increasing the reactor temperature and consequently activity of methane oxidation catalysts.^{14,55} The finding that water-induced deactivation tapers off around 575 °C means that a pre-TC position not only raises activity, it could also alleviate deactivation from water. If a durable catalyst cannot be developed in time, this might be a way to realize the potential of LNG as a transitory maritime fuel.

The importance of a realistic model gas composition and testing conditions is a recurring theme in this thesis. Based on the observations made and the literature digested, agreeing on a common set of model conditions for a given application, in this case emission control of large marine engines, would very likely be greatly beneficial for the catalyst community and continued development.

7.2 Future perspectives

A variety of spectroscopic methods were employed to characterize deactivated palladium oxide, but for various reasons they never worked as well as hypothesised. Potentially, either EXAFS, a well resolved Raman spectrum, or some advanced diffraction method would be able to shed further light on the nature of the structural changes in PdO caused by deactivation. When water-induced deactivation has been fully understood, coupling it with SO₂-poisoning is an important next step as the two types of deactivation have been shown to worsen each other.

It is to be seen if the results from this project will reignite the field of methane oxidation, which has seen a lower publication frequency recently than between 2017 and 2020 when the topic attracted more attention. E-fuels like methanol have gained significant traction recently, and since the geopolitics around natural gas changed in 2022, perhaps LNG will never be the dominant marine fuel, not even during a transition period as previously proposed. Further, the International Council on Clean Transportation released a report⁸ in 2020 concluding that "...factoring in higher upstream emissions for all systems and crankcase emissions for low-pressure systems, there is no climate benefit from using LNG, regardless of the engine technology". Complete oxidation of methane has several other potential applications however, with similar deactivation challenges, so continued development of durable catalysts will likely still be relevant. These include catalytic combustion,^{202–204} CO₂ purification,²⁰⁵ oxidation of ventilation air methane,^{141,206} and landfill gas deoxygen treatment.²⁰⁷

References

- ¹ P. R. Shukla, J. Skea, R. Slade, A. Al Khourdajie, R. van Diemen, D. McCollum, M. Pathak, S. Some, P. Vyas, R. Fradera, M. Belkacemi, A. Hasija, G. Lisboa, S. Luz, and J. Malley (eds.). *IPCC, 2022: Summary for Policymakers. In: Climate Change 2022: Mitigation of Climate Change. Contribution of Working Group III to the Sixth Assessment Report of the Intergovernmental Panel on Climate Change*, Cambridge University Press, Cambridge, UK and New York, NY, USA.
- ² V. Masson-Delmotte, P. Zhai, A. Pirani, S. L. Connors, C. Péan, S. Berger, N. Caud, Y. Chen, L. Goldfarb, M. I. Gomis, M. Huang, K. Leitzell, E. Lonnoy, J. B. R. Matthews, T. K. Maycock, T. Waterfield, O. Yelekçi, R. Yu, and B. Zhou. *IPCC: Climate Change 2021: The Physical Science Basis. Contribution of Working Group I to the Sixth Assessment Report of the Intergovernmental Panel on Climate Change*, Cambridge University Press, 2021.
- ³ The Intergovernmental Panel on Climate Change. *Synthesis report of the IPCC sixth assessment report (AR6), summary for policy makers*, Cambridge University Press, 2023.
- ⁴ M. Etminan, G. Myhre, E. J. Highwood, and K. P. Shine. Radiative forcing of carbon dioxide, methane, and nitrous oxide: A significant revision of the methane radiative forcing. *Geophysical Research Letters*, 43(24):12,614–12,623, 2016.
- ⁵ National Oceanic and Atmospheric Administration. The noaa annual greenhouse gas index (aggi). <https://gml.noaa.gov/aggi/aggi.html>, 30-04-2023, 09:57.
- ⁶ National Aeronautics and Space Administration. The atmosphere: Getting a handle on carbon dioxide. <https://climate.nasa.gov/news/2915/the-atmosphere-getting-a-handle-on-carbon-dioxide/>, 27-05-2023, 08:18.
- ⁷ R. B. Jackson, S. Abernethy, J. G. Canadell, M. Cargnello, S. J. Davis, S. Féron, S. Fuss, A. J. Heyer, C. Hong, C. D. Jones, H. Damon Matthews, F. M. O'Connor, M. Pisciotta, H. M. Rhoda, R. de Richter, E. I. Solomon, J. L. Wilcox, and K. Zickfeld. Atmospheric methane removal: a research agenda. *Philosophical Transactions of the Royal Society A: Mathematical, Physical and Engineering Sciences*, 379(2210):20200454, 2021.
- ⁸ N. Pavlenko, B. Comer, Y. Zhou, N. Clark, and D. Rutherford. The climate implications of using LNG as a marine fuel. *ICCT Working Paper 2020-02*, 2(January), 2020.
- ⁹ D. Stenersen and O. Thonstad. GHG and NO_x emissions from gas fuelled engines. *SINTEF Report*, pages 1–51, 2017.
- ¹⁰ R. L. Mortensen, H.-D. Noack, K. Pedersen, S. Mossin, and J. Mielby. Recent Advances in Complete Methane Oxidation using Zeolite-Supported Metal Nanoparticle Catalysts. *ChemCatChem*, 14(16), 2022.
- ¹¹ K. Lehtoranta, P. Koponen, H. Vesala, K. Kallinen, and T. Maunula. Performance and Regeneration of Methane Oxidation Catalyst for LNG Ships. *Journal of Marine Science and Engineering*, 9(2):111, 2021.
- ¹² K. J. Laidler. A glossary of terms used in chemical kinetics, including reaction dynamics (IUPAC Recommendations 1996). *Pure and Applied Chemistry*, 68(1):149–192, 1996.

-
- ¹³ I. Chorkendorff & J. W. Niemantsverdriet. *Concepts of Modern Catalysis and Kinetics*, 2. Ed, Wiley-VCH Verlag GmbH & Co. KGaA, 2007.
- ¹⁴ A. Gremminger, A. Boubnov, B. Torkashvand, M. Casapu, and M. Merts. Methane catalytic II. Methane oxidation catalysts: influence of catalyst composition, pressure and gas composition on activity, aging and reactivation. *FVV report*, 2017.
- ¹⁵ P. G  lin and M. Primet. Complete oxidation of methane at low temperature over noble metal based catalysts: a review. *Applied Catalysis B: Environmental*, 39(1):1–37, 2002.
- ¹⁶ D. Ciuparu, M. R. Lyubovsky, E. Altman, L. D. Pfefferle, and A. Datye. Catalytic combustion of methane over palladium-based catalysts. *Catalysis Reviews - Science and Engineering*, 44(4):593–649, 2002.
- ¹⁷ T. V. Choudhary, S. Banerjee, and V. R. Choudhary. Catalysts for combustion of methane and lower alkanes. *Applied Catalysis A: General*, 234(1-2):1–23, 2002.
- ¹⁸ M. Cargnello, J. J. D. Jaen, J. C. H. Garrido, K. Bakhmutsky, T. Montini, J. J. C. Gamez, R. J. Gorte, and P. Fornasiero. Exceptional Activity for Methane Combustion over Modular Pd@CeO₂ Subunits on Functionalized Al₂O₃. *Science*, 337(6095):713–717, 2012.
- ¹⁹ K. Keller, P. Lott, H. Stotz, L. Maier, and O. Deutschmann. Microkinetic Modeling of the Oxidation of Methane Over PdO Catalysts—Towards a Better Understanding of the Water Inhibition Effect. *Catalysts*, 10(8):922, 2020.
- ²⁰ P. Auvinen, J. T. Hirvi, N. M. Kinnunen, and M. Suvanto. PdSO₄ Surfaces in Methane Oxidation Catalysts: DFT Studies on Stability, Reactivity, and Water Inhibition. *ACS Catalysis*, 10(21):12943–12953, 2020.
- ²¹ P. Auvinen, N. M. Kinnunen, J. T. Hirvi, T. Maunula, K. Kallinen, M. Keenan, R. Baert, E. van den Tillaart, and M. Suvanto. Development of a rapid ageing technique for modern methane combustion catalysts in the laboratory: Why does SO₂ concentration play an essential role? *Applied Catalysis B: Environmental*, 258:117976, 2019.
- ²² T. W. Hansen, A. T. Delariva, S. R. Challa, and A. K. Datye. Sintering of catalytic nanoparticles: Particle migration or ostwald ripening? *Accounts of Chemical Research*, 46(8):1720–1730, 2013.
- ²³ Z. Li and G. B. Hoflund. A Review on Complete Oxidation of Methane at Low Temperatures. *Journal of Natural Gas Chemistry*, 12(3):153–160, 2003.
- ²⁴ M. Monai, T. Montini, R. J. Gorte, and P. Fornasiero. Catalytic Oxidation of Methane: Pd and Beyond. *European Journal of Inorganic Chemistry*, 2018(25):2884–2893, 2018.
- ²⁵ J. Chen, H. Arandiy  n, X. Gao, and J. Li. Recent Advances in Catalysts for Methane Combustion. *Catalysis Surveys from Asia*, 19(3):140–171, 2015.
- ²⁶ P. Lott and O. Deutschmann. Lean-Burn Natural Gas Engines: Challenges and Concepts for an Efficient Exhaust Gas Aftertreatment System. *Emission Control Science and Technology*, 7(1):1–6, 2021.
-

-
- ²⁷ L. He, Y. Fan, J. Bellettre, J. Yue, and L. Luo. A review on catalytic methane combustion at low temperatures: Catalysts, mechanisms, reaction conditions and reactor designs. *Renewable and Sustainable Energy Reviews*, 119(November 2019):109589, 2020.
- ²⁸ R. Gholami, M. Alyani, and K. Smith. Deactivation of Pd Catalysts by Water during Low Temperature Methane Oxidation Relevant to Natural Gas Vehicle Converters. *Catalysts*, 5(2):561–594, 2015.
- ²⁹ A. Raj. Methane Emission Control. *Johnson Matthey Technology Review*, 60(4):228–235, 2016.
- ³⁰ M. Keenan, R. Pickett, E. Tronconi, I. Nova, N. Kinnunen, M. Suvanto, T. Maunula, K. Kallinen, and R. Baert. The Catalytic Challenges of Implementing a Euro VI Heavy Duty Emissions Control System for a Dedicated Lean Operating Natural Gas Engine. *Topics in Catalysis*, 62(1-4):273–281, 2019.
- ³¹ I. Friberg, N. Sadokhina, and L. Olsson. Complete methane oxidation over Ba modified Pd/Al₂O₃: The effect of water vapor. *Applied Catalysis B: Environmental*, 231(March):242–250, 2018.
- ³² I. Friberg, N. Sadokhina, and L. Olsson. The effect of Si/Al ratio of zeolite supported Pd for complete CH₄ oxidation in the presence of water vapor and SO₂. *Applied Catalysis B: Environmental*, 250(February):117–131, 2019.
- ³³ H. Stotz, L. Maier, A. Boubnov, A.T. Gremminger, J.-D. Grunwaldt, and O. Deutschmann. Surface reaction kinetics of methane oxidation over PdO. *Journal of Catalysis*, 370:152–175, 2019.
- ³⁴ A. Gremminger, J. Pihl, M. Casapu, J.-D. Grunwaldt, T. J. Toops, and O. Deutschmann. PGM based catalysts for exhaust-gas after-treatment under typical diesel, gasoline and gas engine conditions with focus on methane and formaldehyde oxidation. *Applied Catalysis B: Environmental*, 265(January 2019):118571, 2020.
- ³⁵ F. Huang, J. Chen, W. Hu, G. Li, Y. Wu, S. Yuan, L. Zhong, and Y. Chen. Pd or PdO: Catalytic active site of methane oxidation operated close to stoichiometric air-to-fuel for natural gas vehicles. *Applied Catalysis B: Environmental*, 219:73–81, 2017.
- ³⁶ N. M. Kinnunen, J. T. Hirvi, T. Venäläinen, M. Suvanto, and T. A. Pakkanen. Procedure to tailor activity of methane combustion catalyst: Relation between Pd/PdOx active sites and methane oxidation activity. *Applied Catalysis A: General*, 397(1-2):54–61, 2011.
- ³⁷ P. Losch, W. Huang, O. Vozniuk, E. D. Goodman, W. Schmidt, and M. Cargnello. Modular Pd/Zelite Composites Demonstrating the Key Role of Support Hydrophobic/Hydrophilic Character in Methane Catalytic Combustion. *ACS Catalysis*, 9(6):4742–4753, 2019.
- ³⁸ A. W. Petrov, D. Ferri, F. Krumeich, M. Nachtegaal, J. A. van Bokhoven, and O. Kröcher. Stable complete methane oxidation over palladium based zeolite catalysts. *Nature Communications*, 9(1):2545, 2018.
- ³⁹ Z. Zhang, L. Sun, X. Hu, Y. Zhang, H. Tian, and X. Yang. Anti-sintering Pd@silicalite-1 for methane combustion: Effects of the moisture and SO₂. *Applied Surface Science*, 494(July):1044–1054, 2019.
- ⁴⁰ F. Arosio, S. Colussi, G. Groppi, and A. Trovarelli. Regeneration of S-poisoned Pd/Al₂O₃ catalysts for the combustion of methane. *Catalysis Today*, 117(4):569–576, 2006.
-

-
- ⁴¹ M. S. Wilburn and W. S. Epling. A Summary of Sulfur Deactivation, Desorption, and Regeneration Characteristics of Mono- and Bimetallic Pd-Pt Methane Oxidation Catalysts: Pd:Pt Mole Ratio and Particle Size Dependency. *Emission Control Science and Technology*, 4(2):78–89, 2018.
- ⁴² N. M. Kinnunen, V. H. Nissinen, J. T. Hirvi, K. Kallinen, T. Maunula, M. Keenan, and M. Suvanto. Decomposition of Al_2O_3 -Supported PdSO_4 and $\text{Al}_2(\text{SO}_4)_3$ in the Regeneration of Methane Combustion Catalyst: A Model Catalyst Study. *Catalysts*, 9(5):427, 2019.
- ⁴³ H. Nassiri, R. E. Hayes, and N. Semagina. Stability of Pd-Pt catalysts in low-temperature wet methane combustion: Metal ratio and particle reconstruction. *Chemical Engineering Science*, 186:44–51, 2018.
- ⁴⁴ H. Nassiri, K. Lee, Y. Hu, R. E. Hayes, R. W. J. Scott, and N. Semagina. Water shifts PdO-catalyzed lean methane combustion to Pt-catalyzed rich combustion in Pd-Pt catalysts: In situ X-ray absorption spectroscopy. *Journal of Catalysis*, 352:649–656, 2017.
- ⁴⁵ W. Huang, E. D. Goodman, P. Losch, and M. Cargnello. Deconvoluting Transient Water Effects on the Activity of Pd Methane Combustion Catalysts. *Industrial & Engineering Chemistry Research*, 57(31):10261–10268, 2018.
- ⁴⁶ J. Lampert, M. Kazi, and R. Farrauto. Palladium catalyst performance for methane emissions abatement from lean burn natural gas vehicles. *Applied Catalysis B: Environmental*, 14(3-4):211–223, 1997.
- ⁴⁷ P. Gélin, L. Urfels, M. Primet, and E. I. Tena. Complete oxidation of methane at low temperature over Pt and Pd catalysts for the abatement of lean-burn natural gas fuelled vehicles emissions: influence of water and sulphur containing compounds. *Catalysis Today*, 83(1-4):45–57, 2003.
- ⁴⁸ P. Velin, M. Ek, M. Skoglundh, A. Schaefer, A. Raj, D. Thompsett, G. Smedler, and P. A. Carlsson. Water Inhibition in Methane Oxidation over Alumina Supported Palladium Catalysts. *Journal of Physical Chemistry C*, 123(42):25724–25737, 2019.
- ⁴⁹ E. D. Goodman, A. C. Johnston-Peck, E. M. Dietze, C. J. Wrasman, A. S. Hoffman, F. Abild-Pedersen, S. R. Bare, P. N. Plessow, and M. Cargnello. Catalyst deactivation via decomposition into single atoms and the role of metal loading. *Nature Catalysis*, 2(9):748–755, 2019.
- ⁵⁰ A. W. Petrov, D. Ferri, M. Tarik, O. Kröcher, and J. A. van Bokhoven. Deactivation Aspects of Methane Oxidation Catalysts Based on Palladium and ZSM-5. *Topics in Catalysis*, 60(1-2):123–130, 2017.
- ⁵¹ I. Friberg, A. Wang, and L. Olsson. Hydrothermal Aging of Pd/LTA Monolithic Catalyst for Complete CH_4 Oxidation. *Catalysts*, 10(5):517, 2020.
- ⁵² P. Lott, M. Eck, D. E. Doronkin, R. Popescu, M. Casapu, J.-D. Grunwaldt, and O. Deutschmann. Regeneration of Sulfur Poisoned Pd-Pt/ CeO_2 - ZrO_2 - Y_2O_3 - La_2O_3 and Pd-Pt/ Al_2O_3 Methane Oxidation Catalysts. *Topics in Catalysis*, 62(1-4):164–171, 2019.
- ⁵³ M. Honkanen, J. Wang, M. Kärkkäinen, M. Huuhtanen, H. Jiang, K. Kallinen, R. L. Keiski, J. Akola, and M. Vippola. Regeneration of sulfur-poisoned Pd-based catalyst for natural gas oxidation. *Journal of Catalysis*, 358:253–265, 2018.
-

-
- ⁵⁴ T. Franken, M. Roger, A. W. Petrov, A. H. Clark, M. Agote-Arán, F. Krumeich, O. Kröcher, and D. Ferri. Effect of Short Reducing Pulses on the Dynamic Structure, Activity, and Stability of Pd/Al₂O₃ for Wet Lean Methane Oxidation. *ACS Catalysis*, 11(8):4870–4879, 2021.
- ⁵⁵ C. Haas, M. Friedrichshafen, P. Hildenbrand, and B. Torkashvand. Pre-turbine Catalytic Methane Oxidation for Lean-burn Natural Gas Engines. *CIMAC Congress 2019*, 240, 2020.
- ⁵⁶ N. M. Kinnunen, J. T. Hirvi, K. Kallinen, T. Maunula, M. Keenan, and M. Suvanto. Case study of a modern lean-burn methane combustion catalyst for automotive applications: What are the deactivation and regeneration mechanisms? *Applied Catalysis B: Environmental*, 207:114–119, 2017.
- ⁵⁷ M. Tang, S. Li, S. Chen, Y. Ou, M. Hiroaki, W. Yuan, B. Zhu, H. Yang, Y. Gao, Z. Zhang, and Y. Wang. Facet-Dependent Oxidative Strong Metal-Support Interactions of Palladium–TiO₂ Determined by In Situ Transmission Electron Microscopy. *Angewandte Chemie International Edition*, 60(41):22339–22344, 2021.
- ⁵⁸ S. Chen, S. Li, R. You, Z. Guo, F. Wang, G. Li, W. Yuan, B. Zhu, Y. Gao, Z. Zhang, H. Yang, and Y. Wang. Elucidation of Active Sites for CH₄ Catalytic Oxidation over Pd/CeO₂ Via Tailoring Metal-Support Interactions. *ACS Catalysis*, 11(9):5666–5677, 2021.
- ⁵⁹ G. Corro, R. Torralba, U. Pal, O. Olivares-Xometl, and J. L. G. Fierro. Total Oxidation of Methane over Pt/Cr₂O₃ Catalyst at Low Temperature: Effect of Pt⁰–Pt^{x+} Dipoles at the Metal-Support Interface. *The Journal of Physical Chemistry C*, 123(5):2882–2893, 2019.
- ⁶⁰ K. Murata, D. Kosuge, J. Ohyama, Y. Mahara, Y. Yamamoto, S. Arai, and A. Satsuma. Exploiting Metal-Support Interactions to Tune the Redox Properties of Supported Pd Catalysts for Methane Combustion. *ACS Catalysis*, 10(2):1381–1387, 2020.
- ⁶¹ J. Xiong, J. Yang, X. Chi, K. Wu, L. Song, T. Li, Y. Zhao, H. Huang, P. Chen, J. Wu, L. Chen, M. Fu, and D. Ye. Pd-Promoted Co₂NiO₄ with lattice Co–O–Ni and interfacial Pd–O activation for highly efficient methane oxidation. *Applied Catalysis B: Environmental*, 292(February), 2021.
- ⁶² S. B. Kang, K. Karinshak, P. W. Chen, S. Golden, and M. P. Harold. Coupled methane and NO_x conversion on Pt + Pd/Al₂O₃ monolith: Conversion enhancement through feed modulation and Mn_{0.5}Fe_{2.5}O₄ spinel addition. *Catalysis Today*, 360:284–293, 2021.
- ⁶³ T. Wang, L. Qiu, H. Li, C. Zhang, Y. Sun, S. Xi, J. Ge, Z. J. Xu, and C. Wang. Facile synthesis of palladium incorporated NiCo₂O₄ spinel for low temperature methane combustion: Activate lattice oxygen to promote activity. *Journal of Catalysis*, 404:400–410, 2021.
- ⁶⁴ J. Xiong, S. Mo, L. Song, M. Fu, P. Chen, J. Wu, L. Chen, and D. Ye. Outstanding stability and highly efficient methane oxidation performance of palladium-embedded ultrathin mesoporous Co₂MnO₄ spinel catalyst. *Applied Catalysis A: General*, 598(March):117571, 2020.
- ⁶⁵ X. Zou, J. Chen, Z. Rui, and H. Ji. Sequential growth reveals multi-spinel interface promotion for methane combustion over alumina supported palladium catalyst. *Applied Catalysis B: Environmental*, 273(March 2019):119071, 2020.
-

-
- ⁶⁶ T. M. Onn, M. Monai, S. Dai, E. Fonda, T. Montini, X. Pan, G. W. Graham, P. Fornasiero, and R. J. Gorte. Smart Pd Catalyst with Improved Thermal Stability Supported on High-Surface-Area LaFeO₃ Prepared by Atomic Layer Deposition. *Journal of the American Chemical Society*, 140(14):4841–4848, 2018.
- ⁶⁷ G. Ercolino, P. Stelmachowski, A. Kotarba, and S. Specchia. Reactivity of Mixed Iron–Cobalt Spinel in the Lean Methane Combustion. *Topics in Catalysis*, 60(17-18):1370–1379, 2017.
- ⁶⁸ G. Ercolino, A. Grodzka, G. Grzybek, P. Stelmachowski, S. Specchia, and A. Kotarba. The Effect of the Preparation Method of Pd-Doped Cobalt Spinel on the Catalytic Activity in Methane Oxidation Under Lean Fuel Conditions. *Topics in Catalysis*, 60(3-5):333–341, 2017.
- ⁶⁹ Y. Wang, H. Arandian, J. Scott, M. Akia, H. Dai, J. Deng, K. F. Aguey-Zinsou, and R. Amal. High Performance Au-Pd Supported on 3D Hybrid Strontium-Substituted Lanthanum Manganite Perovskite Catalyst for Methane Combustion. *ACS Catalysis*, 6(10):6935–6947, 2016.
- ⁷⁰ G. Ercolino, G. Grzybek, P. Stelmachowski, S. Specchia, A. Kotarba, and V. Specchia. Pd/Co₃O₄-based catalysts prepared by solution combustion synthesis for residual methane oxidation in lean conditions. *Catalysis Today*, 257(P1):66–71, 2015.
- ⁷¹ A. Eyssler, A. Winkler, O. Safonova, M. Nachtegaal, S. K. Matam, P. Hug, A. Weidenkaff, and D. Ferri. On the State of Pd in Perovskite-Type Oxidation Catalysts of Composition A(B,Pd)O_{3δ} (A = La, Y; B = Mn, Fe, Co). *Chemistry of Materials*, 24(10):1864–1875, 2012.
- ⁷² A. Eyssler, P. Mandaliev, A. Winkler, P. Hug, O. Safonova, R. Figi, A. Weidenkaff, and D. Ferri. The Effect of the State of Pd on Methane Combustion in Pd-Doped LaFeO₃. *The Journal of Physical Chemistry C*, 114(10):4584–4594, 2010.
- ⁷³ S. Cimino, M. P. Casaletto, L. Lisi, and G. Russo. Pd–LaMnO₃ as dual site catalysts for methane combustion. *Applied Catalysis A: General*, 327(2):238–246, 2007.
- ⁷⁴ S. Petrović, L. Karanović, P. K. Stefanov, M. Zdujić, and A. Terlecki-Baričević. Catalytic combustion of methane over Pd containing perovskite type oxides. *Applied Catalysis B: Environmental*, 58(1-2):133–141, 2005.
- ⁷⁵ K. Persson, A. Ersson, K. Jansson, N. Iverlund, and S. Jaras. Influence of co-metals on bimetallic palladium catalysts for methane combustion. *Journal of Catalysis*, 231(1):139–150, 2005.
- ⁷⁶ B. Kucharczyk and W. Tylus. Effect of Pd or Ag additive on the activity and stability of monolithic LaCoO₃ perovskites for catalytic combustion of methane. *Catalysis Today*, 90(1-2):121–126, 2004.
- ⁷⁷ M. Stoian, V. Rogé, L. Lazar, T. Maurer, J. C. Védrine, I.-C. Marcu, and I. Fechete. Total Oxidation of Methane on Oxide and Mixed Oxide Ceria-Containing Catalysts. *Catalysts*, 11(4):427, 2021.
- ⁷⁸ S. Colussi, P. Fornasiero, and A. Trovarelli. Structure-activity relationship in Pd/CeO₂ methane oxidation catalysts. *Chinese Journal of Catalysis*, 41(6):938–950, 2020.
-

-
- ⁷⁹ M. A. Mashkovtsev, A. K. Khudorozhkov, I. E. Beck, A. V. Porsin, I. P. Prosvirin, V. N. Rychkov, and V. I. Bukhtiyarov. Selection of modifying additives for improving the steam tolerance of methane afterburning palladium catalysts. *Catalysis in Industry*, 3(4):350–357, 2011.
- ⁸⁰ H. AlMohamadi and K. J. Smith. The Impact of CeO₂ Loading on the Activity and Stability of PdO/ γ -AlOOH/ γ -Al₂O₃ Monolith Catalysts for CH₄ Oxidation. *Catalysts*, 9(6):557, 2019.
- ⁸¹ D. J. Fullerton, A. V. K. Westwood, R. Brydson, M. V. Twigg, and J. M. Jones. Deactivation and regeneration of Pt/ γ -alumina and Pt/ceria–alumina catalysts for methane combustion in the presence of H₂S. *Catalysis Today*, 81(4):659–671, 2003.
- ⁸² M. Alyani and K. J. Smith. Kinetic Analysis of the Inhibition of CH₄ Oxidation by H₂O on PdO/Al₂O₃ and CeO₂/PdO/Al₂O₃ Catalysts. *Industrial & Engineering Chemistry Research*, 55(30):8309–8318, 2016.
- ⁸³ H.-Y. Chen, J. Lu, J. M. Fedeyko, and A. Raj. Zeolite supported Pd catalysts for the complete oxidation of methane: A critical review. *Applied Catalysis A: General*, 633(February):118534, 2022.
- ⁸⁴ L. Wu, W. Fan, X. Wang, H. Lin, J. Tao, Y. Liu, J. Deng, L. Jing, and H. Dai. Methane Oxidation over the Zeolites-Based Catalysts. *Catalysts*, 13(3):604, 2023.
- ⁸⁵ J. Yang and Y. Guo. Nanostructured perovskite oxides as promising substitutes of noble metals catalysts for catalytic combustion of methane. *Chinese Chemical Letters*, 29(2):252–260, 2018.
- ⁸⁶ N. Bahlawane. Kinetics of methane combustion over CVD-made cobalt oxide catalysts. *Applied Catalysis B: Environmental*, 67(3-4):168–176, 2006.
- ⁸⁷ T. H. Lim, S. J. Cho, H. S. Yang, M. H. Engelhard, and D. H. Kim. Effect of Co/Ni ratios in cobalt nickel mixed oxide catalysts on methane combustion. *Applied Catalysis A: General*, 505:62–69, 2015.
- ⁸⁸ D. Trong On, S. V. Nguyen, and S. Kaliaguine. New SO₂ resistant mesoporous mixed oxide catalysts for methane oxidation. *Studies in Surface Science and Catalysis*, 146:641–644, 2003.
- ⁸⁹ S. Royer, A. Van Neste, R. Davidson, S. McIntyre, and S. Kaliaguine. Methane Oxidation over Nanocrystalline LaCo_{1-x}Fe_xO₃: Resistance to SO₂ Poisoning. *Industrial & Engineering Chemistry Research*, 43(18):5670–5680, 2004.
- ⁹⁰ J. Wu, K. Du, J. Che, S. Zou, L. Xiao, H. Kobayashi, and J. Fan. Deactivation Mechanism Study for Sulfur-Tolerance Enhanced NiO Nanocatalysts of Lean Methane Oxidation. *The Journal of Physical Chemistry C*, 125(4):2485–2491, 2021.
- ⁹¹ A. Choya, B. de Rivas, J. I. Gutiérrez-Ortiz, and R. López-Fonseca. On the Effect of the Synthesis Route of the Support in Co₃O₄/CeO₂ Catalysts for the Complete Oxidation of Methane. *Industrial & Engineering Chemistry Research*, 61(49):17854–17865, 2022.
- ⁹² A. Choya, B. de Rivas, J. R. González-Velasco, J. I. Gutiérrez-Ortiz, and R. López-Fonseca. Oxidation of lean methane over cobalt catalysts supported on ceria/alumina. *Applied Catalysis A: General*, 591:117381, 2020.
-

-
- ⁹³ A. Choya, B. de Rivas, J. R. González-Velasco, J. I. Gutiérrez-Ortiz, and R. López-Fonseca. Optimisation of bimetallic Co-Ni supported catalysts for oxidation of methane in natural gas vehicles. *Applied Catalysis B: Environmental*, 284:119712, 2021.
- ⁹⁴ J. Chen, T. Buchanan, E. A. Walker, T. J. Toops, Z. Li, P. Kunal, and E. A. Kyriakidou. Mechanistic Understanding of Methane Combustion over Ni/CeO₂: A Combined Experimental and Theoretical Approach. *ACS Catalysis*, 11(15):9345–9354, 2021.
- ⁹⁵ G. N. Mazo, O. A. Shlyakhtin, A. S. Loktev, and A. G. Dedov. Methane oxidation catalysts based on the perovskite-like complex oxides of cobalt and nickel. *Russian Chemical Bulletin*, 68(11):1949–1953, 2019.
- ⁹⁶ J. Li, X. Liang, S. Xu, and J. Hao. Catalytic performance of manganese cobalt oxides on methane combustion at low temperature. *Applied Catalysis B: Environmental*, 90(1-2):307–312, 2009.
- ⁹⁷ T. C. Xiao, S. F. Ji, H. T. Wang, K. S. Coleman, and M. L. H. Green. Methane combustion over supported cobalt catalysts. *Journal of Molecular Catalysis A: Chemical*, 175(1-2):111–123, 2001.
- ⁹⁸ U. Zavyalova, P. Scholz, and B. Ondruschka. Influence of cobalt precursor and fuels on the performance of combustion synthesized Co₃O₄/γ-Al₂O₃ catalysts for total oxidation of methane. *Applied Catalysis A: General*, 323:226–233, 2007.
- ⁹⁹ G. Caravaggio, L. Nossiova, and M. J. Turnbull. Nickel-magnesium mixed oxide catalyst for low temperature methane oxidation. *Chemical Engineering Journal*, 405:126862, 2021.
- ¹⁰⁰ Wärtsilä. Wärtsilä engine upgrades to reduce ghg emissions. <https://www.wartsila.com/services-catalogue/engine-services-4-stroke/ghg-emissions-reduction-upgrades>, 11-05-2023, 14:17.
- ¹⁰¹ S. Ushakov, D. Stenersen, and P. M. Einang. Methane slip from gas fuelled ships: a comprehensive summary based on measurement data. *Journal of Marine Science and Technology (Japan)*, 24(4):1308–1325, 2019.
- ¹⁰² MAN Energy Solutions. Can methane slip be controlled? <https://www.man-es.com/discover/can-methane-slip-be-controlled>, 11-05-2023, 11:27.
- ¹⁰³ B. Comer, J. O’malley, L. Osipova, and N. Pavlenko. Comparing the future demand for, supply of, and life-cycle emissions from bio, synthetic, and fossil LNG marine fuels in the European Union. *ICCT Report*, September:12–13, 2022.
- ¹⁰⁴ D. J. Zimmerle, L. L. Williams, T. L. Vaughn, C. Quinn, R. Subramanian, G. P. Duggan, B. Willson, J. D. Opsomer, A. J. Marchese, D. M. Martinez, and A. L. Robinson. Methane Emissions from the Natural Gas Transmission and Storage System in the United States. *Environmental Science & Technology*, 49(15):9374–9383, 2015.
- ¹⁰⁵ Daphne Technology. Future-proofing gas engines with slippure™ technology. <https://daphnetechology.com/solutions/slippure>, 11-05-2023, 14:30.
- ¹⁰⁶ Maersk Mc-Kinney Møller Center for Zero Carbon Shipping. Reducing methane emissions onboard vessels, Vessel Emission Reduction Technologies & Solutions. Technical Report October, 2022.
-

-
- ¹⁰⁷ M. Keenan, J. Nicole, and B. Rogers. A novel low-cost aftertreatment solution for lean-burn gas engines. In *Heavy-duty-, On- Und Off-highway-motoren*, pages 53–67. Springer, 2020.
- ¹⁰⁸ K. S. Hui, C. W. Kwong, and C. Y. H. Chao. Methane emission abatement by Pd-ion-exchanged zeolite 13X with ozone. *Energy & Environmental Science*, 3(8):1092, 2010.
- ¹⁰⁹ S. M. Jin, K.-Y. Lee, and D.-W. Lee. Ozone-induced lean methane oxidation over cobalt ion-exchanged BEA catalyst under dry reaction conditions. *Journal of Industrial and Engineering Chemistry*, 112:296–306, 2022.
- ¹¹⁰ W. Li and S. T. Oyama. Catalytic Methane Oxidation at Low Temperatures Using Ozone. *ACS Symposium Series*, 638:363–373, 1996.
- ¹¹¹ L. Zhu, Q. Xu, B. Liu, C. Xie, Y. Li, H. Wang, H. Lou, Q. Zhu, S. Panigrahy, H. Curran, Z. Wang, Y. Ju, and Z. Wang. Ozone-assisted low-temperature oxidation of methane and ethane. *Proceedings of the Combustion Institute*, pages 1–10, 2022.
- ¹¹² F. H. Verhoff and J. T. Banchemo. Predicting dew points of flue gases. *Chemical Engineering Progress*, 70(8):71–72, 1974.
- ¹¹³ N. Wang, Q. Sun, R. Bai, X. Li, G. Guo, and J. Yu. In Situ Confinement of Ultrasmall Pd Clusters within Nanosized Silicalite-1 Zeolite for Highly Efficient Catalysis of Hydrogen Generation. *Journal of the American Chemical Society*, 138(24):7484–7487, 2016.
- ¹¹⁴ K. H. Rasmussen, F. Goodarzi, D. B. Christensen, J. Mielby, and S. Kegnaes. Stabilization of Metal Nanoparticle Catalysts via Encapsulation in Mesoporous Zeolites by Steam-Assisted Recrystallization. *ACS Applied Nano Materials*, 2(12):8083–8091, 2019.
- ¹¹⁵ Y. Ding, S. Wang, L. Zhang, L. Lv, D. Xu, W. Liu, and S. Wang. Investigation of supported palladium catalysts for combustion of methane: The activation effect caused by SO₂. *Chemical Engineering Journal*, 382(September 2019):122969, 2020.
- ¹¹⁶ Lara S. Escandón, Salvador Ordóñez, Aurelio Vega, and Fernando V. Díez. Sulphur poisoning of palladium catalysts used for methane combustion: Effect of the support. *Journal of Hazardous Materials*, 153(1-2):742–750, 2008.
- ¹¹⁷ H. Peng, C. Rao, N. Zhang, X. Wang, W. Liu, W. Mao, L. Han, P. Zhang, and S. Dai. Confined Ultrathin Pd-Ce Nanowires with Outstanding Moisture and SO₂ Tolerance in Methane Combustion. *Angewandte Chemie*, 130(29):9091–9095, 2018.
- ¹¹⁸ J. Lin, X. Chen, Y. Y. Zheng, Y. Xiao, Y. Y. Zheng, and L. Jiang. Sulfur-resistant methane combustion invoked by surface property regulation on palladium-based catalysts. *Applied Surface Science*, 587(January):152835, 2022.
- ¹¹⁹ M. Monai, T. Montini, M. Melchionna, T. Duchoň, P. Kúš, C. Chen, N. Tsud, L. Nasi, K. C. Prince, K. Veltruská, V. Matolín, M. M. Khader, R. J. Gorte, and P. Fornasiero. The effect of sulfur dioxide on the activity of hierarchical Pd-based catalysts in methane combustion. *Applied Catalysis B: Environmental*, 202:72–83, 2017.
-

-
- ¹²⁰ Y. Chen, X. Zhu, X. Wang, and Y. Su. A reliable protocol for fast and facile constructing multi-hollow silicalite-1 and encapsulating metal nanoparticles within the hierarchical zeolite. *Chemical Engineering Journal*, 419:129641, 2021.
- ¹²¹ D. T. Bregante, D. S. Potts, O. Kwon, E. Z. Ayla, J. Z. Tan, and D. W. Flaherty. Effects of Hydrofluoric Acid Concentration on the Density of Silanol Groups and Water Adsorption in Hydrothermally Synthesized Transition-Metal-Substituted Silicalite-1. *Chemistry of Materials*, 32(17):7425–7437, 2020.
- ¹²² I. Grosskreuz, H. Gies, and B. Marler. Alteration and curing of framework defects by heating different as-made silica zeolites of the MFI framework type. *Microporous and Mesoporous Materials*, 291(May 2019):109683, 2020.
- ¹²³ P. Caullet, J.-L. Paillaud, A. Simon-Masseron, M. Soulard, and J. Patarin. The fluoride route: a strategy to crystalline porous materials. *Comptes Rendus Chimie*, 8(3-4):245–266, 2005.
- ¹²⁴ Z. Qin, L. Lakiss, J.-P. Gilson, K. Thomas, J.-M. Goupil, C. Fernandez, and V. Valtchev. Chemical Equilibrium Controlled Etching of MFI-Type Zeolite and Its Influence on Zeolite Structure, Acidity, and Catalytic Activity. *Chemistry of Materials*, 25(14):2759–2766, 2013.
- ¹²⁵ H. Hosseiniamoli, A. Setiawan, A. A. Adesina, E. M. Kennedy, and M. Stockenhuber. The stability of Pd/TS-1 and Pd/silicalite-1 for catalytic oxidation of methane – understanding the role of titanium. *Catalysis Science & Technology*, 10(4):1193–1204, 2020.
- ¹²⁶ A. W. Petrov, D. Ferri, O. Kröcher, and J. A. van Bokhoven. Design of Stable Palladium-Based Zeolite Catalysts for Complete Methane Oxidation by Postsynthesis Zeolite Modification. *ACS Catalysis*, 9(3):2303–2312, 2019.
- ¹²⁷ T. Li, A. Beck, F. Krumeich, L. Artiglia, M. K. Ghosal, M. Roger, D. Ferri, O. Kröcher, V. Sushkevich, O. V. Safonova, and J. A. van Bokhoven. Stable Palladium Oxide Clusters Encapsulated in Silicalite-1 for Complete Methane Oxidation. *ACS Catalysis*, 11(12):7371–7382, 2021.
- ¹²⁸ X. Feng, T. Wang, L. Mu, Z. Chen, J. Liang, and C. Xiao. Excellent stability for catalytic oxidation of methane over core-shell Pd@silicalite-1 with complete zeolite shell in wet conditions. *Catalysis Today*, 400-401:66–72, 2022.
- ¹²⁹ W. Wang, W. Zhou, W. Li, X. Xiong, Y. Y. Wang, K. Cheng, J. Kang, Q. Zhang, and Y. Y. Wang. In-situ confinement of ultrasmall palladium nanoparticles in silicalite-1 for methane combustion with excellent activity and hydrothermal stability. *Applied Catalysis B: Environmental*, 276(May):119142, 2020.
- ¹³⁰ Panos Dimitriou. *Deactivation of zeolite based methane oxidation catalysts.*, MSc. project, Department of Chemistry, Technical University of Denmark, 2021.
- ¹³¹ X. Zhang, Y. Liu, J. Deng, L. Jing, L. Wu, and H. Dai. Catalytic performance and SO₂ resistance of zirconia-supported platinum-palladium bimetallic nanoparticles for methane combustion. *Catalysis Today*, 402(February):138–148, 2022.
-

-
- ¹³² Z. Liu, G. Xu, L. Zeng, W. Shi, Y. Wang, Y. Sun, Y. Yu, and H. He. Anchoring Pt-doped PdO nanoparticles on γ -Al₂O₃ with highly dispersed La sites to create a methane oxidation catalyst. *Applied Catalysis B: Environmental*, 324(December 2022):122259, 2023.
- ¹³³ Signe Tronsen and Frederik Feddersen. *Development of palladium and platinum containing zeolite based methane oxidation catalysts.*, BSc. project, Department of Chemistry, Technical University of Denmark, 2021.
- ¹³⁴ A. L. Patterson. The Scherrer Formula for X-Ray Particle Size Determination. *Physical Review*, 56(10):978–982, 1939.
- ¹³⁵ Q. Sun, N. Wang, Q. Fan, L. Zeng, A. Mayoral, S. Miao, R. Yang, Z. Jiang, W. Zhou, J. Zhang, T. Zhang, J. Xu, P. Zhang, J. Cheng, D. C. Yang, R. Jia, L. Li, Q. Zhang, Y. Wang, O. Terasaki, and J. Yu. Subnanometer Bimetallic Platinum–Zinc Clusters in Zeolites for Propane Dehydrogenation. *Angewandte Chemie - International Edition*, 59(44):19450–19459, 2020.
- ¹³⁶ B. Zhang, G. Li, Z. Zhai, D. Chen, Y. Tian, R. Yang, L. Wang, X. Zhang, and G. Liu. PtZn intermetallic nanoalloy encapsulated in silicalite-1 for propane dehydrogenation. *AIChE Journal*, 67(7):1–12, 2021.
- ¹³⁷ T. Dong, W. Liu, M. Ma, H. Peng, S. Yang, J. Tao, C. He, L. Wang, P. Wu, and T. An. Hierarchical zeolite enveloping Pd-CeO₂ nanowires: An efficient adsorption/catalysis bifunctional catalyst for low temperature propane total degradation. *Chemical Engineering Journal*, 393(February), 2020.
- ¹³⁸ M. Yabushita, M. Yoshida, R. Osuga, F. Muto, S. Iguchi, S. Yasuda, A. Neya, M. Horie, S. Maki, K. Kanie, I. Yamanaka, T. Yokoi, and A. Muramatsu. Mechanochemical Route for Preparation of MFI-Type Zeolites Containing Highly Dispersed and Small Ce Species and Catalytic Application to Low-Temperature Oxidative Coupling of Methane. *Industrial and Engineering Chemistry Research*, 60(28):10101–10111, 2021.
- ¹³⁹ Y. Chen, X. Wang, and L. Zhang. A strategy for fast and facile embedding platinum nanoparticles in silicalite-1 crystallites with a stable and catalytic active structure. *Chemical Engineering Journal*, 394(April):124990, 2020.
- ¹⁴⁰ United States Environmental Protection Agency (EPA). Basics of green chemistry, green chemistry’s 12 principles. <https://www.epa.gov/greenchemistry/basics-green-chemistry#twelve>, 01-05-2023, 10:55.
- ¹⁴¹ H. Hosseiniamoli, G. Bryant, E. M. Kennedy, K. Mathisen, D. Nicholson, G. Sankar, A. Setiawan, and M. Stockenhuber. Understanding Structure–Function Relationships in Zeolite-Supported Pd Catalysts for Oxidation of Ventilation Air Methane. *ACS Catalysis*, 8(7):5852–5863, 2018.
- ¹⁴² J. B. Lim, D. Jo, and S. B. Hong. Palladium-exchanged small-pore zeolites with different cage systems as methane combustion catalysts. *Applied Catalysis B: Environmental*, 219:155–162, 2017.
- ¹⁴³ M. Liu, X. Chen, Z. Wang, Y. Zhang, R. Li, H. Zheng, D. Ye, and J. Wu. Size-Controlled Palladium Nanoparticles Encapsulated in Silicalite-1 for Methane Catalytic Combustion. *ACS Applied Nano Materials*, 6(5):3637–3646, 2023.
-

-
- ¹⁴⁴ R. Niu, P. Liu, W. Li, S. Wang, and J. Li. High performance for oxidation of low-concentration methane using ultra-low Pd in silicalite-1 zeolite. *Microporous and Mesoporous Materials*, 284(February):235–240, 2019.
- ¹⁴⁵ S. M. Vickers, R. Gholami, K. J. Smith, and M. J. MacLachlan. Mesoporous Mn- and La-Doped Cerium Oxide/Cobalt Oxide Mixed Metal Catalysts for Methane Oxidation. *ACS Applied Materials & Interfaces*, 7(21):11460–11466, 2015.
- ¹⁴⁶ G. Corro, J. Cruz-Mérida, D. Montalvo, and U. Pal. Performance of Pt/Cr₂O₃, Pt/ZrO₂, and, Pt/ γ -Al₂O₃ Catalysts in Total Oxidation of Methane: Effect of Metal-Support Interaction. *Industrial & Engineering Chemistry Research*, 60(51):18841–18852, 2021.
- ¹⁴⁷ Y. Wang, C. Liu, X. Liao, Y. Liu, J. Hou, and C. Pham-Huu. Enhancing oxygen activation on high surface area Pd-SnO₂ solid solution with isolated metal site catalysts for catalytic CH₄ combustion. *Applied Surface Science*, 564:150368, 2021.
- ¹⁴⁸ J. Huang, J. Lin, X. Chen, Y. Zheng, Y. Xiao, and Y. Zheng. Optimizing the Microstructure of SnO₂-CeO₂ Binary Oxide Supported Palladium Catalysts for Efficient and Stable Methane Combustion. *ACS Applied Materials & Interfaces*, 14(14):16233–16244, 2022.
- ¹⁴⁹ M. J. Koponen, T. Venäläinen, M. Suvanto, K. Kallinen, T.-J. J. Kinnunen, M. Härkönen, and T. A. Pakkanen. Methane conversion and SO₂ resistance of LaMn_{1-x}Fe_xO₃ (x=0.4, 0.5, 0.6, 1) perovskite catalysts promoted with palladium. *Journal of Molecular Catalysis A: Chemical*, 258(1-2):246–250, 2006.
- ¹⁵⁰ C. Li, B. Tang, A. T. Ogunbiyi, S. Tang, W. Li, Q. Lu, and L. Yuan. The effects of facet-dependent palladium-titania interactions on the activity of Pd/Rutile catalysts for lean methane oxidation. *Molecular Catalysis*, 528(May):112475, 2022.
- ¹⁵¹ Q. Li, X. Chu, Y. Wang, Q. Yang, Z. Su, Y. Peng, W. Si, and J. Li. Metal-Support Interactions within a Dual-Site Pd/YMn₂O₅ Catalyst during CH₄ Combustion. *ACS Catalysis*, 12(8):4430–4439, 2022.
- ¹⁵² S. Colussi, A. Trovarelli, C. Cristiani, L. Lietti, and G. Groppi. The influence of ceria and other rare earth promoters on palladium-based methane combustion catalysts. *Catalysis Today*, 180(1):124–130, 2012.
- ¹⁵³ M. Varbar, S. M. Alavi-Amleshi, M. Rezaei, and E. Akbari. Catalytic Oxidation of Lean Methane over Ni/MgAl₂O₄ Synthesized by a Novel and Facile Mechanochemical Preparation Method. *Combustion Science and Technology*, 195(8):1819–1839, 2023.
- ¹⁵⁴ M. Wu, M. Miao, W. Li, X. Zhang, L. Zhang, T. Zhen, Y. Fu, J. Jin, and L. Yuan. Metal-organic framework-derived one-dimensional Pd@CeO₂ catalysts with enhanced activity for methane oxidation. *Fuel*, 331(P1):125575, 2023.
- ¹⁵⁵ F. Klingstedt, H. Karhu, A. K. Neyestanaki, L.-E. Lindfors, T. Salmi, and J. Väyrynen. Barium Promoted Palladium Catalysts for the Emission Control of Natural Gas Driven Vehicles and Biofuel Combustion Systems. *Journal of Catalysis*, 206(2):248–262, 2002.
- ¹⁵⁶ P. O. Thevenin, E. Poceroba, L. J. Pettersson, H. Karhu, I. J. Väyrynen, and S. G. Järås. Characterization and activity of supported palladium combustion catalysts. *Journal of Catalysis*, 207(1):139–149, 2002.
-

-
- ¹⁵⁷ J. Du, M. Guo, A. Zhang, H. Zhao, D. Zhao, C. Wang, T. Zheng, Y. Zhao, and Y. Luo. Performance, structure and kinetics of Pd catalyst supported in Ba modified γ -Al₂O₃ for low temperature wet methane oxidation. *Chemical Engineering Journal*, 430(P4):133113, 2022.
- ¹⁵⁸ L. Liotta and G. Deganello. Thermal stability, structural properties and catalytic activity of Pd catalysts supported on Al₂O₃-CeO₂-BaO mixed oxides prepared by sol-gel method. *Journal of Molecular Catalysis A: Chemical*, 204-205:763-770, 2003.
- ¹⁵⁹ X. Auvray, A. Lindholm, M. Milh, and L. Olsson. The addition of alkali and alkaline earth metals to Pd/Al₂O₃ to promote methane combustion. Effect of Pd and Ca loading. *Catalysis Today*, 299(April 2017):212-218, 2018.
- ¹⁶⁰ Y. Jing, G. Wang, S. Mine, Z. Maeno, S. M. A. Hakim Siddiki, M. Kobayashi, S. Nagaoka, K. Shimizu, and T. Toyao. Role of Ba in an Al₂O₃ -Supported Pd-based Catalyst under Practical Three-Way Catalysis Conditions. *ChemCatChem*, 14(8), 2022.
- ¹⁶¹ R. Burch, F. Urbano, and P. Loader. Methane combustion over palladium catalysts: The effect of carbon dioxide and water on activity. *Applied Catalysis A: General*, 123(1):173-184, 1995.
- ¹⁶² R. Burch and F. J. Urbano. Investigation of the active state of supported palladium catalysts in the combustion of methane. *Applied Catalysis A, General*, 124(1):121-138, 1995.
- ¹⁶³ D. L. Mowery, M. S. Graboski, T. R. Ohno, and R. L. McCormick. Deactivation of PdO-Al₂O₃ oxidation catalyst in lean-burn natural gas engine exhaust: aged catalyst characterization and studies of poisoning by H₂O and SO₂. *Applied Catalysis B: Environmental*, 21(3):157-169, 1999.
- ¹⁶⁴ D. L. Mowery and R. L. McCormick. Deactivation of alumina supported and unsupported PdO methane oxidation catalyst: the effect of water on sulfate poisoning. *Applied Catalysis B: Environmental*, 34:287-297, 2001.
- ¹⁶⁵ D. Ciuparu and L. Pfefferle. Support and water effects on palladium based methane combustion catalysts. *Applied Catalysis A: General*, 209(1-2):415-428, 2001.
- ¹⁶⁶ D. Ciuparu, N. Katsikis, and L. Pfefferle. Temperature and time dependence of the water inhibition effect on supported palladium catalyst for methane combustion. *Applied Catalysis A: General*, 216(1-2):209-215, 2001.
- ¹⁶⁷ D. Ciuparu and L. Pfefferle. Contributions of lattice oxygen to the overall oxygen balance during methane combustion over PdO-based catalysts. *Catalysis Today*, 77(3):167-179, 2002.
- ¹⁶⁸ D. Ciuparu, E. Perkins, and L. Pfefferle. In situ DR-FTIR investigation of surface hydroxyls on γ -Al₂O₃ supported PdO catalysts during methane combustion. *Applied Catalysis A: General*, 263(2):145-153, 2004.
- ¹⁶⁹ C. F. Cullis, T. G. Nevell, and D. L. Trimm. Role of the catalyst support in the oxidation of methane over palladium. *Journal of the Chemical Society, Faraday Transactions 1: Physical Chemistry in Condensed Phases*, 68(4978):1406, 1972.
-

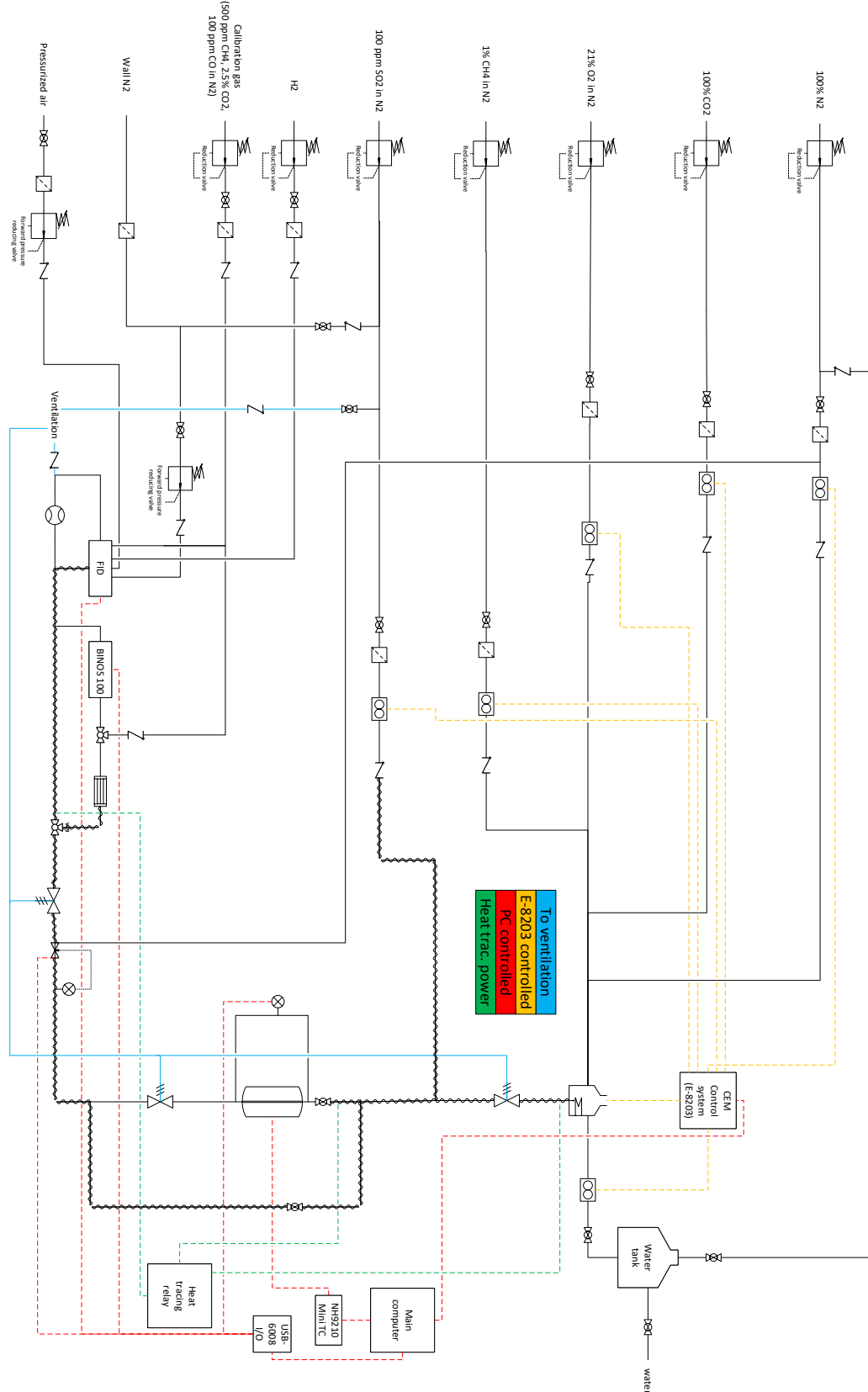
-
- ¹⁷⁰ R. J. Card, J. L. Schmitt, and J. M. Simpson. Palladium-carbon hydrogenolysis catalysts: The effect of preparation variables on catalytic activity. *Journal of Catalysis*, 79(1):13–20, 1983.
- ¹⁷¹ K. Persson, L. D. Pfefferle, W. Schwartz, A. Ersson, and S. G. Järås. Stability of palladium-based catalysts during catalytic combustion of methane: The influence of water. *Applied Catalysis B: Environmental*, 74(3-4):242–250, 2007.
- ¹⁷² W. R. Schwartz and L. D. Pfefferle. Combustion of methane over palladium-based catalysts: Support interactions. *Journal of Physical Chemistry C*, 116(15):8571–8578, 2012.
- ¹⁷³ W. R. Schwartz, D. Ciuparu, and L. D. Pfefferle. Combustion of methane over palladium-based catalysts: Catalytic deactivation and role of the support. *Journal of Physical Chemistry C*, 116(15):8587–8593, 2012.
- ¹⁷⁴ O. Mihai, G. Smedler, U. Nylén, M. Olofsson, and L. Olsson. The effect of water on methane oxidation over Pd/Al₂O₃ under lean, stoichiometric and rich conditions. *Catalysis Science & Technology*, 7(14):3084–3096, 2017.
- ¹⁷⁵ N. Sadokhina, F. Ghasempour, X. Auvray, G. Smedler, U. Nylén, M. Olofsson, and L. Olsson. An Experimental and Kinetic Modelling Study for Methane Oxidation over Pd-based Catalyst: Inhibition by Water. *Catalysis Letters*, 147(9):2360–2371, 2017.
- ¹⁷⁶ A. Toso, S. Colussi, S. Padigapaty, C. de Leitenburg, and A. Trovarelli. High stability and activity of solution combustion synthesized Pd-based catalysts for methane combustion in presence of water. *Applied Catalysis B: Environmental*, 230(December 2017):237–245, 2018.
- ¹⁷⁷ A. Toso, S. Colussi, J. Llorca, and A. Trovarelli. The dynamics of PdO-Pd phase transformation in the presence of water over Si-doped Pd/CeO₂ methane oxidation catalysts. *Applied Catalysis A: General*, 574(January):79–86, 2019.
- ¹⁷⁸ A. Boucly, L. Artiglia, M. Roger, M. Zabilskiy, A. Beck, D. Ferri, and J. A. van Bokhoven. Water inhibition and role of palladium adatoms on Pd/Al₂O₃ catalysts during methane oxidation. *Applied Surface Science*, 606(July):154927, 2022.
- ¹⁷⁹ A. Boubnov, A. Gremminger, M. Casapu, O. Deutschmann, and J.-D. Grunwaldt. Dynamics of the Reversible Inhibition during Methane Oxidation on Bimetallic Pd-Pt Catalysts Studied by Modulation-Excitation XAS and DRIFTS. *ChemCatChem*, 14(22), 2022.
- ¹⁸⁰ P. Velin, F. Hemmingsson, A. Schaefer, M. Skoglundh, K. A. Lomachenko, A. Raj, D. Thompsett, G. Smedler, and P.-A. Carlsson. Hampered PdO Redox Dynamics by Water Suppresses Lean Methane Oxidation over Realistic Palladium Catalysts. *ChemCatChem*, 13(17):3765–3771, 2021.
- ¹⁸¹ X. Li, X. Wang, K. Roy, J. A. van Bokhoven, and L. Artiglia. Role of Water on the Structure of Palladium for Complete Oxidation of Methane. *ACS Catalysis*, 10(10):5783–5792, 2020.
- ¹⁸² F. Zhang, C. Hakanoglu, J. A. Hinojosa, and J. F. Weaver. Inhibition of methane adsorption on PdO(101) by water and molecular oxygen. *Surface Science*, 617:249–255, 2013.
-

-
- ¹⁸³ K. Murata, J. Ohyama, Y. Yamamoto, S. Arai, and A. Satsuma. Methane Combustion over Pd/Al₂O₃ Catalysts in the Presence of Water: Effects of Pd Particle Size and Alumina Crystalline Phase. *ACS Catalysis*, 10(15):8149–8156, 2020.
- ¹⁸⁴ J. C. Van Giezen, F. R. Van Den Berg, J. L. Kleinen, A. J. Van Dillen, and J. W. Geus. The effect of water on the activity of supported palladium catalysts in the catalytic combustion of methane. *Catalysis Today*, 47(1-4):287–293, 1999.
- ¹⁸⁵ Peter Atkins and Julio de Paula. *Atkins’ Physical Chemistry*, 10th Ed, p. 827-831. Oxford University Press, Oxford, 2014.
- ¹⁸⁶ Mikkel Jørgensen. *Kinetics of Nanoparticle Catalysis from First Principles*. PhD thesis, Chalmers University of Technology, 2019.
- ¹⁸⁷ F. Arosio, S. Colussi, A. Trovarelli, and G. Groppi. Effect of alternate CH₄-reducing/lean combustion treatments on the reactivity of fresh and S-poisoned Pd/CeO₂/Al₂O₃ catalysts. *Applied Catalysis B: Environmental*, 80(3-4):335–342, 2008.
- ¹⁸⁸ A. Baylet, P. Marécot, D. Duprez, P. Castellazzi, G. Groppi, and P. Forzatti. In situ Raman and in situ XRD analysis of PdO reduction and Pd⁰ oxidation supported on γ -Al₂O₃ catalyst under different atmospheres. *Physical Chemistry Chemical Physics*, 13(10):4607, 2011.
- ¹⁸⁹ A. Paredes-Nunez, I. Jbir, D. Bianchi, and F. C. Meunier. Spectrum baseline artefacts and correction of gas-phase species signal during diffuse reflectance FT-IR analyses of catalysts at variable temperatures. *Applied Catalysis A: General*, 495:17–22, 2015.
- ¹⁹⁰ E. J. Jang, J. Lee, D. G. Oh, and J. H. Kwak. CH₄ Oxidation Activity in Pd and Pt–Pd Bimetallic Catalysts: Correlation with Surface PdO_x Quantified from the DRIFTS Study. *ACS Catalysis*, 11(10):5894–5905, 2021.
- ¹⁹¹ P. Du, O. Kokhan, K. W. Chapman, P. J. Chupas, and D. M. Tiede. Elucidating the Domain Structure of the Cobalt Oxide Water Splitting Catalyst by X-ray Pair Distribution Function Analysis. *Journal of the American Chemical Society*, 134(27):11096–11099, 2012.
- ¹⁹² S. J. L. Billinge. The rise of the X-ray atomic pair distribution function method: a series of fortunate events. *Philosophical Transactions of the Royal Society A: Mathematical, Physical and Engineering Sciences*, 377(2147):20180413, 2019.
- ¹⁹³ D. Chakraborty, T. Erik L. Smitshuysen, A. Kakekhani, S. P. F. Jespersen, S. Banerjee, A. Krabbe, N. Hagen, H. Silva, J. Just, C. D. Damsgaard, S. Helveg, A. M. Rappe, J. K. Nørskov, and I. Chorkendorff. Reversible Atomization and Nano-Clustering of Pt as a Strategy for Designing Ultra-Low-Metal-Loading Catalysts. *Journal of Physical Chemistry C*, 126(38):16194–16203, 2022.
- ¹⁹⁴ E. D. Goodman, A. A. Ye, A. Aitbekova, O. Mueller, A. R. Riscoe, N. Taylor, A. S. Hoffman, A. Boubnov, K. C. Bustillo, M. Nachtegaal, S. R. Bare, and M. Cargnello. Palladium oxidation leads to methane combustion activity: Effects of particle size and alloying with platinum. *J. Chem. Phys.*, 151:154703, 2019.
-

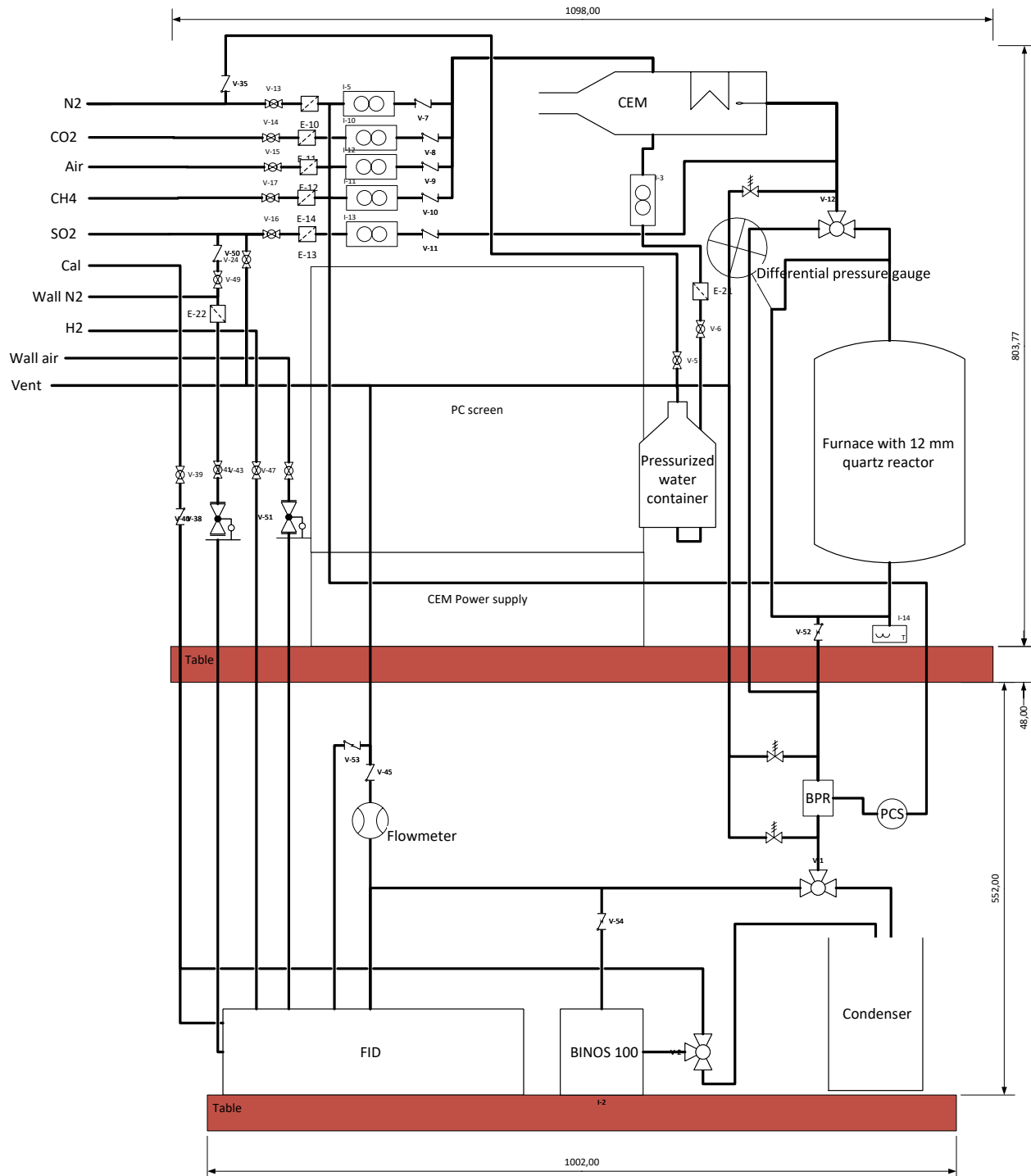
-
- ¹⁹⁵ K. Murata, Y. Mahara, J. Ohyama, Y. Yamamoto, S. Arai, and A. Satsuma. The Metal-Support Interaction Concerning the Particle Size Effect of Pd/Al₂O₃ on Methane Combustion. *Angewandte Chemie*, 129(50):16209–16213, 2017.
- ¹⁹⁶ Z. P. Liu and P. Hu. General rules for predicting where a catalytic reaction should occur on metal surfaces: A density functional theory study of C-H and C-O bond breaking/making on flat, stepped, and kinked metal surfaces. *Journal of the American Chemical Society*, 125(7):1958–1967, 2003.
- ¹⁹⁷ G. Groppi, W. Ibashi, M. Valentini, and P. Forzatti. High-temperature combustion of CH₄ over PdO/Al₂O₃: kinetic measurements in a structured annular reactor. *Chemical Engineering Science*, 56(3):831–839, 2001.
- ¹⁹⁸ G. Groppi, W. Ibashi, E. Tronconi, and P. Forzatti. Structured reactors for kinetic measurements in catalytic combustion. *Chemical Engineering Journal*, 82(1-3):57–71, 2001.
- ¹⁹⁹ C. Cui, Y. Zhang, W. Shan, Y. Yu, and H. He. Influence of NO on the activity of Pd/ θ -Al₂O₃ catalyst for methane oxidation: Alleviation of transient deactivation. *Journal of Environmental Sciences*, 112:38–47, 2022.
- ²⁰⁰ P. Auvinen, N. M. Kinnunen, J. T. Hirvi, T. Maunula, K. Kallinen, M. Keenan, and M. Suvanto. Effects of NO and NO₂ on fresh and SO₂ poisoned methane oxidation catalyst – Harmful or beneficial? *Chemical Engineering Journal*, 417(2):128050, 2021.
- ²⁰¹ J. Chen, H. N. Pham, T. Mon, T. J. Toops, A. K. Datye, Z. Li, and E. A. Kyriakidou. Ni/CeO₂ Nanocatalysts with Optimized CeO₂ Support Morphologies for CH₄ Oxidation. *ACS Applied Nano Materials*, 6(6):4544–4553, 2023.
- ²⁰² Y. Zhao, Z. Gu, D. Li, J. Yuan, L. Jiang, H. Xu, C. Lu, G. Deng, M. Li, W. Xiao, and K. Li. Catalytic combustion of lean methane over MnCo₂O₄/SiC catalysts: Enhanced activity and sulfur resistance. *Fuel*, 323(February):124399, 2022.
- ²⁰³ H. S. F. Ramos, J. P. Mmbaga, and R. E. Hayes. Catalyst optimization in a catalytic flow reversal reactor for lean methane combustion. *Catalysis Today*, 407(December 2021):182–193, 2023.
- ²⁰⁴ J. H. Lee and D. L. Trimm. Catalytic combustion of methane. *Fuel Processing Technology*, 42(2-3):339–359, 1995.
- ²⁰⁵ Q. Zheng, S. Zhou, M. Lail, and K. Amato. Oxygen Removal from Oxy-Combustion Flue Gas for CO₂ Purification via Catalytic Methane Oxidation. *Industrial & Engineering Chemistry Research*, 57(6):1954–1960, 2018.
- ²⁰⁶ T. Guo, J. Du, J. Wu, S. Wang, and J. Li. Structure and kinetic investigations of surface-stepped CeO₂-supported Pd catalysts for low-concentration methane oxidation. *Chemical Engineering Journal*, 306:745–753, 2016.
- ²⁰⁷ H. Gong, Z. Chen, M. Wang, W. Wu, and W. Wang. A study on the feasibility of the catalytic methane oxidation for landfill gas deoxygen treatment. *Fuel*, 120:179–185, 2014.
-

Appendices

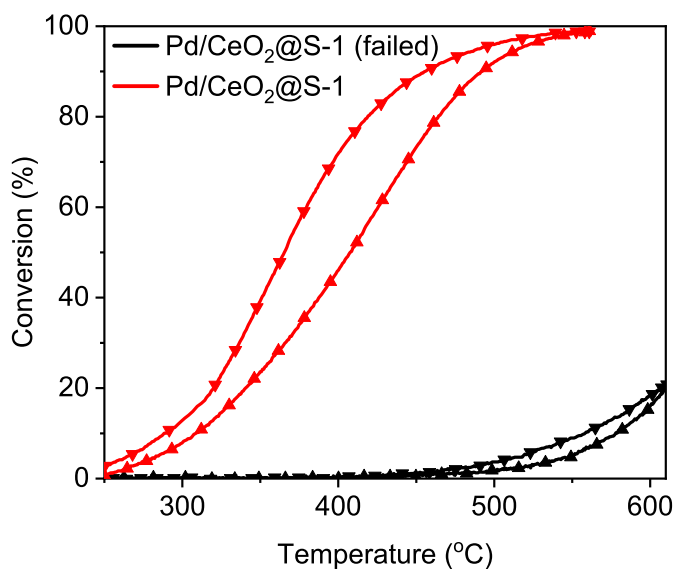
Appendix A - P&I diagram of test setup



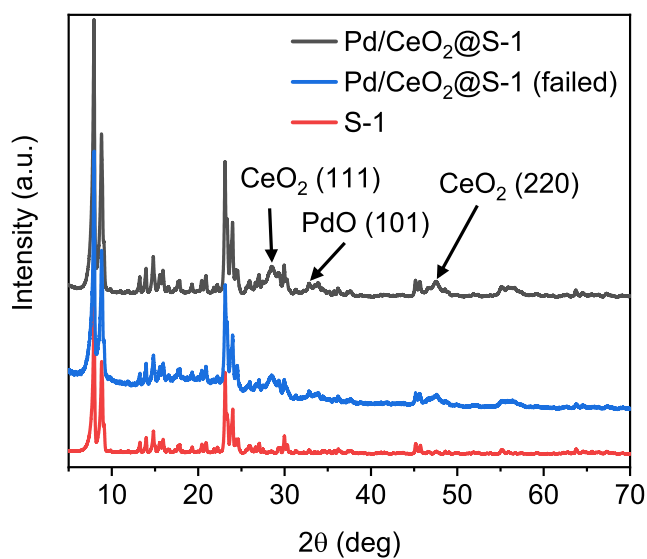
Appendix B - Construction drawing of test setup



Appendix C - Example of poorly reproducible synthesis

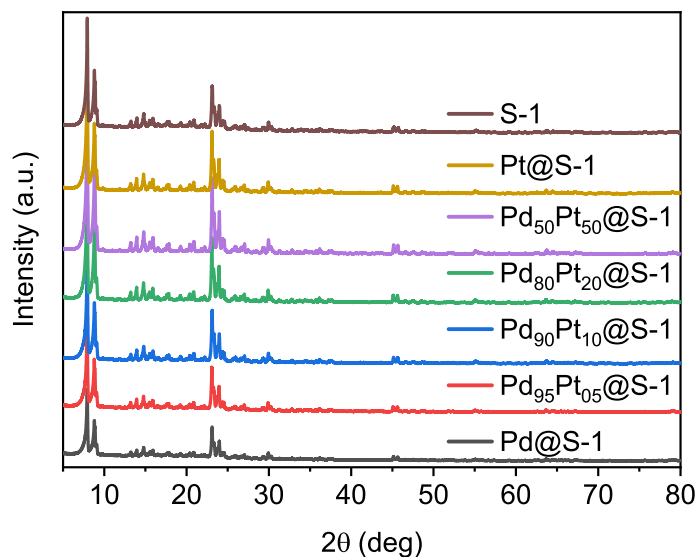


Light-off experiment of Pd/CeO₂@S-1 materials synthesized with identical procedures. Reaction conditions: 1000 ppm CH₄, 10% O₂, 5% CO₂, N₂ balance, WHSV = 126 000 ml h⁻¹ g⁻¹.

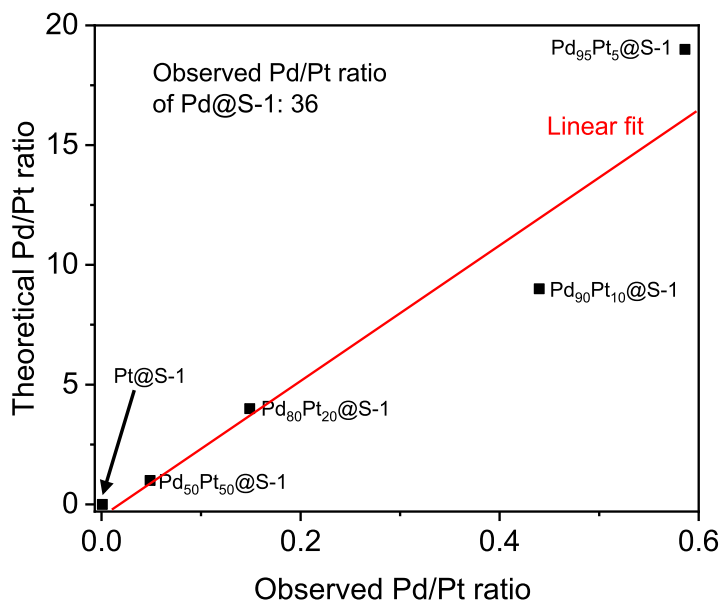


X-ray powder diffraction of Pd/CeO₂@S-1 catalysts with different activities for complete methane oxidation with diffractogram of pure S-1 as reference. Although the activities of the samples were very different, they were indistinguishable in both characterization and visual inspection.

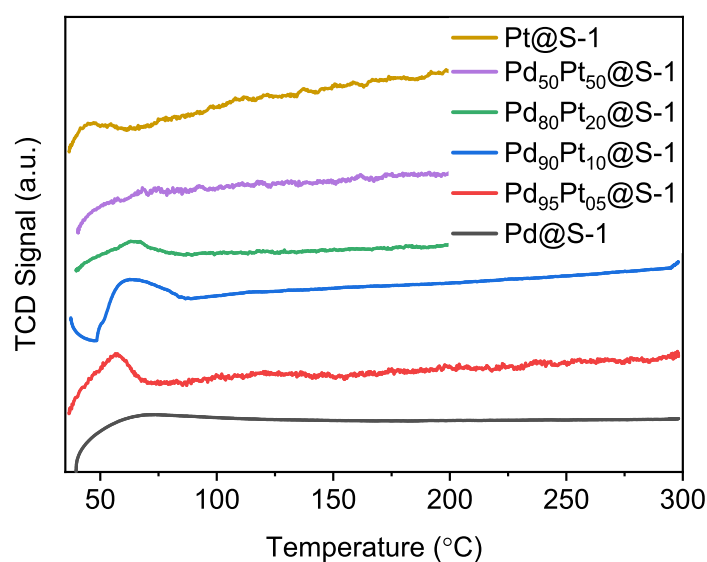
Appendix D - Characterization of PdPt@S-1 materials synthesized by BSc. students



X-ray powder diffraction of PdPt@S-1 catalysts. All diffractograms show the MFI structure, but metal nanoparticles are too small or too few to be observed. Adapted from BSc. project by Frederik Feddersen and Signe Tronsen.¹³³

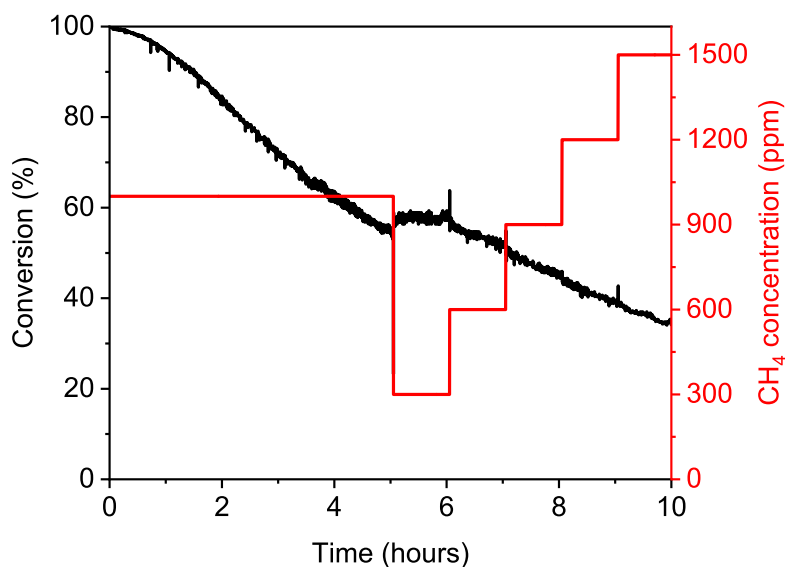


X-ray fluorescence study of PdPt@S-1 catalysts. Using the samples themselves as an internal standard, it was shown that the amounts of precious metals incorporated into materials could be controlled relatively accurately. Adapted from BSc. project by Frederik Feddersen and Signe Tronsen.¹³³

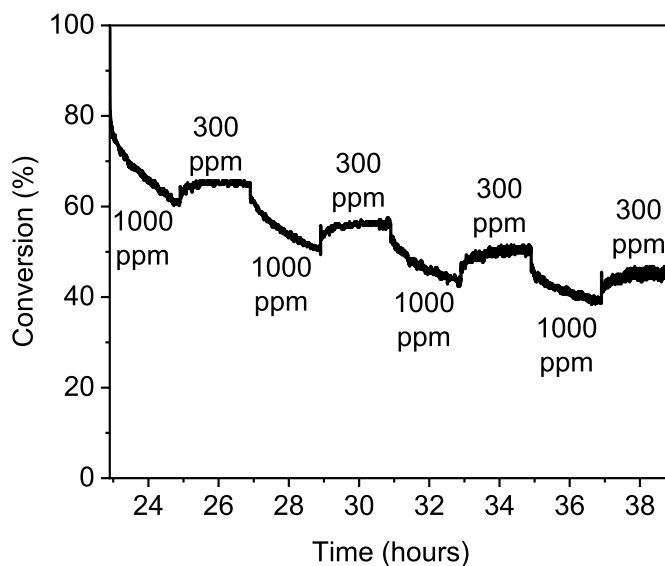


H₂-TPR of PdPt@S-1 catalysts. The reduction temperature of palladium oxide in hydrogen is around 75 °C.³⁹ Assuming that platinum is a little easier to reduce due to being more noble, the expectation was that the reduction temperature would follow the Pd/Pt ratio. The Pt@S-1 sample has its reduction peak at 45 °C, and several of the mixed metal catalysts have reduction peaks between 45 and 75 °C, although their exact locations are not as expected. Adapted from BSc. project by Frederik Feddersen and Signe Tronsen.¹³³

Appendix E - Origin of discovery of methane dependence

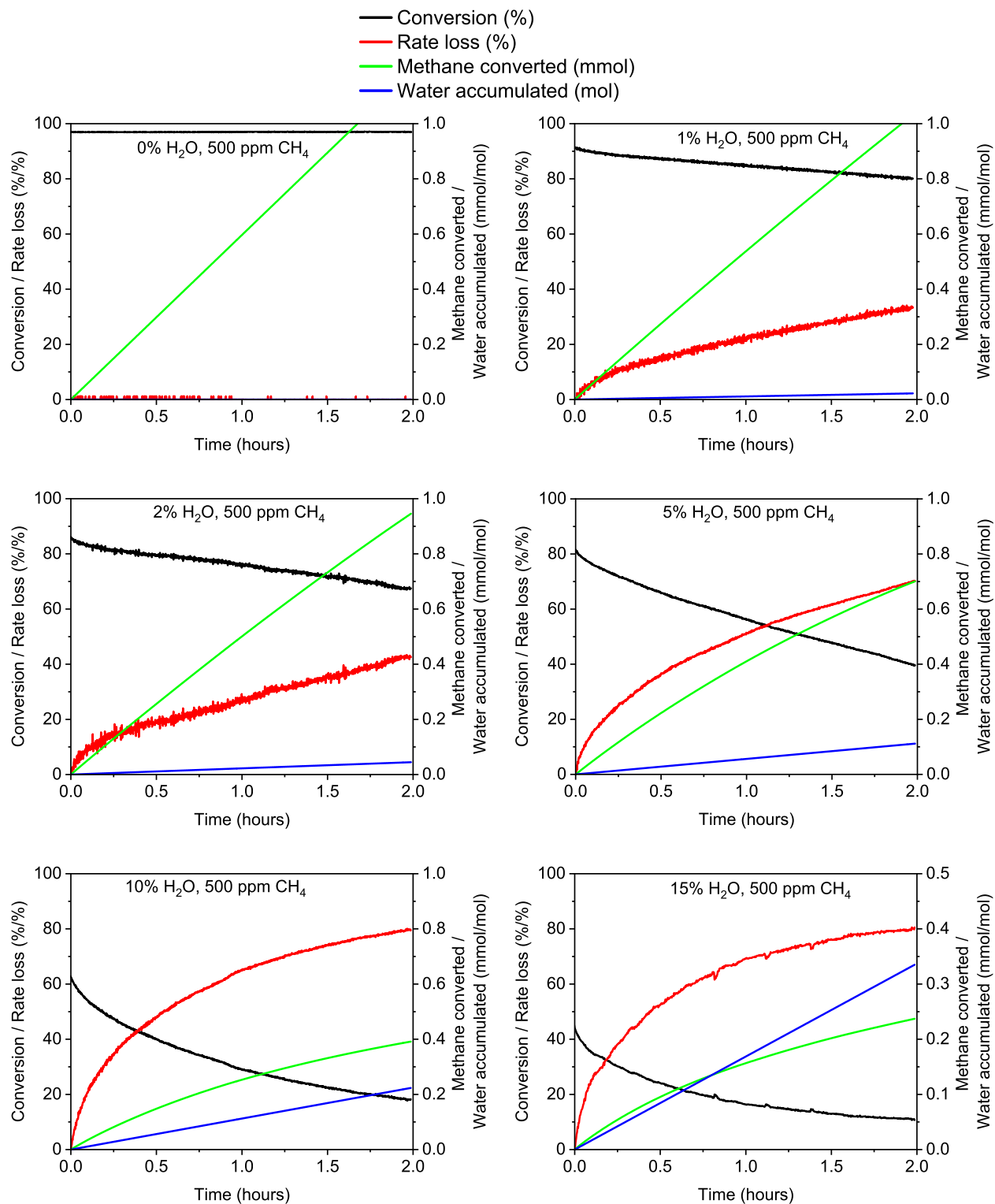


Attempt at estimating the reaction order of methane in complete methane oxidation in the presence of water. As the methane concentration is lowered at the 5-hour mark, the conversion unsurprisingly increases. It was however surprising that the slope of the deactivation curve flattened out. Reaction conditions: 300-1500 ppm CH₄, 10% O₂, 5% H₂O, N₂ balance, WHSV = 126 000 ml h⁻¹ g⁻¹, T = 400 °C.



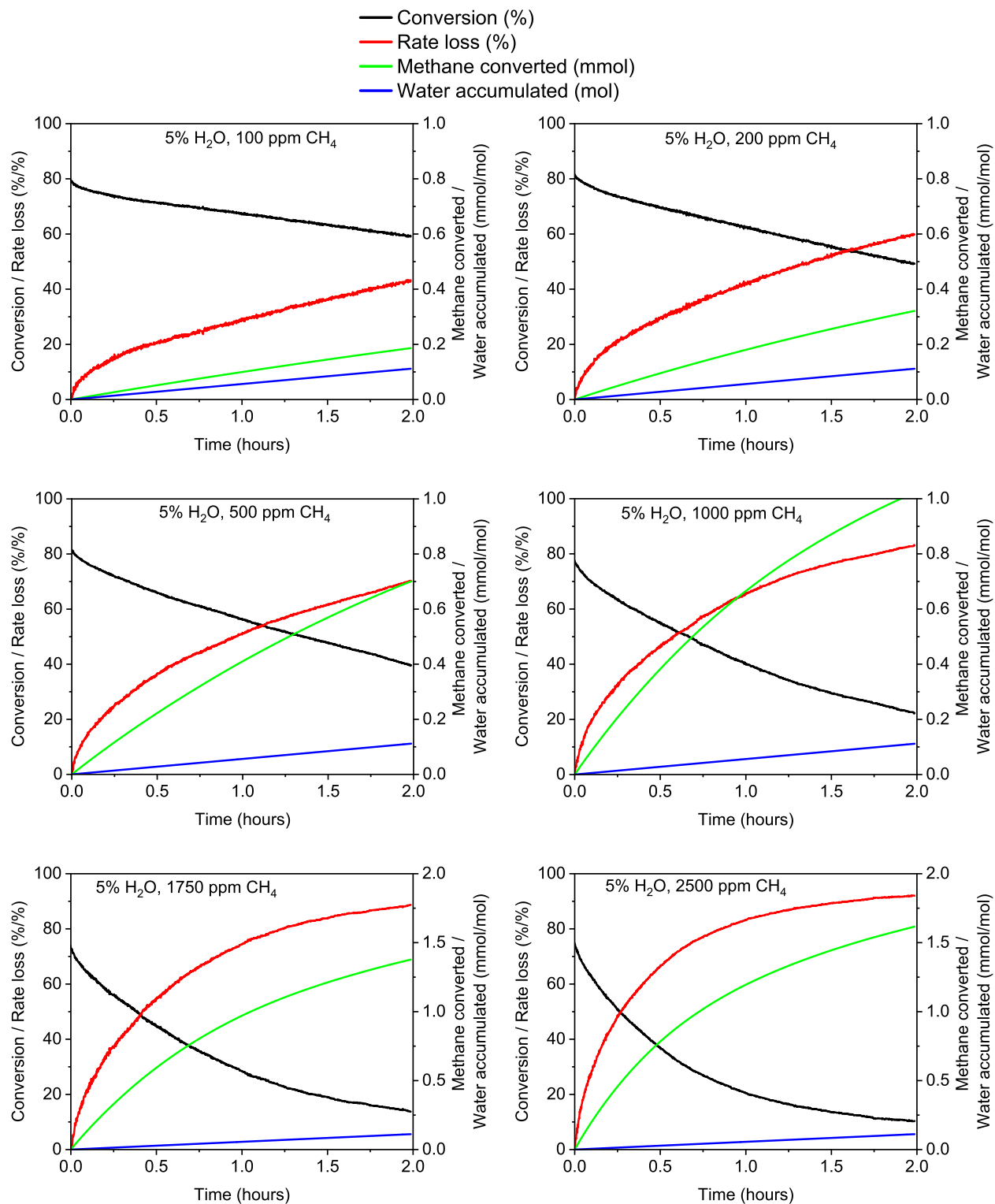
Followup experiment to verify that the slope of the deactivation curve depends on the concentration of methane. This result did not fit with the leading hypothesis for water-induced deactivation revolving around accumulation of hydroxyl groups on the PdO surface. Reaction conditions: 300 or 1000 ppm CH₄, 10% O₂, 5% H₂O, N₂ balance, WHSV = 126 000 ml h⁻¹ g⁻¹, T = 400 °C.

Appendix F - Calculations for accumulation plots (500 ppm CH₄)



Figures showing the results of the calculations for the accumulation plots used in the analysis in Section 6.5. Reaction conditions are described in Paper 3. The data extraction are described in Section 6.5.

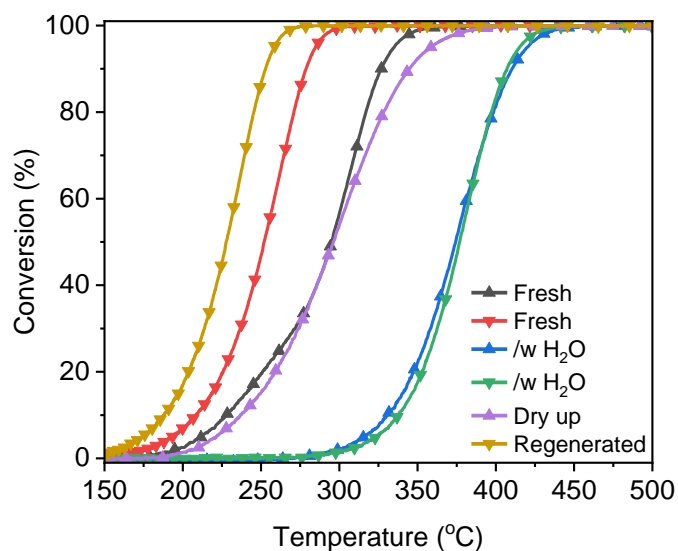
Appendix G - Calculations for accumulation plots (5% H₂O)



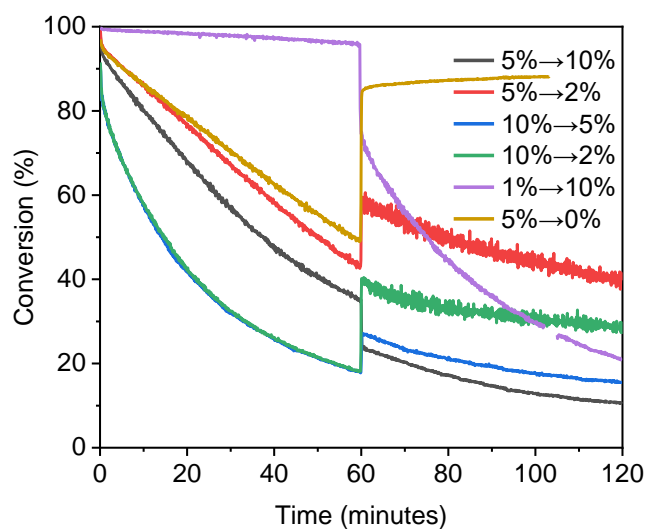
Figures showing the results of the calculations for the accumulation plots used in the analysis in Section 6.5. Reaction conditions are described in Paper 3. The data extraction are described in Section 6.5.

Appendix H - Supporting information for Paper 3

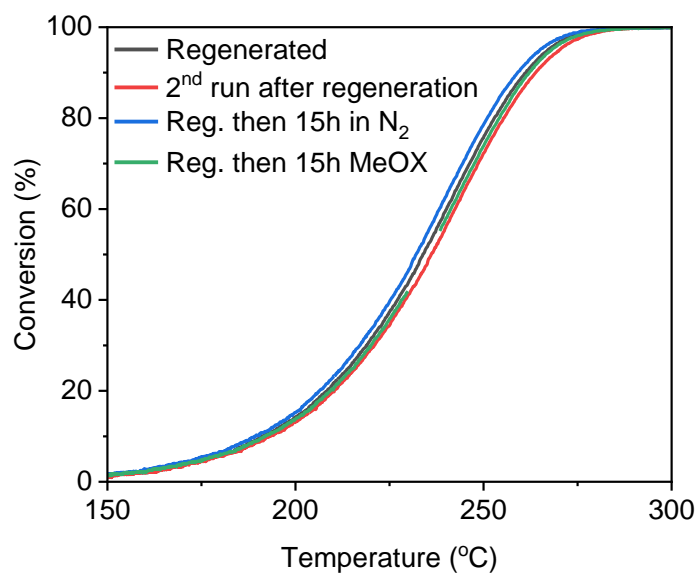
See the following pages.



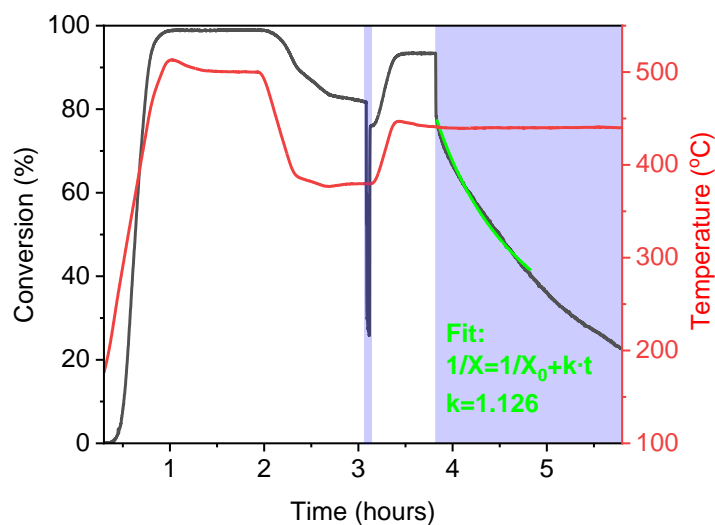
Supplementary Figure 1 | Light-off and light-down curves of Pd/Al₂O₃ catalyst under various conditions. Arrows indicate direction of temperature ramp and are shown for every 40th data point. Experiments were run in sequence, without regeneration in between, using the following reaction conditions: 1000 ppm CH₄, 10% O₂, 10% H₂O (when present), N₂ balance, ramp rate = 5 °C/min, WHSV = 126 000 ml h⁻¹ g⁻¹. Under dry conditions, the sample exhibits a hysteresis typical for palladium-based methane oxidation catalysts. Adding water to the feed gas significantly reduces the methane conversion, but the light-off in presence of water does not cause significant deactivation of the sample, as seen when comparing the purple and black curves. Finally, regenerating the catalyst with a reducing pulse increases activity beyond that of the fresh sample. The regenerated state is very reproducible, both in terms of activity (Figure 3) and reducibility (Supplementary Fig. 10).



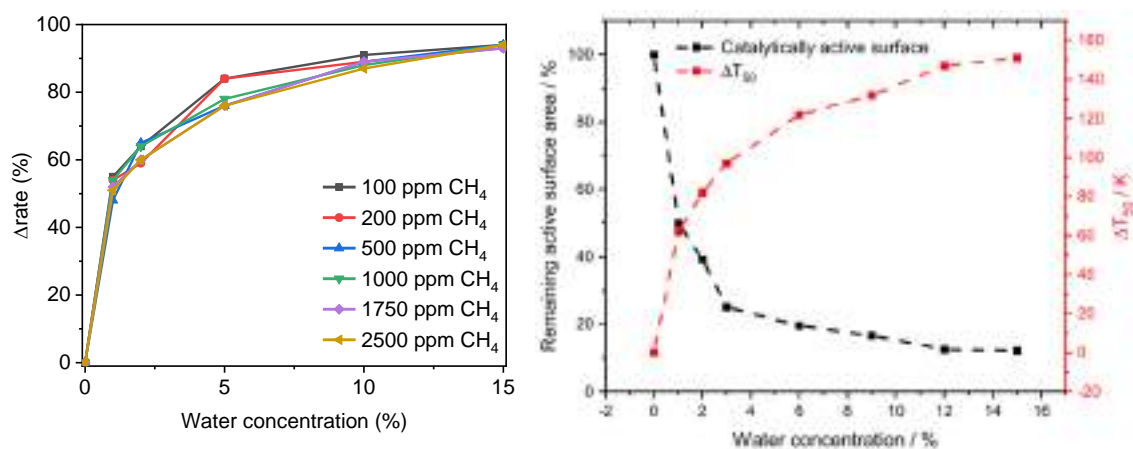
Supplementary Figure 2 | Experiments where the water concentration is changed according to the legend in the upper right corner. The catalyst bed was regenerated between experiments by a reducing pulse. The experiment shown in golden brown ended prematurely. The FID performed an autocalibration at 100 minutes in the purple experiment, leaving a few minutes blank in the data. The experiments with 2% water had a fluctuating liquid flow controller resulting in unstable conversion. Reaction conditions: 1000 ppm CH₄, 10% O₂, H₂O concentration in figure, N₂ balance, T = 430 °C, WHSV = 126 000 ml h⁻¹ g⁻¹.



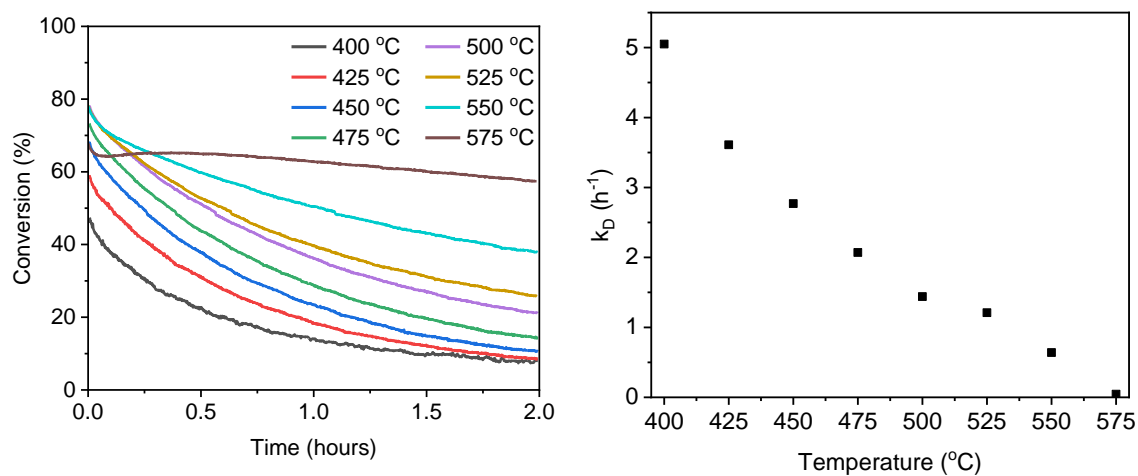
Supplementary Figure 3 | Light-down tests of regenerated catalysts. Reaction conditions: 1000 ppm CH₄, 10% O₂, N₂ balance, ramp = 5 °C/min, WHSV = 126 000 ml h⁻¹ g⁻¹. MeOX conditions refer to the same dry gas mixture. Upon regeneration, some report on a highly active state with a limited lifetime. For the catalyst used in this study, the activity gained from regenerating the fresh material is stable. This further qualifies the approach of reusing catalytic beds for multiple experiments, removing the uncertainties of preparing a new reactor every time. For the green experiment, the FID performed an auto-calibration mid-experiment causing a short gap in the data.



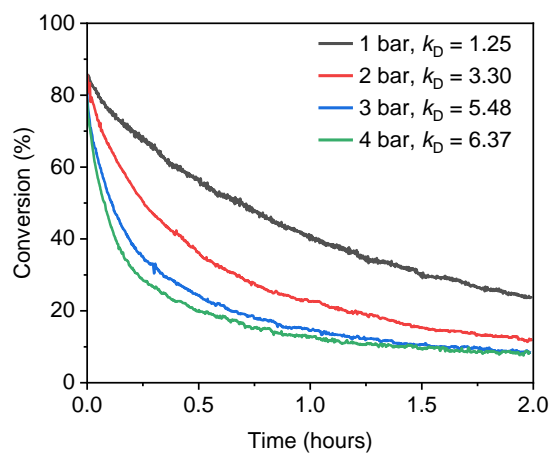
Supplementary Figure 4 | Example of kinetic experiment used to determine Δ rate and k_D for different concentrations of water and methane. To run the experiments at industrially relevant conditions and still stay within an acceptable conversion range (below 80%), the catalyst mass was reduced to 20 mg. The experiment consisted of 3 segments: First the reactor was heated to 500 °C and the catalyst degreened for one hour. Next, the temperature was lowered to 380 °C and water added for just two minutes to measure the inhibition depth, Δ rate. Finally, the temperature was raised to 440 °C and water added for two hours to record a deactivation curve. A second order kinetics fit (green line) was performed on the first hour of the deactivation curve. Reaction conditions for experiment shown in this figure: 1000 ppm CH₄, 10% O₂, 5% CO₂, 5% H₂O (when present, blue areas), N₂ balance, WHSV = 1 260 000 ml h⁻¹ g⁻¹.



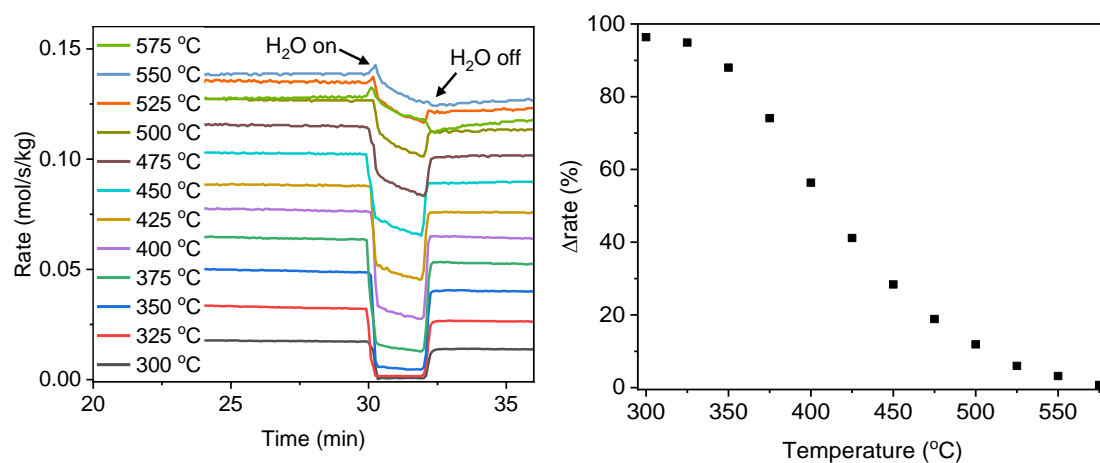
Supplementary Figure 5 | Comparison between the influence of inhibition on water concentration compared to that found by Keller et al. Left: Inhibition data as function of water concentration to the power of 1. Right: Inhibition measurements by Keller et al. Reprinted with permission. Copyright 2020 MDPI. Keller, K.; Lott, P.; Stotz, H.; Maier, L.; Deutschmann, O. Microkinetic Modeling of the Oxidation of Methane Over PdO Catalysts—Towards a Better Understanding of the Water Inhibition Effect. *Catalysts* 2020, 10, 922.



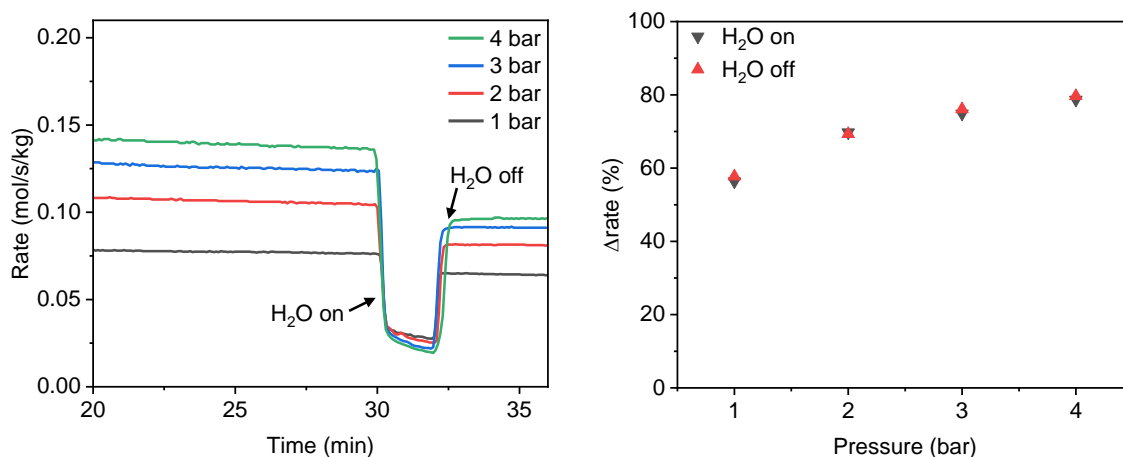
Supplementary Figure 6 | Deactivation experiments at different temperatures. The deactivation rate constant k_D decreases at high temperatures until 575 °C where it essentially stops. In order to run the experiment above 500 °C without exceeding 90% conversion, the catalyst mass was decreased significantly. Reaction conditions: 1000 ppm CH₄, 10% O₂, 5% H₂O, N₂ balance, WHSV = 5 040 000 ml h⁻¹ g⁻¹.



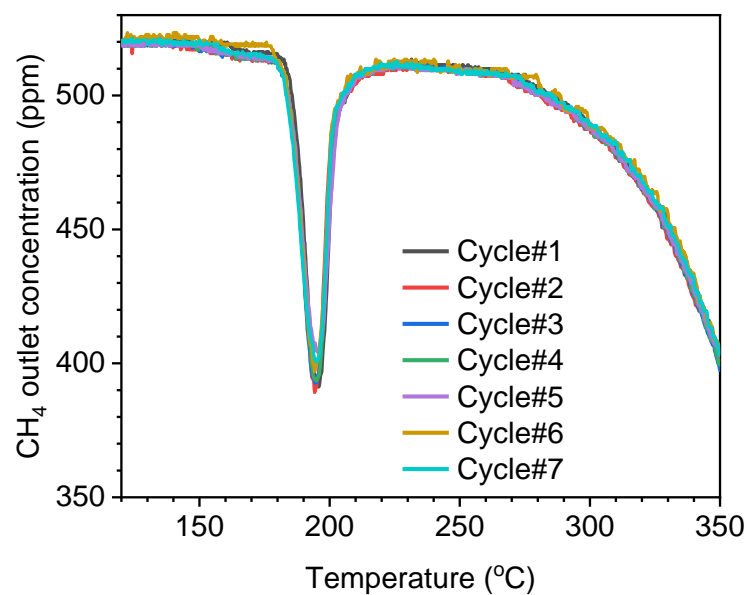
Supplementary Figure 7 | Deactivation experiments at different reactor pressures. The deactivation rate constant k_D increases at elevated pressure, drastically between 1 and 3 bar, but then more slowly. Reaction conditions: 1000 ppm CH_4 , 10% O_2 , 5% H_2O , N_2 balance, $T = 400^\circ\text{C}$, $\text{WHSV} = 1\,260\,000\text{ ml h}^{-1}\text{ g}^{-1}$.



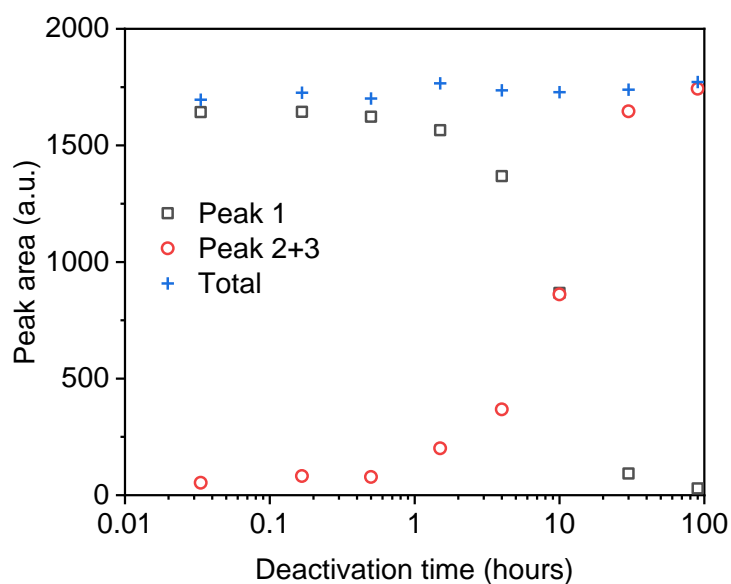
Supplementary Figure 8 | Reversible inhibition as function of temperature. As the temperature is increased, the inhibitory effect of water is gradually diminished, likely due to water adsorption being temperature dependent. Reaction conditions: 1000 ppm CH₄, 10% O₂, 5% H₂O (when present), N₂ balance, WHSV = 5 040 000 ml h⁻¹ g⁻¹.



Supplementary Figure 9 | Reversible inhibition as function of pressure. As the pressure is elevated, the inhibitory effect of water is gradually increased, likely due to water adsorption being pressure dependent. Curiously, irreversible deactivation is so fast that, although water is only being added to the feed gas for only two minutes, the catalyst does not recover to the original dry conversion rate when water is no longer added. Although the height of the climb up looks significantly smaller than the drop down, they are in fact identical in terms of the percentage they make out of their respective dry reaction rates, as shown in the figure to the right. This is critical, as it underlines the complete reversibility of the inhibition phenomenon, and thereby separates it from irreversible deactivation. Raising the pressure at constant molar flow results in an increased residence time which causes the dry conversion rate to increase with the pressure. Upon water addition however, the methane oxidation rate is very similar across the four experiments. Interestingly, this means that the increased inhibition exactly counters out the activity increase from increased pressure. Reaction conditions: 1000 ppm CH₄, 10% O₂, 5% H₂O (when present), N₂ balance, T = 400 °C, WHSV = 5 040 000 ml h⁻¹ g⁻¹.



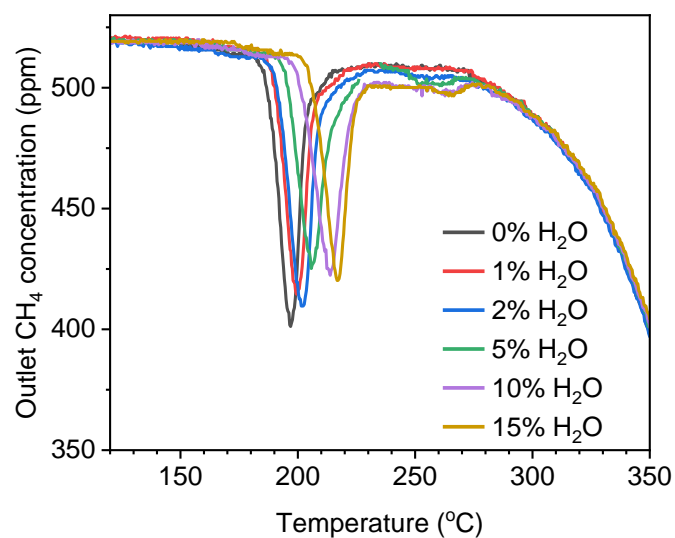
Supplementary Figure 10 | Reduction peaks for regenerated catalyst beds prior to each TPR experiment on deactivated catalyst. Regenerating the catalyst bed between deactivation cycles resulted in an identical reduction peak every time. Using the same regenerated bed for all deactivation experiments removed the uncertainty of preparing new beds, i.e. weighing catalyst, positioning it on quartz sand base, etc. Conditions during CH₄-TPR: 500 ppm CH₄ in N₂, 2.5°C/min, GHSV = 111 000 ml h⁻¹ g⁻¹.



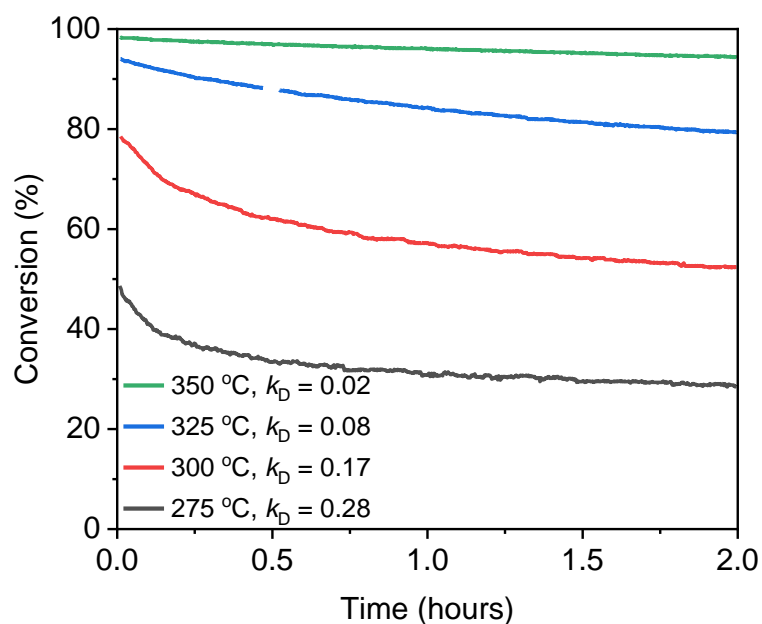
Supplementary Figure 11 | Evolution of peak areas in CH₄-TPR experiments on catalysts deactivated for different amounts of time. The time axis is logarithmic to see both the sample deactivated for 2 minutes and the one deactivated for 90 hours in the wide time span. The total peak area is relatively constant, corresponding to 100% PdO reduction. The peak integration was challenging due to severely overlapping peaks. Peak deconvolution was performed by fitting gauss curves to each set of TPR peaks.

Supplementary Table 1 | Elemental composition of catalyst determined by inductively coupled plasma optical emission spectrometry (ICP-OES). The promoters are irreducible base metal oxides not directly participating in the methane oxidation reaction, deactivation mechanisms, or PdO reduction during CH₄-TPR experiments.

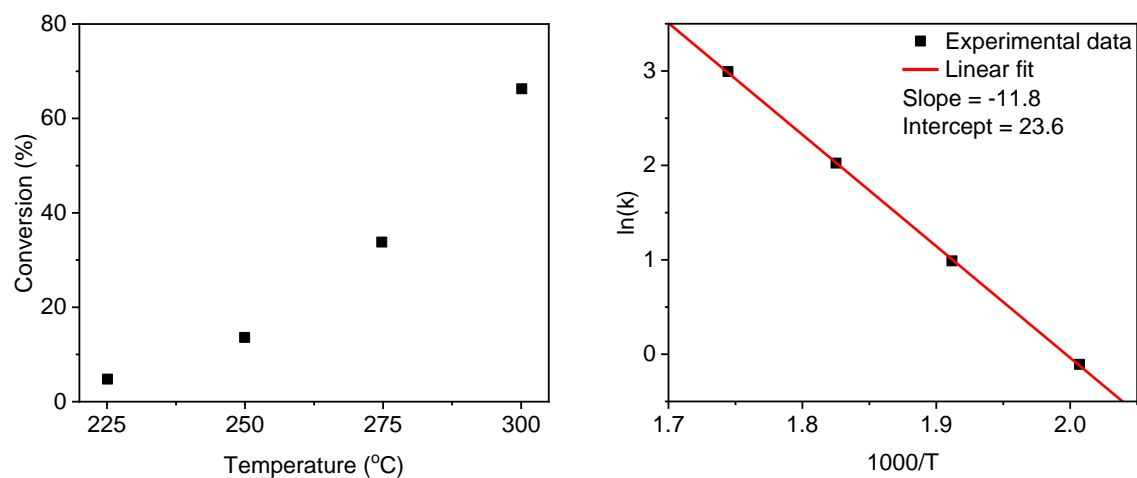
Element	wt%
Pd	2.4
Al ₂ O ₃	Confidential
Promoter 1	Confidential
Promoter 2	Confidential



Supplementary Figure 12 | CH₄-TPR experiments on catalysts deactivated in presence of different amounts of water. Each experiment consisted of 2 hours of deactivation in the presence of an amount of water corresponding to the figure legend. Each deactivation cycle resulted in a catalyst bed with different PdO reduction temperature. For the experiments with high water concentrations, the contours of the new peaks can even be spotted around 260 °C. Conditions during CH₄-TPR: 500 ppm CH₄ in N₂, 2.5°C/min, GHSV = 111 000 ml h⁻¹ g⁻¹.



Supplementary Figure 13 | Deactivation experiments at low temperature without water. At sufficiently low temperatures, the regenerated catalyst deactivates even when there is no water in the feed gas. We are still investigating the reason for this, and its potential links to water-induced deactivation. Reaction conditions: 1000 ppm CH₄, 10% O₂, N₂ balance, WHSV = 1 260 000 ml h⁻¹ g⁻¹. After 0.5 hours in the experiment at 325 °C the FID performs an autocalibration, creating a gap in the data of a few minutes.



Supplementary Figure 14 | Determination of pre-exponential factor A and activation energy E_a of Arrhenius expression for kinetic model. First, the steady state conversion at four different temperatures was determined, shown to the left. The rate constant at the four temperatures was then calculated and $\ln(k)$ was plotted against $1000/T$. The intercept of the linear fit was then $\ln(A)$ meaning $A = \exp(23.6) = 1.78 \cdot 10^{10} \text{ mol}/(\text{m}^2 \text{ s})$. The slope of the linear fit was $-E_a/R$ meaning $E_a = 11.8 R = 98.1 \text{ kJ/mol}$. Reaction conditions: 1000 ppm CH_4 , 10% O_2 , 5% CO_2 , N_2 balance, WHSV = 150 000 $\text{ml h}^{-1} \text{ g}^{-1}$.

Appendix I - Pictures of test setup



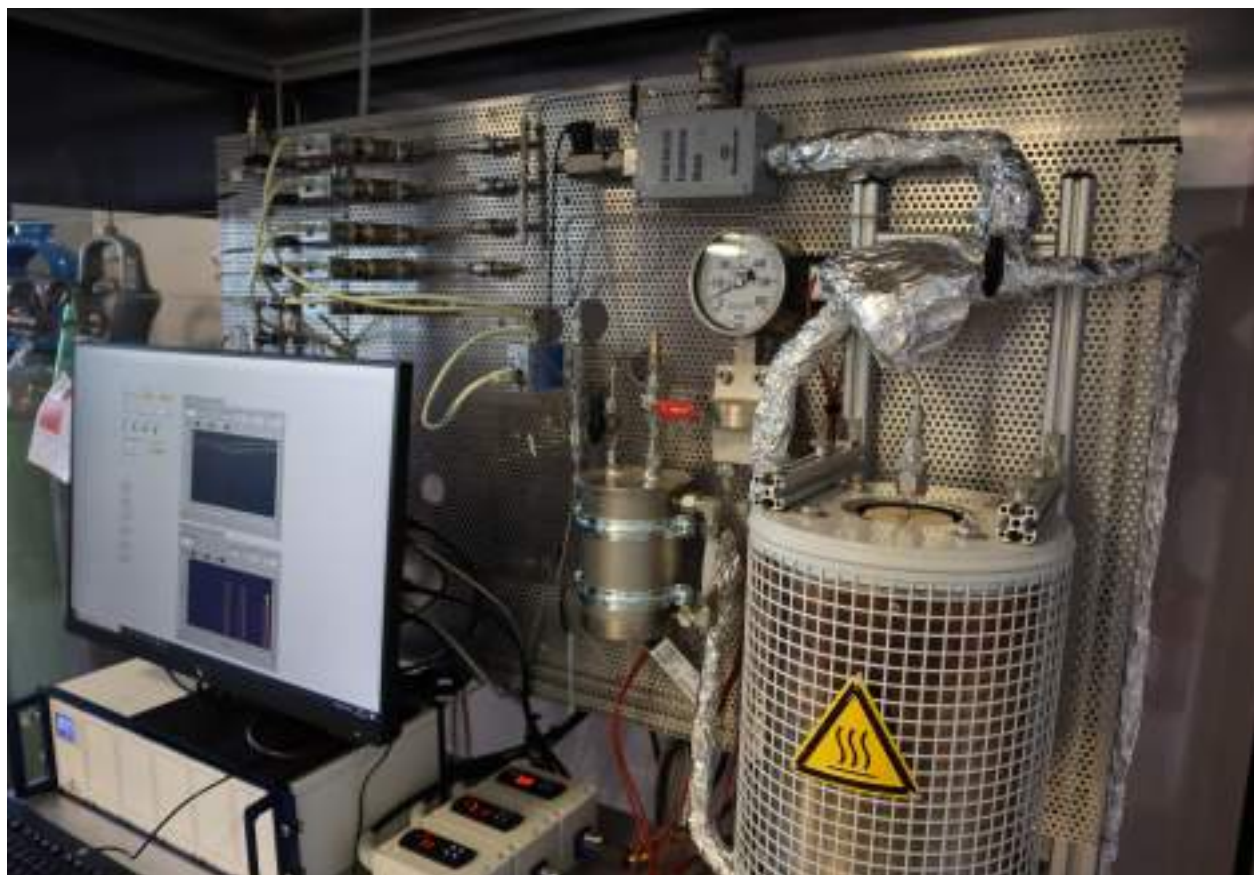
Overview of test setup inside polycarbonate casing.



Gas mixing section with N_2 lines for the back-pressure regulator and the water container feeding the CEM system.



Section delivering working gasses for the detectors. Lines are equipped with forward pressure reducing valves to deliver exact pressures of burner air, hydrogen, calibration gas, etc.

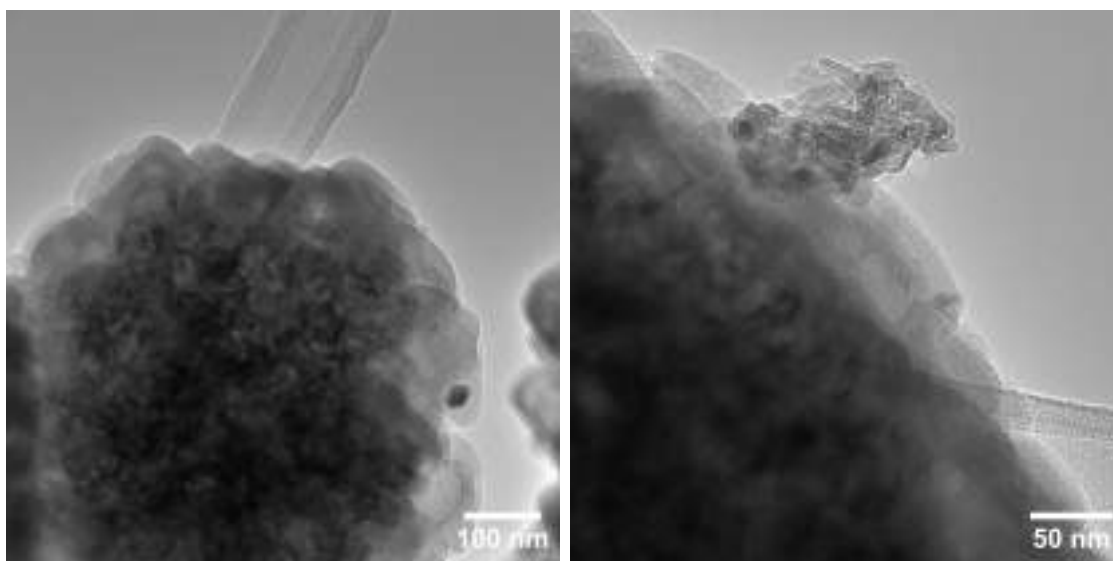


Reactor section showing the CEM and water flow meter, the pressurized water container, the differential pressure gauge, the bypass line, the three heat tracing control units, and the PC setup. Just prior to entering the reactor, the gas line is bent to a three dimensional double figure-8 shape to provide flexibility for mounting and dismounting reactors. This manifold is heat traced and insulated which is the triangular bulge seen just above the furnace.



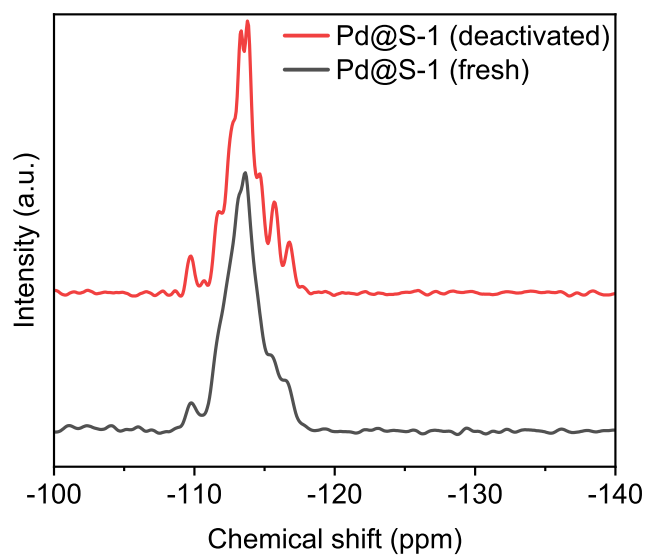
Quantification segment including the BINOS and FID instruments. Before the BINOS is a condenser to remove moisture before the sensitive IR detector. In the upper right corner is the back-pressure regulator wrapped in heat tracing and insulation. To the left of that are the relays which collect data from thermocouples and instruments. The main gas line is heat traced to 140 °C from the reactor to the FID detector to avoid condensation of sulfuric acid.

Appendix J - TEM of Pd/CeO₂@S-1 without methane oxidation activity



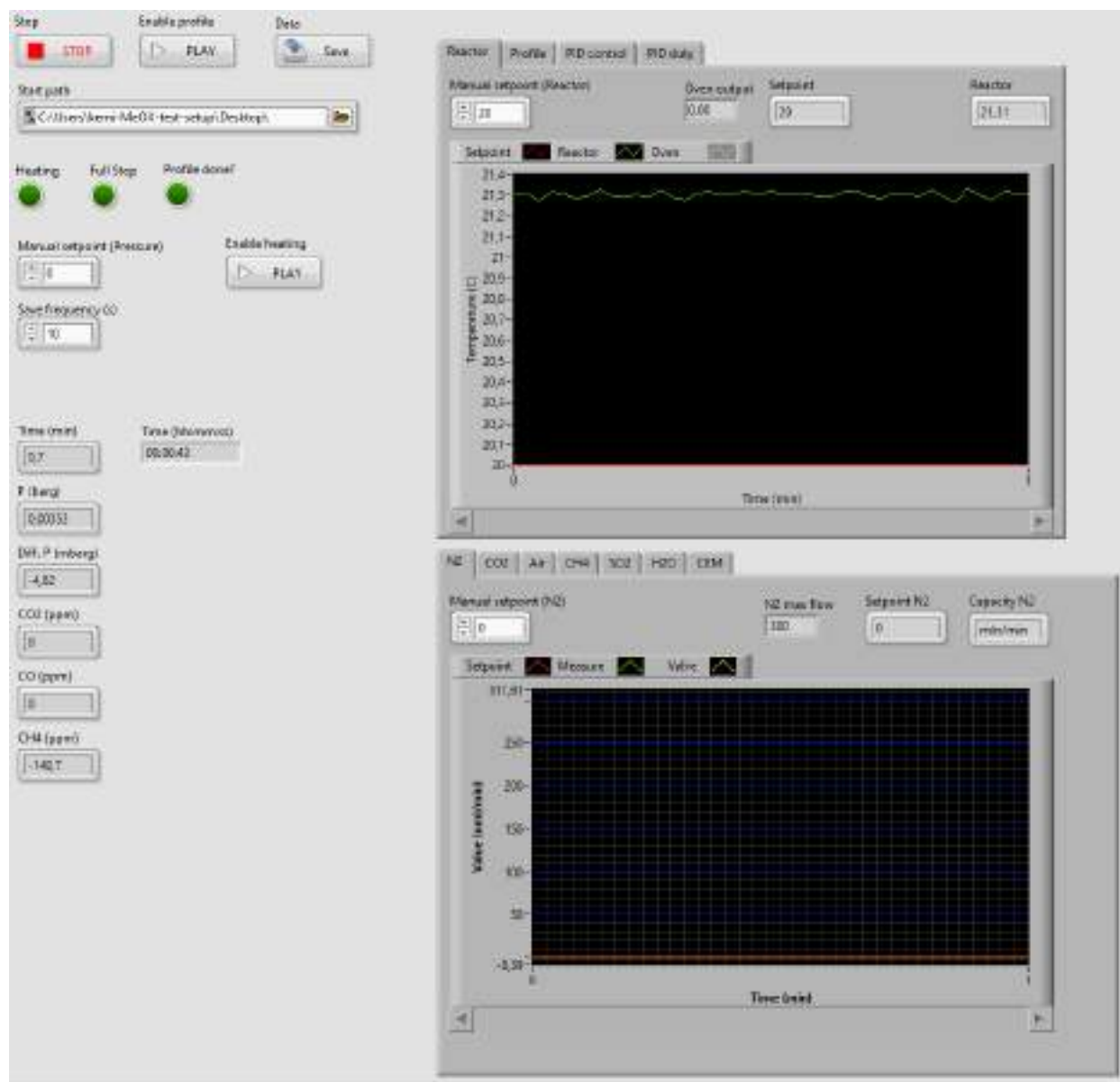
Bright-field TEM micrographs of a batch of Pd/CeO₂@S-1 which had close to no activity for methane oxidation. Other than some inhomogeneities around the surface of the particles, the sample looks very similar to the active one presented in Figure 17 which was synthesized in the same manner from the same starting materials.

Appendix K - Solid-state ^{29}Si NMR of fresh and deactivated Pd@S-1



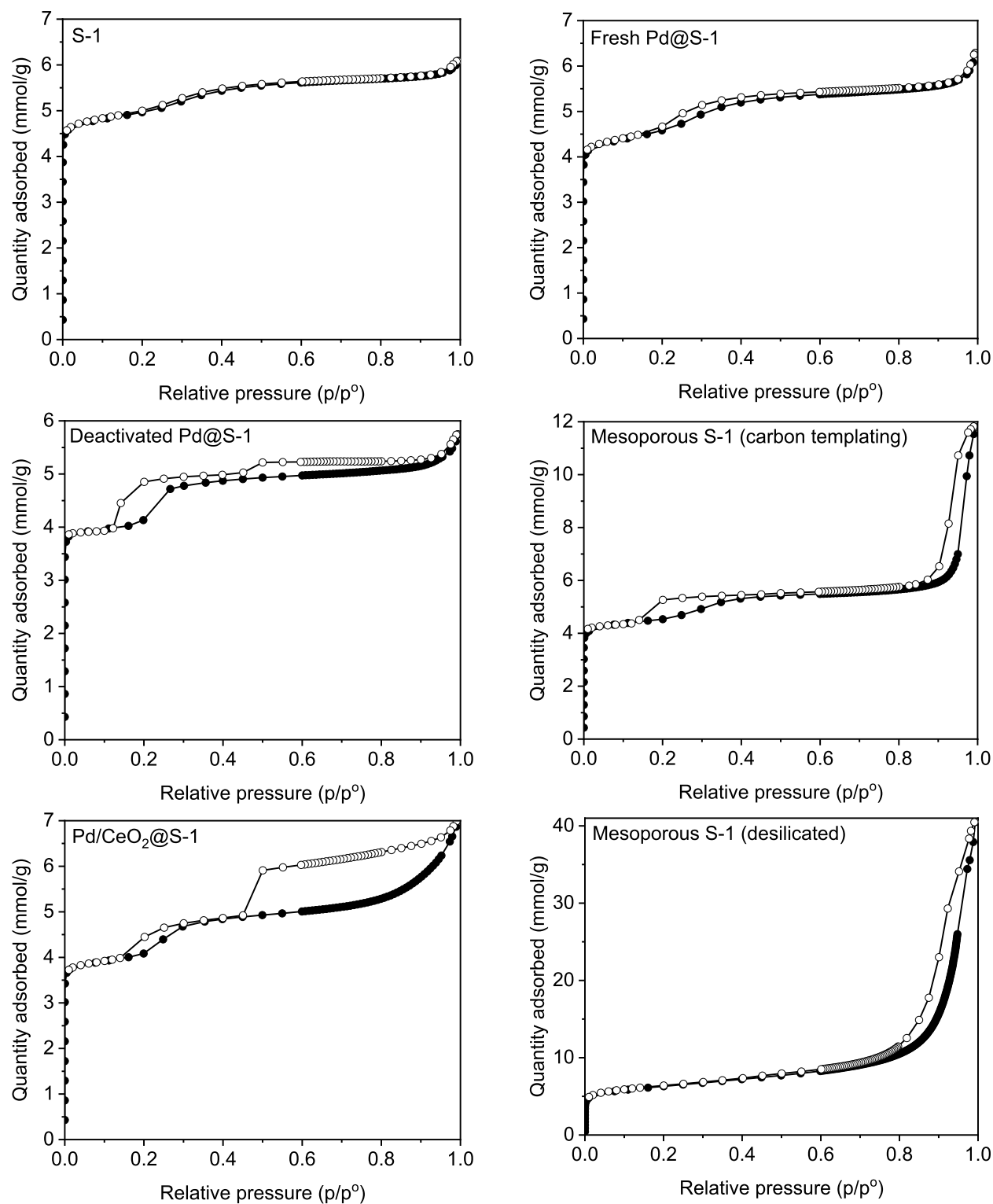
Solid-state ^{29}Si NMR of fresh and deactivated Pd@S-1 performed to assess the change in extra-framework aluminum. The analysis was inconclusive. Adapted from MSc. project by Panagiotis Dimitriou.¹³⁰

Appendix L - Virtual control panel for catalytic test setup



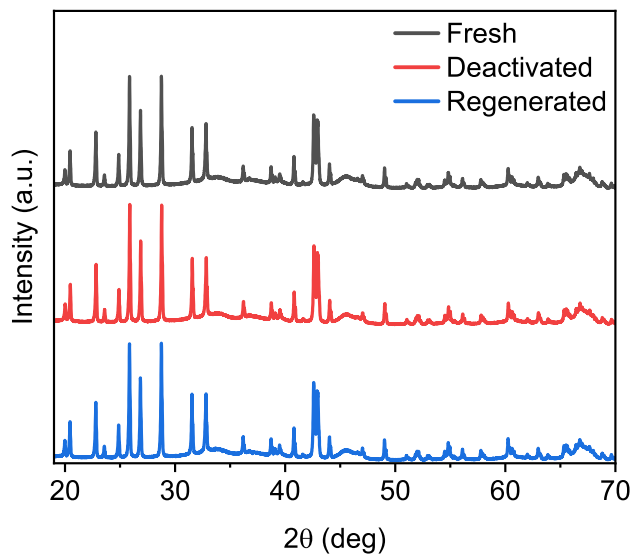
LabView control panel used for running catalytic tests and CH₄-TPR experiments.

Appendix M - N₂-physisorption isotherms



Nitrogen physisorption isotherms of Silicalite-1 derived materials. Measurements were performed on a Micrometrics 3Flex system at 77 K. All samples were degassed for 24 hours in a Micrometrics VacPrep 061 Sample Degas System at 400 °C.

Appendix N - XRD of fresh, deactivated, and regenerated catalyst for water deactivation project


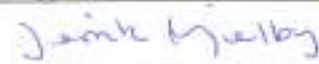



X-ray diffraction of Pd/Al₂O₃ catalyst in its fresh, deactivated and regenerated states, as described in Section 6.6. Although the PdO structure changes significantly during deactivation it was not visible from the diffraction patterns.

Appendix O - Co-author statements



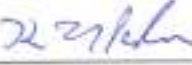
See the following pages.

Title of article		
Recent Advances in Complete Methane Oxidation using Zeolite-Supported Metal Nanoparticle Catalysts		
Journal/conference		
ChemCatChem		
Author(s)		
Rasmus Lykke Mortensen, Hendrik-David Noack, Kim Pedersen, Susanne Mossin, and Jerrik Mielby		
Name (capital letters)		
RASMUS LYKKE MORTENSEN		
Name of principal supervisor		
Susanne Mossin		
Declaration of the PhD student's contribution		
For each category in the table below, please specify the PhD student's contribution to the article as appropriate (please do not fill in with names or x's)		
Category	Minor contribution to the work (please specify the nature of the PhD student's contribution)	Substantial contribution to the work (please specify the nature of the PhD student's contribution)
Formulation of the conceptual framework and/or planning of the design of the study including scientific questions		Contributed with the initial outline of the review and the topics to be covered.
Carrying out of experiments/data collection and analysis/interpretation of results		Contributed with collecting, reading, and analyzing all the key literature to be covered in the review.
Writing of the article/revising the manuscript for intellectual content		Wrote the initial draft of the paper and took charge of the first round of editing. Created most of the figures for the article.
Signature of the PhD student 16/5-23 Rasmus Lykke Mortensen		

Title of article			
Recent Advances in Complete Methane Oxidation using Zeolite-Supported Metal Nanoparticle Catalysts			
Journal/conference			
ChemCatChem			
Author(s)			
Rasmus Lykke Mortensen, Hendrik-David Noack, Kim Pedersen, Susanne Mossin, and Jerrik Mielby			
Name (capital letters)			
RASMUS LYKKE MORTENSEN			
Name of principal supervisor			
Susanne Mossin			
Date	Name	Title	Signature
24/5-23	Susanne Mossin	Assoc. Prof.	
9/5-23	Jerrik Mielby	Dr.	
24/5-23	Kim Pedersen	Dr.	

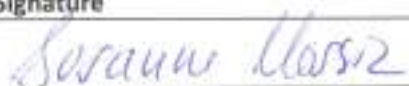
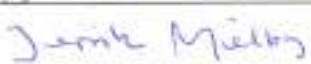
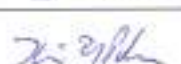
Please note that by signing this declaration, co-authors permit the PhD student to reuse whole or parts of co-authored articles in their PhD thesis, under the condition that co-authors are acknowledged in connection with the reused text or figure.

Title of article		
The Effect of Zeolite Counter-Ion on a Pd/H-CHA Methane Oxidation Catalyst with Remarkable Tolerance to SO ₂		
Journal/conference		
Author(s)		
Rasmus Lykke Mortensen, Hendrik-David Noack, Kim Pedersen, Susanne Mossin, and Jerrik Mielby		
Name (capital letters)		
RASMUS LYKKE MORTENSEN		
Name of principal supervisor		
Susanne Mossin		
Declaration of the PhD student's contribution		
For each category in the table below, please specify the PhD student's contribution to the article as appropriate (please do not fill in with names or x's)		
Category	Minor contribution to the work (please specify the nature of the PhD student's contribution)	Substantial contribution to the work (please specify the nature of the PhD student's contribution)
Formulation of the conceptual framework and/or planning of the design of the study including scientific questions	Assisted the conceptualization of the project	
Carrying out of experiments/data collection and analysis/interpretation of results		Contributed with all the experimental work, developed the methodology
Writing of the article/revising the manuscript for intellectual content		Wrote the initial draft and took charge of the first round of editing. Created all the figures for the manuscript.
Signature of the PhD student 16/5-23 Rasmus Lykke Mortensen		

Title of article			
The Effect of Zeolite Counter-Ion on a Pd/H-CHA Methane Oxidation Catalyst with Remarkable Tolerance to SO ₂			
Journal/conference			
Author(s)			
Rasmus Lykke Mortensen, Hendrik-David Noack, Kim Pedersen, Susanne Mossin, and Jerrik Mielby			
Name (capital letters)			
RASMUS LYKKE MORTENSEN			
Name of principal supervisor			
Susanne Mossin			
Date	Name	Title	Signature
24/5-23	Susanne Mossin	Assoc. Prof.	
9/5-23	Jerrik Mielby	Dr.	
24/5-23	Kim Pedersen	Dr.	

Please note that by signing this declaration, co-authors permit the PhD student to reuse whole or parts of co-authored articles in their PhD thesis, under the condition that co-authors are acknowledged in connection with the reused text or figure.

Title of article		
Understanding Water-Induced Reversible Inhibition and Irreversible Deactivation of Methane Oxidation Catalysts		
Journal/conference		
Author(s)		
Rasmus Lykke Mortensen, Hendrik-David Noack, Kim Pedersen, Susanne Mossin, and Jerrik Mielby		
Name (capital letters)		
RASMUS LYKKE MORTENSEN		
Name of principal supervisor		
Susanne Mossin		
Declaration of the PhD student's contribution		
For each category in the table below, please specify the PhD student's contribution to the article as appropriate (please do not fill in with names or x's)		
Category	Minor contribution to the work (please specify the nature of the PhD student's contribution)	Substantial contribution to the work (please specify the nature of the PhD student's contribution)
Formulation of the conceptual framework and/or planning of the design of the study including scientific questions	Assisted the conceptualization of the overall project	
Carrying out of experiments/data collection and analysis/interpretation of results		Contributed with all the experimental work, developed the methodology
Writing of the article/revising the manuscript for intellectual content		Wrote the initial draft and assisted revision of the manuscript. Created all the figures for the manuscript.
Signature of the PhD student 16/5-23 Rasmus Lykke Mortensen		

Title of article			
Understanding Water-Induced Reversible Inhibition and Irreversible Deactivation of Methane Oxidation Catalysts			
Journal/conference			
Author(s)			
Rasmus Lykke Mortensen, Hendrik-David Noack, Kim Pedersen, Susanne Mossin, and Jerrik Mielby			
Name (capital letters)			
RASMUS LYKKE MORTENSEN			
Name of principal supervisor			
Susanne Mossin			
Date	Name	Title	Signature
24/5-23	Susanne Mossin	Assoc. Prof.	
9/5-23	Jerrik Mielby	Dr.	
24/5-23	Kim Pedersen	Dr.	

Please note that by signing this declaration, co-authors permit the PhD student to reuse whole or parts of co-authored articles in their PhD thesis, under the condition that co-authors are acknowledged in connection with the reused text or figure.